Design and Synthesis of Poly(HydroxyUrethane) Hot-Melt Adhesives from CO_2 and Bio-Based Monomers

by

Ghuge Gorakh Hiraman

10CC19J26028

A thesis submitted to the

Academy of Scientific & Innovative Research

for the award of the degree of

DOCTOR OF PHILOSOPHY

in

SCIENCE

Under the supervision of

Dr. S. Kiran



CSIR-National Chemical Laboratory, Pune



Academy of Scientific and Innovative Research
AcSIR Headquarters, CSIR-HRDC campus
Sector 19, Kamla Nehru Nagar,
Ghaziabad, U.P. – 201 002, India

October, 2024

Certificate

This is to certify that the work incorporated in this Ph.D. thesis entitled, *"Design and Synthesis of Poly(HydroxyUrethane) Hot-Melt Adhesives from CO_2 and Bio-Based Monomers"*, submitted by *Ghuge Gorakh Hiraman* to the Academy of Scientific and Innovative Research (AcSIR) in fulfillment of the requirements for the award of the Degree of *Doctor of Philosophy in Science*, embodies original research work carried-out by the student. We, further certify that this work has not been submitted to any other University or Institution in part or full for the award of any degree or diploma. Research material(s) obtained from other source(s) and used in this research work has/have been duly acknowledged in the thesis. Image(s), illustration(s), figure(s), table(s) etc., used in the thesis from other source(s), have also been duly cited and acknowledged.

Gorakh Hiraman Ghuge
(Research Student)
Date: 07/10/2024

Dr. S. Kiran
(Research Supervisor)
Date: 07/10/24

STATEMENTS OF ACADEMIC INTEGRITY

I, Ghuge Gorakh Hiraman, a Ph.D. student of the Academy of Scientific and Innovative Research (AcSIR) with Registration No. 10CC19J26028 hereby undertake that, the thesis entitled "Design and Synthesis of Poly(HydroxyUrethane) Hot-Melt Adhesives from CO_2 and Bio-Based Monomers", has been prepared by me and that the document reports original work carried out by me and is free of any plagiarism in compliance with the UGC Regulations on "*Promotion of Academic Integrity and Prevention of Plagiarism in Higher Educational Institutions (2018)*" and the CSIR Guidelines for "*Ethics in Research and in Governance (2020)*".

(Ghuge)
Signature of the Student

Date : 07/10/2024

Place : Pune

It is hereby certified that the work done by the student, under my/our supervision, is plagiarism-free in accordance with the UGC Regulations on "*Promotion of Academic Integrity and Prevention of Plagiarism in Higher Educational Institutions (2018)*" and the CSIR Guidelines for "*Ethics in Research and in Governance (2020)*".

Signature of the Supervisor

Name : Dr. S. Kiran

Date : 07/10/24

Place : Pune



DEDICATED TO MY GRANDPARENTS AND PARENTS,

MY GREATEST INSPIRATIONS.

Acknowledgements

This thesis would not have been possible without the guidance, support, and encouragement of many individuals. I would like to take this opportunity to express my deepest gratitude to all of them.

First and foremost, I extend my sincere thanks to Dr. S. Kiran, my thesis supervisor, for his invaluable guidance, support, and encouragement throughout my research. His expertise and insights greatly contributed to the success of this work.

I also wish to express my heartfelt gratitude to the members of my Doctoral Advisory Committee (Dr. Santosh Mhaske, Dr. Ashootosh Ambade, Dr. S. Kadhiravan, Dr. Anuya Nisal, Dr. Shubhangi Umbarkar, and Dr. Vilas Rane) for their insightful feedback, and helpful suggestions. Their recommendations have significantly helped to improve the quality of my thesis.

I want to thank Dr. Vijay Bokade for all his great advice and mentorship during my initial time at NCL. I am also grateful to Dr. Prashant Niphadkar, Dr. Nagesh Mulik, and Mr. Jagtap for their help and assistance.

I would like to extend my heartfelt thanks to Dr. Prakash Wadgaonkar for his timely suggestions and encouragement.

I would also like to sincerely thank Dr. Schin Nandanwar and Dr. Dinesh Sawant for their valuable suggestions and support throughout my thesis work.

I would like to express my gratitude to my postgraduate faculty for their invaluable guidance in helping me succeed in the CSIR-NET exam and encouraging me to pursue a Ph.D. I am particularly thankful for the timely support and mentorship of Prof. Padwal, Dr. N. K. Jadhav, Dr. R. R. Kale, Dr. N. D. Gaikwad, Dr. Keshav Mahale, Dr. Koli, and Dr. Kardel.

I am especially grateful to Mr. Uday Jadhav, Dr. Pravin Salunkhe, Dr. Amol Ichake, Dr. Deepak Maher, and Mr. Swami for their help and cooperation during the early stages of my research at the PSE division. They always guided me in conducting experiments, synthesizing and purifying compounds, and analyzing data.

I also wish to acknowledge Dr. Paresh Dhepe and his students, Mr. Tufeil Khan, for allowing me to use the high-pressure reactor, and Dr. Harshwardhan Pol and his students for their assistance with rheological and tensile analysis.

I feel fortunate to have been part of a supportive lab environment where I spent more time with my colleagues than with my own family. This work would not have been possible without the collective support of everyone in the lab. I am deeply grateful to both my former and current colleagues: Dr. Samadhan Nagane, Dr. Aniket Talanikar, Ms. Srilatha Naga, Ms. Sonali Naik, Ms. VK Karthika, Ms. Durga, Mr. Adebayo Olosho, and Disiya Davis. I also appreciate the cooperation of Ms. Sayali Mahajan, Mr. Shantanu Vedpathak, Ms. Safa, Ms. Amrutha, Ms. Nila Krishna, Ms. Jagruti Chavan, Ms. Bhadra P. B., Ms. Shazia, Ms. Tejaswini, Ms. Amruta Phegade, and Ms. Sanjana Kasturi during their internship projects.

I am profoundly grateful to CSIR-National Chemical Laboratory, Pune, for providing the resources and facilities necessary for the completion of this work. I also extend my thanks to the AcSIR office (Ms. Vaishali, Ms. Vijaya, and Ms. Komal) and the SAAC office for their assistance and cooperation with the academic paperwork.

I am also grateful to Dr. Shivshankar Mane, Dr. Shivaji Markand, Mr. Dnyaneshwar Mache, Mr. Shakeb Chaudhari, Dr. Nitin Basutkar, Mr. Shankar Avhad, Mr. Shafi Alam, Mr. Rahul Yede, Mr. Anil Patil, Mr. Apparao Wale, Ms. Pragati Hetkale, Mr. Nitin Thorat, Mr. Ritesh, Mr. Fayis, Mr. Navnath Kakade, Ms. Devika, Ms. Rachna for their help and support during my research.

I want to extend my appreciation to Dr. Arun Torris, Mr. Chetan, Ms. Sangeeta Hambir, Ms. Nita Patil, and Dr. Purvi Purohit for their help and cooperation in analyzing samples.

I would like to express my deepest appreciation to my best friends: Mr. Ajay Kumar, Mr. Gangadhar Hattale, Mr. Vishal Virole, Mr. Chetan Galave, Mr. Atul Ugale, Mr. Onkar Dube, Mr. Vaibhav, Mr. Vinod Lohar, Ms. Rutuja Kadam, Ms. Revati Dokhe, Ms. Pallavi, Mr. Ganesh Kambale, Mr. Akshay, Mr. Avinash Jadhav, Mr. Indrajit, Mr. Kiran Ingole, Mr. Yogesh Gaikwad, Mr. Siddharth Barik, Ms. Priyanka PP, Mr. Amit Gavit, Mr. Sameer Sonawane, Mr. Sachin Mahale, Raj Birajdar, Mr. Radhakisan Kurgude, Ms. Ashwini Deshpande.

I am forever thankful to my family for their unwavering love and support throughout this journey. Without their encouragement, this thesis would not have been possible.

I am also deeply grateful to my friends, whose belief in my ability to produce quality research motivated me to complete this work successfully. Special thanks to Mr. Gorakh Kale, Mr. Ravindra Ugale, Mr. Deepak Ugale, Mr. Ravindra Aghav, Mr. Manoj Vairagar, Mr. Kishor Bidgar, Mr. Sainath Guru, Mr. Ramkrishna Chavhan, Ms. Poonam Chavhan, Mr. Haridas Sarode, Mr. Nayan Vairagar, Mr. Tushar Dhatrak, and Dr. Pankaj Harkal.

Finally, I would like to acknowledge the CSIR, New Delhi for providing the financial support necessary to carry out this research. Their funding allowed me to focus on my work without financial concerns.

To anyone I may have unintentionally missed in this acknowledgment, I sincerely thank you for your contributions and support throughout this process. This thesis is a reflection of the combined efforts of many individuals, and I am truly grateful to everyone who has been part of this journey.

Thank you all.

Gorakh Ghuge

Abbreviations and Symbols

Synthesized compounds

V-DL	2-methoxybenzene-1,4-diol
V-DGE	Vanillin diglycidyl ether
V-DC	Vanillin dicarbonate
ISO-DAE	Isosorbide diallyl ether
ISO-DGE	Isosorbide diglycidyl ether
ISO-DC	Isosorbide dicarbonate
DVS-DL	Divanillin-spiro-diol
DVS-DGE	Divanillin-spiro-diglycidyl ether
DVS-DC	Divanillin-spiro-dicarbonate
VA	Vanillyl alcohol
BGF-DL	Bisguaiacol diol
BGF-DGE	Bisguaiacol diglycidyl ether
BGF-DC	Bisguaiacol dicarbonate
BGF-PF-DL	Bisguaiacol-diol bearing pendant furyl group
BGF-PF-DGE	Bisguaiacol-diglycidyl ether bearing pendant furyl group
BGF-PF-DC	Bisguaiacol-dicarbonate bearing pendant furyl group

Symbols

T_g	Glass transition temperature
$T_{d,\,10\,\%}$	Decomposition temperature after 10% weight loss
M_n	Number-average molar mass
M_w	Weight-average molar mass
Đ	Dispersity
G’	Storage modulus
G’’	Loss modulus
wt%	Weight percentage
Al	Aluminum
SS	Stainless steel
mol %	Mole percentage
ωc	Relaxation time
π	Pi

$I_A/I_BI/_C$	Integration of A/B/C
MPa	Megapascals
$R_{p/s}$	Ratio of the primary to secondary hydroxyl groups

Polymers

PU	Polyurethane
NIPU	Non-isocyanate polyurethane
PHU	Polyhydroxyurethane
HMA	Hot melt adhesives
PHU-HMA	Polyhydroxyurethane based hot melt adhesives
EVA	Ethylene vinyl acetate
PMMA	Polymethyl methacrylate

Reagents and Solvents

DMC	Dimethyl Carbonate
CNSL	Cashew nut shell liquid
PDMS	Polydimethylsiloxane
APTES	3-Aminopropyl) triethoxysilane
TBAB	Tetrabutylammonium bromide
TBD	1,5,7-triazabicyclo-[4.4.0] dec-5-ene
NaOH	Sodium hydroxide pellets
HCl	Hydrochloric acid
DMSO-d_6	Deuterated dimethyl sulfoxide
NMP	N-methyl pyrrolidinone
DMF	N, N-Dimethylformamide
CaH_2	Calcium hydride
CO_2	Carbon dioxide
LiBr	Lithium bromide
THF	Tetrahydrofuran
Na_2CO_3	Sodium percarbonate
Na_2SO_4	Sodium sulphate
pTSA.H_2O	Para-toluene sulfonic acid monohydrate
DCM	Dichloromethane

Acetone-d_6	Deuterated acetone
$NaHCO_3$	Sodium bicarbonate
BMI	1, 1′-(methylenedi-1, 4-phenylene) bismaleimide
H_2SO_4	Sulfuric acid
TCE-d_2	Deuterated 1, 1, 2, 2-tetrachloroethane-d_2
$CDCl_3$	Deuterated $CDCl_3$
$NaBH_4$	Sodium borohydride
DMAc	N, N-dimethyl acetamide

Characterization techniques

FTIR	Fourier transform infrared spectroscopy
HRMS	High-resolution mass spectrometer
GPC	Gel permeation chromatography
SEC	Size exclusion chromatography
TGA	Thermogravimetric analysis
XRD	X-ray diffraction
DSC	Differential scanning calorimeter
WCA	Water contact angle

Others

ASTM	American society for testing and materials
ISO	International organization for standardization
EN	European committee for standardization
LSS	Lap shear strength
VOC	Volatile organic compounds
ROP	Ring opening polymerization
5CC/6CC/7CC/8CC	Five/six/seven/eight membered cyclic carbonate
CESBO	Carbonated-epoxidized soybean oil
REACH	Registration, evaluation, authorization, and restriction of chemicals
ECHA	European chemicals agency
M.P.	Melting point
LVR	Linear viscoelastic region

DA	Diels-alder
rDA	Reverse diels-alder
PF	Pendant furyl group
RCC	Renewable carbon content
L*W*T	Length, width, and thickness
CAGR	Compound annual growth rate
USD	US dollar

Table of Contents

List of Tables i

List of Schemes ii

List of Figures iii

Chapter 1

Introduction and Literature Survey 2

1.1 Adhesives and their applications 3

1.2 Theories of adhesion 4

1.3 Classification of adhesives 5

1.4 Factors influencing the performance of the adhesive 6

1.5 Test methods for assessing the adhesive performance 8

1.5.1 Lap shear strengths 9

1.6 Adhesive technologies 10

1.6.1 Polyurethane hot melt adhesives (PU-HMAs) 12

1.7 Isocyanate-free polyurethanes 13

1.7.1 Synthetic pathways for producing NIPUs 14

1.7.1.1 NIPUs from aziridine and CO_2 copolymerization 14

1.7.1.2 Ring-opening-polymerization of cyclic carbamate 14

1.7.1.3 Transurethanization 15

1.7.1.4 Aminolysis of carbonates 15

1.7.2 Limitations in PHU production 19

1.7.2.1 Side reactions 19

1.7.2.2 Hydrogen bonds 20

1.8 Literature survey on PHU-based adhesives 21

1.8.1 Bio-derived PHU-adhesives 21

1.8.2 Fossil-derived PHU-adhesives 23

1.9 Objective of the thesis 28

1.10 References 30

Chapter 2

Evaluation of the Adhesive Properties of Vanillin-Derived Poly(HydroxyUrethane)s ... 38

2.1 Introduction 39

2.2 Experimental section 40

2.2.1 Materials 40

2.2.2 Characterization techniques....40
2.2.3 Methods....41
2.2.3.1 Synthesis of vanillin and CO_2-derived cyclic dicarbonate....41
2.2.3.2 Synthesis of PHU series....44
2.3 Result and Discussion....44
2.3.1 Synthesis of vanillin-CO_2-derived cyclic dicarbonate....44
2.3.1.1 Synthesis of 2-methoxybenzene-1, 4-diol....44
2.3.1.2 Synthesis vanillin diglycidyl ether....45
2.3.1.3 Synthesis of vanillin dicarbonate....45
2.3.2 Optimization of polymerization conditions....50
2.3.3 Synthesis of PHU series....52
2.3.3.1 Spectral analysis of PHUs....53
2.3.3.2 Molecular weight analysis of PHUs....56
2.3.3.3 Thermal properties of PHUs....57
2.3.3.4 Adhesive properties of PHUs....59
2.4 Conclusion....62
2.5 References....62
Chapter 3
Biobased Reusable Poly(HydroxyUrethane) Hot-Melt Adhesives with Potential Chemical Degradability....67
3.1 Introduction....68
3.2 Experimental section....69
3.2.1 Materials....69
3.2.2 Characterization techniques....69
3.2.3 Methods....71
3.2.3.1 Preparation of isosorbide-derived cyclic carbonate....71
3.2.3.2 Preparation of vanillin and pentaerythritol-derived cyclic carbonate....73
3.2.3.3 General procedure for the synthesis of PHUs....76
3.2.3.4 Acid degradability of PHUs....77
3.3 Result and Discussion....77
3.3.1 Preparation of isosorbide-derived cyclic carbonate....77
3.3.2 Preparation of vanillin and pentaerythritol-derived cyclic carbonate....83
3.3.3 PHU formulations and their structural characterization....89
3.3.3.1 Analysis of the ^{1}H NMR recorded at various temperatures....98

3.3.3.2 Size Exclusion Chromatography....99
3.3.3.3 Thermal properties....100
3.3.3.4 Water contact angle measurements....101
3.3.3.5 X-ray diffraction spectroscopy....102
3.3.3.6 Rheological measurements....103
3.3.3.7 Adhesive properties....105
3.3.3.8 Mechanical properties....110
3.3.3.9 Acid degradability of PHUs....111
3.4 Conclusion....115
3.5 References....116
Chapter 4
Post-Functionalizable and Reusable Biobased Polyhydroxyurethane Adhesives with Pendant Furyl Groups....120
4.1 Introduction....123
4.2 Experimental section....124
4.2.1 Materials....124
4.2.2 Characterization techniques....125
4.2.3 Methods....126
4.2.3.1 Preparation of vanillin and guaiacol-derived cyclic carbonate....126
4.2.3.2 Preparation of guaiacol and furfural-derived cyclic carbonate....127
4.2.3.3 General procedure for diglycidyl ether preparation....128
4.2.3.4 General procedure for dicarbonate preparation....130
4.2.3.5 A typical procedure for the synthesis of PHU polymers....131
4.2.3.6 Preparation of the cross-linked PHU/BMI networks....132
4.3 Result and Discussion....132
4.3.1 Preparation of vanillin and guaiacol-derived cyclic carbonate....132
4.3.2 Preparation of guaiacol and furfural-derived cyclic carbonate....139
4.3.3 Synthesis and Characterization of PHUs.....144
4.3.3.1 Size Exclusion Chromatography....149
4.3.3.2 Thermal properties....150
4.3.3.3 X-ray diffraction....152
4.3.3.4 Water contact angle....153
4.3.3.5 Rheological behavior of PHU materials....154
4.3.3.6 Adhesive properties....156

4.3.4 Thermal and adhesive properties of cross-linked PHU/BMI networks.....161
4.4 Conclusion 166
4.5 References.....166
Chapter 5
Conclusion and Future Outlook 173
5.1 Conclusion 174
5.2 Future Outlook.....176
Abstract.....178
List of Publications 179

List of Tables

Table 1.1. A list of bio-derived cyclic carbonates utilized to prepare the PHU-based adhesives. 22

Table 1.2. A list of fossil-derived cyclic carbonates utilized to prepare the PHU-based adhesives. 25

Table 2.1. The nomenclature of synthesized PHUs. 44

Table 2.2. The molecular weight of the PHUs synthesized at different temperatures. 51

Table 2.3. Experimental data from SEC and ^{1}H NMR. 56

Table 2.4. Thermal properties of PHUs. 58

Table 2.5. Lap shear strength of PHUs evaluated on aluminum and stainless-steel substrates. 60

Table 3.1. Molar compositions of the precursors utilized in PHUs preparation……..90

Table 3.2. Renewable carbon contents for cyclic dicarbonate monomers developed from the sugar and lignin-derived precursors. 97

Table 3.3. Renewable carbon contents of PHU adhesives. 97

Table 3.4. Incorporated mole percentage of dicarbonate monomers in the final PHU copolymers, determined using the integrals of ^{1}H NMR signals. 97

Table 3.5. Molecular weight distribution and Thermal properties of the PHUs. 99

Table 3.6. Water contact angle measurements of PHU polymers. 102

Table 3.7. Lap shear strength of PHUs on the aluminum substrate. 110

Table 3.8. Mechanical properties of the PHU samples. 110

Table 4.1. Molar compositions and molecular weight of the PHUs……132

Table 4.2. Thermal properties and molecular weights distribution of the PHUs. 152

Table 4.3. Experimental values from rheological measurements and water contact angle…155

Table 4.4. Incorporated mole percentage of dicarbonate monomers in the final NIPU copolymers, were determined using the integrals of ^{1}H NMR signals. 166

List of Schemes

Scheme 1.1. Conventional method for producing isocyanate-based polyurethanes. 13
Scheme 2.1. Synthetic process for the V-DL compound. 42
Scheme 2.2. Synthetic method for V-DGE compound. 42
Scheme 2.3. Preparation of V-DC monomer. 43
Scheme 2.4. Synthetic scheme for PHUs made at various temperatures. 50
Scheme 2.5. Syntheses of bio-based PHUs from vanillin-derived dicarbonate and diamines of different chain lengths. 52
Scheme 3.1. Synthesis of ISO-DAE……..71
Scheme 3.2. Preparation of ISO-DGE via epoxidation. 72
Scheme 3.3. Synthesis of ISO-DC monomer through carbonation. 73
Scheme 3.4. Procedure for synthesizing the DVS-DL compound. 74
Scheme 3.5. Epoxidation method for producing the DVS-DGE compound. 75
Scheme 3.6. Synthesis of the DVS-DC monomer by carbonation. 76
Scheme 3.7. Preparation of the PHU-based hot melt adhesives from isosorbide and vanillin-derived cyclic carbonates (a) structure of the copolymers when two cyclic carbonates were used, (b, c) structure of homopolymers when individual monomers were used. 89
Scheme 4.1. Reduction of vanillin to vanillyl alcohol (VA) using $NaBH_4$ as a reducing agent. 125
Scheme 4.2. Preparation of BGF-DL by condensation of vanillyl alcohol with guaiacol….127
Scheme 4.3. Synthesis of BGF-PF-DL from the reaction of guaiacol with furfural. 127
Scheme 4.4. Method for synthesizing the BGF-DGE using glycidation. 129
Scheme 4.5. Synthetic scheme for BGF-PF-DGE compound. 129
Scheme 4.6. Preparation of BGF-DC monomer using carbonation. 130
Scheme 4.7. Carbonation process for synthesizing the BGF-PF-DC monomer. 131
Scheme 4.8. Design and synthesis of PHU-derived hot melt adhesives bearing pendant furyl groups. 144

List of Figures

Figure 1.1. Key application areas for adhesive. 3
Figure 1.2. Overview of adhesive classification by origin, curing process, composition, and application. 6
Figure 1.3. Overview of the main factors affecting the strength of adhesive joints. 6
Figure 1.4. (a) Schematic illustration of an adhesive joint specimen used in a single-lap shear test, and (b) modes of adhesive bond failure. 10
Figure 1.5. Types of the adhesive technologies and the polymers used in their formulation, 2023 (Market share data added from multiple sources and may vary slightly)… 11
Figure 1.6. The key sectors of global hot melt adhesives and their approximate market share. 12
Figure 1.7. Principal synthesis routes for non-isocyanate polyurethanes. 14
Figure 1.8. Mechanism of the aminolysis reaction between cyclic carbonate and diamine. 16
Figure 1.9. Principal pathways for 5-membered cyclic carbonate synthesis. 17
Figure 1.10. Mechanism for producing five-membered cyclic carbonates from carbon dioxide and epoxide. 18
Figure 1.11. The synthesis of larger ring cyclic carbonates (a) 6CCs from oxetane and CO_2, (b) 6CCs from 1, 3 diols and DMC (c) 7CCs from 1, 4 diols and triphosgene, and (d) 8CCs from 1, 5 diols and triphosgene. 18
Figure 1.12. Potential secondary reactions occur during the polyaddition reaction between 5CC and amine. 20
Figure 1.13. Inter and intra-molecular hydrogen bonds are present in the PHU chains. 21
Figure 1.14. Structure of the thesis chapters. 29
Figure 2.1. ^{1}H NMR spectrum of V-DL. 46
Figure 2.2. ^{13}C NMR spectrum of V-DL. 47
Figure 2.3. ^{1}H NMR spectrum of V-DGE. 47
Figure 2.4. ^{13}C NMR spectrum of V-DGE. 48
Figure 2.5. ^{1}H NMR spectrum of V-DC. 48
Figure 2.6. ^{13}C NMR spectrum of V-DC. 49
Figure 2.7. HRMS spectrum of V-DC. 49
Figure 2.8. FTIR spectrum of V-DL, V-DGE, and V-DC compounds. 50
Figure 2.9. GPC chromatograms of PHUs synthesized at different temperatures. 51
Figure 2.10. ^{1}H NMR spectrum of PHUs prepared at different temperatures. 52

Figure 2.11. Photographs of the synthesized PHUs. 53
Figure 2.12. FTIR spectrum of PHUs. 54
Figure 2.13. ^{1}H NMR spectrum of PHUs. 55
Figure 2.14. ^{13}C NMR spectrum of PHUs. 56
Figure 2.15. GPC curves of developed PHUs. 57
Figure 2.16. The second heating curves of PHUs were obtained from DSC. 58
Figure 2.17. TGA results of PHUs (a) TGA thermograms (b) DTG curves of PHU-4. 59
Figure 2.18. Lap shear strength of PHUs evaluated on aluminum and stainless-steel substrates. The error bars show the representative standard deviation of each sample set of five samples. 60
Figure 2.19. Fractured test specimen showing the mixture of cohesive and adhesive failure of PHU-4. 61
Figure 2.20. Load vs displacement curves of (a) PHU-2, PHU-3, PHU-6 and (b) PHU-4, PHU-5 were evaluated for aluminum substrates. 61
Figure 2.21. Load vs displacement curves of (a) PHU-2, PHU-3, PHU-6 and (b) PHU-4, PHU-5 were evaluated for stainless steel substrates. 61
Figure 3.1. FTIR spectrum of ISO-DL, ISO-DGE, and ISO-DC compounds……79
Figure 3.2. ^{1}H NMR spectrum of ISO-DAE. 79
Figure 3.3. ^{13}C NMR spectrum of ISO-DAE. 80
Figure 3.4. ^{1}H NMR spectrum of ISO-DGE. 80
Figure 3.5. ^{13}C NMR spectrum of ISO-DGE. 81
Figure 3.6. ^{1}H NMR spectrum of ISO-DC. 81
Figure 3.7. ^{13}C NMR spectrum of ISO-DC. 82
Figure 3.8. HRMS spectrum of ISO-DC. 82
Figure 3.9. FTIR spectrum of DVS-DL, DVS-DGE, and DVS-DC compounds. 85
Figure 3.10. ^{1}H NMR spectrum of DVS-DL. 85
Figure 3.11. ^{13}C NMR spectrum of DVS-DL. 86
Figure 3.12. ^{1}H NMR spectrum of DVS-DGE. 86
Figure 3.13. ^{13}C NMR spectrum of DVS-DGE. 87
Figure 3.14. ^{1}H NMR spectrum of DVS-DC. 87
Figure 3.15. ^{13}C NMR spectrum of DVS-DC. 88
Figure 3.16. HRMS spectrum of DVS-DC. 88
Figure 3.17. The photographs of PHU polymers. 90
Figure 3.18. FTIR spectrum of the PHUs. 91

Figure 3.19. ^{1}H NMR spectrum of PHU1-0 (Homo). 92
Figure 3.20. ^{1}H NMR spectrum of PHU6-100 (Homo). 92
Figure 3.21. ^{1}H NMR spectrum of PHU copolymers. 93
Figure 3.22. ^{13}C NMR spectrum of PHU1-0 (Homo). 94
Figure 3.23. ^{13}C NMR spectrum of PHU6-100 (Homo). 94
Figure 3.24. ^{13}C NMR spectrum of PHU copolymers. 95
Figure 3.25. The % molar compositions of PHU copolymers were determined by ^{1}H NMR spectroscopy. 96
Figure 3.26. ^{1}H NMR spectrum of PHU3-40 taken at different temperatures (a) displaying the shifting of primary and secondary hydroxyl groups, and (b) the shifting of urethane -NH. ... 99
Figure 3.27. GPC traces of PHUs. 100
Figure 3.28. Overlay of the DSC curves (second heating cycles). 100
Figure 3.29. TGA results of PHUs (a) TGA thermograms (b) DTG curve of PHU4-60. 101
Figure 3.30. Water contact angle measurement images of PHUs. 102
Figure 3.31. X-ray diffractogram profile of PHUs. 103
Figure 3.32. Plot of (a) storage and loss modulus vs strain (b) storage and loss modulus vs angular frequency. 103
Figure 3.33. Plot of (a) complex viscosity vs angular frequency. (b) storage modulus vs temperature, (c) loss modulus vs temperature, and (d) tan δ vs temperature, obtained from rheological measurement for PHUs. 104
Figure 3.34. a) Schematic diagram of the bonding of PHU adhesives to aluminum substrate (b) Original and recycled lap shear strength of PHU hot melt adhesives assessed on aluminum (c) Adhesive strength after water soaking for 12 h and (d) Lap shear strength of PHU3-40 at different temperature. 106
Figure 3.35. Schematic representation of the possible non-covalent interactions and structural arrangement of cycloaliphatic and aromatic segments in PHU1-0 (a), PHU3-40 (b), and PHU6-100 (c). 107
Figure 3.36. Force vs. displacement curves of PHU adhesives. 108
Figure 3.37. (a) Two aluminum joints bonded by a PHU3-40 held 100 kg of weight. (b) Lap shear strength of PHU3-40 compared against thermoplastic PHU-based hot melt adhesives reported in the literature. 109
Figure 3.38. Fracture interfaces of the PHU adhesives (a) PHU1-0 and (b) PHU2-20 (c) PHU3-40 (d) PHU4-60 (e) PHU5-80 (f) PHU6-100. 109

Figure 3.39. Tensile test curves (stress-strain) of the (a) PHU1-0, PHU2-20, and b) PHU3-40, PHU4-60, PHU5-80, and PHU6-100. 111
Figure 3.40. The change in color of DVS-DC solutions in NMR tubes at room temperature (a) 0 mol/L (b) 0.1 mol/L (c) 1.0 mol/L (d) 2.0 mol/L. 111
Figure 3.41. ^{1}H NMR spectra of DVS-DC (a) after 5 h (b) after 24 h (c) after 120 h (d) possible degradation mechanism of DVS-DC in HCl solutions. 112
Figure 3.42. ^{1}H NMR spectrum of possible degradation products (1.0 mol/L, 5 h). 113
Figure 3.43. Photographs of the PHU samples before and after adding to 1 mol/L HCl solutions. 114
Figure 3.44. ^{1}H NMR spectrum of (a) PHU1-0, (b) PHU3-40, and (c) PHU6-100, before and after degradation (1 mol/L HCl). (d) weight loss of the PHUs with different times (under 1 mol/L HCl). 114
Figure 3.45. FTIR spectra of (a) PHU1-0, (b) PHU3-40, and (c) PHU6-100 before and after degradation under 1 mol/L HCl. 115
Figure 4.1. FTIR spectrum of Vanillin, BGF-DL, BGF-DGE, and BGF-DC compounds….. 134
Figure 4.2. ^{1}H NMR spectrum of VA. 134
Figure 4.3. ^{13}C NMR spectrum of VA. 135
Figure 4.4. ^{1}H NMR spectrum of BGF-DL. 135
Figure 4.5. ^{13}C NMR spectrum of BGF-DL. 136
Figure 4.6. ^{1}H NMR spectrum of BGF- DGE. 136
Figure 4.7. ^{13}C NMR spectrum of BGF- DGE. 137
Figure 4.8. ^{1}H NMR spectrum of BGF-DC. 137
Figure 4.9. ^{13}C NMR spectrum of BGF-DC. 138
Figure 4.10. HRMS spectrum of BGF-DC. 138
Figure 4.11. FTIR spectrum of BGF-PF-DL, BGF-PF-DGE, and BGF-PF-DC compounds bearing pendant furyl groups. 140
Figure 4.12. ^{1}H NMR spectrum of BGF-PF-DL. 140
Figure 4.13. ^{13}C NMR spectrum of BGF-PF-DL. 141
Figure 4.14. ^{1}H NMR spectrum of BGF-PF-DGE. 141
Figure 4.15. ^{13}C NMR spectrum of BGF-PF-DGE. 142
Figure 4.16. ^{1}H NMR spectrum of BGF-PF-DC. 142
Figure 4.17. ^{13}C NMR spectrum of BGF-PF-DC. 143
Figure 4.18. HRMS spectrum of BGF-PF-DC. 143
Figure 4.19. FTIR spectrum of PHUs bearing pendant furyl groups. 145

Figure 4.20. ^{1}H NMR spectrum of PHU1-PF0 (Homo). 146
Figure 4.21. ^{1}H NMR spectrum of PHU6-PF100 (Homo). 146
Figure 4.22. ^{1}H NMR spectrum of PHUs (Copolymers). 147
Figure 4.23. ^{1}H NMR spectrum of PHU4-PF60 recorded at different temperatures. 148
Figure 4.24. ^{13}C NMR spectrum of PHU1-PF0 (Homo). 148
Figure 4.25. ^{13}C NMR spectrum of PHU6-PF100 (Homo). 149
Figure 4.26. ^{13}C NMR spectrum of PHUs (Copolymers). 150
Figure 4.27. SEC curves for PHUs bearing pendant furyl group. 149
Figure 4.28. DSC thermograms of PHUs bearing pendant furyl groups. 151
Figure 4.29. TGA results of PHUs bearing furyl groups (a) TGA thermograms (b) DTG curve of PHU6-PF100. 152
Figure 4.30. XRD pattern of PHUs bearing pendant furyl group. 153
Figure 4.31. Contact angle measurements of PHUs bearing pendant furyl groups. 153
Figure 4.32. Plot of (a) storage and loss modulus vs strain (b) storage and loss modulus vs angular frequency for PHUs bearing pendant furyl group.....154
Figure 4.33. A plot of (a) storage modulus vs temperature (b) loss modulus vs temperature (c) tan δ vs temperature (d) complex viscosity vs angular frequency acquired from rheological measurement for PHUs bearing pendant furyl group. 156
Figure 4.34. The lap shear strength of PHUs bearing pendant furyl groups (a) evaluated on the aluminum (b) evaluated on the stainless steel and (c) evaluated under the water environment. 157
Figure 4.35. Force vs. displacement curves of PHUs bearing pendant furyl group (an aluminum substrate). 159
Figure 4.36. Force vs. displacement curves of PHUs bearing pendant furyl group (stainless-steel substrate).....159
Figure 4.37. Photos of the representative cohesive failure for (a) PHU1-PF0 (b) PHU2-PF20 (c) PHU3-PF40 (d) PHU4-PF60, and the mixture of cohesive/adhesive failure for (e) PHU5-PF80 (f) PHU6-PF100, after the lap shear test assessed on an aluminum substrate. 160
Figure 4.38. Photos of the representative cohesive failure for (a) PHU1-PF0 (b) PHU2-PF20 (c) PHU3-PF40 (d) PHU4-PF60, and the mixture of cohesive/adhesive failure for (e) PHU5-PF80 (f) PHU6-PF100, after the lap shear test assessed on stainless-steel. 161
Figure 4.39. DSC curves of the cross-linked PHU/BMI polymers (a) first heating curves (b) second heating curves. 162
Figure 4.40. Preparation of crosslinked PHU/BMI network via Diels-Alder reaction. 163

Figure 4.41. (a) Comparison of adhesion strength (aluminum) and glass transition temperature, and (b) force-displacement curves of the crosslinked PHU/BMI network. 164

Figure 4.42. Failure images of crosslinked PHU/BMI network (a) PHU6/BMI-1, (b) PHU6/BMI-5, (c) PHU6/BMI-10, and (d) (a) PHU6/BMI-20. 164

Figure 4.43. Incorporated mole percentage of dicarbonate monomers in the final NIPU copolymers, were determined using the integrals of ^{1}H NMR signals. The $I_{A(CH)}$, $I_{B(OCH3)}$, and $I_{C(OCH3)}$ represent the integrals of one bridge-head proton of BGF-PF-DC (signal 1), six methoxy protons of BGF-DC (signals 2), and six methoxy protons of BGF-PF-DC (signal 3), respectively. 165

Figure 5.1. Schematic representation illustrating the chapter-wise (working) improvements in renewable carbon content (RCC) and lap shear strength (LSS) of PHU hot melt adhesives. 176

Chapter 1

Introduction and Literature Survey

1.1 Adhesives and their applications

The practice of bonding various materials together using adhesives has been a well-documented technique throughout human history. Early humans utilized beeswax to affix feathers to arrows and enhance their tools, while evidence from around 1300 BC depicts the use of natural adhesives by the ancient Egyptians, as indicated by carvings portraying glue pots and brushes employed for bonding wood.[1] In the early 1900s, synthetic adhesives gained popularity in industries such as construction and aerospace, as well as allied application.[1] Today, adhesives play a vital role in numerous industries, with ongoing enhancements improving their strength, versatility, and environmental sustainability.[2,3]

In contemporary times, adhesives play an integral role, being employed in commonplace household settings as well as in advanced industrial sectors including construction, automotive, aerospace, packaging, and electronics (**Figure 1.1**).[4] They are esteemed for their adaptability, robustness, and capacity to form strong bonds with an array of materials, encompassing metals, plastics, wood, and ceramics.[5] Within the realm of packaging, adhesives are pivotal for activities such as carton sealing, product labeling, film lamination, and the production of flexible packaging materials. Water-based and hot melt adhesives are particularly favored in packaging due to their expeditious curing times and formidable bonds, which serve to streamline production processes and augment efficiency.

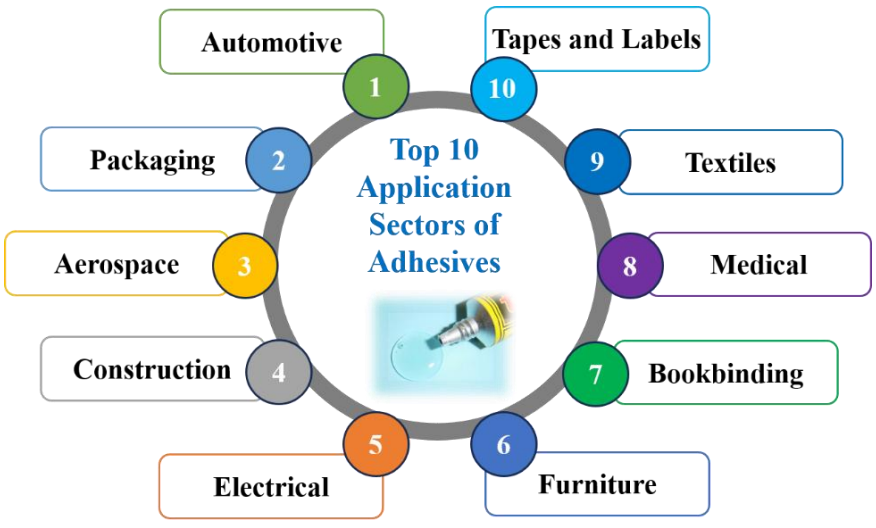

Figure 1.1. *Key application areas for adhesive.*

Moreover, pressure-sensitive adhesives (PSAs) are extensively employed for labels and tapes, facilitating straightforward application, robust adhesion, and often, removability or repositionability, attributes that are instrumental for diverse packaging requisites.[2] In the

automotive industry, adhesives have revolutionized manufacturing by enabling the use of lighter materials, thus contributing to improved fuel efficiency and vehicle performance. They are used for bonding body panels, installing windshields, securing interior components, and providing structural integrity.[5] Epoxy, polyurethane, and acrylic adhesives are commonly employed in automotive applications due to their high strength, flexibility, and durability. The construction industry benefits immensely from adhesives, which are used in a in a several areas like flooring installation, wall coverings, roofing, insulation, and structural bonding.[5]

1.2 Theories of adhesion

Adhesion, the phenomenon where two surfaces are bonded by interfacial forces, is explained by several theories.[6,7] Each theory provides a different perspective on how and why materials stick together. The key adhesion theories are outlined below,

(a) Mechanical interlocking theory

This theory suggests that adhesion occurs when the adhesive material physically locks into the pores, voids, or surface irregularities of the substrate. As the adhesive hardens, it forms a strong mechanical bond.

(b) Chemical bonding theory

This bonding theory proposes that adhesion results from the creation of chemical bonds between the adhesive and the substrate. These bonds can be covalent, ionic, or hydrogen bonds, which create a strong attachment at the molecular level.

(c) Physical adsorption (Van der Waals) theory

According to this theory, adhesion is caused by Van der Waals forces, which are weak inter-molecular interactions like dipole-dipole forces and London dispersion forces. These forces act over very short distances and can cause adhesion when molecules of the adhesive and substrate are in close contact.

(d) Diffusion theory

Diffusion theory explains adhesion through the interpenetration of polymer molecules from the adhesive into the substrate, leading to the formation of a bonded interface. This is particularly relevant for polymeric materials where the molecules can diffuse across the interface.

(e) Electrostatic theory

This theory is centered on the electrostatic attraction between two opposite charged materials. When an adhesive and a substrate come into contact, they may exchange or redistribute electrons, creating an electrostatic force that holds them together.

(f) Weak boundary layer theory

The weak boundary layer theory suggests that poor adhesion occurs when there is a weak layer at the junction between the glue and the substrate. This layer could be due to contamination, oxidation, or a phase with poor cohesive properties, and it acts as a weak link in the adhesive bond. In many practical situations, adhesion is a result of a combination of the above mechanisms. The contribution of each theory may vary depending on the materials involved and the conditions under which adhesion occurs. These theories help scientists and engineers understand the principles behind adhesion and develop better adhesives and surface treatments for various applications.

1.3 Classification of adhesives

Adhesives can be categorized in various ways, as illustrated in **Figure 1.2**, according to their origin, curing methods, chemical composition, and intended application.[1] Based on origin, they are classified into natural and synthetic types.[1,5] Natural adhesives, derived from plants or animals, include starch, and animal glue, commonly used in everyday applications. In contrast, synthetic adhesives, like epoxy, silicone, and superglue, are produced through chemical processes and are typically stronger, making them suitable for construction and manufacturing. Moving to curing methods, adhesives can be one-part or two-part.[1,5] One-part adhesives are ready to use and harden when exposed to specific conditions like air, heat, or moisture, examples being silicone sealants and super glue. Two-part adhesives, like epoxy, require mixing before use and begin curing without external factors. In terms of chemical composition, adhesives can be thermoset, thermoplastic, or elastomeric.[1,5] Thermoset adhesives, such as epoxy, form a strong, permanent bond when heated, while thermoplastic adhesives, like hot glue, soften with heat and can be reshaped. Elastomeric adhesives, like rubber-based glues, offer flexibility and are suitable for materials that expand or move. Lastly, adhesives are classified by application into structural and non-structural types.[1] Structural adhesives, like epoxy and certain polyurethanes, are used in load-bearing applications in industries like construction and automotive, where bond strength is crucial. Non-structural adhesives, like glue sticks or tape, are used for lighter tasks such as packaging, crafting, or temporary fixes,

where strength is less important. All these classifications help determine the right adhesive for different needs.

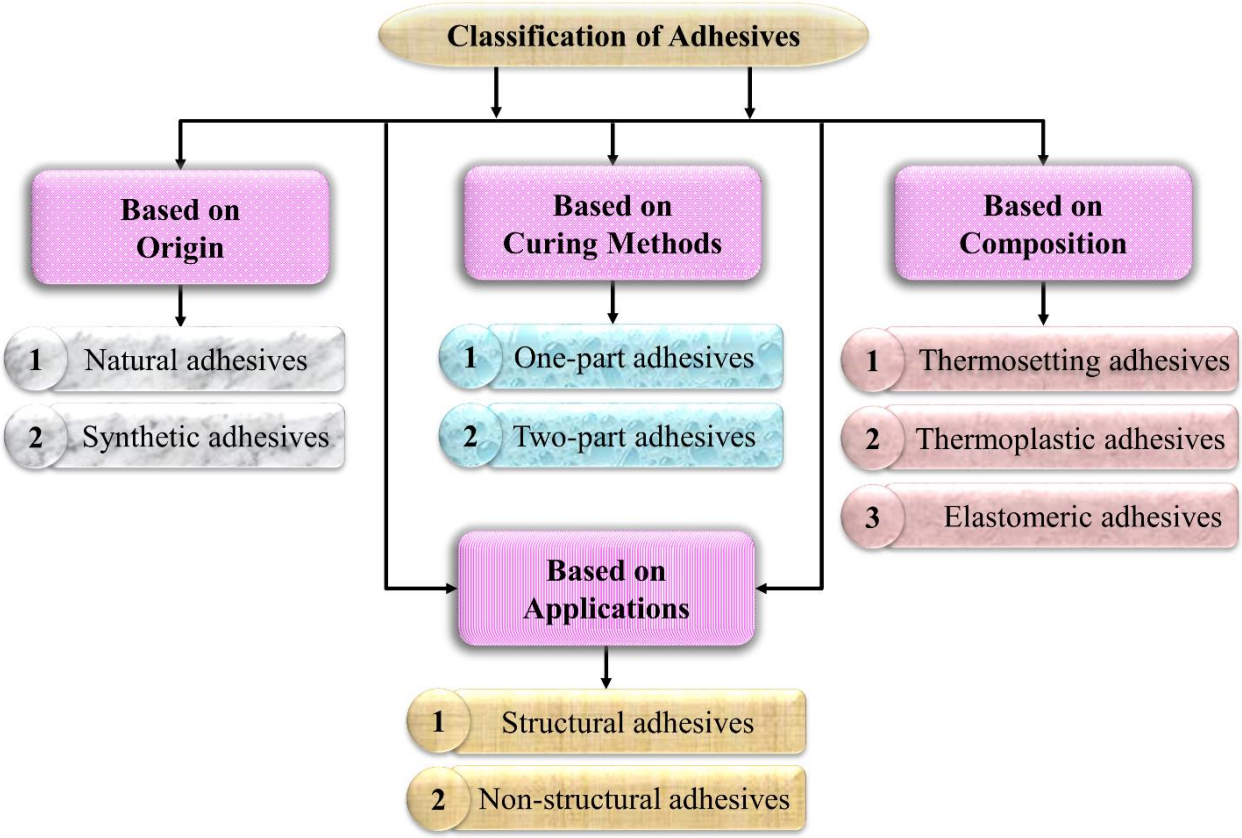

Figure 1.2. *Overview of adhesive classification by origin, curing process, chemical composition, and application.*

1.4 Factors influencing the performance of the adhesive

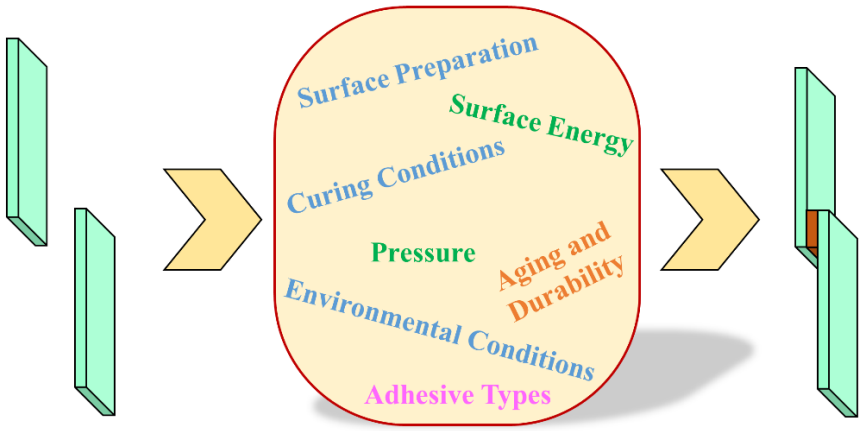

Figure 1.3. *Overview of the main factors affecting the strength of adhesive joints.*

Several factors can impact the strength of an adhesive bond (**Figure 1.3**). Some of the common factors include the follows,

(a) Adhesive types

The chemical composition and working mechanism are different for each adhesive, so the type of adhesive significantly affects adhesion strengths.[1] For example, epoxy adhesives offer high strength and chemical resistance, making them suitable for structural applications. Acrylic adhesives cure quickly and provide good environmental resistance, while polyurethane adhesives are flexible and impact-resistant, ideal for dynamic loads. Furthermore, cyanoacrylates form bonds rapidly but can be brittle, suited for small, precise applications, whereas silicone adhesives provide excellent flexibility and temperature resistance, perfect for sealing and bonding in harsh environments.[3]

(b) Surface preparation

Surface preparation is a critical factor affecting adhesion strength, as it directly influences the capability of an adhesive to bond effectively with a substrate. However, proper surface preparation involves cleaning the surface to remove contaminants such as dust, oil, grease, and moisture, which can interfere with adhesive bonding.[8,9] Without adequate surface preparation, even the best adhesives may fail to achieve optimal bond strength and durability.

(c) Surface energy

Materials such as metals and glass, which possess high surface energy, typically form strong bonds because the adhesive can easily wet and adhere to the surface.[10] In contrast, low surface energy materials, like polyethylene and Teflon, present a challenge for adhesion due to their resistance to wetting, often requiring specialized adhesives or surface treatments to improve bonding. [11] Depending on the surface type and the required strength, the appropriate adhesive for different substrates can be selected. For example, epoxy, and polyurethane is excellent for strong bonds on metal, wood, and ceramics,[12,13] while cyanoacrylate (super glue) and silicon quickly bonds to non-porous materials like plastic and glass.[12,14]

(d) Curing conditions

Proper curing involves the right combination of time, temperature, and humidity to allow the adhesive to achieve its optimal properties. Insufficient curing can lead to weak bonds, as the adhesive may not fully cross-link or reach its intended strength. Conversely, excessive heat or

incorrect curing times can degrade the adhesive or cause thermal stresses that weaken the bond. Therefore, controlling and optimizing curing conditions is essential to ensure strong, durable adhesive bonds in various applications.[15,16]

(e) Environmental conditions

Environmental conditions are crucial in determining adhesion strength, as factors such as temperature, UV radiation, corrosion, humidity, and chemical exposure can significantly influence the performance of an adhesive bond.[16] Extreme temperatures can cause adhesives to soften, harden, or become brittle, leading to bond failure. High humidity levels can interfere with the curing process and introduce moisture into the bond line, weakening the adhesive.[15] Exposure to chemicals, such as solvents, acids, or bases, can change the adhesive material and compromise its integrity.[17] Therefore, understanding and mitigating the impact of environmental conditions are essential for ensuring durable and reliable adhesive bonds in various applications.

(f) Pressure

The magnitude of pressure applied during the bonding process significantly influences the strength of adhesion. Diverse levels of pressure are utilized based on the specific adhesive and the nature of the substrate being bonded. Furthermore, the application of appropriate pressure enhances the adhesive wetting and facilitates effective surface penetration.[18]

(g) Aging and Durability

Aging refers to the gradual changes an adhesive undergoes due to exposure to environmental factors such as UV light, temperature fluctuations, and moisture. These factors can lead to degradation, loss of adhesion, or changes in adhesive properties.[19] Durability assesses the ability of adhesives to maintain bond strength and resist wear, stress, and environmental challenges throughout their service life.[16] Proper selection of adhesive and consideration of aging effects are essential to ensure long-lasting, reliable performance and to prevent premature bond failure.

1.5 Test methods for assessing the adhesive performance

Adhesion is a complex process that requires specially designed tests due to the different substrates, types of adhesives, surface treatments, and adhesion enhancement techniques. Various test methods have been developed and established for evaluating adhesively bonded

joints in different industrial sectors and trades. These methods adhere to the standards established by prominent organizations such as the International Organization for Standardization (ISO), the European Committee for Standardization (CEN), and the American Society for Testing and Materials (ASTM).[1] Based on their intended application, the standard tests utilized for assessing adhesives encompass the peel test, tack test, and lap shear test. Peel testing measures the force needed to remove an adhesive from a substrate (ASTM D903). The main types include the 90° peel, 180° peel, and T-peel method. The 90° peel method measures the force needed to peel the adhesive at a 90-degree angle; the 180° peel test measures the force needed at a 180-degree angle; and the T-peel test measures the bond strength between two flexible materials by pulling them apart (ASTM D1876). However, peel tests are widely used in industries like packaging, footwear, electronics, and automotive to ensure the durability and reliability of adhesive bonds in products such as labels, tapes, and laminated materials. Tack testing evaluates how sticky an adhesive is when it first touches a surface (ASTM D 2979). It includes tests like the loop tack test, which assess the force needed to remove an adhesive loop from a surface (ASTM D6195), and the probe tack test, which evaluates the force needed to detach a probe from the adhesive (ASTM D2979). These tests are essential for assessing the immediate bonding performance of adhesives and they are often used in industries like packaging, medical devices, and consumer goods to evaluate the stickiness of labels, bandages, and tapes.

1.5.1 Lap shear strength

Lap shear strength serves as a metric for assessing the adhesive strength of a bonded joint, specifically gauging the adhesive's ability to bond two substrates together under a shear load, as outlined in ASTM D1002. This testing procedure involves the application of a load parallel to the bonded surfaces until adhesive failure occurs (**Figure 1.4a**). The determination of lap shear strength involves dividing the force at failure by the bonded area, with the resulting value commonly expressed in units of force per area, such as psi or MPa. Furthermore, this method is cost-effective and easy to execute, rendering it widely employed in the automotive, aerospace, packaging, electronics, and construction industries for assessing adhesive performance and durability.

1.5.1.1 Types of failure in adhesive joints:

Identifying, comprehending, and categorizing the types of failure that may arise in adhesive bonds during lap shear testing can yield valuable insights into the performance and applicability of an adhesive for specific industrial or commercial applications (**Figure 1.4b**).[13]

(a) Adhesive failure: It occurs when the adhesive separates cleanly from one of the substrates. This indicates that the bonding between the glue and the substrate is weaker than the internal strength of the adhesive or the substrate itself.[13,20]

(b) Cohesive failure: It occurs within the adhesive layer itself, meaning the adhesive breaks apart while still bonded to both substrates. This type of failure suggests that the bonding between the glue and the substrate is stronger than the internal strength of the glue.[13]

(c) Substrate failure: It occurs when the substrate material fails before the adhesive bond (for example glass). This indicates that the adhesive is stronger than the substrate, which can be desirable or problematic depending on the application.[20]

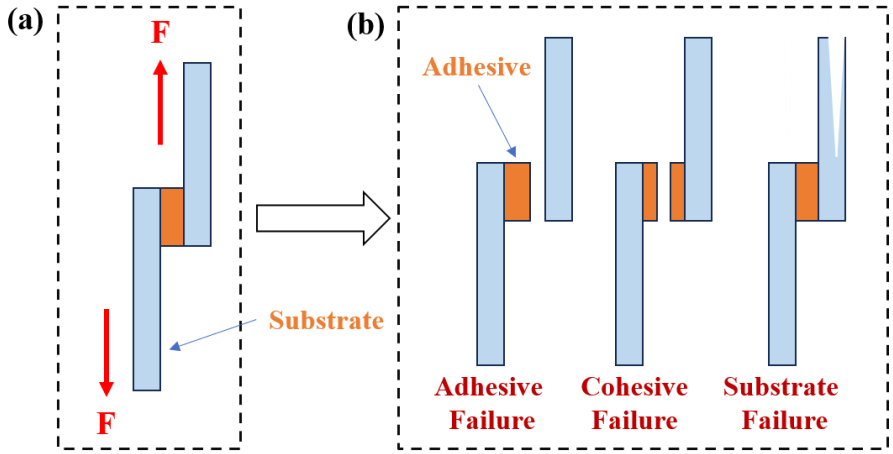

Figure 1.4. *(a) Schematic illustration of an adhesive joint specimen used in a single-lap shear test, and (b) modes of adhesive bond failure.*

1.6 Adhesive technologies

Adhesive technologies provide a variety of formulations and application methods designed to meet specific bonding needs. The adhesive technologies can be categorized into several types, including solvent-based, water-based, hot melt, reactive, and pressure-sensitive adhesives, as presented in **Figure 1.5**.[21] Further, the subsequent discussion was centered on HMA-based adhesives, as the current research delves into their advancements and potential applications.

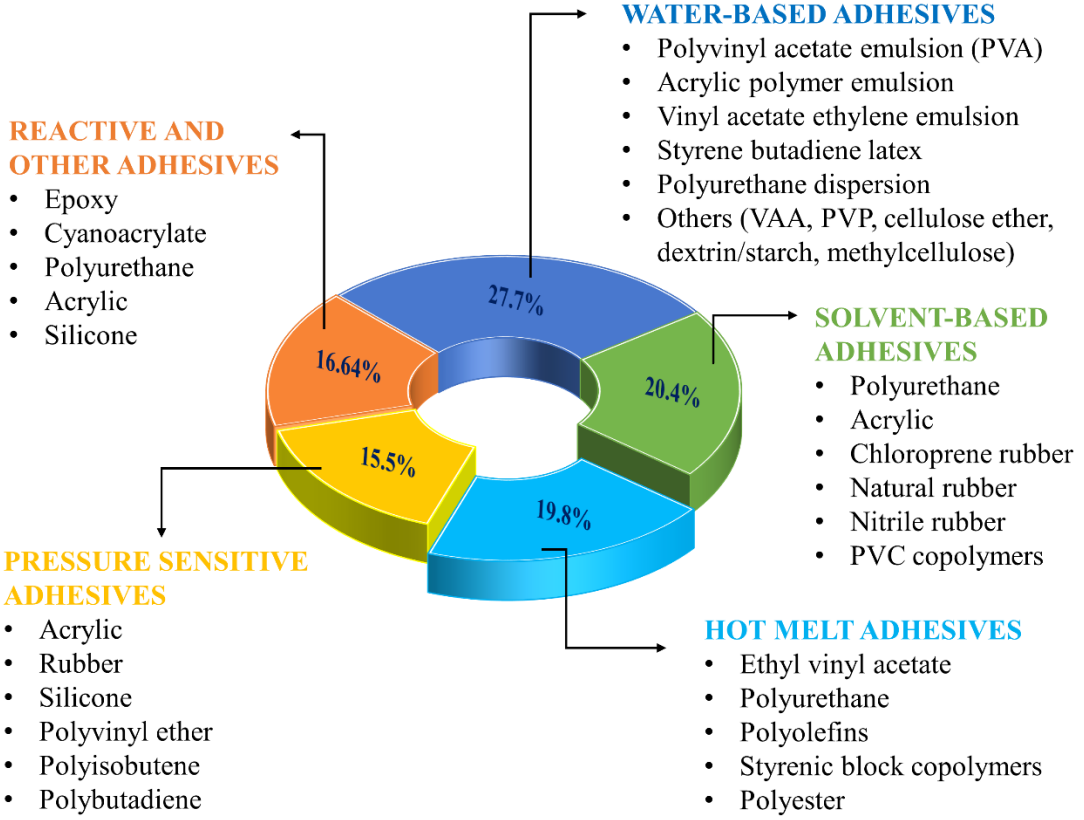

Figure 1.5. *Types of the adhesive technologies and the polymers used in their formulation, 2023 (Market share data added from multiple sources and may vary slightly).*[22–26]

Hot melt adhesives (HMAs), often referred to as hot glue, are thermoplastic adhesives applied in a molten form that solidify upon cooling to create a strong bond.[21] However, the value of global HMAs was assessed at USD 13.8 billion in 2023 and is projected to expand at a CAGR of 9 % between 2023 and 2030, reaching USD 29.1 billion by 2032. Indeed, the HMAs are expected to grow faster than water-based and other types of adhesives. This is because they have key benefits like quick setting times, making them easy to use, being environmentally friendly, and allowing re-adhesion.[27] Additionally, since they don't release harmful chemicals like volatile organic compounds, they are suitable for various sectors, including consumer goods, packaging, bookbinding, footwear and leather, construction, woodworking, automotive, electronics, and healthcare (**Figure 1.6**).[2,21,27] In 2020, the packaging sector accounted for more than 30 % of total revenue. The increasing need for packaging and nonwoven products significantly contributes to market growth, as HMAs do not require drying or curing like solvent and water-based adhesives.[28] Key companies in the global HMA market include Henkel, 3M, Sika , H.B. Fuller, Arkema, Dow, Jowat, Ashland, 3M, Beardow Adams, and Avery Dennison.[29a]

Hot melt adhesives are available in a variety of types, each offering distinct advantages and tailored for specific applications. These types include ethylene vinyl acetate (EVA), polyurethane, polyamide, polyolefin, styrenic block copolymer (SBC), and polyester.[28] Notably, EVA constitutes the majority of the volume.[29a] However, it gradually releases acetic acid over time, which can lead to corrosion of the applied surface. Additionally, the raw materials used in its production are derived from petroleum sources.[29b]

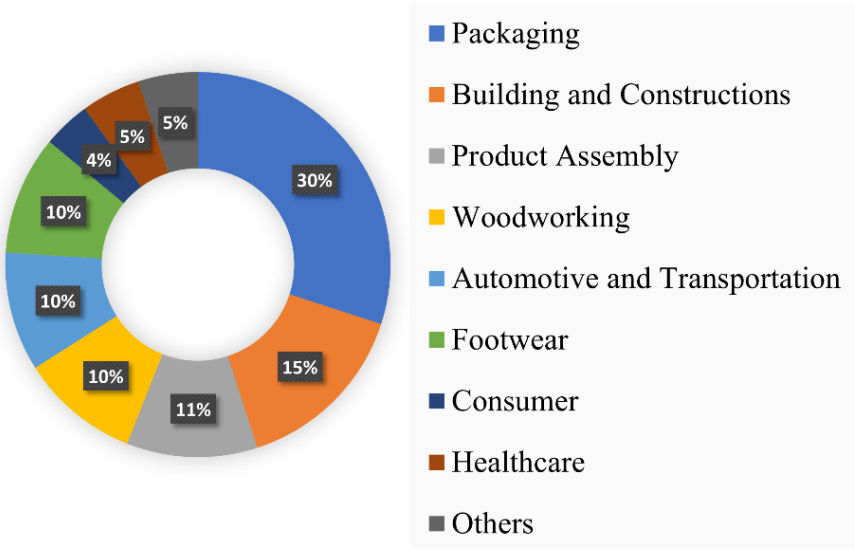

Figure 1.6. *The key sectors of global hot melt adhesives and their approximate market share.*[30]

Despite the advantages of HMAs, they also have some disadvantages. One major drawback is their limited heat resistance, as they can soften or lose bond strength at elevated temperatures, making them unsuitable for high-temperature applications. Additionally, compared to other adhesives like epoxy or cyanoacrylate, HMAs often provide weaker bonding strength, which may not meet the requirements for certain applications. They also tend to have poor chemical resistance, limiting their use in environments exposed to harsh chemicals. Another concern is the environmental impact, as many HMAs are derived from fossil fuels, contributing to resource depletion and environmental issues. Furthermore, the rapid setting time of HMAs can be challenging in high-speed production environments, requiring quick application. Despite these challenges, ongoing research aims to improve the performance and sustainability of hot melt adhesives.

1.6.1 Polyurethane hot melt adhesives (PU-HMAs)

Polyurethanes (PUs) were first developed by Dr. Otto Bayer and his team in 1937.[34] They are versatile polymers with a wide range of applications, including packaging, construction,

automotive, foams, elastomers, adhesives, coatings, and sealants. Among these, adhesives are one of the primary areas of application.[33] However, polyurethane hot melt adhesives (PU-HMAs) are known for their excellent bonding properties and capability to create strong bonds with various surfaces, including fabrics, metals, plastics, and wood. The PU-HMAs market was assessed at USD 1,311 million in 2021 and is projected to grow to USD 2,537 million by 2030, with a CAGR of 7.61 % over the projected period from 2023 to 2030.[31] Their low cost, exceptional flexibility, along with strong resistance to extreme temperatures, water vapor, chemicals, and solvents, has made them more popular in the market compared to other hot melt adhesives.[32,33] The synthesis process of PUs generally involves two main components: a polyol, often a polyester or polyether, and the isocyanate, which can be aromatic or aliphatic. The reaction between these two components leads to the formation of urethane linkages (**Scheme 1.1**), which are responsible for the strength and elasticity of the material.[33]

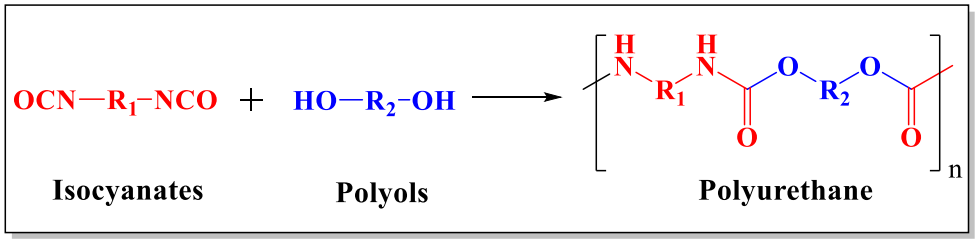

Scheme 1.1. *Conventional method for producing isocyanate-based polyurethanes.*

Despite its many advantages, PU synthesis and usage come with certain health and environmental concerns.[35] The primary issue is related to the use of isocyanates, which are hazardous chemicals. Exposure to isocyanates can cause respiratory problems, and skin irritation, and, in severe cases, can be life-threatening.[36] The Bhopal disaster of 1984, where a leak of methyl isocyanate resulted in thousands of deaths, highlighted the risks associated with these chemicals.[37] Moreover, the production of isocyanates often involves the use of phosgene, a toxic gas with a history of use as a chemical weapon during World War I. This raises significant concerns about the safety of the production process.

1.7 Isocyanate-free polyurethanes

To overcome the limitations discussed earlier, researchers have explored alternative methods to create polymers with properties similar to traditional PUs without using isocyanates as starting materials. This focus led to the development of non-isocyanate polyurethane (NIPUs).[33] Currently, various synthetic pathways exist to produce these isocyanate-free PU materials (**Figure 1.7**).

1.7.1 Synthetic pathways for producing NIPUs

The aminolysis of cyclic carbonates is one of the most discussed methods, gaining significant attention for its advantages in producing PUs. Other promising alternatives include the polymerization of aziridine with carbon dioxide, transurethanization, and ROP of cyclic carbamates.[38,39]

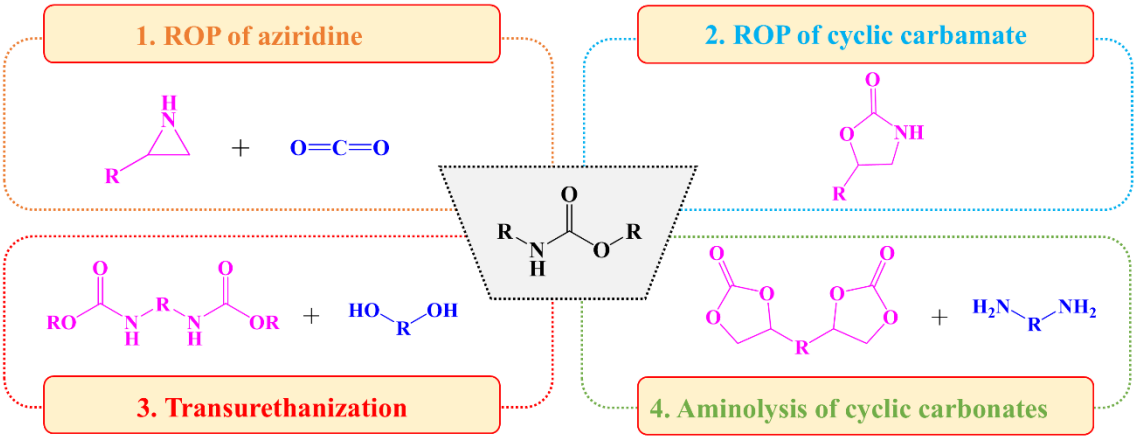

Figure 1.7. *Principal synthesis routes for non-isocyanate polyurethanes.*

1.7.1.1 NIPUs from aziridine and CO_2 copolymerization

In 1969, Inoue et al. were the first to synthesize polycarbonate from carbon dioxide and epoxide.[40] This pioneering work inspired several research groups in the 1970s to explore the synthesis of NIPUs from carbon dioxide and aziridine [**Figure 1.7 (1)**].[41,42] However, recent years have seen limited use of aziridine copolymerization in developing NIPUs due to their several drawbacks. The process still requires improvements in the yield of urethane linkages, and the presence of amine residues can negatively impact material properties. The most significant limitation is the toxicity of aziridines, which are harmful substances, greatly restricting their use.[38]

1.7.1.2 Ring-opening-polymerization of cyclic carbamate

The ROP of cyclic carbamates presents notable benefits over other common methods for synthesizing NIPUs [**Figure 1.7 (2)**].[38] It effectively addresses the low reactivity issues associated with aminolysis reactions and promotes atom economy and waste reduction. However, the ring-opening polymerization of cyclic carbamate precursors has certain

limitations that need to be addressed. The process involves multiple synthesis steps to achieve the carbamate and final polymer, which is not cost effective and can reduce overall yield. Additionally, in many cases, carbamates are developed using amines and hazardous phosgene or its derivatives, which conflicts with the principles of sustainable PU production.[43]

1.7.1.3 Transurethanization

A third method is transurethanization, in which alcohol condenses with a carbamate to make urethanes [**Figure 1.7 (3)]**. [43,44] Carbamates can be synthesized through various methods. Henri Cramail's group reviewed the transurethanization reaction in detail, focusing on various types of alkylated carbamate structures, all developed using phosgene-free processes.[38] Nonetheless, the transurethanization method has several benefits, including the scalability of producing dicarbamates from DMC and diamines. Furthermore, various renewable polyols, commercially available for isocyanate-based PUs, can also be used in NIPUs through this approach. The NIPUs produced through transurethanization have similar properties to those made with isocyanates, allowing them to replace existing PUs.[38] However, there are challenges. Transurethanization is a polycondensation process, meaning the alcohol byproduct must be removed, which can complicate industrial-scale production. Also, the reaction parameters are harsh, requiring high temperatures (100-200 °C) and a catalyst.[38]

1.7.1.4 Aminolysis of carbonates

The most commonly used method for synthesizing isocyanate-free PUs involves the reaction between cyclic dicarbonates and diamines [**Figure 1.7 (4)]**. This method is gaining attention in the industry due to stricter regulations on the use of toxic compounds.[38] Among the bis-cyclic carbonates, 5-membered bis-cyclic carbonate monomers (5CC) have emerged as the most extensively studied and utilized for NIPU synthesis.[45] This preference is largely due to their easy synthesis from epoxides and CO_2. Furthermore, CO_2 serves as a sustainable, bio-renewable, environmentally friendly, and readily available C1 feedstock.[46] The use of non-toxic precursors in PHU synthesis positions them as promising candidates for traditional PUs. Also, the aminolysis reaction is known for its high atom efficacy. The reaction between carbonates and amines results in the creation of PHUs featuring hydroxyl groups on its backbone. Studies indicate that when substituted carbonates are used as precursors, the reaction tends to favor the production of PHUs containing secondary -OH groups.[47] This preference arises because electron-withdrawing substituents increase the acidity of the negatively charged oxygen, thereby stabilizing the transition phase. As a result, the reaction selectively promotes

the generation of PHUs containing secondary -OH groups.[48] These hydroxyl groups offer several advantages over conventional PUs; they enable post-functionalization and facilitate the formation of multiple hydrogen bond interactions.[33] These interactions enhance mechanical strength and improve chemical resistance compared to polyurethanes. The increased thermal stability and chemical resistance could be due to the absence of unstable biuret and allophanate units.[38] Further, the carbonate and amine precursors are non-moisture sensitive, eliminating the need for special storage precautions and preventing the generation of byproducts like isocyanurates during storage.[38] In addition, PHUs demonstrate strong adhesion properties facilitated by their rich network of hydrogen bonds.[49,50] This enables them to adhere effectively to various surfaces, including metals (aluminum, stainless steel, copper, etc.), glass, wood, and polymers (PTFE, HDPE, etc.). The mechanism of the carbonate/amine reaction is depicted in **Figure 1.8**.

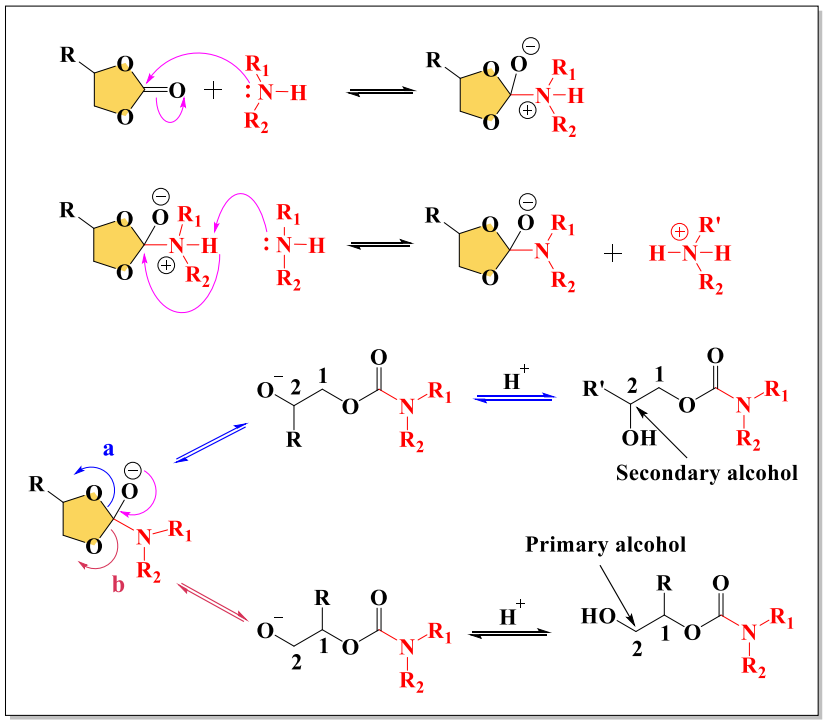

Figure 1.8. *Mechanism of the aminolysis reaction between cyclic carbonate and diamine.*

1.7.1.4.1 Synthesis of five-membered cyclic dicarbonates

Five-membered cyclic carbonates were traditionally made by reacting diols with phosgene or its derivatives, which produced high yields because phosgene is very reactive.[51] However, since phosgene is toxic, several alternative methods have been developed. Some of the common methods are shown in **Figure 1.9**. The most common industrial method involves the incorporation of carbon dioxide into epoxides under extreme temperature and pressure [**Figure**

1.9 (7)]. This method is advantageous in green and sustainable chemistry because it utilizes carbon dioxide, a renewable, inexpensive, non-toxic, and readily available reactant. CO_2,[46,52] generated in large quantities from both natural processes (such as decomposition, ocean release, and respiration) and human activities (like industrial production, deforestation, and fossil fuel combustion), is often considered waste and contributes to global warming and climate change. By incorporating this waste CO_2 into the production of cyclic carbonates, researchers have turned a harmful by-product into a valuable resource. The mechanism for the synthesis of five membered cyclic carbonates is presented in **Figure 1.10**.[53,54] First, the oxirane ring is activated by a catalyst, leading to ring opening; next, carbon dioxide is inserted, forming a carbonate intermediate; finally, the intermediate undergoes intramolecular ring-closing to yield the desired cyclic carbonate, with the catalyst being regenerated. Various catalytic systems have been developed for this process, primarily focusing on homogeneous, metal-free organo-catalysts, including alkali metal salts, organic or ammonium salts, organic bases, and different types of ionic liquids (such as phosphonium, imidazolium, pyridinium, and pyrrolidinium ILs).[55,56]

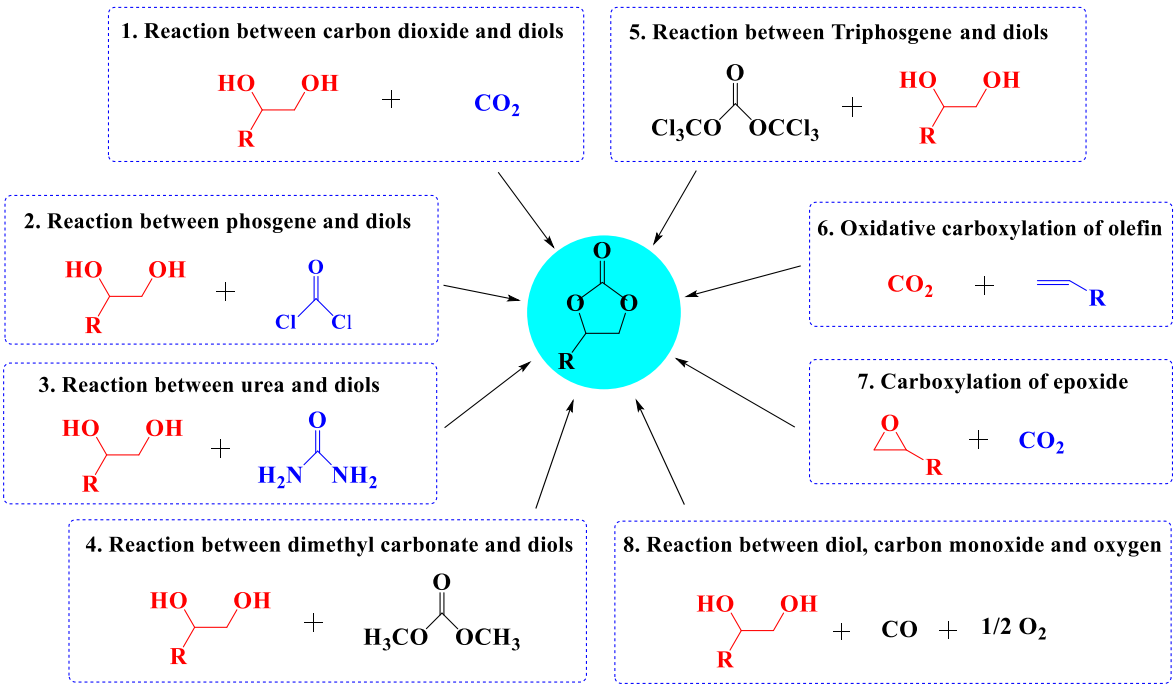

Figure 1.9. *Principal pathways for 5-membered cyclic carbonate synthesis.*

Among these, ammonium salts are the most commonly used catalysts for CO_2/epoxide coupling, as they are efficient at high temperatures, providing high yields with low catalyst loading.[57]

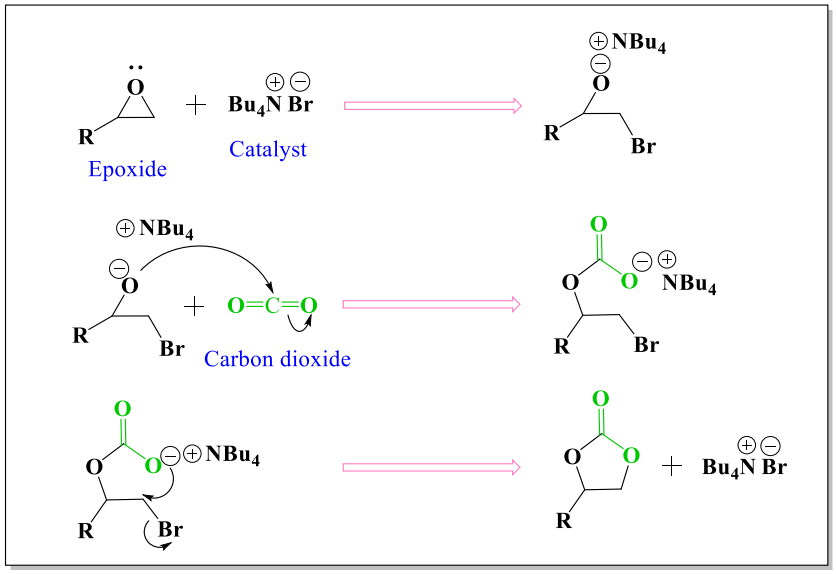

Figure 1.10. *Mechanism for producing five-membered cyclic carbonates from carbon dioxide and epoxide.*

1.7.1.4.2 Synthesis of larger ring cyclic carbonates

The synthesis of 6CCs or bigger size rings can be accomplished in addition to the typical 5CCs. **Figure 1.11 (a, b)** shows the reaction of oxetane with CO_2 yields 6CCs. However, the primary disadvantage of this approach is that oxetanes, which are four-membered cyclic ether rings exhibit greater stability compared to epoxides, making them less reactive towards CO_2, which leads to lower yields.[58]

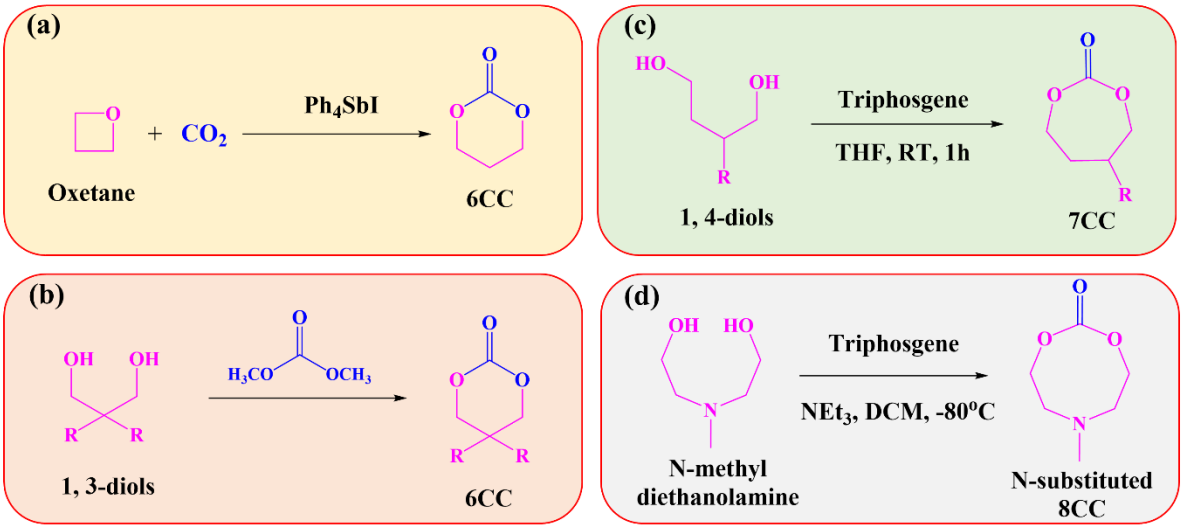

Figure 1.11. *The synthesis of larger ring cyclic carbonates (a) 6CCs from oxetane and CO_2, (b) 6CCs from 1, 3 diols and DMC (c) 7CCs from 1, 4 diols and triphosgene, and (d) 8CCs from 1, 5 diols and triphosgene.*

Besides oxetane, 1,3-diols can also be employed to produce 6CCs.[59] H. Tomita et al. synthesized seven-membered cyclic carbonates (7CCs) from 1, 4-diol and triphosgene [**Figure 1.11 (c)**].[60] They further reported that 6- and 7-membered rings exhibited greater reactivity compared to traditional 5CCs. Furthermore, the eight-membered cyclic carbonates (8CCs) were synthesized by reacting N-methyl-diethanolamine with triphosgene [**Figure 1.11 (d)**]. They demonstrated that N-substituted 8CCs were much more reactive than smaller 5CCs and 6CCs, based on the molecular weight of the synthesized polymers.[61] Although these studies show that larger ring cyclic carbonates (6CCs, 7CCs, and 8CCs) are more reactive than the standard 5CCs, they are less frequently used in the synthesis of non-isocyanate polyurethane due to their more challenging preparation, often requiring multiple steps and lower yields.[38]

1.7.2 Limitations in PHU production

Extensive research has been conducted on the parameters affecting PHU chemistry, highlighting their potential as a superior alternative to conventional PUs.[38] However, their industrial development faces significant hurdles, including issues with reaction kinetics, conversion rates, and molar mass due to limitations that occurred during polymerization. These significant factors, like side reactions and hydrogen bonds, that restrict the potential applicability of PHUs have been reviewed here.[33,38]

1.7.2.1 Side reactions

Side reactions present major challenges in PHU synthesis. Factors such as catalyst type and concentration, polymerization conditions (including time and temperature), and reaction stoichiometry can lead to various secondary reactions, as illustrated in **Figure 1.12**.[33] These side reactions include amine carbonation,[62,63] trans-urethanation,[64] urea formation,[65] oxazolidinone formation,[66,67] amidification,[68] and in-situ CO_2 generation.[66] These issues contribute to low monomer conversion rates and result in lower molar masses of PHUs.

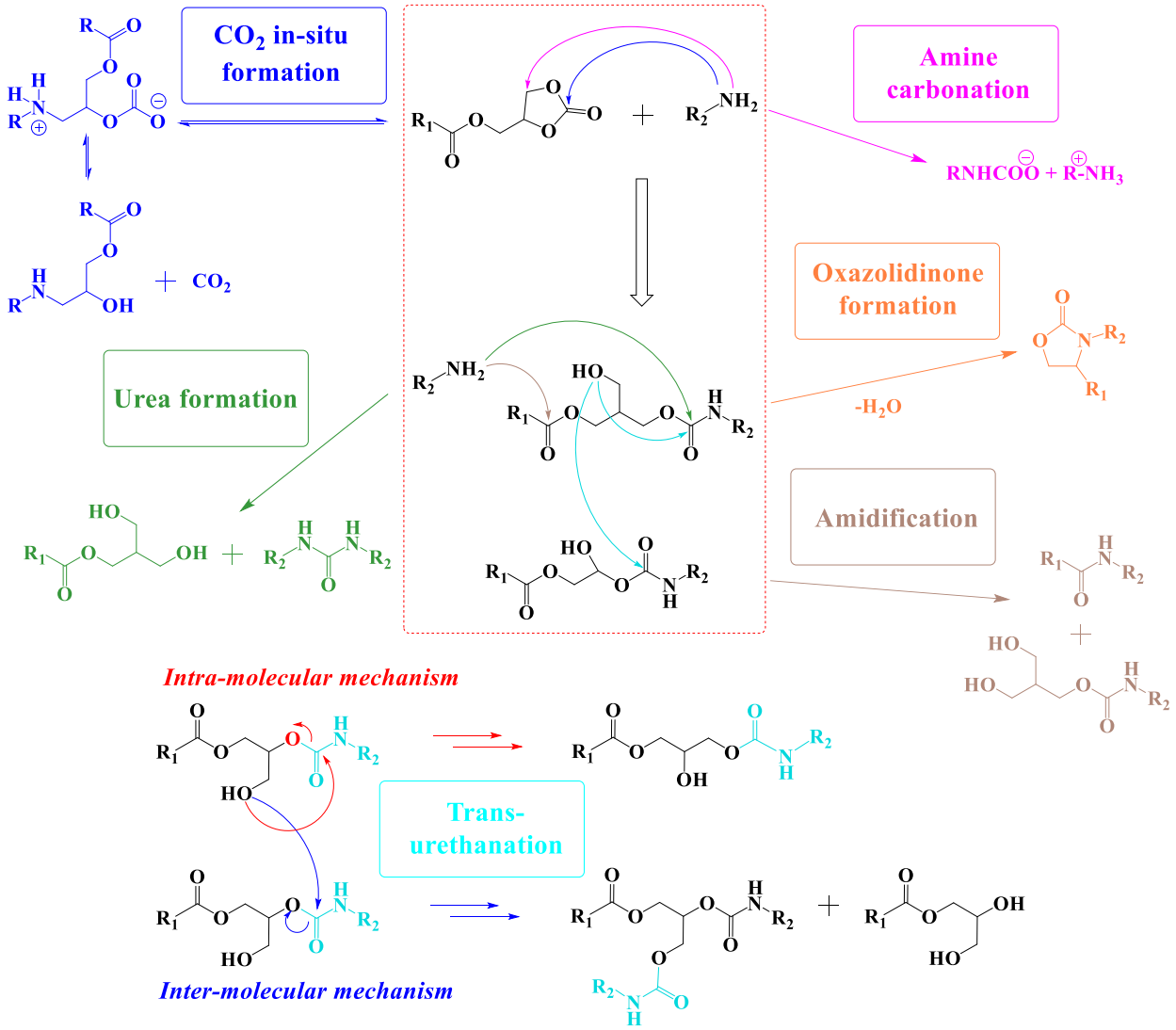

Figure 1.12. *Potential secondary reactions occur during the polyaddition reaction between 5CC and amine.*

1.7.2.2 Hydrogen bonds

The dangling of hydroxyl groups on the PHU polymer backbone leads to a higher number of hydrogen bond interactions, both inter- and intramolecular, compared to conventional PUs (**Figure 1.13**).[38] These hydrogen bonds contribute significantly to the enhanced mechanical and thermal properties of PHUs.[36] However, they are also responsible for posing disadvantages. During polymerization, these intra- and intermolecular hydrogen bonds restrict the mobility of polymer chains, thereby hindering the attainment of high monomer conversion and high molar masses.[33]

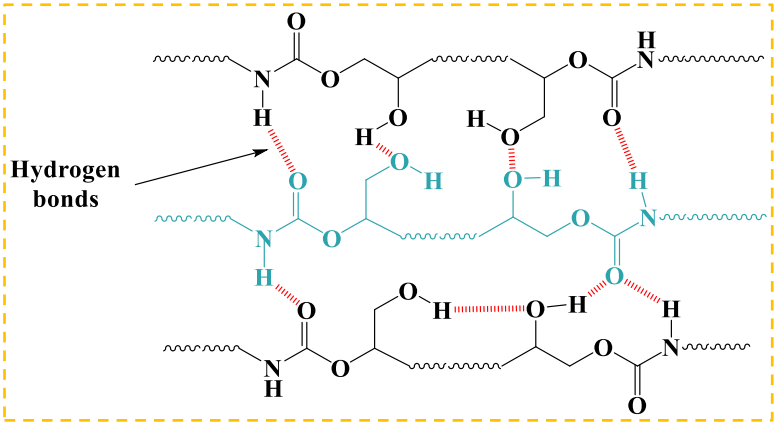

Figure 1.13. *Inter and intra-molecular hydrogen bonds are present in the PHU chains.*

1.8 Literature survey on PHU-based adhesives

The hydroxyl groups in PHUs enhances in PHUs enhances adhesion with various substrates through multiple hydrogen bonds. As a result, PHU-based adhesives are regarded as an emerging technology in the adhesive sector, offering safer and more sustainable methods compared to conventional PU-based HMAs.[33] **Table 1.1**, and **Table 1.2** respectively provide overviews of the bio-derived and fossil-derived PHU adhesives described in various literature sources, respectively.[13] These PHU adhesives have been discussed here based on two main categories: thermoset and thermoplastic adhesives. Thermoset adhesives undergo a chemical reaction during the curing process that forms a cross-linked, three-dimensional network. This reaction is often initiated by heat, light, or curing additives. Once cured, the adhesive becomes rigid and cannot be melted or reshaped. This irreversible bonding process results in superior mechanical properties, making them ideal for structural applications where high strength and stiffness are essential to withstand loads.[69] On the other hand, thermoplastic adhesives, including hot melt adhesives, do not undergo a chemical change when they solidify. Instead, they melt upon heating and solidify upon cooling. This process is reversible, allowing thermoplastic adhesives to be reheated, melted, and reshaped multiple times. They are particularly valuable in applications requiring quick bonding and the potential for future disassembly or repair.[69]

1.8.1 Bio-derived PHU-adhesives

As discussed previously, PHUs synthesized from cyclic carbonates and diamines offer an eco-friendly alternative to traditional PUs. The current challenge is to replace fossil-derived resources with renewable ones to produce new, sustainable PUs because the chemical industry traditionally relies on crude oil and natural gas for their starting materials.[70] This dependence

on fossil resources is threatened by potential shortages and price volatility. Additionally, global warming from CO_2 emissions and growing environmental concerns are driving the development of biobased PHUs.[71,72]

Table 1.1. *A list of bio-derived cyclic carbonates utilized to prepare the PHU-based adhesives.*

Sr. No.	Cyclic carbonates	Curing conditions	Lap shear strength (MPa) and Substrates	Ref.
(a) Thermoset adhesives				
1	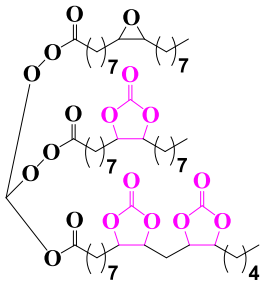	RT, 7 days	7 (Al) 10 (carbon steel)	74
2	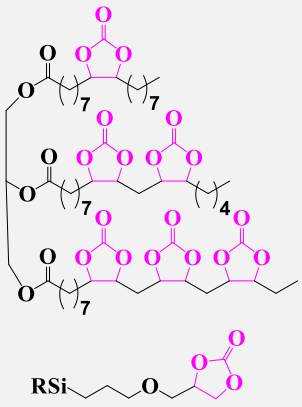 R: SiO_2/ZnO nanofillers	70 °C, 12 h and 100 °C, 4 h	11.3 (Al) 10.1 (SS)	75
(b) Thermoplastic adhesives (hot melt)				
3	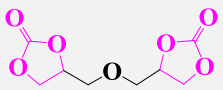	130 °C, 1.18 MPa, 30 min	0.67 (Birchwood)	77
4	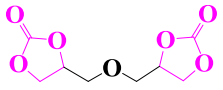	130 °C, 1.18 MPa, 30 min	3.19 (Birchwood)	78

Nevertheless, the renewable PHUs found in the literature are primarily synthesized from various biobased materials, including lignocellulose, vegetable oils, CNSL, glycerol, tannins, and terpenes.[53,73] However, reports on thermoset PHUs for adhesive applications have largely focused on those derived from vegetable oil and glycerol. There are only a couple of studies

on thermoset biobased PHU adhesives (**Table 1.1**). One such study by Figovsky et al. involved the creation of PHU-epoxy adhesive formulations by combining carbonated-epoxidized soybean oil (CESBO) with an epoxy resin (DER 331) and Vestamin TMD as a hardener, curing the mixture at room temperature over 7 days. The formulations exhibited the highest lap shear strength when 10 mol% of CESBO was used, achieving approximately 10 MPa for carbon steel and 7 MPa for aluminum.[74] Another study (Panchireddy et al.) addressed the issue of wet delamination in PHU adhesives by incorporating water-repellent vegetable oil-derived cyclic carbonates into their formulations. This method was designed to reduce water absorption, as some studies suggest that hydroxyl groups in PHUs may contribute to easier wet delamination.[75] To further enhance the formulations, they added SiO_2 or ZnO nanofillers, which effectively reduced water uptake and improved both the adhesion as well as thermo-mechanical properties. These soybean oil-derived PHUs attained adhesion values reaching as high as 12 MPa for aluminum and steel substrates.[75] This enhancement was due to the higher cross-linking density from the aminolysis of cyclic carbonates on the nanoparticle surfaces. A similar group also used PDMS as a hydrophobic segment in place of soybean oil.[76] A significant improvement was achieved with the incorporation of 5 wt% ZnO nanomaterial modified with carbonate functionality, leading to a adhesion strength reaching 16.3 MPa.

On the other hand, biobased thermoplastic PHU adhesives have also received limited attention, with only two studies reported in the literature. Both of these studies, conducted by Mariusz Tryznowski and his team, developed thermoplastic adhesives from glycerol-derived carbonates designed for wood joints. They initially prepared the hydrophobic amino-telechelic oligoamides via condensation of dimethyl succinate [77] or diethyl tartrate [78] with 1, 3-diamino propane, followed by polyaddition with diglycerol dicarbonate to get the amide backbone containing materials. Prior to joining the wood specimens, the polymers were melted at 130 °C, and these polymers demonstrated moderate adhesive strength of up to 3.19 MPa.

1.8.2 Fossil-derived PHU-adhesives

Petroleum-based thermoset PHU adhesives have been more extensively studied than their biobased counterparts which might be due to the straightforward synthesis of carbonate monomers from commercially available epoxy precursors (**Table 1.2**). This simpler process eliminates the need for multiple synthesis steps and improves reaction yield. However, limitations such as sustainability concerns, and longer curing times have restricted their broader application. The use of neat PHUs as adhesives was initially reported by Cornille et al.[49] They prepared the thermoset adhesive formulations by mixing the dicyclic and tricyclic carbonates

with aliphatic and cycloaliphatic diamines, which were then thermally cured to bond similar surfaces like glass, aluminum and beech wood. The adhesive performance was compared to that of two traditional polyurethanes made from isocyanates. The optimum PHU sample with a cycloaliphatic diamine reached lap-shear strengths exceeding 15 MPa, resulting in wood failure before the adhesive bond failed, whereas the control PUs showed adhesion strengths of only 3 to 6 MPa. Additionally, PU formulations made with diisocyanates and structurally similar diols exhibited lower adhesion strengths, highlighting the stronger hydrogen bond interactions in PHUs due to hydroxyl groups.

Moreover, one significant limitation noted in reports is the longer curing time required for PHU adhesives due to the low reactivity of cyclic carbonates. [74,79] To improve this, various cross-linking agents were used in PHU formulations. For example, alkoxysilane molecules (APTES) were one of the widely studied curing agents used in most reports of PHU adhesives because of their ability to crosslink and form a siloxane-linked network through condensation reactions.[80] They can also react with functional molecules on the surfaces of various substrates, including glass and metals, creating covalent silicon-oxygen and silicon-metal bonds, which significantly improve both adhesion and the curing process. Rossi de Aguiar et al.[81] reacted PDMS-derived cyclic dicarbonate (CC-PDMS) with APTES or blends of APTES and IPDA. When the formulations were cured at 60 °C, the blended PHUs showed optimal shear strengths of 1.3 MPa for aluminum-glass and 3 MPa for glass substrates, with the highest strength achieved using only APTES. However, raising the setting temperature up to 180 °C drastically reduced adhesive strength by more than 50 %. However, the group of Haritz Sardon et al. utilized different types of curing and adhesion promoters to improve the curing conditions as well as the adhesion of PHUs. Initially, they developed a two-step process to develop a thermoset PHU adhesive. By step-growth copolymerization of PPG- and resorcinol-derived cyclic carbonates blends with fatty acid based amine, they produced cyclic carbonate terminated PHU prepolymers, which were then functionalized with APTES.[80] The study highlighted the importance of temperature and catalysts (MSA, and DBU) in the curing kinetics. At ambient temperature, the curing reaction proceeded slowly, but it accelerated significantly at 100 °C, creating a cross-linked network in under an hour. Further, the addition of small amount of MSA catalyst (1 wt%) reduced the gelation time to just 9 minutes. The highest adhesion strength was achieved up to 3 MPa for stainless steel. The same team demonstrated PHU hybrid polymers that achieved adhesion strength up to 21 MPa by modifying the PHU composition and incorporating dopamine as an adhesion promoter and APTMS as a curing promoter.[82] Recently, they incorporated a trifunctional thiol additive

(TMPTMP) as a curing agent into PHU formulations prepared from an amino-ended PHU prepolymer (based on a composition of PPG- and Resorcinol carbonates treated with an excessive amount of 1, 12-diamine), along with a commercial epoxy resin. This formulation achieved a maximum adhesion strength of 12.8 ± 1.0 MPa.[83] Detrembleur et al.[50] synthesized biomimetic thermoset adhesives by incorporating dopamine as an adhesion promoter into a formulation of TMPTC and 1, 6-HMDA. With a low dopamine content (3.9 mol %), the adhesives achieved lap-shear strengths of 24 MPa for aluminum and 28 MPa for wood. They also showed adhesion strength of up to 4.76 MPa on HDPE and effectively bonded dissimilar substrates like aluminum to stainless steel or plastics, with strengths ranging from 6.7 to 25 MPa. These glues were comparable with commercial resins (Teromix and Araldite), given proper thermal curing. Lambeth et al. recently optimized the formulation of PHU-epoxy networks by examining the reactivity of oxirane and cyclic carbonate functionality. They found that amine-epoxide reaction was somewhat faster, leading to uniform PHU-epoxy networks with an initial preference for epoxide ring-opening. Using trifunctional epoxide (TMPT-GE), trifunctional carbonate (TMP-TC), and 4, 4′-methylene bis-(cyclohexylamine), they prepared thermoset adhesives and achieved a maximum adhesion of 27 MPa for a 50/50 TMPT-GE/TMP-TC composition. This was significantly higher than pure epoxy or PHU formulations.[84]

Table 1.2. *A list of fossil-derived cyclic carbonates utilized to prepare the PHU-based adhesives.*

Sr. No.	Cyclic carbonates	Curing conditions	Lap shear strength (MPa) and Substrates	Ref.
(a) Thermoset adhesives				
1	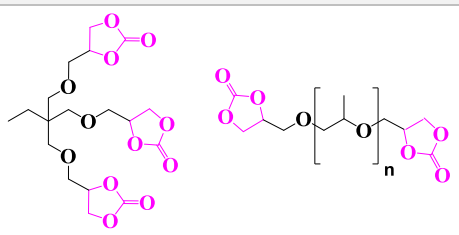	80 °C, 12 h, and 150 °C, 30 min	2.0 to 3.0 (Al), 15.0 ± 1.5 (wood)	49
2	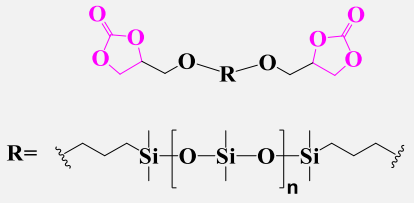	60 °C, 24 h	1.0 (Glass) 1.5 (SS) 0.9 (Titanium)	81

	Curing agent: 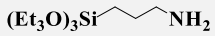			
3	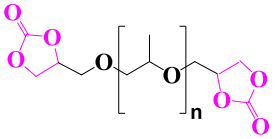 Curing agent: 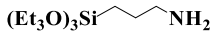	100 °C, 24 h	2.9 ± 0.6 (SS) 1.1	80
4	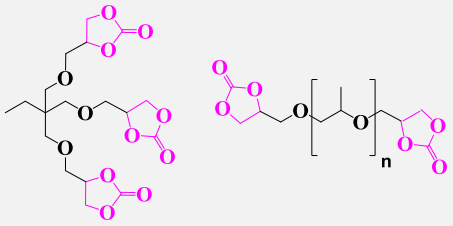 Adhesion promoter: 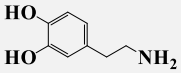 Curing agent: 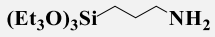	100 °C, 24 h	20.9 ± 0.9 (Al) 21.6 ± 0.7 (SS) 12.8 ± 2.4 (Oak wood) 2.8 ± 0.7 (Polyamide) 140.8 ± 0.2 (HDPE) 1.8 ± 0.2 (PMMA)	82
5	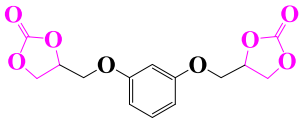 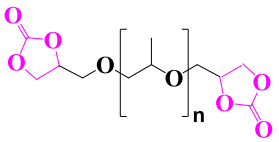 Curing agent: 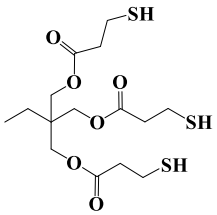	Mixing: 50 °C, 2 min, followed by RT at 1 min Bonding: RT, 24 h	7.6 ± 0.9 to 12.8 ± 1.0 (SS)	83
6	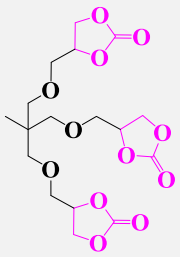	100 °C, 18 h	24.1 ± 1.7 (Al), 22.1 ± 0.9 (SS), 28 ± 1.7 (Beech), 17.9 ± 1.3 (PMMA),	50

	Adhesion promoter: 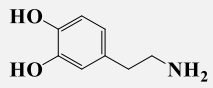		4.76 ± 2.5 (HDPE), 6.7 to 25.0 (dissimilar substrates)	
7	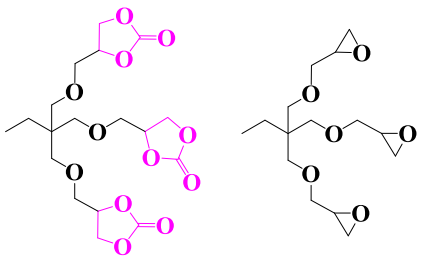	80 °C, 48 h	27 (Al)	84
8	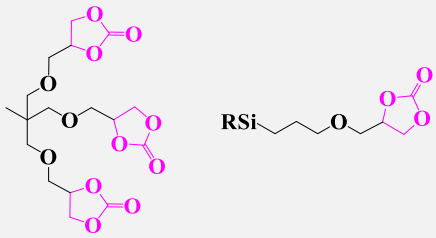 R: SiO_2/ZnO nanofillers	70 °C, 12 h and 100 °C, 3 h	16.3 ± 1.4 (Al)	76
(b) Thermoplastic adhesives (hot melt)				
10	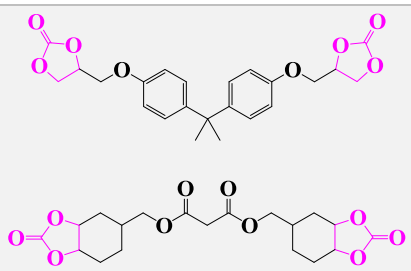	T not reported, 24 h	5.0 to 9.0 (Al) 1.5 to 2 (HDPE)	85
11	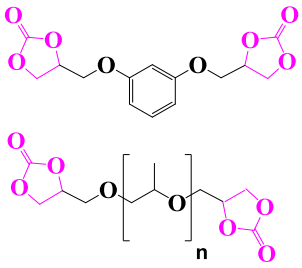	80-120 °C, 5-10 min	2.4 ± 0.8 to 7.0 ± 0.8 (SS)	86

Thermoplastic PHU adhesives offer moderate adhesion strength relative to thermoset adhesives, but their quick setting time and reversible properties make them more attractive. However, Anitha Nair et. al.[85] developed the PHU-HMAs using rigid, and flexible carbonates along with amino-terminated oligo- (propylene glycol). The specimens were prepared at polymer softening temperature (80-100 °C) and the researchers found strong adhesion values

of up to 5 to 9 MPa on Al-Al and 1.5 to 2 MPa on HDPE-HDPE. The researchers further examined the recyclability to assess the reusability of adhesives and discovered nearly the same adhesive strength after one-time recycling. Another group (Alvaro Gomez-Lopez et. al.) [86] recently prepared PHU-HMAs by varying the composition between two cyclic carbonate monomers based on resorcinol (RdiCC) and polypropylene glycol (PPGdiCC); they employed two different temperatures to bind stainless-steel joints, at 80 °C, the adhesion was measured to be between 1.9 ± 0.6 to 3 MPa, while at 100 °C, it increased upto 7 MPa in the case of 50/50-MXDA. The authors also studied the impact of diamine structures on the adhesion of HMAs, finding that the MXDA-based HMA (7 MPa) had higher shear strength than CBMA (5.8 MPa) and PXDA (3.5 MPa). Additionally, to enhance the thermo-mechanical behavior and service temperature of HMAs, they developed hybrid PHUs by incorporating 15 wt% of an epoxy crosslinker into two PHU compositions (50/50-MXDA and 50/50- PXDA). The addition of the epoxy resin reduced the lap shear strength of HMAs due to persistent cross-linking without impeding thermos-reversibility.

A review of the literature reveals that research on biobased PHU-HMAs is quite limited, underscoring the need for more extensive development of high-performance PHU-HMAs using eco-friendly methods, particularly those involving renewable resources. Biobased PHU-HMAs present several advantages over their petroleum-based counterparts, making them a more sustainable and environmentally friendly option.

1.9 Objective of the thesis

The detailed review of HMAs indicate the majority of polymers for this application are derived from non-renewable resources, and nearly half of the material ends up in landfills, and one-third escapes the collection system resulting in economic and energy losses. To reduce pollution and promote sustainability, governments and international organizations are implementing stricter regulations more frequently. Policies such as the European Union's REACH (Registration, Evaluation, Authorization, and Restriction of Chemicals) and similar regulations in other regions are driving the chemical industry to find greener alternatives.[87] Meeting these regulations often requires the reduction of harmful emissions and the adoption of safer, more sustainable production methods. Hence, there is substantial interest in the development of HMAs from sustainable feedstocks, aiming to diminish reliance on fossil resources and mitigate environmental impacts. This endeavor holds the potential to significantly decrease greenhouse gas emissions and energy consumption.

This thesis endeavors to investigate the potential use of CO_2, lignin, and sugar-derived precursors, namely vanillin, guaiacol, isosorbide, and furfural, in the synthesis of biobased PHU-HMAs.

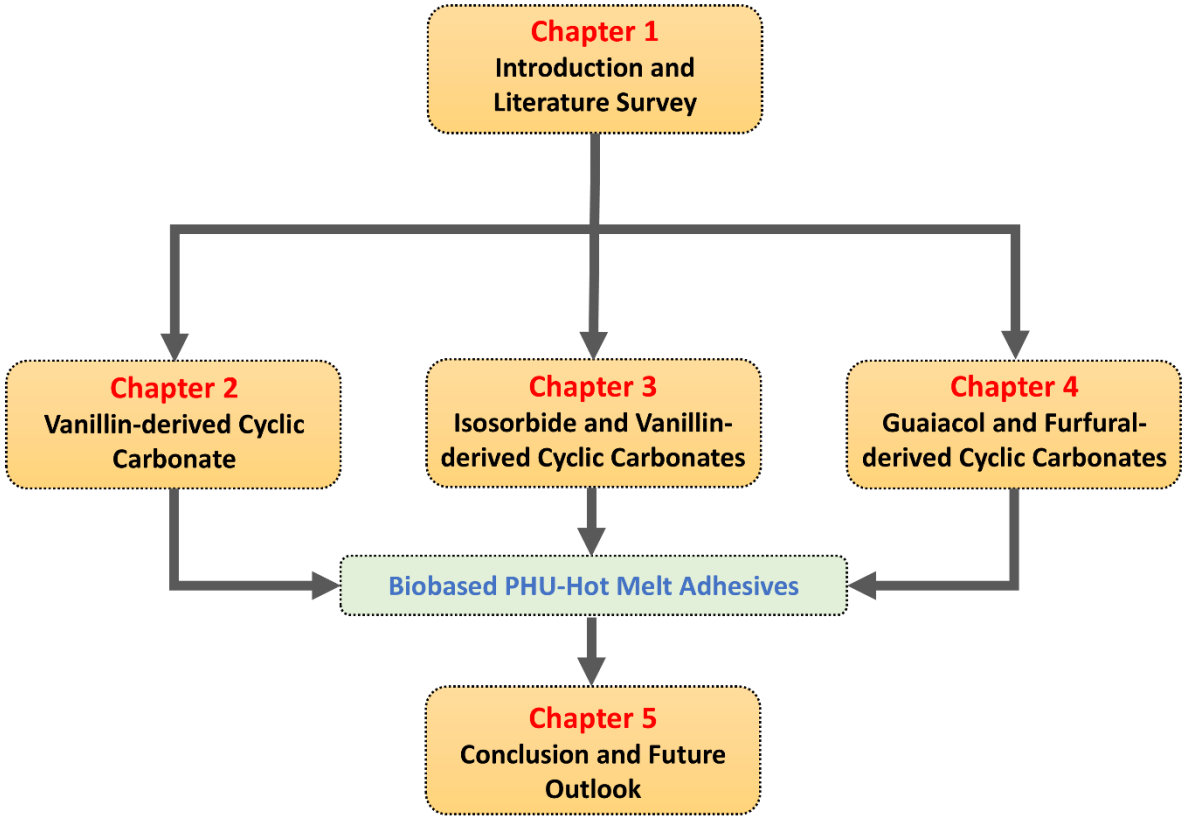

Figure 1.14. *Structure of the thesis chapters.*

The key objectives of this thesis are outlined as follows:

- ✓ Development and synthesis of difunctional five-membered cyclic carbonates using sustainable resources such as CO_2 and lignocellulose-derived precursors.
- ✓ Development of thermoplastic polyurethanes through a non-isocyanate route, by entails the polymerization of cyclic carbonates with diamines via step-growth polymerization.
- ✓ Enhancing the renewable carbon content and adhesive strength of PHU hot melt adhesives.
- ✓ Assessing the bonding properties of polymers through lap shear tests on metal surfaces, like aluminum and stainless steel.
- ✓ Investigating the relationship between structure and behaviour, as well as the thermo-mechanical properties of the synthesized polymers
- ✓ Study of the impact of combining rigid and flexible precursors on the thermal-mechanical and adhesive properties of PHUs.

- ✓ Investigation of the influence of Diels-Alder network on the adhesive properties of sustainable PHU.
- ✓ Diels-Alder cross-linking of PHUs containing pendant furyl groups with maleimide derivatives and their influence on adhesive properties.

The findings elucidated in this thesis have the potential to enhance our comprehension of the precursors and formulations necessary to achieve hot melt properties characterized by high adhesion and renewable carbon content. This acquired knowledge is poised to play a pivotal role in the identification of suitable industrial applications for PHU adhesives, thereby potentially streamlining the integration of more environmentally sustainable materials into the adhesive market.

1.10 References

(1) Edward, M. P.; Handbook of Adhesives and Sealants, **2007**.

(2) Heinrich, L. A. Future Opportunities for Bio-Based Adhesives-Advantages beyond Renewability. *Green Chem.* **2019**, *21* (8), 1866–1888.

(3) Mair, G. Joining Processes. *Mastering Manuf.* **1993**, 150–167.

(4) Marques, A. C.; Mocanu, A.; Tomić, N. Z.; Balos, S.; Stammen, E.; Lundevall, A.; Abrahami, S. T.; Günther, R.; de Kok, J. M. M.; de Freitas, S. T. Review on Adhesives and Surface Treatments for Structural Applications: Recent Developments on Sustainability and Implementation for Metal and Composite Substrates. *Materials (Basel).* **2020**, *13* (24), 1–43.

(5) Dinte, E.; Sylvester, B. Adhesives: Applications and Recent Advances. *Appl. Adhes. Bond. Sci. Technol.* **2018**.

(6) Wake, W. C. Theories of Adhesion and Uses of Adhesives: A Review. *Polymer (Guildf).* **1978**, *19* (3), 291–308.

(7) Gharde, S.; Sharma, G.; Kandasubramanian, B. Hot-Melt Adhesives: Fundamentals, Formulations, and Applications: A Critical Review. *Rev. Adhes. Adhes.* **2020**, *8* (1), 1–28.

(8) Borges, C. S. P.; Marques, E. A. S.; Carbas, R. J. C.; Ueffing, C.; Weißgraeber, P.; Silva, L. F. M. D. Review on the Effect of Moisture and Contamination on the Interfacial Properties of Adhesive Joints. *Proc. Inst. Mech. Eng. Part C J. Mech. Eng. Sci.* **2021**, *235* (3), 527–549.

(9) Musiari, F.; Moroni, F. Experimental Study of the Influence of the Surface Preparation

on the Fatigue Behavior of Polyamide Single Lap Joints. *Materials (Basel).* **2021**, *14* (4), 1–22.

(10) Müller, M.; Hrabě, P.; Chotěborský, R.; Herák, D. Evaluation of Factors Influencing Adhesive Bond Strength. *Res. Agric. Eng.* **2006**, *52* (1), 30–37.

(11) Liu, Y.; Shigemoto, Y.; Hanada, T.; Miyamae, T.; Kawasaki, K.; Horiuchi, S. Role of Chemical Functionality in the Adhesion of Aluminum and Isotactic Polypropylene. *ACS Appl. Mater. Interfaces* **2021**, *13* (9), 11497–11506.

(12) Bumbrah, G. S. Cyanoacrylate Fuming Method for Detection of Latent Fingermarks: A Review. *Egypt. J. Forensic Sci.* **2017**, *7* (1), 1-8.

(13) Gomez-Lopez, A.; Panchireddy, S.; Grignard, B.; Calvo, I.; Jerome, C.; Detrembleur, C.; Sardon, H. Poly(Hydroxyurethane) Adhesives and Coatings: State-of-the-Art and Future Directions. *ACS Sustain. Chem. Eng.* **2021**, *9* (29), 9541–9562.

(14) Silvestru, V. A.; Englhardt, O.; Schneider, J. Investigations on Linear Silicone Joints for Glass-Metal Elements with Composite Structural Behavior. *Challenging Glas. 6 Conf. Archit. Struct. Appl. Glas. CGC 2018 - Proc.* **2018**, No. May, 389–398.

(15) Viana, G.; Costa, M.; Banea, M. D.; Da Silva, L. F. M. A Review on the Temperature and Moisture Degradation of Adhesive Joints. *Proc. Inst. Mech. Eng. Part L J. Mater. Des. Appl.* **2017**, *231* (5), 488–501.

(16) Gualberto, H. R.; do Carmo Amorim, F.; Costa, H. R. M. A Review of the Relationship between Design Factors and Environmental Agents Regarding Adhesive Bonded Joints. *J. Brazilian Soc. Mech. Sci. Eng.* **2021**, *43* (8), 1–19.

(17) Cognard, J. Environmental Attack on Adhesive Joints Studied by Cleavage Fracture. *J. Adhes.* **1988**, *26* (2–3), 155–169.

(18) Kim, J. K.; Lee, D. G. Effects of Applied Pressure and Temperature during Curing Operation on the Strength of Tubular Single-Lap Adhesive Joints. *J. Adhes. Sci. Technol.* **2004**, *18* (1), 87–107.

(19) Ameli, A.; Papini, M.; Spelt, J. K. Hygrothermal Degradation of Two Rubber-Toughened Epoxy Adhesives: Application of Open-Faced Fracture Tests. *Int. J. Adhes. Adhes.* **2011**, *31* (1), 9–19.

(20) Pethrick, R. A. Design and Ageing of Adhesives for Structural Adhesive Bonding-A Review. *Proc. Inst. Mech. Eng. Part L J. Mater. Des. Appl.* **2015**, *229* (5), 349–379.

(21) Vineeth, S. K.; Gadhave, R. V. Sustainable Raw Materials in Hot Melt Adhesives: A Review. *Open J. Polym. Chem.* **2020**, *10* (August), 49–65.

(22) https://www.marketresearchfuture.com/reports/water-base DAdhesive-market-6987 (accessed on 08 August 2024).

(23) https://www.thebusinessresearchcompany.com/report/solventbaseDAdhesives-global-market-report (accessed on 08 August 2024).

(24) https://www.gminsights.com/industry-analysis/hot-melt-adhesives-market# (accessed on 08 August 2024).

(25) https://www.researchnester.com/reports/pressure-sensitive-adhesives-market/4337 (accessed on 08 August 2024).

(26) https://www.thebusinessresearchcompany.com/report/reactive-and-other-adhesives-global-market-report (accessed on 08 August 2024).

(27) Li, W.; Bouzidi, L.; Narine, S. S. Current Research and Development Status and Prospect of Hot-Melt Adhesives: A Review. *Ind. Eng. Chem. Res.* **2008**, *47* (20), 7524–7532.

(28) https://www.fortunebusinessinsights.com/industry-reports/hot-melt-adhesives-market-101724 (accessed on 10 August 2024).

(29) (a) https://www.grandviewresearch.com/industry-analysis/hot-melt-adhesives-market (accessed on 10 August 2024).

(b) María, A. M.; Rodrigo P.; José Miguel M. Viscoelastic and adhesion properties of hot-melts made with blends of ethylene-co-n-butyl acrylate (EBA) and ethylene-co-vinyl acetate (EVA) copolymers. *Intern. J. of Adhesion and Adhesives.* **2019**, *88*, 34-42.

(30) https://www.chemanager-online.com/en/news/adhesives-and-sealants-are-gaining-demand (accessed on 10 August 2024).

(31) Fristrup, C. J.; Jankova, K.; Hvilsted, S. Hydrophilization of Poly(Ether Ether Ketone) Films by Surface-Initiated Atom Transfer Radical Polymerization. *Polym. Chem.* **2010**, *1* (10), 1696–1701.

(32) Tang, Q.; He, J.; Yang, R.; Ai, Q. Study of the Synthesis and Bonding Properties of Reactive Hot-Melt Polyurethane Adhesive. *J. Appl. Polym. Sci.* **2013**, *128* (3), 2152–2161.

(33) Ecochard, Y.; Caillol, S. Hybrid Polyhydroxyurethanes: How to Overcome Limitations and Reach Cutting Edge Properties? *Eur. Polym. J.* **2020**, *137* (August), 109915.

(34) Engels, H. W.; Pirkl, H. G.; Albers, R.; Albach, R. W.; Krause, J.; Hoffmann, A.; Casselmann, H.; Dormish, J. Polyurethanes: Versatile Materials and Sustainable Problem Solvers for Today's Challenges. *Angew. Chemie - Int. Ed.* **2013**, *52* (36), 9422–9441.

(35) Allport, D. MDI and TDI – Safety, Health and the Environment. *Manag. Environ. Qual. An Int. J.* **2003**, *14* (4), 540–540.

(36) Delavarde, A.; Savin, G.; Derkenne, P.; Boursier, M.; Morales-Cerrada, R.; Nottelet, B.; Pinaud, J.; Caillol, S. Sustainable Polyurethanes: Toward New Cutting-Edge Opportunities. *Prog. Polym. Sci.* **2024**, *151*.

(37) Jasanoff, S. The Bhopal Disaster and the Right to Know. *Soc. Sci. Med.* **1988**, *27* (10), 1113–1123.

(38) Maisonneuve, L.; Lamarzelle, O.; Rix, E.; Grau, E.; Cramail, H. Isocyanate-Free Routes to Polyurethanes and Poly(Hydroxy Urethane)S. *Chem. Rev.* **2015**, *115* (22), 12407–12439.

(39) Sardon, H.; Pascual, A.; Mecerreyes, D.; Taton, D.; Cramail, H.; Hedrick, J. L. Synthesis of Polyurethanes Using Organocatalysis: A Perspective. *Macromolecules* **2015**, *48* (10), 3153–3165.

(40) Vol, P. L.; Carbon, C. D. Copolymerization O F Carbon Dioxide. **1969**, *7*, 287–292.

(41) Ihata, O.; Kayaki, Y.; Ikariya, T. Synthesis of Thermoresponsive Polyurethane from 2-Methylaziridine and Supercritical Carbon Dioxide. *Angew. Chemie - Int. Ed.* **2004**, *43* (6), 717–719.

(42) Kuran, W.; Rokicki, A.; Romanowska, D. New Route for Synthesis of Oligomeric Polyurethanes. Alternating Copolymerization of Carbon Dioxide and Aziridines. *J Polym Sci Polym Chem Ed* **1979**, *17* (7), 2003–2011.

(43) Zhang, D.; Zhang, Y.; Fan, Y.; Rager, M. N.; Guérineau, V.; Bouteiller, L.; Li, M. H.; Thomas, C. M. Polymerization of Cyclic Carbamates: A Practical Route to Aliphatic Polyurethanes. *Macromolecules* **2019**, *52* (7), 2719–2724.

(44) Prenveille, T.; Garreau, C.; Matner, M.; Dijkstra, D.; Oppermann, W.; Johannsmann, D. Reactivity of Urethanes at High Temperature: Transurethanization and Side Reactions. *J. Polym. Sci. Part A Polym. Chem.* **2019**, *57* (5), 621–629.

(45) North, M.; Pasquale, R.; Young, C. Synthesis of Cyclic Carbonates from Epoxides and CO2. *Green Chem.* **2010**, *12* (9), 1514–1539.

(46) Grignard, B.; Gennen, S.; Jérôme, C.; Kleij, A. W.; Detrembleur, C. Advances in the Use of CO2 as a Renewable Feedstock for the Synthesis of Polymers. *Chem. Soc. Rev.* **2019**, *48* (16), 4466–4514.

(47) Tomita, H.; Sanda, F.; Endo, T. Structural Analysis of Polyhydroxyurethane Obtained by Polyaddition of Bifunctional Five-Membered Cyclic Carbonate and Diamine Based on the Model Reaction. *J. Polym. Sci. Part A Polym. Chem.* **2001**, *39* (6), 851–859.

(48) Tomita, H.; Sanda, F.; Endo, T. Model Reaction for the Synthesis of Polyhydroxyurethanes from Cyclic Carbonates with Amines: Substituent Effect on the Reactivity and Selectivity of Ring-Opening Direction in the Reaction of Five-Membered Cyclic Carbonates with Amine. *J. Polym. Sci. Part A Polym. Chem.* **2001**, *39* (21), 3678–3685.

(49) Cornille, A.; Michaud, G.; Simon, F.; Fouquay, S.; Auvergne, R.; Boutevin, B.; Caillol, S. Promising Mechanical and Adhesive Properties of Isocyanate-Free Poly(Hydroxyurethane). *Eur. Polym. J.* **2016**, *84*, 404–420.

(50) Panchireddy, S.; Grignard, B.; Thomassin, J.-M.; Jerome, C.; Detrembleur, C. Catechol Containing Polyhydroxyurethanes as High-Performance Coatings and Adhesives. *ACS Sustain. Chem. & Eng.* **2018**, *6* (11), 14936–14944.

(51) Burk, R. M.; Roof, M. B. A Safe and Efficient Method for Conversion of 1,2- and 1,3-Diols to Cyclic Carbonates Utilizing Triphosgene. *Tetrahedron Lett.* **1993**, *34* (3), 395–398.

(52) Pescarmona, P. P. Cyclic Carbonates Synthesised from CO2: Applications, Challenges and Recent Research Trends. *Curr. Opin. Green Sustain. Chem.* **2021**, *29*, 1–9.

(53) Carré, C.; Ecochard, Y.; Caillol, S.; Avérous, L. From the Synthesis of Biobased Cyclic Carbonate to Polyhydroxyurethanes: A Promising Route towards Renewable Non-Isocyanate Polyurethanes. *ChemSusChem* **2019**, *12* (15), 3410–3430.

(54) North, M.; Pasquale, R. Mechanism of Cyclic Carbonate Synthesis from Epoxides and CO2. *Angew. Chemie - Int. Ed.* **2009**, *48* (16), 2946–2948.

(55) He, Q.; O'Brien, J. W.; Kitselman, K. A.; Tompkins, L. E.; Curtis, G. C. T.; Kerton, F. M. Synthesis of Cyclic Carbonates from CO2 and Epoxides Using Ionic Liquids and Related Catalysts Including Choline Chloride-Metal Halide Mixtures. *Catal. Sci. Technol.* **2014**, *4* (6), 1513–1528.

(56) Lan, D. H.; Fan, N.; Wang, Y.; Gao, X.; Zhang, P.; Chen, L.; Au, C. T.; Yin, S. F. Recent Advances in Metal-Free Catalysts for the Synthesis of Cyclic Carbonates from CO2 and Epoxides. *Cuihua Xuebao/Chinese Journal of Catalysis*. 2016, pp 826–845.

(57) Alves, M.; Grignard, B.; Mereau, R.; Jerome, C.; Tassaing, T.; Detrembleur, C. Organocatalyzed Coupling of Carbon Dioxide with Epoxides for the Synthesis of Cyclic Carbonates: Catalyst Design and Mechanistic Studies. *Catal. Sci. Technol.* **2017**, *7* (13), 2651–2684.

(58) Rintjema, J.; Guo, W.; Martin, E.; Escudero-Adán, E. C.; Kleij, A. W. Highly Chemoselective Catalytic Coupling of Substituted Oxetanes and Carbon Dioxide. *Chem.*

- *A Eur. J.* **2015**, *21* (30), 10754–10762.

(59) Tomita, H.; Sanda, F.; Endo, T. Reactivity Comparison of Five- and Six-Membered Cyclic Carbonates with Amines: Basic Evaluation for Synthesis of Poly(Hydroxyurethane). *J. Polym. Sci. Part A Polym. Chem.* **2001**, *39* (1), 162–168.

(60) Tomita, H.; Sanda, F.; Endo, T. Polyaddition of Bis(Seven-Membered Cyclic Carbonate) with Diamines: A Novel and Efficient Synthetic Method for Polyhydroxyurethanes. *J. Polym. Sci. Part A Polym. Chem.* **2001**, *39* (23), 4091–4100.

(61) Yuen, A.; Bossion, A.; Gómez-Bengoa, E.; Ruipérez, F.; Isik, M.; Hedrick, J. L.; Mecerreyes, D.; Yang, Y. Y.; Sardon, H. Room Temperature Synthesis of Non-Isocyanate Polyurethanes (NIPUs) Using Highly Reactive N-Substituted 8-Membered Cyclic Carbonates. *Polym. Chem.* **2016**, *7* (11), 2105–2111.

(62) Astarita, G.; Marrucci, G.; Gioia, F. The Influence of Carbonation Ratio and Total Amine Concentration on Carbon Dioxide Absorption in Aqueous Monoethanolamine Solutions. *Chem. Eng. Sci.* **1964**, *19* (2), 95–103.

(63) Blain, M.; Jean-Gérard, L.; Benazet, D.; Boutevin, B.; Andrioletti, B.; Caillol, S. Synthesis of Aminotelechelic Prepolymers to Circumvent the Carbonation of Amines in Epoxy Coatings. *Macromol. Mater. Eng.* **2016**, *301* (6), 682–693.

(64) Steblyanko, A.; Choi, W.; Sanda, F.; Endo, T. Addition of Five-Membered Cyclic Carbonate with Amine and Its Application to Polymer Synthesis. *J. Polym. Sci. Part A Polym. Chem.* **2000**, *38* (13), 2375–2380.

(65) Bossion, A.; Aguirresarobe, R. H.; Irusta, L.; Taton, D.; Cramail, H.; Grau, E.; Mecerreyes, D.; Su, C.; Liu, G.; Müller, A. J.; Sardon, H. Unexpected Synthesis of Segmented Poly(Hydroxyurea-Urethane)s from Dicyclic Carbonates and Diamines by Organocatalysis. *Macromolecules* **2018**, *51* (15), 5556–5566.

(66) Clements, J. H. Reactive Applications of Cyclic Alkylene Carbonates. *Ind. Eng. Chem. Res.* **2003**, *42* (4), 663–674.

(67) Dyer, E.; Scott, H. The Preparation of Polymeric and Cyclic Urethans and Ureas from Ethylene Carbonate and Amines. *J. Am. Chem. Soc.* **1957**, *79* (3), 672–675.

(68) Boyer, A.; Cloutet, E.; Tassaing, T.; Gadenne, B.; Alfos, C.; Cramail, H. Solubility in CO2 and Carbonation Studies of Epoxidized Fatty Acid Diesters: Towards Novel Precursors for Polyurethane Synthesis. *Green Chem.* **2010**, *12* (12), 2205–2213.

(69) Niu, X.; Gao, J.; Wang, K.; Miao, Q.; Dong, M.; Wang, G.; Fan, W.; Qin, Z.; Wang, J. Influence of Crystal Size on the Catalytic Performance of H-ZSM-5 and Zn/H-ZSM-5 in the Conversion of Methanol to Aromatics. *Fuel Process. Technol.* **2017**, *157*, 99–107.

(70) Polo Fonseca, L.; Duval, A.; Luna, E.; Ximenis, M.; De Meester, S.; Avérous, L.; Sardon, H. Reducing the Carbon Footprint of Polyurethanes by Chemical and Biological Depolymerization: Fact or Fiction? *Curr. Opin. Green Sustain. Chem.* **2023**, *41*, 100802.

(71) Henrich, E.; Dahmen, N.; Dinjus, E.; Sauer, J. The Role of Biomass in a Future World without Fossil Fuels. *Chemie-Ingenieur-Technik* **2015**, *87* (12), 1667–1685.

(72) Bos, H. L.; Broeze, J. Circular Bio-Based Production Systems in the Context of Current Biomass and Fossil Demand. *Biofuels, Bioprod. Biorefining* **2020**, *14* (2), 187–197.

(73) Ghasemlou, M.; Daver, F.; Ivanova, E. P.; Adhikari, B. Bio-Based Routes to Synthesize Cyclic Carbonates and Polyamines Precursors of Non-Isocyanate Polyurethanes: A Review. *Eur. Polym. J.* **2019**, *118* (June), 668–684.

(74) Figovsky, O.; Shapovalov, L.; Birukova, O.; Leykin, A. Modification of Epoxy Adhesives by Hydroxyurethane Components on the Basis of Renewable Raw Materials 1. **2013**, *6* (4), 271–274.

(75) Panchireddy, S.; Grignard, B.; Thomassin, J. M.; Jerome, C.; Detrembleur, C. Bio-Based Poly(Hydroxyurethane) Glues for Metal Substrates. *Polym. Chem.* **2018**, *9* (19), 2650–2659.

(76) Panchireddy, S.; Thomassin, J. M.; Grignard, B.; Damblon, C.; Tatton, A.; Jerome, C.; Detrembleur, C. Reinforced Poly(Hydroxyurethane) Thermosets as High Performance Adhesives for Aluminum Substrates. *Polym. Chem.* **2017**, *8* (38), 5897–5909.

(77) Tryznowski, M.; Świderska, A.; Gołofit, T.; Zołek-Tryznowska, Z. Wood Adhesive Application of Poly(Hydroxyurethane)s Synthesized with a Dimethyl Succinate-Based Amide Backbone. *RSC Adv.* **2017**, *7* (48), 30385–30391.

(78) Tryznowski, M.; Gołofit, T.; Świderska, A. Poly(Hydroxyurethane)s with Diethyl Tartrate-Based Amide Backbone by an Isocyanate-Free Route: Use as Adhesives. *Polymer (Guildf).* **2018**, *144*, 1–6.

(79) Stroganov, I. V; Stroganov, V. F. Peculiarities of Structurization and Properties of Nonisocyanate Epoxyurethane Polymers. **2007**, *49* (3), 258–263.

(80) Gomez-Lopez, A.; Grignard, B.; Calvo, I.; Detrembleur, C.; Sardon, H. Monocomponent Non-Isocyanate Polyurethane Adhesives Based on a Sol-Gel Process. *ACS Appl. Polym. Mater.* **2020**, *2* (5), 1839–1847.

(81) Aguiar, K. R.; Santos, V. G.; Eberlin, M. N.; Rischka, K.; Noeske, M.; Tremiliosi-Filho, G.; Rodrigues-Filho, U. P. Efficient Green Synthesis of Bis(Cyclic Carbonate)Poly(Dimethylsiloxane) Derivative Using CO2 Addition: A Novel Precursor for Synthesis of Urethanes. *RSC Adv.* **2014**, *4* (46), 24334–24343.

(82) Gomez-Lopez, A.; Grignard, B.; Calvo, I.; Detrembleur, C.; Sardon, H. Synergetic Effect of Dopamine and Alkoxysilanes in Sustainable Non-Isocyanate Polyurethane Adhesives. *Macromol. Rapid Commun.* **2021**, *42* (3), 1–9.

(83) Gomez-Lopez, A.; Grignard, B.; Calvo, I.; Detrembleur, C.; Sardon, H. Accelerating the Curing of Hybrid Poly(Hydroxy Urethane)-Epoxy Adhesives by the Thiol-Epoxy Chemistry. *ACS Appl. Polym. Mater.* **2022**, *4* (12), 8786–8794.

(84) Lambeth, R. H.; Rizvi, A. Mechanical and Adhesive Properties of Hybrid Epoxy-Polyhydroxyurethane Network Polymers. *Polymer (Guildf).* **2019**, *183*, 121881.

(85) Sukumaran Nair, A.; Cherian, S.; Balachandran, N.; Panicker, U. G.; Kalamblayil Sankaranarayanan, S. K. Hybrid Poly(Hydroxy Urethane)s: Folded-Sheet Morphology and Thermoreversible Adhesion. *ACS Omega* **2019**, *4* (8), 13042–13051.

(86) Gomez-Lopez, A.; Ayensa, N.; Grignard, B.; Irusta, L.; Calvo, I.; Müller, A. J.; Detrembleur, C.; Sardon, H. Enhanced and Reusable Poly(Hydroxy Urethane)-Based Low Temperature Hot-Melt Adhesives. *ACS Polym. Au* **2022**, *2* (3), 194–207.

(87) Marques, A. C.; Mocanu, A.; Tomić, N. Z.; Balos, S.; Stammen, E.; Lundevall, A.; Abrahami, S. T.; Günther, R.; de Kok, J. M. M.; de Freitas, S. T. Review on Adhesives and Surface Treatments for Structural Applications: Recent Developments on Sustainability and Implementation for Metal and Composite Substrates. Materials (Basel). 2020, 13 (24), 1–43.

Chapter 2

Evaluation of the Adhesive Properties of Vanillin-Derived Poly(HydroxyUrethane)s

2.1 Introduction

Synthetic polymers have occupied almost every extent of modern life, and their use and production are increasing exponentially and are expected to exceed 500 million metric tons by 2050.[1] Among them, PUs have found numerous applications in various sectors (transportation, health, construction, etc.).[2–5] It is also ranked as the sixth most-produced polymer globally, with a market size of about USD 81.3 billion in 2022.[6] However, the precursors for their synthesis depend on fossil fuels and involve using hazardous chemicals.[7] Since PUs are extensively used in various sectors, it would be highly advantageous if these polymeric materials could be developed from renewable biomass and by using non-toxic precursors. Intensive studies in this area have aided in the development of alternate methods such as (a) copolymerization of aziridines with carbon dioxide,[8] (b) rearrangement of acyl azide followed by its polycondensation with alcohol,[8] (c) trans-urethanization reaction between a bis-carbamate and a diol,[9] and (d) polyaddition between cyclic carbonates and amines,[10,11] for the development of PUs. The latter method, the polyaddition between cyclic carbonates and amines, is considered as one of the most studied and promising routes for developing PHUs since it involves the usage of much safer precursors. However, the structure of PHUs differs from conventional PUs due to the presence of both primary and secondary hydroxyl groups in the main chain of polymers providing additional benefits such as post-functionalization, improved hydrogen bonding, enhanced adhesion forces,[12–14] and miscibility between phases.[15,16] Furthermore, PHUs designed from bis-5-membered cyclic carbonates are considered more viable than PHUs developed from higher cyclic carbonates since they bypass toxic precursors making the process safer and further involve the utilization of renewable and sustainable resources such as CO_2 as feedstock.[17,18] However, in most current studies on the development of PHUs, the molecules for cyclic carbonate synthesis mainly depended on fossil fuel. It will be highly feasible if CO_2 can be coupled to molecules derived from renewable biomass since it can improve sustainability and aid in developing polymers with a low carbon footprint compared to traditional routes. Vanillin is one such molecule derived from lignin, which is of great interest because of its bioactivity and can represent an inexhaustible resource of monomers for developing sustainable polymers.[19,20] Despite the ease in the availability of vanillin, there are hardly very few reports concerning its utilization in developing PHU.[21,22] Furthermore, the applicability of these polymers as adhesives is yet to be explored. Herein, we elaborate on the potential of bio-renewable vanillin as a dicarbonate precursor for synthesizing novel thermoplastic PHUs suitable for adhesive application. First, a vanillin-derived dicarbonate was

developed and further optimization of polymerization conditions based on molecular weights was carried out. We then prepared a series of PHUs via step-growth polyaddition reaction between dicarbonate monomer with six aliphatic diamines of various chain lengths, and their effect on thermo-mechanical properties has been investigated. Finally, adhesion studies were performed to evaluate the application potential of the above-synthesized PHUs.

2.2 Experimental section

2.2.1 Materials

Vanillin (>98%), tetrabutylammonium bromide (TBAB, >98%), ethylenediamine (anhydrous, >98%), 1, 10-diamino decane (>97%), and 1,5,7-triazabicyclo-[4.4.0] dec-5-ene (TBD, >98%) was purchased from the TCI Chemicals, India. Sodium percarbonate (13%-14% active oxygen, $Na_2CO_3.1.5H_2O_2$) was provided by the Alfa Aesar. Epichlorohydrin (≥99%) and hexamethylene diamine (98%) were procured from Sigma Aldrich. Sodium hydroxide pellets (NaOH, 98%), hydrochloric acid (HCl, 35%–38%), ethyl acetate, and petroleum ether were supplied from the S D fine chemical. Sodium sulfate (anhydrous, ≥99.5%, AR) was delivered by Leonid chemicals. Dimethyl sulfoxide (DMSO-d_6, 99.80% D) and chloroform (99.80% D) were purchased from Eurisotop. CO_2 gas cylinder (99.5%) was obtained from the Vadilal chemical. 1, 8-diamino octane (98%) and 1, 12-diamino dodecane (99%) were received from the Chempure. 1, 4-diaminobutane (99%), and isopropanol (99.5%) were procured from SRL chemicals. N-Methyl pyrrolidinone (NMP), and dimethylformamide (DMF) were distilled over CaH_2 under a nitrogen atmosphere and stored over molecular sieves (4 Å). All chemicals were used as received unless specified.

2.2.2 Characterization techniques

The chemical structure of the molecules was determined by ^{1}H and ^{13}C NMR spectroscopy using a Bruker Advance 500 MHz spectrometer equipped with a QNP z-gradient probe at room temperature. The infrared spectra (IR) were recorded on Bruker alpha Fourier transform infrared spectroscopy (FTIR) spectrometer, where 48 scans were recorded in a frequency range of 4000-500 cm^{-1} at a resolution of 4 cm^{-1}. The high-resolution mass spectrometer (ThermoFisher Scientific) was used to detect the molecular weight of compounds and the data was acquired from a hybrid Quadrapole Q-Exactive orbitrap fitted with an ACCELA PDA detector. Gel permeation chromatography was employed to analyze the molecular weight of PHUs using viscotek GPC max (VE 2001) with a refractive index as a detector. The

measurements were done in DMF (DMF plus lithium bromide $1gL^{-1}$) as an eluent at 1 mL/min. and using the DT6000M column at 50 °C. Molecular weights were estimated relative to polymethyl methacrylate standards. The glass transition temperature (T_g) was analyzed on a DSC-Q10 system from TA instruments. For each sample, two cycles were performed in the range between -40 and 140 °C at 10 °C/min under a nitrogen atmosphere. The T_g was determined from a second heating cycle. Thermogravimetric studies were performed using a TGA-STA 6000 (Perkin Elmer) at a heating rate of 10 °C/min from 50 °C to 800 °C under a nitrogen atmosphere. The adhesive properties of synthesized PHUs were investigated at room temperature using an Instron 5943 with a displacement rate of 1 $mm.min^{-1}$. The lap shear test was performed on aluminum substrates having dimensions of 54 mm × 20 mm × 1.55 mm (L*W*T). Aluminum plates were repeatedly washed three to four times using a 50:50 combination of acetone and isopropanol, followed by water, and then dried in an oven before using it for adhesion studies. 200 mg of polymer materials were applied on the substrate surface by maintaining the adhesive contact area of 300 mm^2 (20 mm × 15 mm). Further, the adhesive specimen was prepared by melting PHU-2, PHU-3, and PHU-6 at 80 °C, whereas the PHU-4 and PHU-5 at 120 °C for 30 min while applying gentle pressure. The measurements of each sample were repeated at least five times. The type of failure was also reported after the test based on visual inspection. The lap shear strength was determined by the following formula,

$\tau = F/A$

where:

τ = lap-shear strength ($N.mm^{-2}$ or MPa),

F = maximum shear force (N), and

A = contact area of the adhesive joints (300 mm^2)

2.2.3 Methods

2.2.3.1 Synthesis of vanillin and CO_2-derived cyclic dicarbonate

The method described in the literature was followed to prepare the synthesis of carbonate monomer.[21]

2.2.3.1.1 Synthesis of 2-methoxybenzene-1, 4-diol

Vanillin (30 g, 0.197 mol) was solubilized in THF (220 mL). To this, deionized water (80 mL) was added followed by the addition of sodium percarbonate ($Na_2CO_3.1.5\ H_2O_2$, 46.43 g, 0.295 mol). The reaction was continuously stirred for another 24 h at RT under an N_2 atmosphere,

followed by quenching the reaction mixture by adding HCl solution (0.1 mol L^{-1}, maintained pH = 3), and the THF was removed using a rotary evaporator at 40°C. The above-attained crude product was extracted with ethyl acetate, dried over Na_2SO_4, and concentrated. Further purified by column chromatography using ethyl acetate and petroleum ether to give a brown-colored powder (yield: 83 %, m. p.: 88 °C).

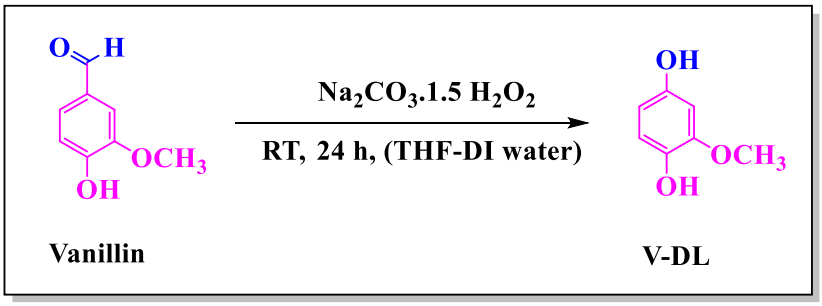

Scheme 2.1. *Synthetic process for the V-DL compound.*

FTIR (cm^{-1}): 3283-3366 (OH), 2951, 2862 (CH stretch).

^{1}H-NMR (500 MHz, DMSO-d$_6$) δ (ppm): 3.69 (s, 3H, OC<u>H</u>$_3$), 6.16 (dd, 1H, aromatic -C<u>H</u>), 6.36 (d, 1H, aromatic -C<u>H</u>), 6.54 (dd, 1H, aromatic -C<u>H</u>), 8.12 (s, 1H, aromatic -O<u>H</u>), 8.72 (s, 1H, aromatic -O<u>H</u>).

^{13}C-NMR (500 MHz, DMSO-d$_6$) δ (ppm): 55.45 (O<u>C</u>H$_3$), 100.78 (<u>C</u>-H, aromatic), 106.30 (<u>C</u>-H, aromatic), 115.76 (<u>C</u>-H, aromatic), 138.93 (<u>C</u>-O, aromatic), 148.14 (<u>C</u>-O, aromatic), 150.37 (<u>C</u>-O, aromatic).

HRMS (ESI) m/z: $[M + H]^+$ calculated for $C_7H_9O_3$: 141.0551; found: 141.0546.

2.2.3.1.2 Synthesis of vanillin diglycidyl ether

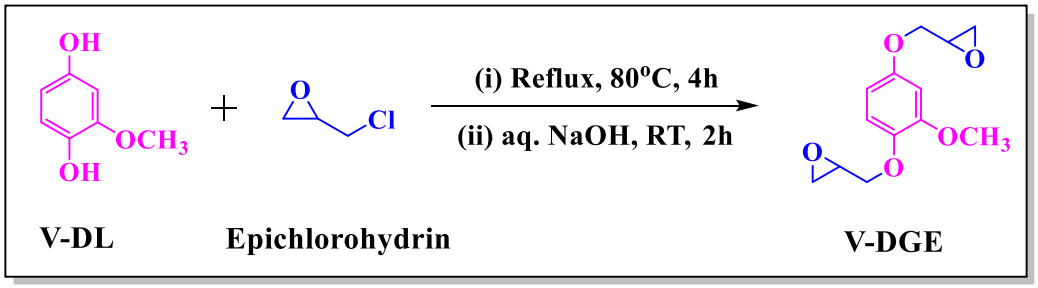

Scheme 2.2. *Synthetic method for V-DGE compound.*

In a typical synthesis, V-DL (20 g, 0.143 mol.), and TBAB (2.65 g, 0.014 mol.) was initially charged into a round bottom flask followed by the addition of epichlorohydrin (145 g, 1.57 mol), and the reaction mixture was stirred for 4 h at 80 °C under inert conditions. The reaction

medium was further allowed to cool down to room temperature followed by the dropwise addition of aqueous NaOH (22.84 g, 0.570 mol.). The reaction was further continued for another 2 h at 16 °C followed by the removal of excess epichlorohydrin by vacuum distillation. The product thus obtained was extracted with ethyl acetate and the crude product was further purified by column chromatography, using petroleum ether and ethyl acetate as eluent to give glycidated V-DGE (yield: 88 %, m. p.: 87 °C).

FTIR (cm^{-1}): 2951, 2862 (CH stretch), 911 (asymmetric C-O stretch, epoxy), 860 (symmetric C-O stretch, epoxy).

^{1}H-NMR (500 MHz, CDCl$_3$) δ (ppm): 2.75 (dd, 2H, epoxy -C$\underline{H}_2$), 2.90 (dd, 2H, epoxy -C$\underline{H}_2$), 3.34 (m, 2H, epoxy -C$\underline{H}$), 3.84 (s, 3H, OC$\underline{H}_3$), 3.95 (dd, 2H, epoxy -C$\underline{H}_2$), 4.20 (dd, 2H, epoxy -C$\underline{H}_2$), 6.39 (dd, aromatic -C$\underline{H}$), 6.56 (s, aromatic -C$\underline{H}$), 6.86 (dd, aromatic -C$\underline{H}$).

^{13}C-NMR (500 MHz, CDCl$_3$) δ (ppm): 44.69 (C$\underline{H}_2$-O, epoxy), 50.19 (CH-O, epoxy), 55.88 (OC$\underline{H}_3$), 69.28 (C$\underline{H}_2$-O-epoxy), 101.28 (C-H, aromatic), 104.13 (C-H, aromatic), 115.75 (C-H, aromatic), 142.65 (C-O, aromatic), 150.82 (C-O, aromatic), 154.05 (C-O, aromatic).

HRMS (ESI) m/z: $[M + H]^+$ calculated for $C_{13}H_{17}O_5$: calculated: 253.1076; found: 253.1071.

2.2.3.1.3 Synthesis of vanillin dicarbonate

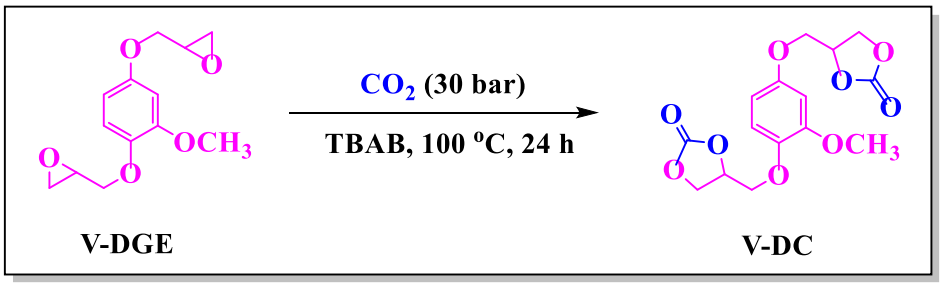

Scheme 2.3. *Preparation of V-DC monomer.*

A solution of DGE compound (10 g, 0.039 mol), and TBAB (5 mol%) in DMF (40 mL) was prepared and added to a 100 mL autoclave. The reactor was filled with carbon dioxide gas, and the reaction was conducted at 100 °C for 24 h. Thus, the obtained reaction mixture was collected and precipitated in cold water. The crude product was then dried on anhydrous Na_2SO_4, purified by column chromatography, and recrystallized in isopropanol to obtain carbonated glycidyl ether (yield: 82 %, m. p.: 110-112 °C).

FTIR (cm^{-1}): 2951, 2862 (CH stretch), 1787 (carbonate C=O stretch).

^{1}H-NMR (500 MHz, DMSO-d_6) δ (ppm): 3.76 (s, 3H, OC$\underline{H}_3$), 4.17 (m, 4H, carbonate -C$\underline{H}_2$), 4.40 (dd, 2H, carbonate -C$\underline{H}_2$), 4.61 (dd, 2H, carbonate -C$\underline{H}_2$), 5.13 (m, 2H, carbonate -C$\underline{H}$), 6.46 (dd, 1H, aromatic -C$\underline{H}$), 6.63 (s, 1H, aromatic -C$\underline{H}$), 6.92 (dd, 1H, aromatic -C$\underline{H}$).
^{13}C-NMR (500 MHz, DMSO-d_6) δ (ppm): 56.21 (O$\underline{C}H_3$), 66.42 ($\underline{C}H_2$-O, carbonate), 68.37 (CH-O, carbonate), 75.36 (CH_2-OAr), 101.69 ($\underline{C}$-H, aromatic), 105.20 ($\underline{C}$-H, aromatic), 116.74 ($\underline{C}$-H, aromatic), 142.54 ($\underline{C}$-O, aromatic), 151.00 ($\underline{C}$-O, aromatic), 154.03 ($\underline{C}$-O, aromatic), 155.35 (C=O, carbonate).
HRMS (ESI) m/z: $[M + H]^+$ calculated for $C_{15}H_{17}O_9$: 341.0872; found: 341.0867.

2.2.3.2 Synthesis of PHU series

Cyclic dicarbonate (1 eq.) was mixed with respective diamines (1 eq.), followed by the addition of TBD (10 mol%). Next, the freshly distilled N-methyl-2-pyrrolidinone (5 mL/1 g) was added, and the polyaddition reaction was carried out at 80 °C for 24 h under an inert atmosphere.[10] The obtained polymers were then further purified by precipitation in diethyl ether. The designation of the obtained polymers is depicted in **Table 2.1.**

Table 2.1. *The nomenclature of synthesized PHUs.*

Polymers	Diamine used
PHU-1	1, 2-Diaminoethane
PHU-2	1, 4-Diaminobutane
PHU-3	1, 6-Diaminohexane
PHU-4	1, 8-Diaminooctane
PHU-5	1, 10-Diaminodecane
PHU-6	1, 12-Diaminododecane

2.3 Result and Discussion

2.3.1 Synthesis of vanillin-CO_2-derived cyclic dicarbonate

2.3.1.1 Synthesis of 2-methoxybenzene-1,4-diol

The preparation of cyclic dicarbonate was carried out in three stages with an overall yield of 59.77 %.[21] The first stage is the Dakin reaction, which leads to the product V-DL with one carbon loss in the presence of sodium percarbonate as an oxidizing agent (**Scheme 2.1.**). NMR (^{1}H, ^{13}C) and FTIR spectroscopy were used to validate their structure. As anticipated, the FTIR

spectrum **(Figure 2.8)** of V-DL showed a broad peak at 3366 cm^{-1}, which is attributed to the aromatic hydroxyl groups, while the peak at 1668 cm^{-1}, has completely disappeared, which was the characteristic peak of the aldehyde functionality (vanillin).[23] In ^{1}H NMR spectra **(Figure 2.1)**, new signals, relating to the two hydroxyl protons were observed at 8.14 ppm and 8.74 ppm, whereas, the protons attributed to the aldehyde group disappeared at 9.83 ppm.[24] Further, the ^{13}C NMR spectrum of V-DL is shown in **Figure 2.2**.

2.3.1.2 Synthesis vanillin diglycidyl ether

The V-DL thus obtained was then glycidylated in the second step using epichlorohydrin as a reagent and TBAB as a phase transfer catalyst (**Scheme 2.2**). The FTIR analyses validated the formation of V-DGE (**Figure 2.8**), where the absorption peak of hydroxyl groups vanished at 3366 cm^{-1}, and the distinct absorption peak of the epoxy rings appeared at 911 and 860 cm^{-1}.[26–28] The ^{1}H NMR spectra of V-DGE (**Figure 2.3**) exhibited new signals in the area of 2.73 ppm and 4.18 ppm, which corresponds to the epoxy ring, and signals corresponding to hydroxyl groups at 8.14 ppm and 8.74 ppm disappeared,[25,26] revealing that the complete conversion of hydroxyl groups into glycidyl rings. Moreover, the epoxy protons showed five signals in the spectrum: three doublets at 2.71, 2.75, and 3.95 ppm (labeled as 1, 1′, and 3′ respectively) and two multiplets at 3.34, and 4.20 ppm (labeled as 2, and 3 respectively). The methoxy group marked as 4 appeared at 3.84 ppm whereas, the aromatic protons labeled as 5, 6, and 7 were observed at 6.36, 6.55, and 6.85 ppm, respectively. The ^{13}C NMR of V-DGE is presented in **Figure 2.4**. The appearance of additional peaks for epoxy carbons at 44.69, 50.19, 69.28-71.32 ppm (labeled as 1, 1′, 2, 2′,3, 3′) also supports the formation of diglycidyl ether compound.

2.3.1.3 Synthesis of vanillin dicarbonate

In the final step, V-DGE was converted into its cyclic carbonate (V-DC) by TBAB-catalyzed CO_2 insertion reaction (**Scheme 2.3**). The chemical structure of V-DC was analyzed by FTIR and NMR (^{1}H, ^{13}C) spectroscopy. FTIR (**Figure 2.8**) and ^{13}C NMR (**Figure 2.6**) analysis indicated the presence of a new absorbance band at 1787 cm^{-1} and 155.35 ppm, respectively, attributed to the C=O of five-membered cyclic carbonate rings.[29,30] Moreover, the evaluation of ^{1}H NMR spectra of V-DC (**Figure 2.5**) confirmed the formation of cyclic carbonates where the signal associated with protons of the cyclic carbonate appeared in the region of 4.10 ppm to 5.15 ppm. Further, the disappearance of epoxide signals from the 2.73 to 4.18 ppm range was noted, indicating the oxirane ring has transformed into carbonate rings.[29–31] The carbonate peaks with the labels 2, and 2′ were observed as multiplets at 4.10-4.23 ppm whereas the peaks

marked as 4, 4′ were found as quartets at 4.39 and 4.59 ppm. The peaks with the designations 3, 3′ were also found to be multiplets at 5.13 ppm.

In addition, it has been observed that the peaks associated with the protons of the carbonate ring shifted toward the high field in comparison to the epoxide protons, this is probably due to the electron-withdrawing effect of the carbonyl group (C=O) (**Figure 2.5**) indicative of the formation of V-DC product.[32]

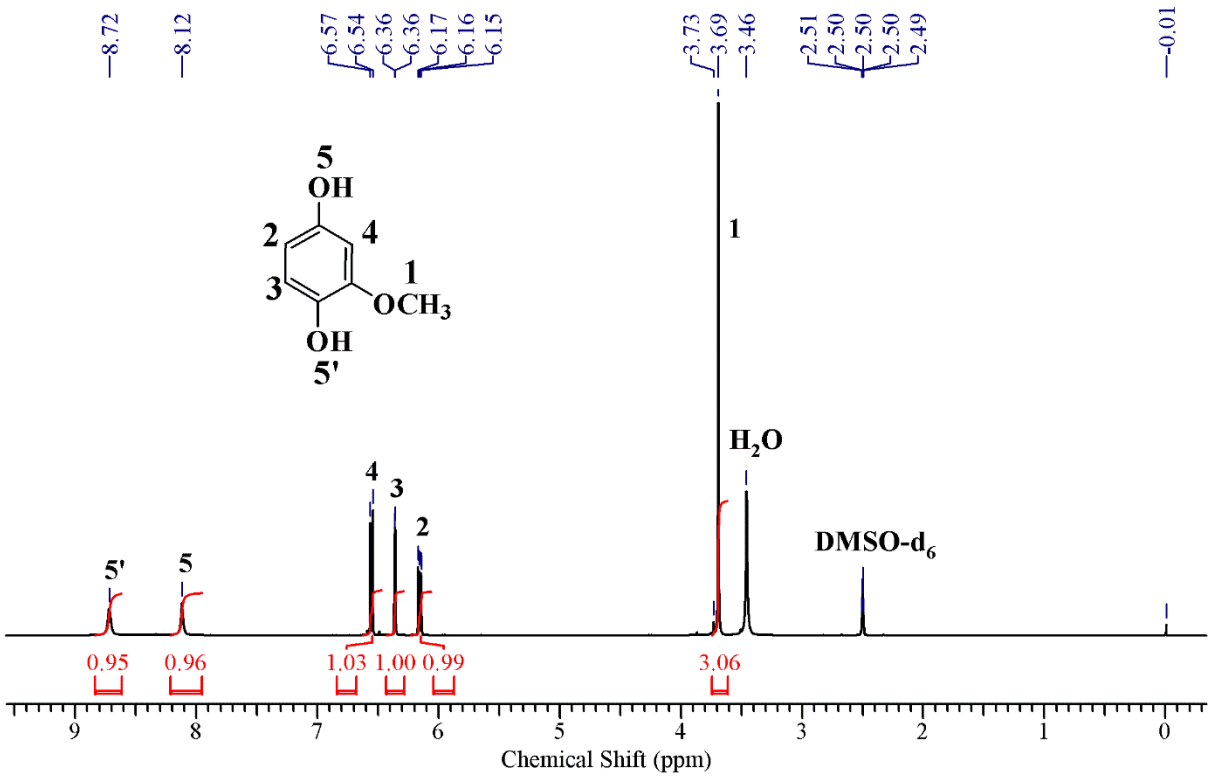

Figure 2.1. *^{1}H NMR spectrum of V-DL.*

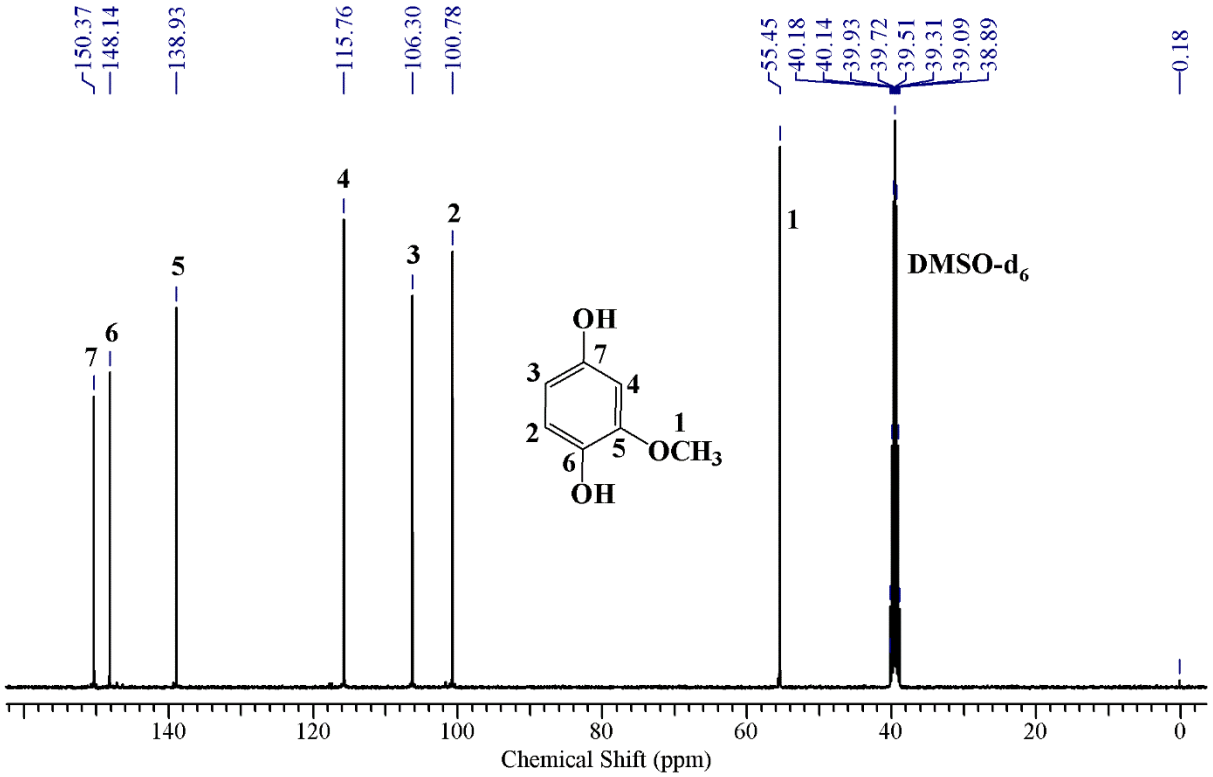

Figure 2.2. *^{13}C NMR spectrum of V-DL.*

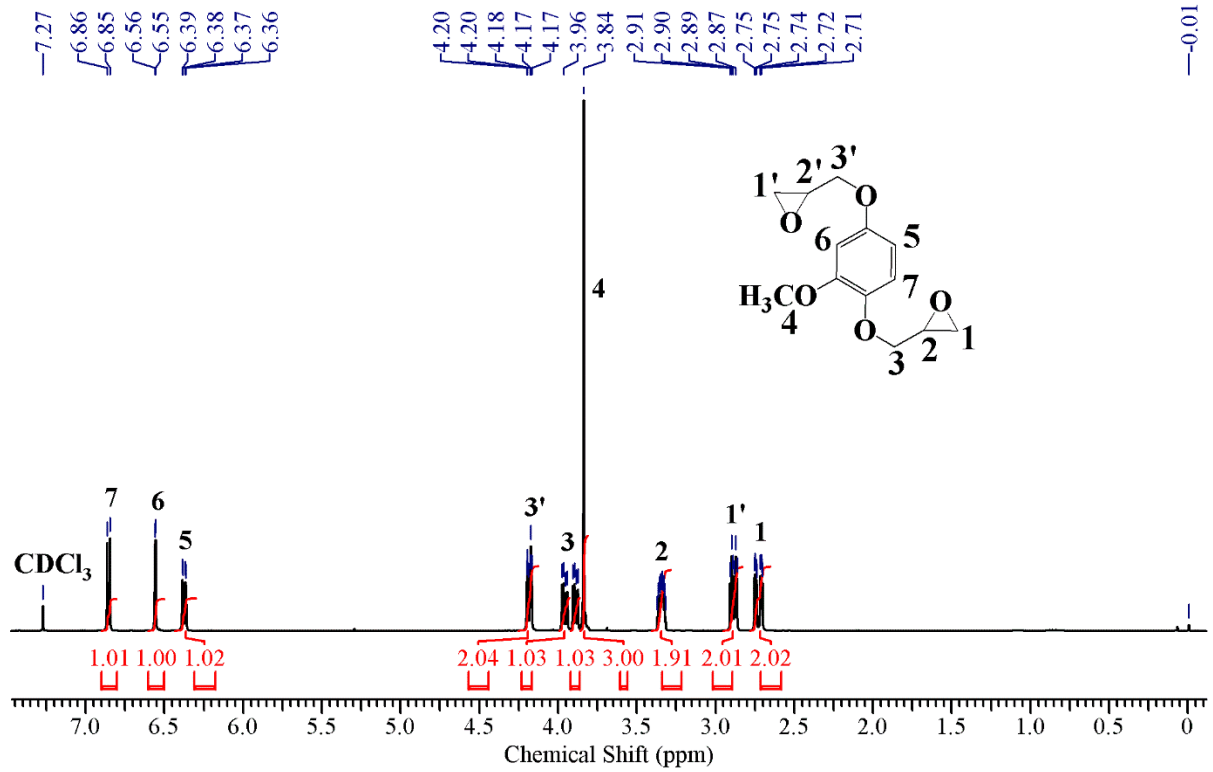

Figure 2.3. *^{1}H NMR spectrum of V-DGE.*

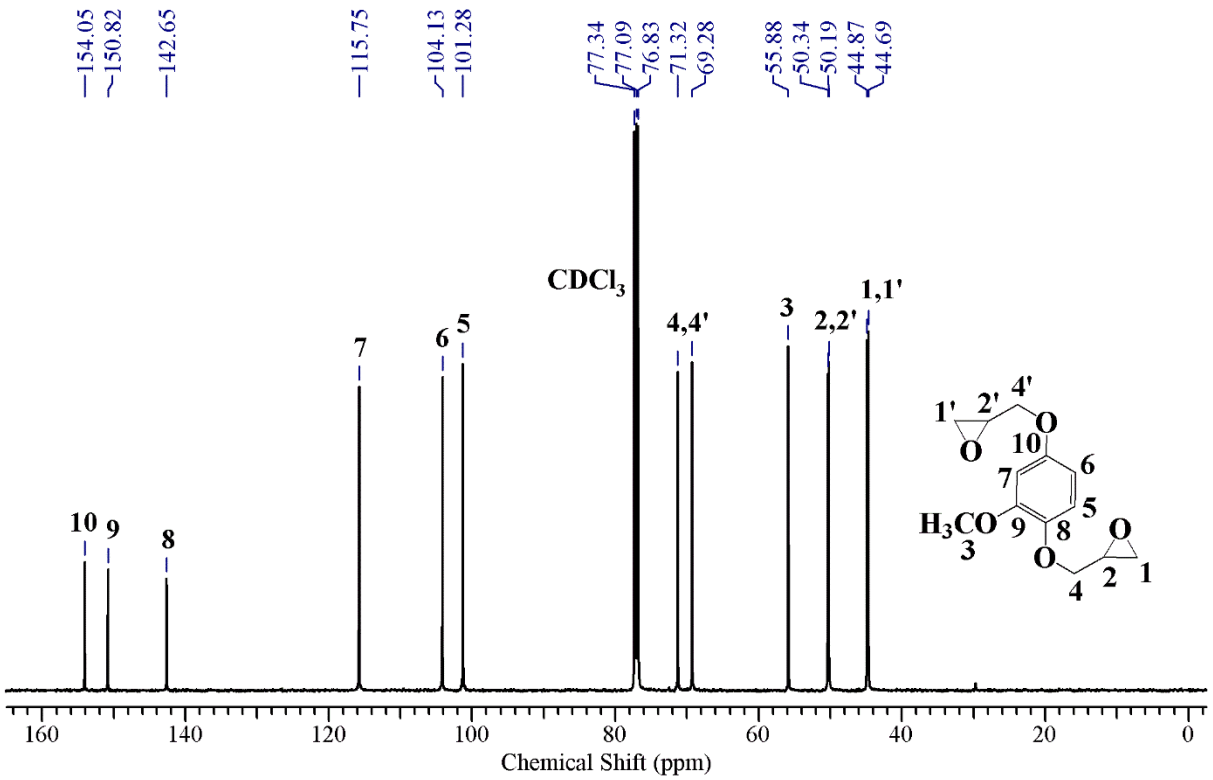

Figure 2.4. *^{13}C NMR spectrum of V-DGE.*

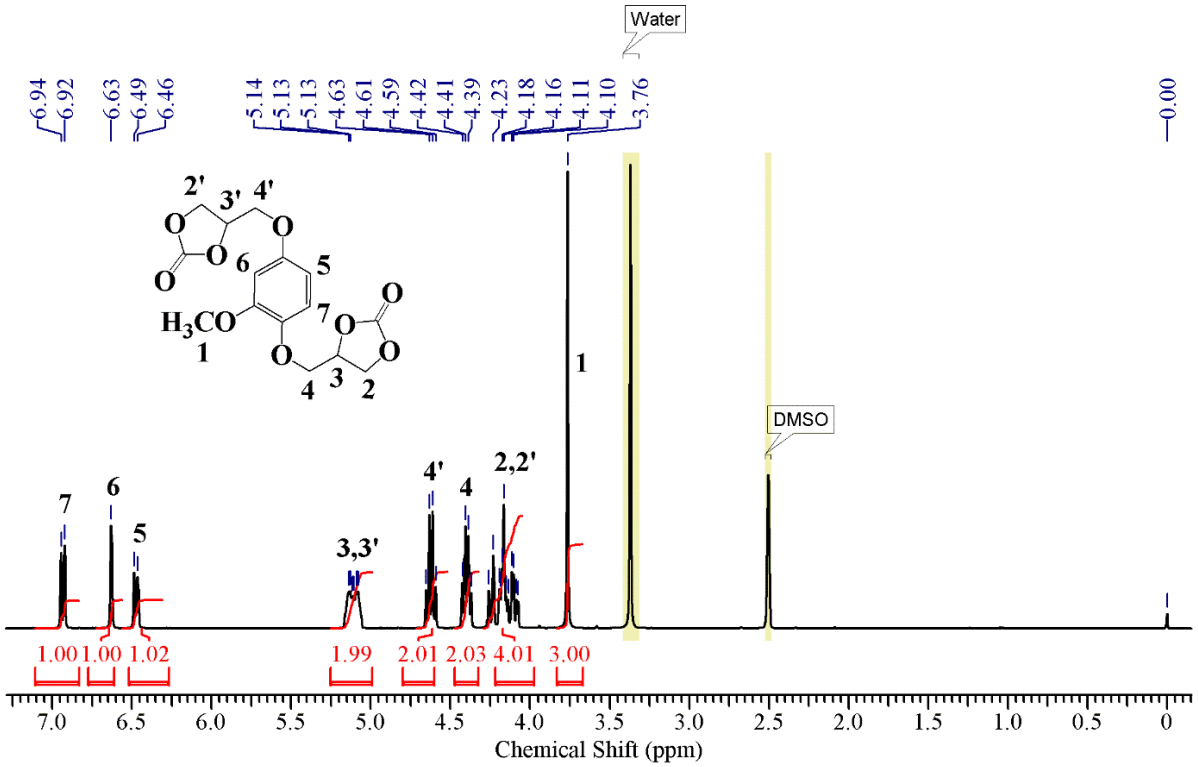

Figure 2.5. *^{1}H NMR spectrum of V-DC.*

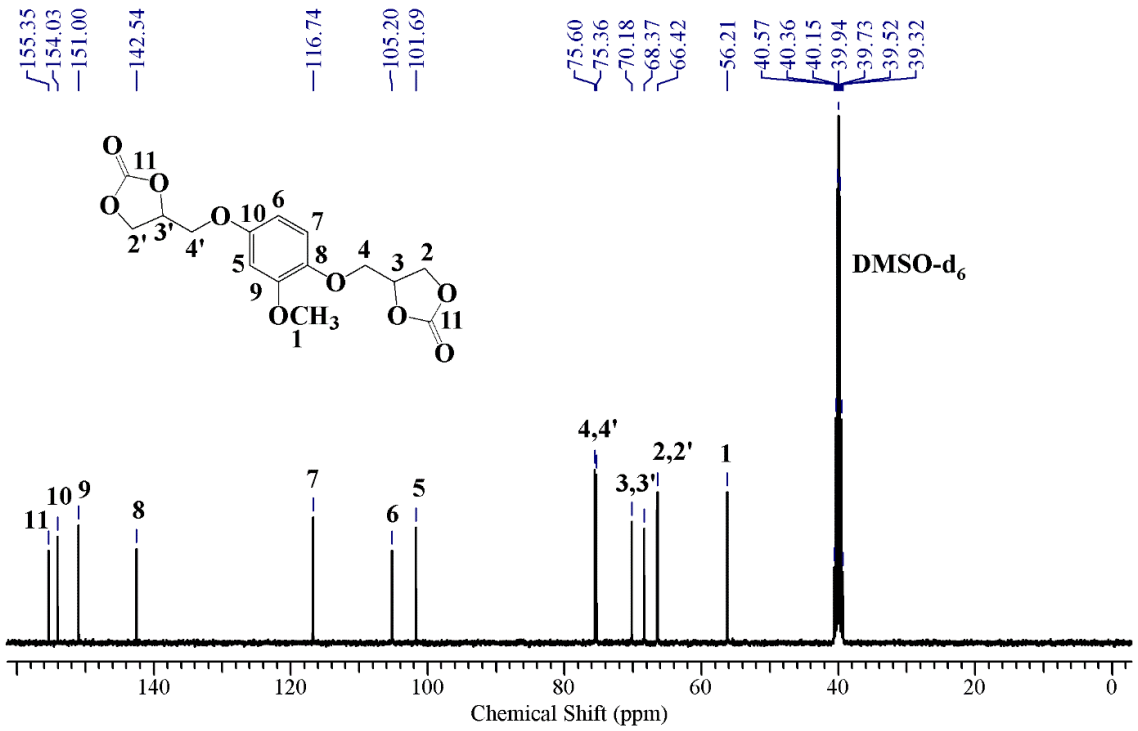

Figure 2.6. *^{13}C NMR spectrum of V-DC.*

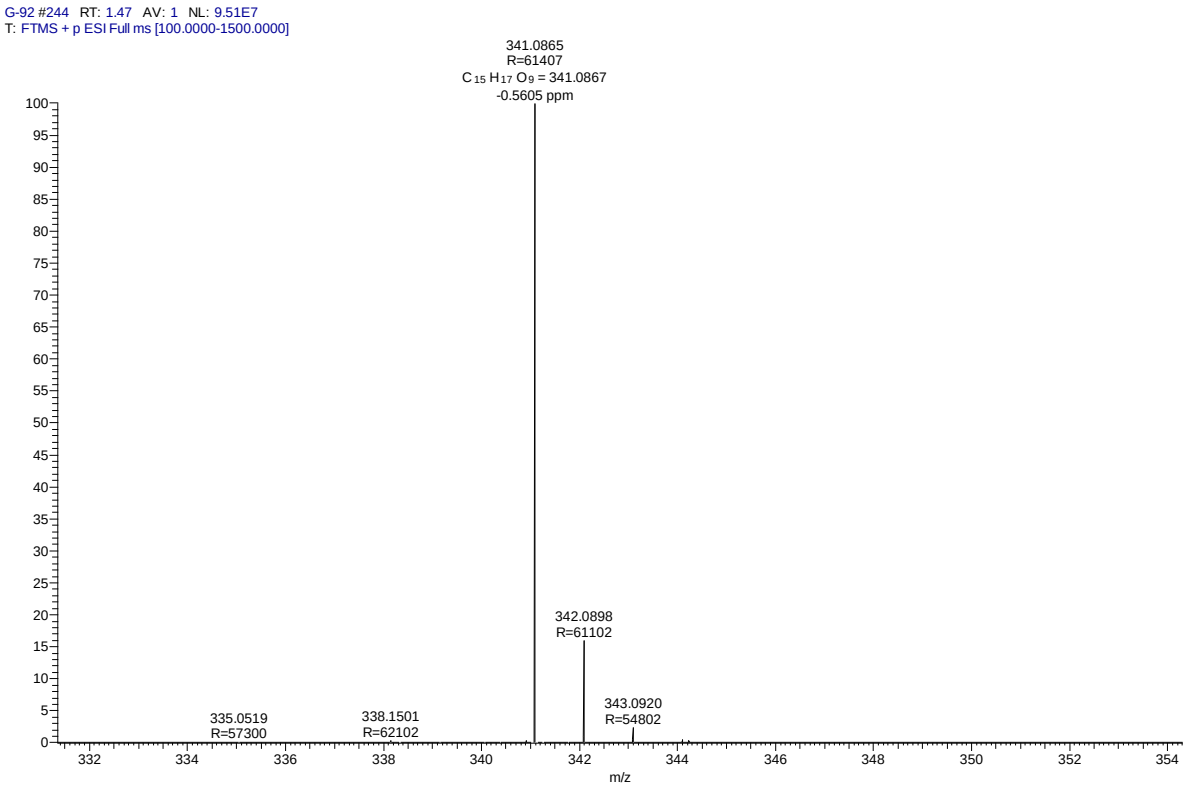

Figure 2.7. *HRMS spectrum of V-DC.*

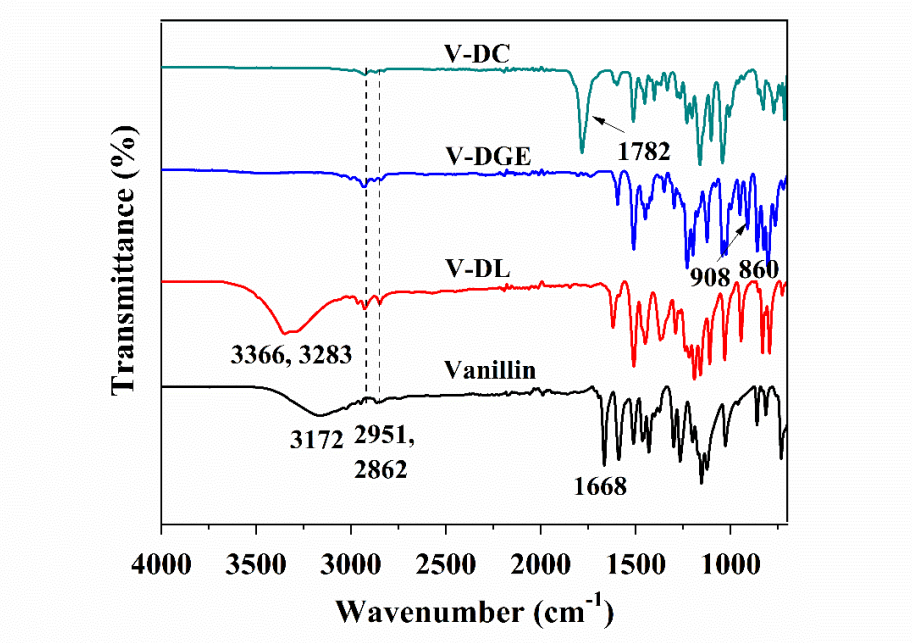

Figure 2.8. *FTIR spectrum of V-DL, V-DGE, and V-DC compounds.*

2.3.2 Optimization of polymerization conditions

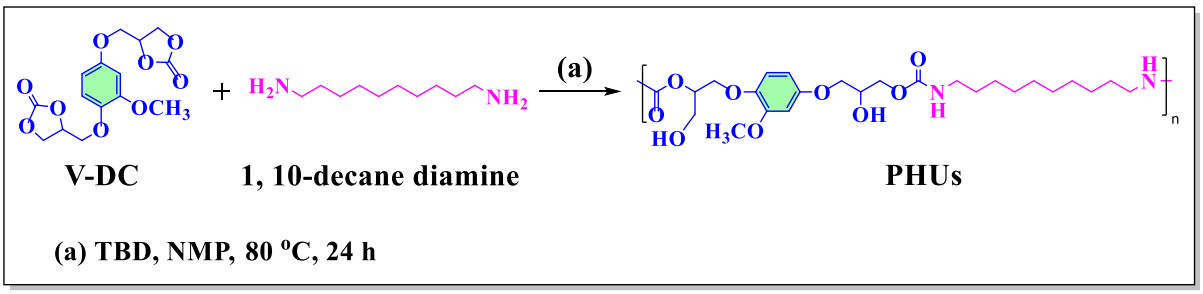

Scheme 2.4*. Synthetic scheme for PHUs made at various temperatures.*

To optimize the polymerization conditions, we performed a series of polyaddition reactions between cyclic dicarbonate and 1, 10-decane diamine at different temperatures from 40 °C to 140 °C (**Scheme 2.4**), and their molecular weight was analyzed by gel permeation chromatography (**Table 2.2**, **Figure 2.9**). The molecular weight of PHUs was initially found to increase with a rise in reaction temperature and a maximum molecular weight was attained at 80°C (6000 g/mol). The molecular weight increase can be associated with the increased reactivity of cyclic dicarbonate with temperatures.[33] Further, the molecular weight of PHUs was found to decrease as the reaction temperature was raised above 80 °C.[13] ^{1}H NMR evaluation of PHUs synthesized at higher temperatures stated the presence of an additional peak at 5.71 ppm (**Figure 2.10**) indicative of urea formation.[11,13] The occurrence of these side reactions could be the probable reason for the reduction in molecular weights of PHUs at higher

temperatures. Therefore, the preferred condition for the polyaddition reaction between V-DC and diamine was chosen as 80 °C.[34]

Table 2.2. *The molecular weight of the PHUs synthesized at different temperatures.*

Entry	Temperature (°C)	SEC		
		M_n (g.mol^{-1})	M_w (g.mol^{-1})	Dispersity
1	40	4,100	6,600	1.59
2	60	4,600	7,000	1.52
3	80	6000	9100	1.34
4	100	5000	6400	1.28
5	120	4,500	6,200	1.50
6	140	4,000	5,100	1.27

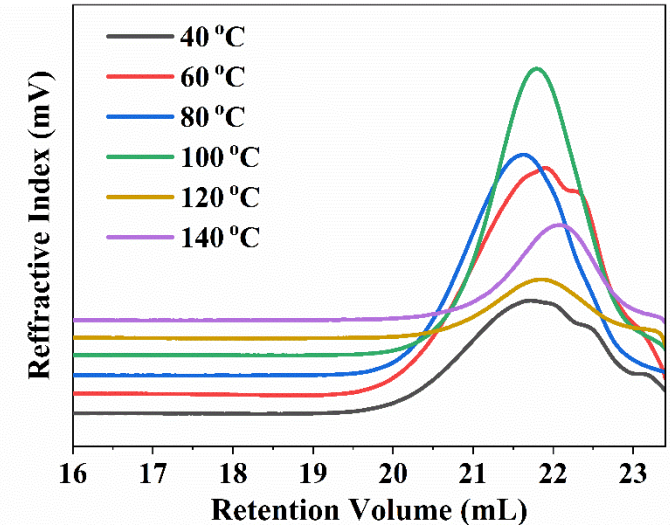

Figure 2.9. *GPC chromatograms of PHUs synthesized at different temperatures.*

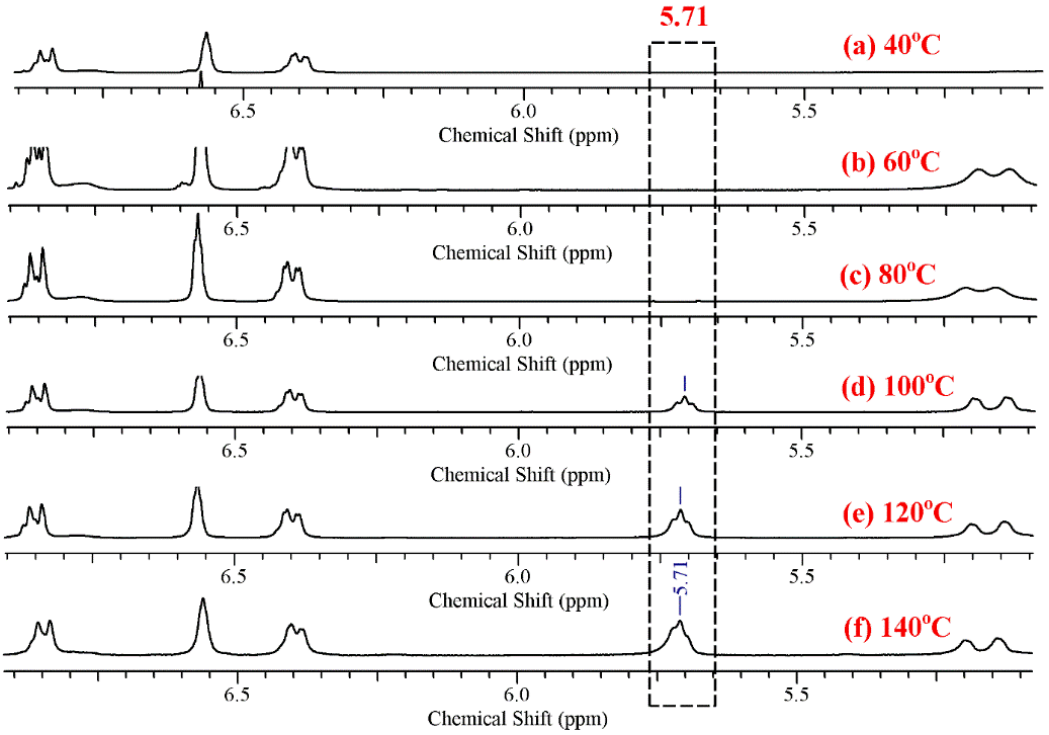

Figure 2.10. *^{1}H NMR spectrum of PHUs prepared at different temperatures.*

2.3.3 Synthesis of PHU series

The PHUs have been considered attractive and safer varieties of conventional polyurethanes (PUs). To improve the requirement of green and sustainable chemistry herein, we propose the synthesis and utilization of cyclic carbonate monomers majorly derived from vanillin, a lignin derivative, and CO_2 for the development of PHUs. In this regard, a step-growth polyaddition reaction between dicarbonate monomer with six aliphatic diamines of various chain lengths was conducted at 80 °C for 24 h utilizing TBD as a catalyst and NMP as a solvent (**Scheme 2.5**), and their impact on thermo-mechanical properties has been examined.

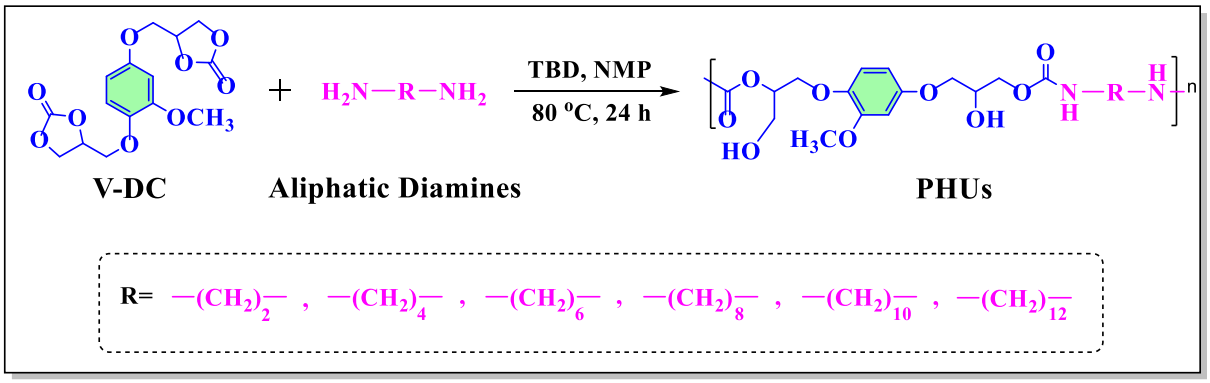

Scheme 2.5. *Syntheses of bio-based PHUs from vanillin-derived dicarbonate and diamines of different chain lengths.*

However, since the PHUs are enriched with pendant hydroxyl groups on their backbone which can promote adhesion. Therefore, the adhesion studies were carried out to evaluate the application potential of the above-synthesized PHUs. This study collectively demonstrates an attractive and environment-friendly pathway for developing novel PHU networks using renewable biobased resources and further explores its applicability as adhesives.

The photographs of the polymers are presented in **Figure 2.11**. It indicated that the viscous behavior of PHUs synthesized from shorter chain diamines (PHU1, PHU2, and PHU3) whereas, the solid nature of PHUs made from longer chain diamines (PHU4, PHU5, and PHU6).

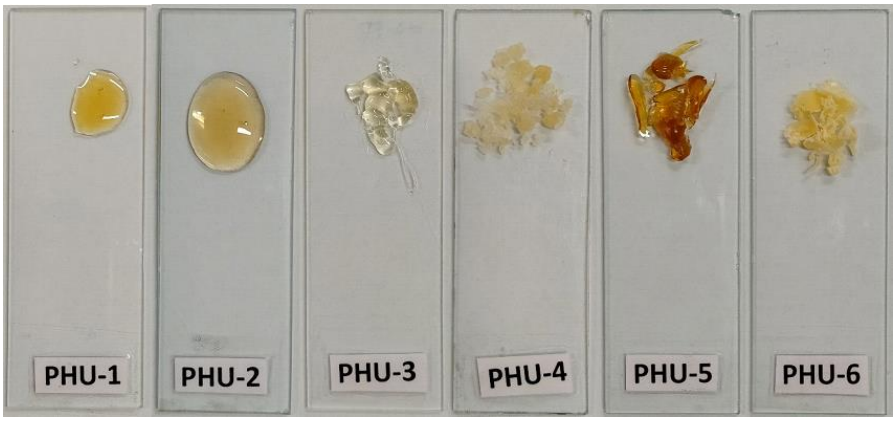

Figure 2.11. *Photographs of the synthesized PHUs.*

2.3.3.1 Spectral analysis of PHUs

The chemical structure of developed PHUs has been evaluated by FTIR and NMR (^{13}C, ^{1}H) spectroscopy. FTIR spectrum (**Figure 2.12**) indicated the existence of signals at 1703 cm^{-1} and 1468 cm^{-1}, which correlates to the C=O stretching and N-H bending of urethane linkages, respectively, while the broad signal at 3375 cm^{-1}, relates to the OH and NH stretch.[31] Moreover, the lack of the absorption band of the carbonyl of the carbonate group at 1787 cm^{-1} reveals the conversion of DC monomer, indicating the formation of PHUs. The ^{1}H NMR spectra of synthesized materials are displayed in **Figure 2.13**, confirming the successful synthesis of PHUs. The formation of urethane bonds (N-H signal) by ring-opening polymerization of cyclic dicarbonate and amine was confirmed by the appearance of signals between 7.10 and 7.21 ppm.[29,31] In fact, the ring opening of cyclic dicarbonates often occurs in two pathways giving two signals, due to the formation of both primary and secondary hydroxyl groups.[35,36]

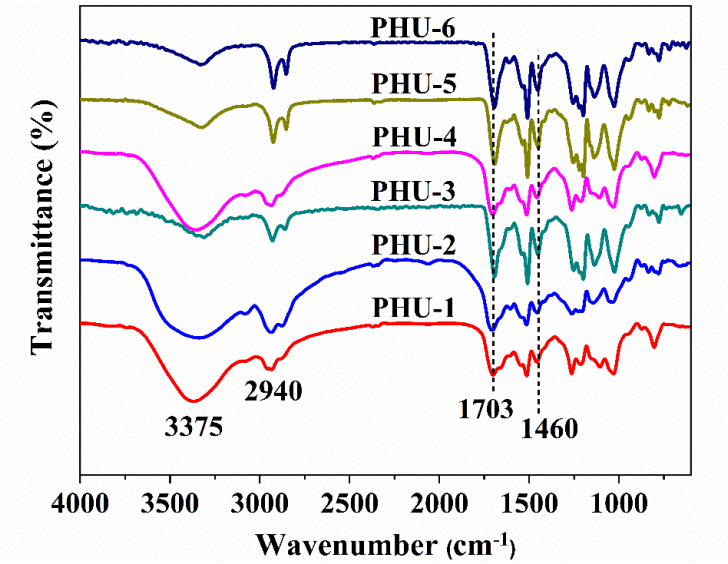

Figure 2.12. *FTIR spectrum of PHUs.*

The ratio of the primary to secondary hydroxyl groups ($R_{P/S}$) has been calculated from the ^{1}H NMR by integrating the protons of the urethane NH (i.e., $R_{P/S}$ for PHU-2 obtained 0.32/0.98 = 25/75), and also by integrating the hydroxyl signal at 4.35-4.92 ppm and at 4.86–5.20 ppm (i.e., $R_{P/S}$ for PHU-2 obtained 0.41/1.06 = 28/72). The determined values of ratios from both signals are included in **Table 2.3.** The results indicate that PHUs are equipped with more secondary hydroxyl groups than primary ones. This can be attributed to the presence of electron-withdrawing groups such as $PhOCH_2$, which favors the better transition and stabilization of the secondary hydroxyl group during the polymerization hence favoring the formation of a higher number of secondary hydroxyl groups.[32]

Furthermore, the aliphatic hydrocarbons (diamine precursors) in PHUs (except for PHU-1) displayed the two types of protons in the ^{1}H NMR spectra, where the alpha protons to the urethane NH were observed at 2.95 ppm while the remaining protons of the aliphatic hydrocarbons appeared in the area of 1.22-1.38 ppm.[29,37] However, in the case of PHU-1, only one signal appeared around 2.95 ppm from the alpha protons adjacent to the urethane NH.[29,37] Moreover, the NMR signals for the protons related to the opening of the five-membered cyclic carbonate were observed at 3.57-4.87 ppm.[29] The ^{13}C NMR spectra are presented in **Figure 2.14**. It revealed the existence of urethane functionality in all PHUs by showing the signal of carbonyl carbon at 156.6 ppm.[37] Both ^{1}H NMR and ^{13}C NMR results confirm the formation of PHU of the desired structure.

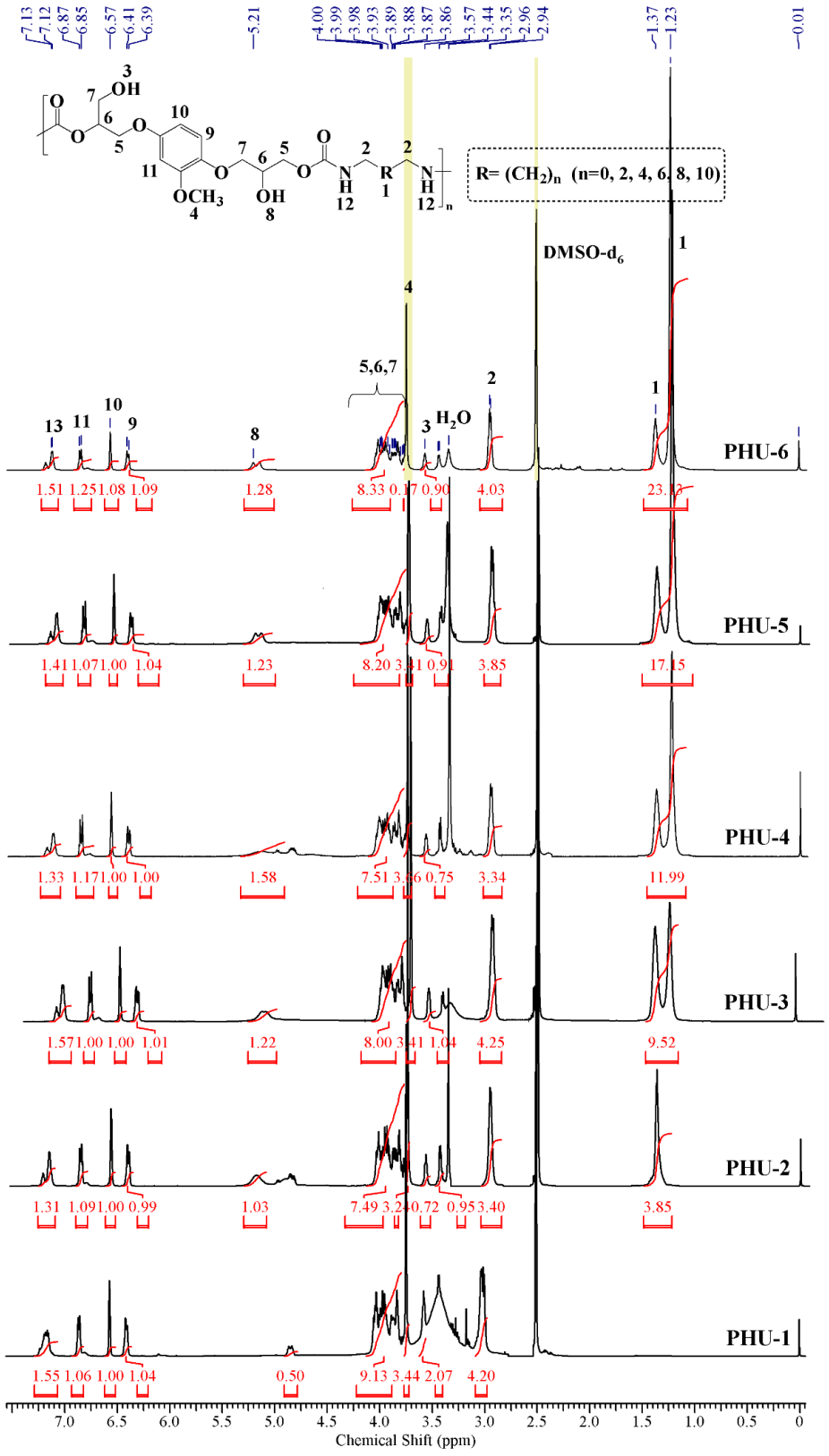

Figure 2.13. *^{1}H NMR spectrum of PHUs.*

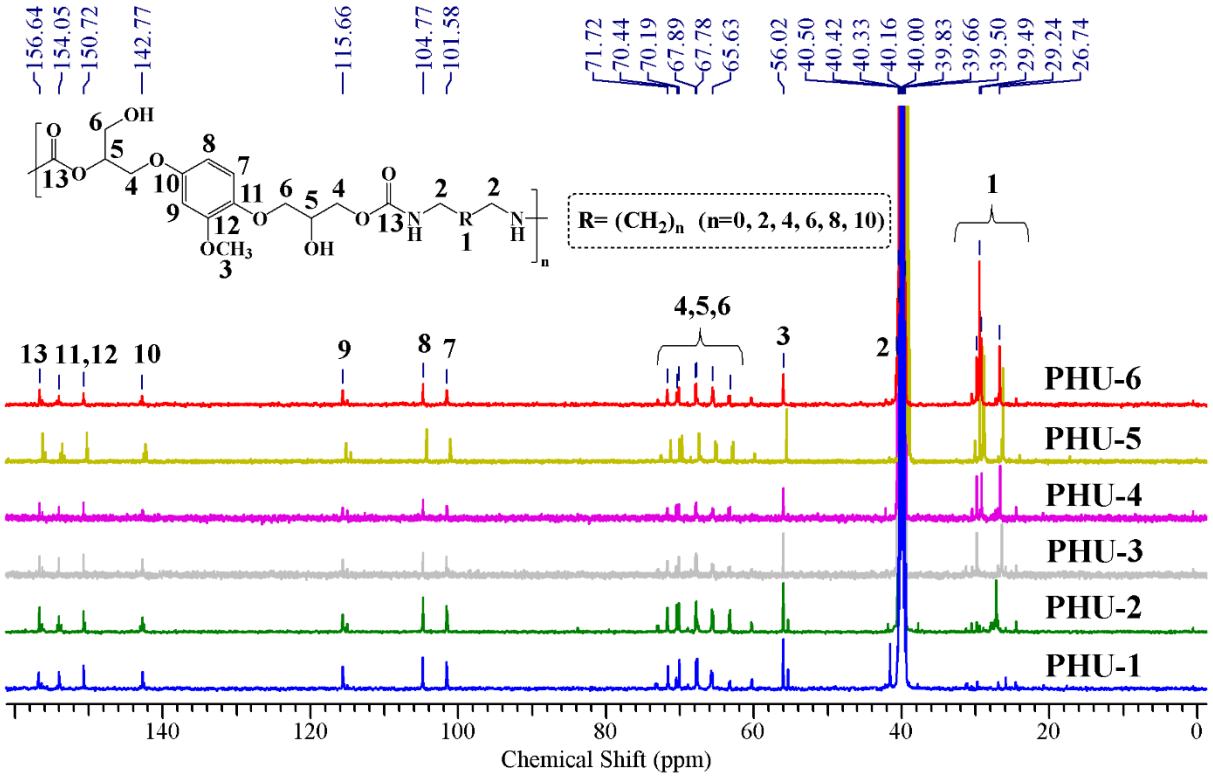

Figure 2.14. *^{13}C NMR spectrum of PHUs.*

Table 2.3. *Experimental data from SEC and ^{1}H NMR.*

Polymers	SEC			^{1}H NMR	
	M_n (g/mol)	M_w (g/mol)	Dispersity	$R_{P/S}$ [a]	$R_{P/S}$ [b]
PHU-1	2,500	2,600	1.03	-	-
PHU-2	4,000	8,100	2.03	28/72	25/75
PHU-3	4,900	8,800	1.77	19/81	24/76
PHU-4	11,100	23,200	2.08	22/78	24/76
PHU-5	6,000	9,100	1.50	19/81	24/76
PHU-6	5,000	7,600	1.50	22/78	25/74

[a] Calculated from the primary and secondary hydroxyl group signals.

[b] Calculated from the urethane signals.

2.3.3.2 Molecular weight analysis of PHUs

The molecular weight of PHUs was determined by GPC and calibrated with PMMA standards, where DMF containing LiBr (0.1 %) was used as the mobile phase. Molecular weights (M_n) of resultant PHUs were observed to vary from 2500 to 11,100 g/mol, and their dispersity was between 1.03 and 2.08 (**Table 2.3**). However, it has been observed that the synthesized PHUs

have a lower molecular weight and polydispersity. The inability of PHUs to achieve higher molecular weights has mainly been attributed to the formation of several oligomers [31] and side reactions during the reaction[11,38] and, secondly, due to the lower reactivity of cyclic carbonate leading to incomplete conversions.[34] Further GPC traces of PHUs further validate the formation of the oligomers, other than a monomodal curve, a multimodel curve was observed for all PHUs (**Figure 2.15**).

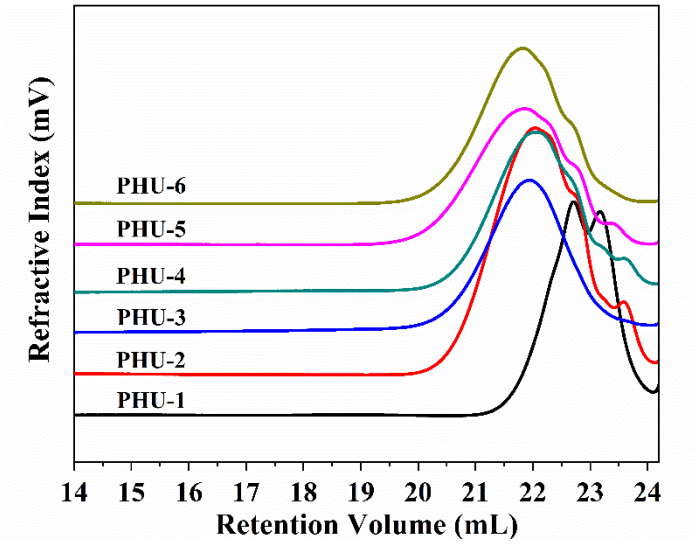

Figure 2.15. *GPC curves of developed PHUs.*

2.3.3.3 Thermal properties of PHUs

The thermal properties of PHUs were determined by DSC and TGA analysis and the results are summarized in **Table 2.4**. DSC measurements indicated the amorphous nature of the resulting PHUs (**Figure 2.16**). The glass transition temperature (T_g) values of the developed PHUs were found to vary in the range of 28 to 42 °C and were found to depend on the chemical structure of diamines. As the length of incorporated diamine in PHU increased, the flexibility of the polymer chain improved, leading to decreased T_g values.[39,40] Moreover, PHUs synthesized from shorter chain diamines can lead to the formation of higher density of hydrogen bonds, which in turn can increase the rigidity of chains.[41] So, the T_g of PHUs with shorter chain diamines was found to be higher than those of PHUs with longer chain diamines.

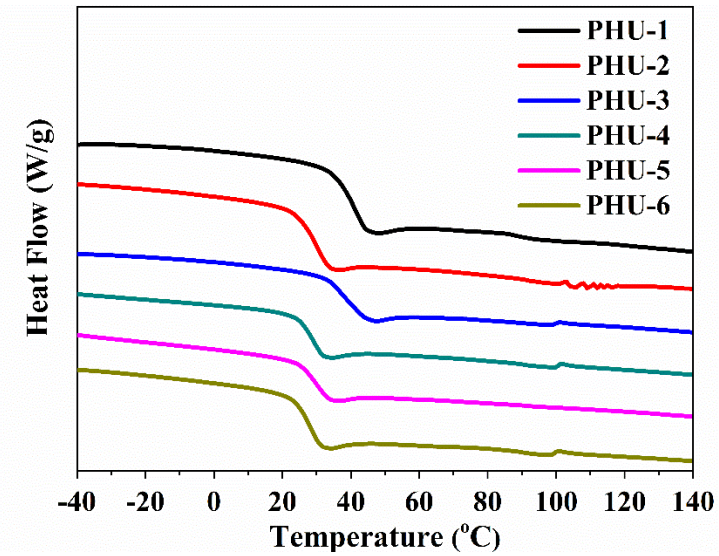

***Figure 2.16**. The second heating curves of PHUs were obtained from DSC.*

Thermogravimetric analyses have been performed to examine the thermal stability of the produced PHU systems. The decomposition temperature after 10 % weight loss ($T_{d,10\%}$) is listed in **Table 2.4** and the corresponding thermograms of all PHUs are depicted in **Figure 2.17a**. The results demonstrated that the developed PHUs remained stable up to 180 °C and primarily exhibited two-step degradation, and the results were similar to those of the previously reported study.[42]

***Table 2.4**. Thermal properties of PHUs.*

Polymers	DSC	TGA
	T_g (°C)	$T_{d,10\%}$ (°C)
PHU-1	42	180
PHU-2	31	214
PHU-3	38	265
PHU-4	30	234
PHU-5	30	247
PHU-6	28	273

However, the curves of first-step degradation corresponded to the decomposition of urethane linkages, whereas the curves of second degradation were related to hydrocarbons of the PHU backbones (aliphatic and aromatic moieties) (**Figure 2.17b**).[43,44] Moreover, it was observed that the chemical nature of diamines influenced the thermal stability of PHUs, and the thermal stability of PHUs was found to increase as the diamine chain length increased.[42,45]

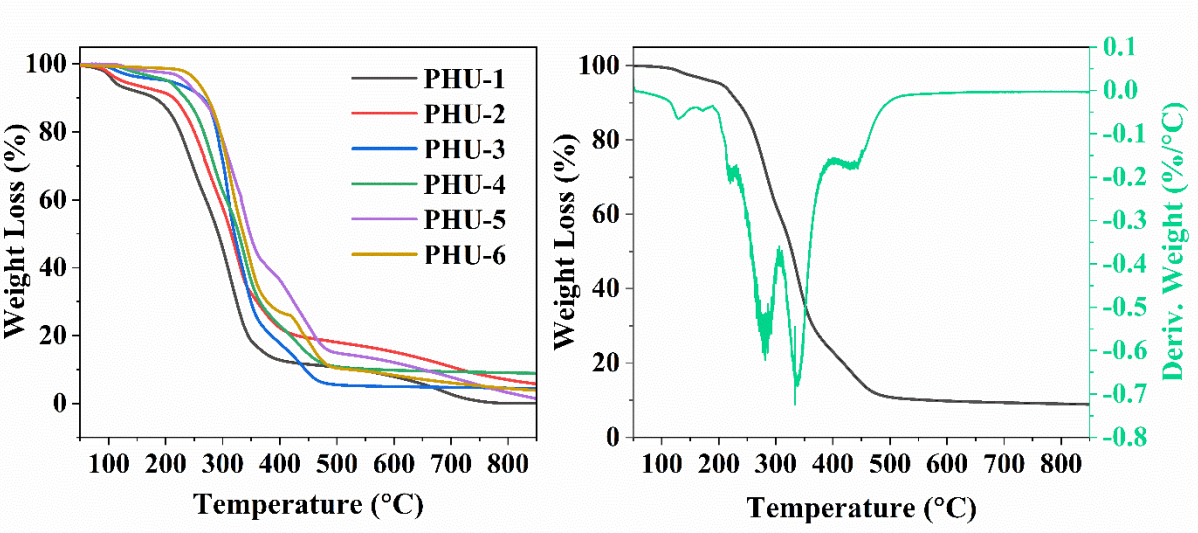

Figure 2.17. *TGA results of PHUs (a) TGA thermograms (b) DTG curves of PHU-4.*

2.3.3.4 Adhesive properties of PHUs

The application potential of the above synthesized PHU was further explored by evaluating the adhesion performance. It will always be advantageous if the above synthesized bio-based PHU from vanillin can exhibit adhesive properties alternative to traditional petroleum-based products because of its inherent bioactivity, and it represents an inexhaustible resource of monomers.[20,21] Hence, to determine the adhesive performance of synthesized materials, we have performed the lap shear measurements on the aluminum (Al) and stainless steel (SS) substrate by employing single lap joints (ASTM D1002). The examined PHUs revealed adhesive strength in the range of 0.0025 to 1.65 MPa for aluminum substrate whereas it was in the range of 0.0025 to 2.24 MPa for SS substrates (**Table 2.5, Figure 2.18**). Interestingly, PHU-4 demonstrated better shear strength on both substrates. This enhanced performance of PHU4 can be attributed to their high molecular weight, which resulted in a higher number of primary and secondary hydroxyl groups (hydrogen bonding) and more units of aromatic moieties (π–π interactions), leading to enhanced adhesion properties.[14,46] However, the shear test was not performed in the case of PHU-1 since the flowable nature of the material prevented it from adhering to the substrate. Further, to explore the adhesive's repeated applicability, the lap shear-tested substrates (aluminum) were rejoined under similar conditions as of the first application, and measurements were made (**Table 2.5, Figure 2.18**).

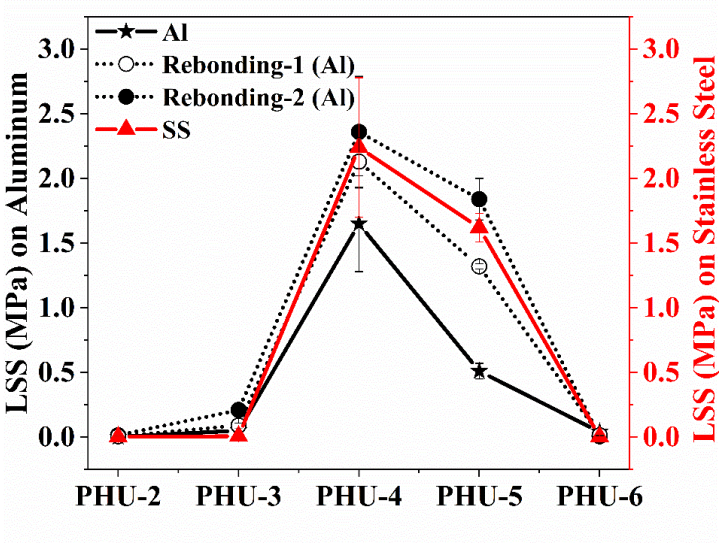

Figure 2.18. *Lap shear strength of PHUs evaluated on aluminum and stainless-steel substrates. The error bars show the representative standard deviation of each sample set of five samples.*

Table 2.5. *Lap shear strength of PHUs evaluated on aluminum and stainless-steel substrates.*

PHUs	Lap shear strength (MPa)			
	Aluminum			Stainless steel
	Original	Rebonding 1	Rebonding 2	
PHU-1	-	-	-	-
PHU-2	0.0025±0.0	0.0066±0.0	0.014±0.0	0.0025±0.0
PHU-3	0.05±0.0	0.09±0.0	0.21±0.0	0.0071±0.0
PHU-4	1.65±0.3	2.13±0.2	2.36±0.4	2.24±0.5
PHU-5	0.51±0.0	1.32±0.0	1.84±0.2	1.62±0.1
PHU-6	0.04±0.0	0.014±0.0	0.0065±0.0	0.0031±0.0

The rebonded PHUs exhibited comparable or better adhesive strength to their original adhesives.[47] In addition to the adhesive strength, the nature of the adhesive failure was also examined by visual inspection of samples. The mixture of cohesive and adhesive failure was observed in PHU-4, which has the highest adhesion strength (**Figure 2.19**). In contrast, cohesive failure was noted in all other PHUs.[14] Even though a few articles explored the applicability of PHUs as adhesives, the dicarbonates utilized for synthesizing these PHUs mainly depend on non-renewable material and often involve further modifications or crosslinking to achieve better adhesive strength.[46–51]

Additionally, the load vs. displacement curves were added in **Figure 2.20** (AL), **and Figure 2.21** (SS).

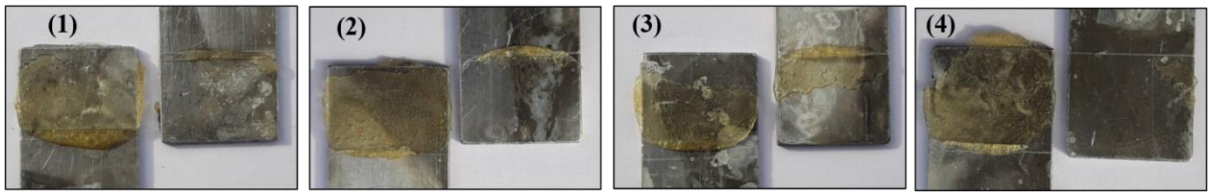

Figure 2.19. *Fractured test specimen showing the mixture of cohesive and adhesive failure of PHU-4.*

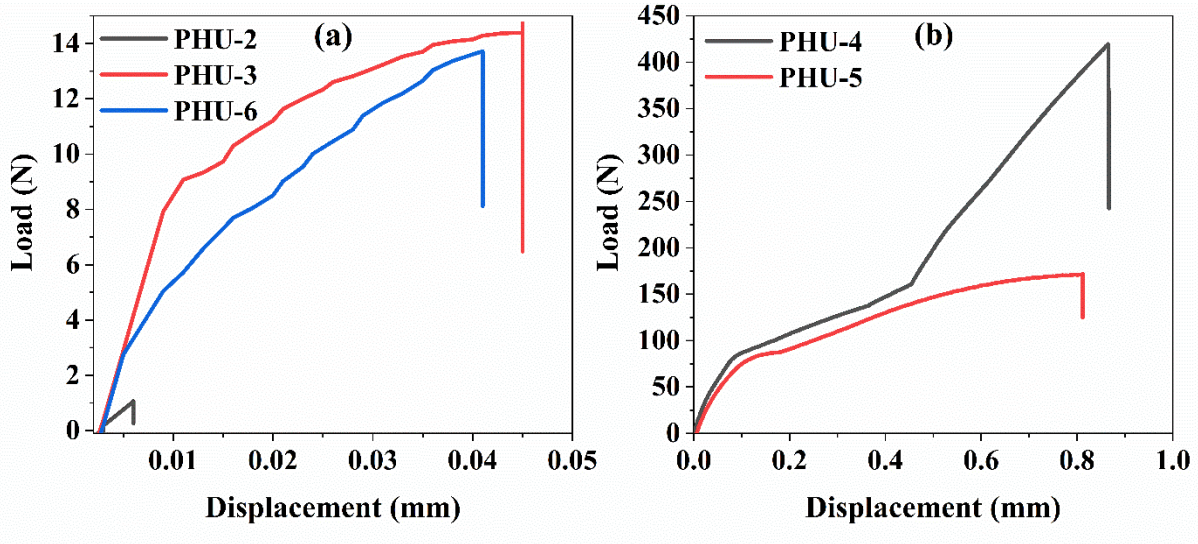

Figure 2.20. *Load vs displacement curves of (a) PHU-2, PHU-3, PHU-6 and (b) PHU-4, PHU-5 were evaluated for aluminum substrates.*

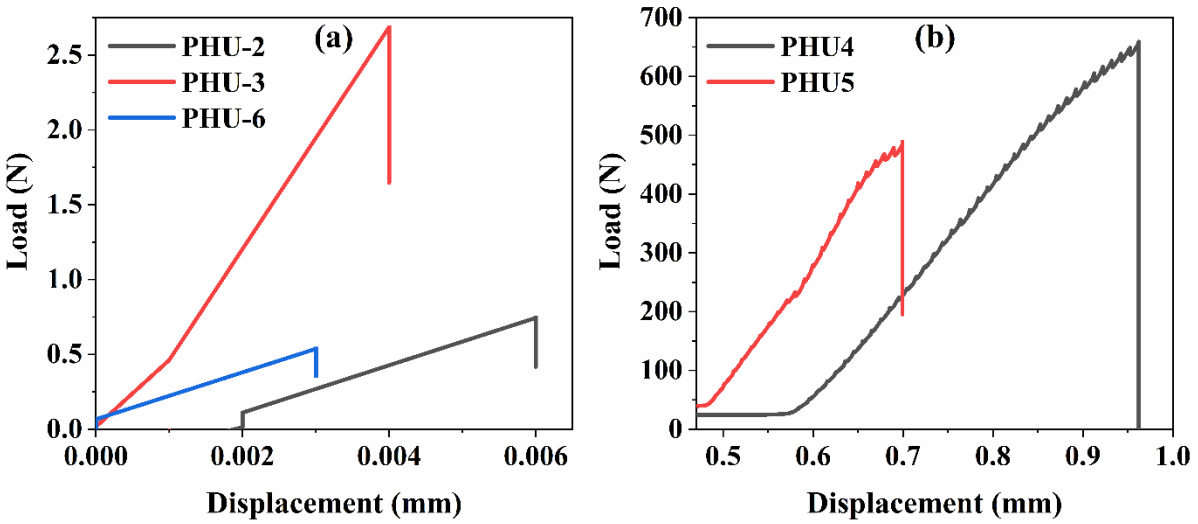

Figure 2.21. *Load vs displacement curves of (a) PHU-2, PHU-3, PHU-6 and (b) PHU-4, PHU-5 were evaluated for stainless steel substrates.*

2.4 Conclusion

In this work, renewable cyclic dicarbonates of vanillin derived by the chemical fixation of greenhouse gas carbon dioxide were reacted with diamines of different chain lengths, yielding a wide range of PHUs. Further, the chemical structure of the diamine strongly influenced the thermal properties, where PHUs with longer chain diamines exhibited lower T_g values than those with shorter chain diamines, leading to flexible and rigid materials. Structural evaluation of PHUs revealed the ring opening of cyclic dicarbonates led to the formation of both primary and secondary hydroxyl groups, which was significantly found to affect the adhesive properties of the polymer. Indeed, the material exhibited an impressive repeatable adhesion strength after several bonding and rebonding studies. Overall, this study highlights the potential of utilizing renewable biobased monomers derived from vanillin for developing PHUs suitable as adhesives

2.5 References

(1) Ellen MacArthur Foundation and World Economic Forum The New Plastics Economy: Rethinking the future of plastics. *Ellen MacArthur Found.* **2016**, 120.

(2) Das, A.; Mahanwar, P. A Brief Discussion on Advances in Polyurethane Applications. *Adv. Ind. Eng. Polym. Res.* **2020**, *3* (3), 93–101.

(3) W. Wang, C. Wang, *Polyurethane for biomedical applications: A review of recent developments,* University of Minnesota, USA, 2012.

(4) Akindoyo, J. O.; Beg, M. D. H.; Ghazali, S.; Islam, M. R.; Jeyaratnam, N.; Yuvaraj, A. R. Polyurethane Types, Synthesis and Applications-a Review. *RSC Adv.* **2016**, *6* (115), 114453–114482.

(5) Joseph, J.; Patel, R. M.; Wenham, A.; Smith, J. R. Biomedical Applications of Polyurethane Materials and Coatings. *Trans. Inst. Met. Finish.* **2018**, *96* (3), 121–129.

(6) https://www.precedenceresearch.com/polyurethane-market (13 May 2023).

(7) Bello, D.; Herrick, C. A.; Smith, T. J.; Woskie, S. R.; Streicher, R. P.; Cullen, M. R.; Liu, Y.; Redlich, C. A. Skin Exposure to Isocyanates: Reasons for Concern. *Environ. Health Perspect.* **2007**, *115* (3), 328–335.

(8) Maisonneuve, L.; Lamarzelle, O.; Rix, E.; Grau, E.; Cramail, H. Isocyanate-Free Routes to Polyurethanes and Poly(Hydroxy Urethane)S. *Chem. Rev.* **2015**, *115* (22), 12407–12439.

(9) Wołosz, D.; Parzuchowski, P. G.; Świderska, A. Synthesis and Characterization of the

Non-Isocyanate Poly(Carbonate-Urethane)s Obtained via Polycondensation Route. *Eur. Polym. J.* **2021**, *155*, 110574.

(10) Dong, W.; Yoshida, Y.; Endo, T. Synthesis of Poly(Hydroxyurethane) from 5-Membered Cyclic Carbonate under Mild Conditions in the Presence of Bicyclic Guanidine and Their Reaction Process. *J. Polym. Sci.* **2021**, *59* (6), 502–509.

(11) Besse, V.; Camara, F.; Méchin, F.; Fleury, E.; Caillol, S.; Pascault, J. P.; Boutevin, B. How to Explain Low Molar Masses in PolyHydroxyUrethanes (PHUs). *Eur. Polym. J.* **2015**, *71*, 1–11.

(12) Pronoitis, C.; Hakkarainen, M.; Odelius, K. Solubility-Governed Architectural Design of Polyhydroxyurethane-: Graft -Poly(ϵ-Caprolactone) Copolymers. *Polym. Chem.* **2021**, *12* (2), 196–208

(13) Blain, M.; Cornille, A.; Boutevin, B.; Auvergne, R.; Benazet, D.; Andrioletti, B.; Caillol, S. Hydrogen Bonds Prevent Obtaining High Molar Mass PHUs. *J. Appl. Polym. Sci.* **2017**, *134* (45), 1–13.

(14) Panchireddy, S.; Grignard, B.; Thomassin, J.-M.; Jerome, C.; Detrembleur, C. Catechol Containing Polyhydroxyurethanes as High-Performance Coatings and Adhesives. *ACS Sustain. Chem. & Eng.* **2018**, *6* (11), 14936–14944.

(15) Younes, G. R.; Marić, M. Bio-Based Thermoplastic Polyhydroxyurethanes Synthesized from the Terpolymerization of a Dicarbonate and Two Diamines: Design, Rheology, and Application in Melt Blending. *Macromolecules* **2021**, *54* (21), 10189–10202.

(16) Aguirresarobe, R. H.; Nevejans, S.; Reck, B.; Irusta, L.; Sardon, H.; Asua, J. M.; Ballard, N. Healable and Self-Healing Polyurethanes Using Dynamic Chemistry. *Prog. Polym. Sci.* **2021**, *114*, 101362.

(17) Leitsch, E. K.; Beniah, G.; Liu, K.; Lan, T.; Heath, W. H.; Scheidt, K. A.; Torkelson, J. M. Nonisocyanate Thermoplastic Polyhydroxyurethane Elastomers via Cyclic Carbonate Aminolysis: Critical Role of Hydroxyl Groups in Controlling Nanophase Separation. *ACS Macro Lett.* **2016**, *5* (4), 424–429.

(18) Bobbink, F. D.; Van Muyden, A. P.; Dyson, P. J. En Route to CO2-Containing Renewable Materials: Catalytic Synthesis of Polycarbonates and Non-Isocyanate Polyhydroxyurethanes Derived from Cyclic Carbonates. *Chem. Commun.* **2019**, *55* (10), 1360–1373.

(19) Saravanan, A.; Senthil kumar, P.; Vo, D. V. N.; Jeevanantham, S.; Bhuvaneswari, V.; Anantha Narayanan, V.; Yaashikaa, P. R.; Swetha, S.; Reshma, B. A Comprehensive Review on Different Approaches for CO_2 Utilization and Conversion Pathways. *Chem.*

Eng. Sci. **2021**, *236*, 116515.

(20) Fache, M.; Boutevin, B.; Caillol, S. Vanillin Production from Lignin and Its Use as a Renewable Chemical. *ACS Sustain. Chem. Eng.* **2016**, *4* (1), 35–46.

(21) Fache, M.; Darroman, E.; Besse, V.; Auvergne, R.; Caillol, S.; Boutevin, B. Vanillin, a Promising Biobased Building-Block for Monomer Synthesis. *Green Chem.* **2014**, *16* (4), 1987–1998.

(22) Fanjul-Mosteirín, N.; Fonseca, L. P.; Dove, A. P.; Sardon, H. Bio-Based Non-Isocyanate Poly(Hydroxy Urethane)s (PHU) Derived from Vanillin and CO_2. *Mater. Adv.* **2023**, *4* (11), 2437–2448.

(23) Zhang, C.; Madbouly, S. A.; Kessler, M. R. Renewable Polymers Prepared from Vanillin and Its Derivatives. *Macromol. Chem. Phys.* **2015**, *216* (17), 1816–1822.

(24) Engelen, S.; Wróblewska, A. A.; De Bruycker, K.; Aksakal, R.; Ladmiral, V.; Caillol, S.; Du Prez, F. E. Sustainable Design of Vanillin-Based Vitrimers Using Vinylogous Urethane Chemistry. *Polym. Chem.* **2022**, 1–18.

(25) Ecochard, Y.; Leroux, J.; Boutevin, B.; Auvergne, R.; Caillol, S. From Multi-Functional Siloxane-Based Cyclic Carbonates to Hybrid Polyhydroxyurethane Thermosets. *Eur. Polym. J.* **2019**, *120* (August), 109280.

(26) Kayan, A. Copolymerization Reactions of Butadiene Monoxide with 3-Glycidyloxypropyltrimethoxysilane and Styrene Oxide and Their Glycol Derivatives. *J. Appl. Polym. Sci.* **2019**, *136* (14), 1–7.

(27) Duraibabu, D.; Alagar, M.; Kumar, S. A. Studies on Mechanical, Thermal and Dynamic Mechanical Properties of Functionalized Nanoalumina Reinforced Sulphone Ether Linked Tetraglycidyl Epoxy Nanocomposites. *RSC Adv.* **2014**, *4* (76), 40132–40140.

(28) González, M. G.; Cabanelas, J. C.; Baselga, J. Applications of FTIR on Epoxy Resins - Identification, Monitoring the Curing Process, Phase Separation and Water Uptake. *Infrared Spectrosc. - Mater. Sci. Eng. Technol.* **2012**, *2*..

(29) Ma, Z.; Li, C.; Fan, H.; Wan, J.; Luo, Y.; Li, B. G. Polyhydroxyurethanes (PHUs) Derived from Diphenolic Acid and Carbon Dioxide and Their Application in Solvent- and Water-Borne PHU Coatings. *Ind. Eng. Chem. Res.* **2017**, *56* (47), 14089–14100.

(30) Mokhtari, C.; Malek, F.; Manseri, A.; Caillol, S.; Negrell, C. Reactive Jojoba and Castor Oils-Based Cyclic Carbonates for Biobased Polyhydroxyurethanes. *Eur. Polym. J.* **2019**, *113*, 18–28.

(31) Ménard, R.; Caillol, S.; Allais, F. Chemo-Enzymatic Synthesis and Characterization of Renewable Thermoplastic and Thermoset Isocyanate-Free Poly(Hydroxy)Urethanes

from Ferulic Acid Derivatives. *ACS Sustain. Chem. Eng.* **2017**, *5* (2), 1446–1456.

(32) Tomita, H.; Sanda, F.; Endo, T. Model Reaction for the Synthesis of Polyhydroxyurethanes from Cyclic Carbonates with Amines: Substituent Effect on the Reactivity and Selectivity of Ring-Opening Direction in the Reaction of Five-Membered Cyclic Carbonates with Amine. *J. Polym. Sci. Part A Polym. Chem.* **2001**, *39* (21), 3678–3685.

(33) Yuen, A.; Bossion, A.; Gómez-Bengoa, E.; Ruipérez, F.; Isik, M.; Hedrick, J. L.; Mecerreyes, D.; Yang, Y. Y.; Sardon, H. Room Temperature Synthesis of Non-Isocyanate Polyurethanes (NIPUs) Using Highly Reactive N-Substituted 8-Membered Cyclic Carbonates. *Polym. Chem.* **2016**, *7* (11), 2105–2111.

(34) Ecochard, Y.; Caillol, S. Hybrid Polyhydroxyurethanes : How to Overcome Limitations and Reach Cutting Edge Properties. *Eur. Polym. J.* **2020**, 109915.

(35) Steblyanko, A.; Choi, W.; Sanda, F.; Endo, T. Addition of Five-Membered Cyclic Carbonate with Amine and its Application to Polymer Synthesis. *J. Polym. Sci. Part A Polym. Chem.* **2000**, *38*, 2375

(36) Tomita, H.; Sanda, F.; Endo, T. Structural Analysis of Polyhydroxyurethane Obtained by Polyaddition of Bifunctional Five-Membered Cyclic Carbonate and Diamine Based on the Model Reaction. *J. Polym. Sci. Part A Polym. Chem.* **2001**, *39* (6), 851–859.

(37) Anders, T.; Keul, H.; Möller, M. Synthesis and Characterization of Polyhydroxyurethanes Prepared from Difunctional Six-Membered Ring Carbonates. *Des. Monomers Polym.* **2011**, *14* (6), 593–608.

(38) Bossion, A.; Aguirresarobe, R. H.; Irusta, L.; Taton, D.; Cramail, H.; Grau, E.; Mecerreyes, D.; Su, C.; Liu, G.; Müller, A. J.; Sardon, H. Unexpected Synthesis of Segmented Poly(Hydroxyurea-Urethane)s from Dicyclic Carbonates and Diamines by Organocatalysis. *Macromolecules* **2018**, *51* (15), 5556–5566.

(39) Ubaghs, L.; Fricke, N.; Keul, H.; Höcker, H. Polyurethanes with Pendant Hydroxyl Groups: Synthesis and Characterization. *Macromol. Rapid Commun.* **2004**, *25* (3), 517–521.

(40) Benyahya, S.; Habas, J. P.; Auvergne, R.; Lapinte, V.; Caillol, S. Structure-Property Relationships in Polyhydroxyurethanes Produced from Terephthaloyl Dicyclocarbonate with Various Polyamines. *Polym. Int.* **2012**, *61* (11), 1666–1674.

(41) Beniah, G.; Fortman, D. J.; Heath, W. H.; Dichtel, W. R.; Torkelson, J. M. Non-Isocyanate Polyurethane Thermoplastic Elastomer: Amide-Based Chain Extender Yields Enhanced Nanophase Separation and Properties in Polyhydroxyurethane.

Macromolecules **2017**, *50* (11), 4425–4434.

(42) Duval, C.; Kébir, N.; Jauseau, R.; Burel, F. Organocatalytic Synthesis of Novel Renewable Non-Isocyanate Polyhydroxyurethanes. *J. Polym. Sci. Part A Polym. Chem.* **2016**, *54* (6), 758–764.

(43) Behnam, R.; Roghani-Mamaqani, H.; Salami-Kalajahi, M.; Mardani, H. Effect of Aliphatic and Aromatic Chain Extenders on Thermal Stability of Graphene Oxide/Polyurethane Hybrid Composites Prepared by Sol-Gel Method. *ChemistrySelect* **2020**, *5* (3), 962–967.

(44) Wang, C.; Auad, M. L.; Marcovich, N. E.; Nutt, S.; Si, À. Synthesis and Characterization of Organically Modified Attapulgite / Polyurethane Nanocomposites. *Journal of Applied Polymer Science,* **2008**, *109*, 2562.

(45) Van Velthoven, J. L. J.; Gootjes, L.; Van Es, D. S.; Noordover, B. A. J.; Meuldijk, J. Poly(Hydroxy Urethane)s Based on Renewable Diglycerol Dicarbonate. *Eur. Polym. J.* **2015**, *70*, 125–135.

(46) Sukumaran Nair, A.; Cherian, S.; Balachandran, N.; Panicker, U. G.; Kalamblayil Sankaranarayanan, S. K. Hybrid Poly(Hydroxy Urethane)s: Folded-Sheet Morphology and Thermoreversible Adhesion. *ACS Omega* **2019**, *4* (8), 13042–13051.

(47) Gomez-Lopez, A.; Ayensa, N.; Grignard, B.; Irusta, L.; Calvo, I.; Müller, A. J.; Detrembleur, C.; Sardon, H. Enhanced and Reusable Poly(Hydroxy Urethane)-Based Low Temperature Hot-Melt Adhesives. *ACS Polym. Au* **2022**, *2* (3), 194–207.

(48) Cornille, A.; Michaud, G.; Simon, F.; Fouquay, S.; Auvergne, R.; Boutevin, B.; Caillol, S. Promising Mechanical and Adhesive Properties of Isocyanate-Free Poly(Hydroxyurethane). *Eur. Polym. J.* **2016**, *84*, 404–420.

(49) Gomez-lopez, A.; Grignard, B.; Detrembleur, C.; Sardon, H. Monocomponent Non-Isocyanate Polyurethane Adhesives Based on a Sol − Gel Process. *ACS Appl. Polym. Mater*. **2020**, *2*, 1839.

(50) Gomez-Lopez, A.; Grignard, B.; Calvo, I.; Detrembleur, C.; Sardon, H. Synergetic Effect of Dopamine and Alkoxysilanes in Sustainable Non-Isocyanate Polyurethane Adhesives. *Macromol. Rapid Commun.* **2021**, *42* (3), 1–9

(51) Gomez-Lopez, A.; Grignard, B.; Calvo, I.; Detrembleur, C.; Sardon, H. Accelerating the Curing of Hybrid Poly(Hydroxy Urethane)-Epoxy Adhesives by the Thiol-Epoxy Chemistry. *ACS Appl. Polym. Mater.* **2022**, *4* (12), 8786–8794.

Chapter 3

Biobased Reusable Poly(HydroxyUrethane) Hot-Melt Adhesives with Potential Chemical Degradability

3.1 Introduction

Adhesives play a significant role in numerous fields of human endeavor, ranging from basic repairs to advanced engineering.[1] Based on the practical implementations, adhesives mainly involve solvent-based adhesives, two-component adhesives, and hot melt adhesives in practice.[2] Even though widely employed from a sustainable and environmental point of view solvent-based adhesives, and two-component adhesives are not much feasible due to pollution arising from solvent vapors and residual quantities of curing agents and monomers. Hot-melt adhesives (HMAs) are a promising green alternative to other adhesives due to their solvent-free nature, ease of use, and cost-effectiveness. These characteristics make them a popular adhesive choice in various industries, including aerospace, automotive, textile, electronics, and packaging.[3] In fact, the growing demand for HMA is driving the global market to expand, and it is projected to achieve USD 11.4 billion by 2027.[4] Among the polymers used for hot melt adhesives, polyurethanes are commonly chosen for creating high-quality hot melt adhesives due to their diverse formulation options, better low-temperature properties, greater flexibility, and excellent adhesion on low-surface roughness material.[3] The global polyurethane hot-melt adhesive market is valued at USD 1311 million in 2021 and is projected to reach USD 2537 million by 2030.[5] However, the synthesis of these PUs entirely depends on fossil fuels and involves using hazardous chemicals such as isocyanates as well as the precursors used for its production such as phosgene is a major drawback of the system.[6] Furthermore, the current forms of PU-HMAs are not environmentally friendly as they are non-biodegradable and most of the material ends up in landfills, resulting in economic and energy losses.

Scientific efforts to produce sustainable PU-HMAs have led to the development of non-isocyanate polyurethanes (PHUs), a promising substitute to conventional PUs as it restricts the usage of allergenic and carcinogenic isocyanates.[7] Additionally, the monomers used in PHUs can be created from precursors utilizing CO_2, an abundant and inexhaustible resource, making the method more sustainable and safer to handle than conventional PU-based HMAs.[8] Despite the recent advancements in the field of PHU-based adhesives, most studies rely on non-renewable fossil fuels to synthesize cyclic carbonate and diamine.[9-13] Moreover, most of these studies concentrate on developing thermoset adhesives that are not reworkable, recyclable, or biodegradable, making disposal/recycling of discarded adhesive products difficult.[14-18] Although limited studies have explored the development of sustainable PHU-HMAs by utilizing bio-derived monomers, they have not yet received much attention as they exhibit inferior adhesion properties and limited recyclable and biodegradable properties.[19-21]

Obviously, there is a need for PHU-HMA systems based on bio-renewable monomers, which are reprocessable and could achieve good adhesion and biodegradation properties.

Efforts to develop sustainable PHUs have led to the utilization of vanillin and isosorbide molecules, which are environmentally friendly, economically viable, sustainable, and produced on an industrial scale. A series of PHU-HMAs were synthesized by reacting different compositions of vanillin and isosorbide carbonates with priamine 1074. This study further explored the effect of structure on the thermal properties, mechanical properties, and adhesive behaviors of the PHUs. In addition to their improved sustainability, the unique molecular architecture of acetal-coupled di-vanillin utilized in the current study aided in the exploration of convenient degradation of PHU-HMAs, which can facilitate biodegradation or chemical recycling. Further, the adhesion strength, thermo-reversible adhesion properties, temperature tolerance, and adhesion under wet conditions of the developed PHUs have been investigated in detail to validate their potential as environmentally friendly and sustainable HMAs.

3.2 Experimental section

3.2.1 Materials

Vanillin (>98%), isosorbide (>98%), pentaerythritol (>98%), allyl bromide (>98%), tetrabutylammonium bromide (TBAB, >98 %), potassium peroxymonosulfate (oxone), and 1,5,7-triazabicyclo-[4.4.0] dec-5-ene (TBD, >98%) was purchased from the TCI Chemicals, India. Priamine 1074 was provided by the Croda, Netherlands. Epichlorohydrin (>99%) and para-toluene sulfonic acid monohydrate (pTSA.H_2O), were procured from Sigma Aldrich. Sodium hydroxide pellets (NaOH, 98%), hydrochloric acid (HCl, 35-38%), and petroleum ether were supplied by the S D fine chemical. Sodium sulfate (anhydrous, >99.5%, AR), ethyl acetate, and dichloromethane (DCM) were delivered by Leonid Chemicals. Dimethyl sulfoxide (DMSO-d_6, 99.80% D), acetone-d6, and chloroform (99.80% D) were purchased from Eurisotop. CO_2 gas cylinder (99.5%) was obtained from Vadilal Chemical. Sodium bicarbonate ($NaHCO_3$) was procured from SRL chemicals. N-methyl pyrrolidinone (NMP), and dimethylformamide (DMF) were distilled over CaH_2 under a nitrogen atmosphere and stored over molecular sieves (4Å). All chemicals were used as received unless specified.

3.2.2 Characterization techniques

The procedure and conditions described in Chapter 2 (Section 2.2.2) were similarly followed in this chapter for the structural, molecular weight, and thermal analysis of the synthesized compounds and polymers. These analyses were conducted using ^{1}H NMR, ^{13}C NMR, FTIR,

HRMS, GPC, DSC, and TGA. Additionally, the adhesive properties of the synthesized PHUs were evaluated using an Instron 33R4204 (load cell: 10 KN). For specimen preparation, 135 mg of polymer material was applied to the substrate surface, maintaining an adhesive contact area of 200 mm^2 (18 mm × 11.15 mm). The adhesive specimens were prepared by melting at 130 °C under gentle pressure. All other conditions were the same as those described in Chapter 2 (Section 2.2.2).

The X-ray diffraction (XRD) measurement was performed at room temperature using a Rigaku SmartLab X-ray Diffractometer equipped with Cu, Kα radiation source (operation at 40 kV and 30 mA, λ= 1.5406 nm). The data was recorded in the 2θ range from 5 to 50°. The water contact angle (WCA) was determined using a KRUSS instrument with droplets of MilliQ water (2 µL). The homogenous film was prepared prior to analysis by casting polymeric solutions (50 mg in one ml of chloroform) on the glass surface (75 × 25 mm). The slides were then kept at room temperature overnight to evaporate the chloroform slowly without leaving any air bubbles on the film. The measurements were made on dried homogeneous polymer film after drying at room temperature for 48 hours in a desiccator equipped with a high vacuum. To calculate the mean contact angle values, a minimum of five repeated measurements were taken at various locations on each PHU surface.

Oscillatory rheological measurements were performed on a stress-controlled rheometer (Physica MCR 301, Anton Paar, Austria) to study the viscoelastic behavior of PHUs. PHUs were subjected to sinusoidal oscillatory shear stress to study their visco-elastic response using parallel plate geometry (plate diameter, 25 mm). Strain sweep measurements were performed in the 1 to 10 % strain range at constant temperature (135 °C) and frequency (1 rad/s). Frequency sweep measurements were performed in the frequency range of 0.5 to 500 rad/s at constant temperature (135 °C) and strain (2.5 %). Temperature ramp measurements were performed in the 5 to 160 °C temperature range, at a constant frequency (10Hz) and strain (2.5 %). The resulting storage modulus, loss modulus, tan delta, and complex viscosity values are recorded and plotted. Tensile testing was performed at room temperature on an Instron 5944 (Load cell: 1 KN) at a speed of 20 $mm.min^{-1}$. The dog-bone-shaped samples were used for analysis, having the dimensions of length = 2.8 cm, and width = 1.2 cm (length and width of narrow fraction = 1.5 cm and 0.6 cm, respectively). The Young's modulus, tensile strength, and elongation at the break of each polymer were calculated using the average values of at least five specimens. Error represents one standard deviation.

3.2.3 Methods

3.2.3.1 Preparation of isosorbide-derived cyclic carbonate

The synthesis of isosorbide dicarbonate has been carried out in three steps using methods described elsewhere in the literature.[22,23]

3.2.3.1.1 Synthesis of isosorbide diallyl ether

In a 250 ml round bottom flask, 30 g of isosorbide (0.2052 mol), and 62.06 g of allyl bromide (0.513 mol) were added. Next, an aqueous solution of NaOH (20.52 g, 0.513 mol) was added dropwise, followed by the addition of 1.983 g of tetrabutylammonium bromide (TBAB, 6.155 mmol) as a phase transfer catalyst. The reaction was performed at 65 °C for 6 h. The obtained crude product was extracted with dichloromethane, dried with anhydrous sodium sulfate, and purified by column chromatography (yield: 76 %).

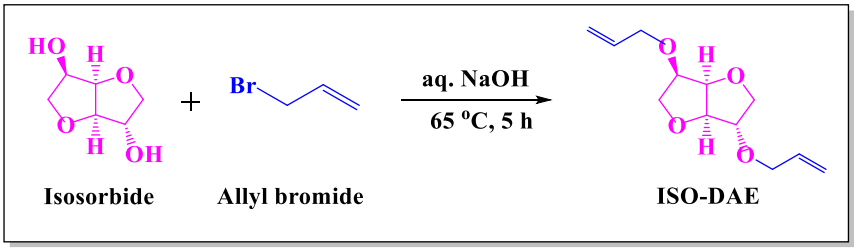

Scheme 3.1. *Synthesis of ISO-DAE.*

FTIR (cm^{-1}): 2980 (CH stretch), 1647 (C=C stretch).

^{1}H-NMR (500 MHz, $CDCl_3$) δ (ppm): 3.57 (t, 1H, isosorbide ring -C<u>H</u>), 3.89-4.05 (m, 5H, isosorbide ring -C<u>H</u>, and C<u>H</u>$_2$), 3.89-4.05 (m, 3H, C<u>H</u>$_2$-CH=CH$_2$), 4.16-4.20 (dd, 1H, C<u>H</u>$_2$-CH=CH$_2$), 4.48 (d, 1H, bridgehead -C<u>H</u>), 4.61 (t, 1H, bridgehead -C<u>H</u>), 5.15-5.30 (m, 4H, -C<u>H</u>$_2$=CH), 5.82-5.96 (m, 2H, -C<u>H</u>=CH$_2$).

^{13}C-NMR (500 MHz, $CDCl_3$) δ (ppm): 69.79-70.47 (-<u>C</u>H$_2$-O, isosorbide ring), 71.59-73.41 (-C=C-<u>C</u>H$_2$-O), 79.43-80.19 (-<u>C</u>H-O, isosorbide ring), 83.75-86.28 (-<u>C</u>H-O, bridgehead), 117.39-117.72 (-CH=<u>C</u>H$_2$-), 134.16-134.49 (-<u>C</u>H=CH$_2$-).

HRMS (ESI) m/z: $[M + H]^+$ calculated for $C_{12}H_{18}O_4$: 227.1283; found:227.1278.

3.2.3.1.2 Synthesis of isosorbide diglycidyl ether

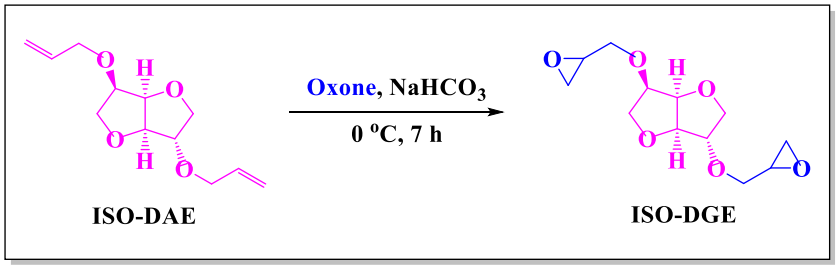

Scheme 3.2*. Preparation of ISO-DGE via epoxidation.*

The ISO-DAE compound (20 g, 0.088 mol) was dissolved in acetone (161 ml) and DI water (380 ml), and the solution was agitated at 0 °C 30 min (temperature was maintained using an ice bath). Afterward, oxone (155 g, 0.251 mol), and sodium bicarbonate (63.08 g, 0.750 mol) were added in three to four parts over the course of 1 h. After the addition, the reaction was allowed to run for 7 h while maintaining the temperature at 5 °C. Thus, obtained reaction mixture was filtered extracted with dichloromethane and purified by column chromatography to obtain the final product (yield: 86.33 %).

FTIR (cm^{-1}): 2980 (CH stretch), 905 (asymmetric C-O stretch, epoxy), 833 (symmetric C-O stretch, epoxy).

^{1}H-NMR (500 MHz, $CDCl_3$) δ (ppm): 2.54-2.61 (m, 2H, epoxy -C$\underline{H}_2$), 2.75-2.78 (m, 2H, epoxy -C$\underline{H}_2$), 3.08-3.18 (m, 2H, epoxy -C$\underline{H}$), 3.32-3.44 (m, 2H, -O-C$\underline{H}_2$), 3.75-3.83 (m, 2H, -O-CH_2), 3.75-3.80 (t, 1H, isosorbide ring -C$\underline{H}$), 3.87-4.01 (m, 5H, isosorbide ring -C$\underline{H}$, and CH_2), 4.47-4.50 (dd, 1H, bridgehead -C$\underline{H}$), 4.60-4.66 (m, 1H, bridgehead -C$\underline{H}$).

^{13}C-NMR (500 MHz, $CDCl_3$) δ (ppm): 44.02-44.19 (-$\underline{C}$H-O, epoxy), 50.53-50.78 (-$\underline{C}H_2$-O, epoxy), 69.79-70.35 (-$\underline{C}H_2$-O), 71.07-73.36 (-$\underline{C}H_2$-O, isosorbide ring), 80.16-80.63 (-$\underline{C}$H-O, isosorbide ring), 84.81-86.16 (-$\underline{C}$H-O, bridgehead).

HRMS (ESI) m/z: $[M + H]^+$ calculated for $C_{12}H_{18}O_6$: 259.1181; found: 259.1176.

3.2.3.1.3 Synthesis of isosorbide dicarbonate

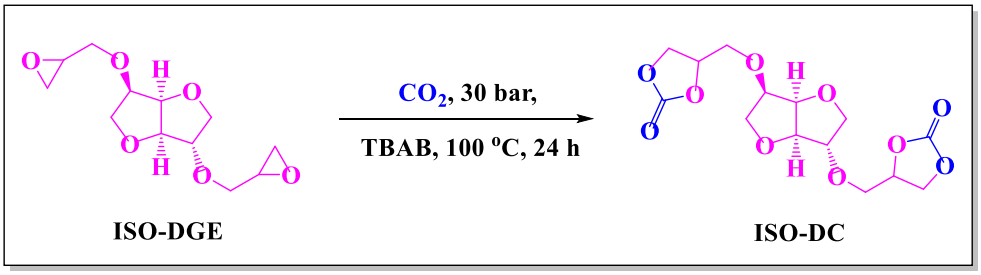

Scheme 3.3. *Synthesis of ISO-DC monomer through carbonation.*

ISO-DGE (11 g, 0.0318 mol) and TBAB catalyst (5 mol %) were dissolved in acetone and added into the 50 mL autoclave reactor. The reactor was pressurized with 20 bars of CO_2 and the mixture was heated at 100 °C for 24 h. Upon completion, the reactor was degassed and allowed to cool to room temperature. The crude product was concentrated, extracted with ethyl acetate, and purified by column chromatography using ethyl acetate and petroleum ether as eluents (yield: 83 %).

FTIR (cm^{-1}): 2980 (CH stretch), 1791 (carbonate C=O stretch).

^{1}H-NMR (500 MHz, $CDCl_3$) δ (ppm): 3.62-3.99 (m, 8H, isosorbide ring -C<u>H</u>, and C<u>H</u>$_2$), 4.05-4.41 (dd, 4H, carbonate -C<u>H</u>$_2$), 4.32-4.56 (dd, 4H, carbonate -C<u>H</u>$_2$), 4.84 (m, 2H, carbonate -C<u>H</u>).

^{13}C-NMR (500 MHz, $DMSOd_6$) δ (ppm): 66.46 (-<u>C</u>H$_2$-O, carbonate), 68.69-70.32 (-<u>C</u>H$_2$-O, isosorbide ring), 72.83-72.94 (-<u>C</u>H-O, carbonate), 75.74-75.94 (-<u>C</u>H$_2$-O), 80.24-80.59 (-<u>C</u>H-O, isosorbide ring), 84.52-85.87 (-<u>C</u>H-O, bridgehead), 155.36-155.43 (C=O, carbonate).

HRMS (ESI) m/z: $[M + H]^+$ calculated for $C_{14}H_{19}O_{10}$: 347.0978; found:347.0973.

3.2.3.2 Preparation of vanillin and pentaerythritol-derived cyclic carbonate

The synthesis of vanillin and pentaerythritol-derived dicarbonate was carried out in three steps.[24]

3.2.3.2.1 Synthesis of spiro-divanillin-diol

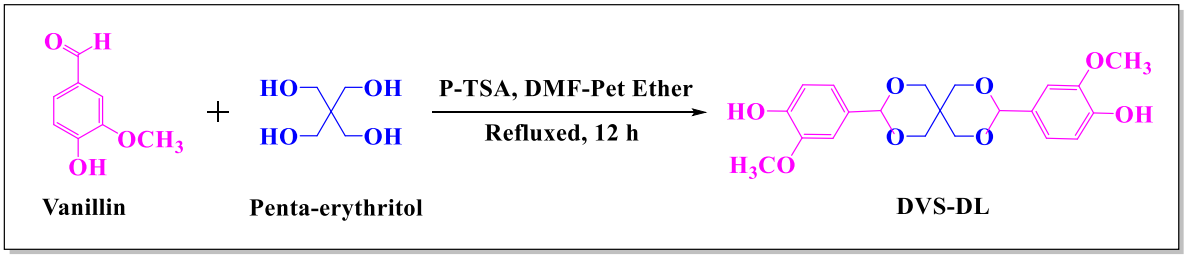

Scheme 3.4. *Procedure for synthesizing the DVS-DL compound.*

Vanillin (10 g, 0.02473 mol) and pentaerythritol (8.95 g, 0.06574 mol) were dissolved in a mixture of DMF (22 ml) and petroleum ether (24 ml) in an RB flask equipped with a reflux condenser and Dean-Stark trap. Then, p-toluenesulfonic acid monohydrate (pTSA.H2O, 0.38 g, 2 wt% of the total weight of vanillin and pentaerythritol) was added, and the reaction was carried out at 105 °C for 15 h. The L-shaped tube of the Dean-Stark trap was charged periodically throughout the reaction using a hot gun to increase the vapor speed towards the condenser. The white solid was precipitated with a 3 wt% aqueous solution of $NaHCO_3$, washed multiple times with water, and purified by precipitation in petroleum ether (yield: 56.43 %, m. p.: 170-171 °C).

FTIR (cm^{-1}): 3488 (OH stretch), 2872, 2969 (CH stretch), 1263 (spiroacetal C-O stretch), 1167 (spiroacetal C-O-C stretch).

^{1}H-NMR (500 MHz, $CDCl_3$) δ (ppm): 3.59 (d, 2H, spirocyclic -CH_2), 3.76 (t, 4H, spirocyclic -CH_2), 3.85 (s, 6H, OCH_3), 4.81 (d, 2H, spirocyclic -CH_2), 5.33 (s, 2H, spirocyclic -CH), 5.59 (s, 2H, aromatic -OH), 6.85 (d, 2H, aromatic -CH), 6.90 (d, 2H, aromatic -CH), 6.96 (s, 2H, aromatic -CH).

^{13}C-NMR (500 MHz, $CDCl_3$) δ (ppm): 32.46 (-C-$(CH_2)_4$-, spirocyclic), 55.94 (OCH_3), 70.59-71.08 (-$CH_2)_4$-O, spirocyclic), 102.29 (O-CH-O, spirocyclic), 108.26-119.51 (C-H, aromatic), 130.15 (C-CH, aromatic), 146.31-146.45 (C-O, aromatic).

HRMS (ESI) m/z: $[M + H]^+$ calculated for $C_{21}H_{24}O_8$: 405.1549; found:405.1544.

3.2.3.2.2 Synthesis of spiro-divanillin-diglycidyl ether (DVS-DGE)

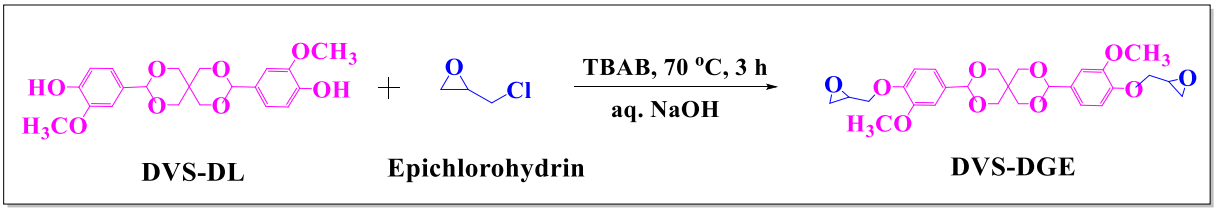

Scheme 3.5. *Epoxidation method for producing the DVS-DGE compound.*

DVS-DL (8.70 g, 0.0215 mol) was added to an RB flask equipped with a reflux condenser and magnetic stirrer followed by the addition of epichlorohydrin (79.64 g, 0.861 mol), and tetrabutylammonium bromide (TBAB, 10 wt%). The reaction was conducted at a temperature of 75 °C for a duration of 3 h. After completion, the reaction mixture was cooled to room temperature, following which a 50 % aqueous solution of NaOH weighing 5.16 g (0.129 mol) was added dropwise. The reaction was then allowed to continue for another 3 h while maintaining a temperature of around 16 °C to promote the ring-closing process. The resulting mixture was filtered, washed with DI water, and dried with anhydrous sodium sulfate. After that, it was precipitated with petroleum ether to obtain a white powder (yield: 72.86 %).

FTIR (cm^{-1}): 2989, 2872 (CH stretch), 1263 (spiroacetal C-O stretch), 1167 (spiroacetal C-O-C stretch), 921 (asymmetric C-O stretch, epoxy), 810 (symmetric C-O stretch, epoxy).

^{1}H-NMR (500 MHz, $CDCl_3$) δ (ppm): 2.73 (m, 2H, epoxy -C$\underline{H}_2$), 2.88 (m, 2H, epoxy -C$\underline{H}_2$), 3.37 (m, 2H, epoxy -C$\underline{H}$), 3.66 (m, 2H, C$\underline{H}_2$-OAr), 3.85 (m, 2H, C$\underline{H}_2$-OAr), 3.85 (m, 2H, spirocyclic -C$\underline{H}_2$), 3.89 (s, 6H, OC$\underline{H}_3$), 4.04 (m, 2H, spirocyclic -C$\underline{H}_2$), 4.22 (dd, 2H, spirocyclic -C$\underline{H}_2$), 4.84 (d, 2H, spirocyclic -C$\underline{H}_2$), 5.40 (s, 2H, spirocyclic -C$\underline{H}$), 6.92 (d, 2H, aromatic -C$\underline{H}$), 6.99 (d, 2H, aromatic -C$\underline{H}$), 7.04 (s, 2H, aromatic -C$\underline{H}$).

^{13}C-NMR (500 MHz, $CDCl_3$) δ (ppm): 32.49 (-$\underline{C}$-$(CH_2)_4$-, spirocyclic), 45.00 (CH_2-O, epoxy), 50.14 (CH-O, epoxy), 55.94 (O$\underline{C}H_3$), 70.26 ($\underline{C}H_2$-OAr), 70.58-71.07 (-$\underline{C}H_2)_4$-O, spirocyclic), 102.09 (O-$\underline{C}$H-O, spirocyclic), 109.51-118.70 ($\underline{C}$-H, aromatic), 131.76 ($\underline{C}$-CH, aromatic), 148.53-149.56 ($\underline{C}$-O, aromatic).

HRMS (ESI) m/z: $[M + H]^+$ calculated for $C_{27}H_{32}O_{10}$: 517.2073; found: 517.2068.

3.2.3.2.3 Synthesis of spiro-divanillin-dicarbonate

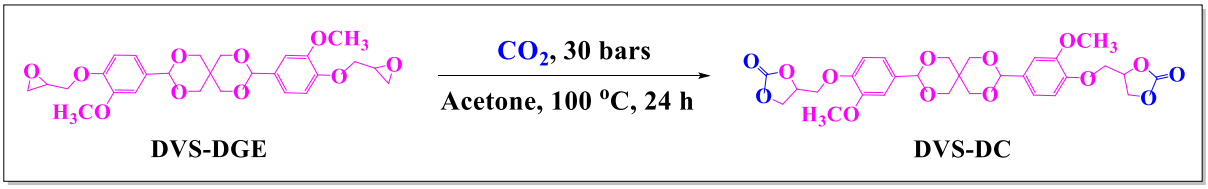

Scheme 3.6. Synthesis of the DVS-DC monomer by carbonation.

The DVS-DGE compound (10 g, 0.0166 mol) and TBAB catalyst (5 mol %) were dissolved in acetone and poured into the 100 mL autoclave reactor which was equipped with a mechanical stirrer and temperature controller. Next, 30 bars of CO_2 were introduced into the reactor and the reaction was performed at 100 °C for 24 h. After completion of the reaction, the reactor was degassed and cooled to room temperature. Then, the white solid was precipitated out by adding the reaction mixture to cold water. The crude product was purified by recrystallization in isopropanol (yield: 88 %).

FTIR (cm^{-1}): 2967, 2872 (CH stretch), 1790 (carbonate C=O stretch), 1263 (spiroacetal C-O stretch), 1167 (spiroacetal C-O-C stretch).

^{1}H-NMR (500 MHz, $CDCl_3$) δ (ppm): 3.64 (d, 2H, spirocyclic -C$\underline{H}_2$), 3.81 (dd, 4H, spirocyclic -C$\underline{H}_2$), 3.86 (s, 6H, OC$\underline{H}_3$), 4.20 (dd, 4H, carbonate -C$\underline{H}_2$), 4.60 (dd, 4H, carbonate -C$\underline{H}_2$), 4.80 (d, 2H, spirocyclic -C$\underline{H}_2$), 4.99 (m, 2H, carbonate -C$\underline{H}$), 5.41 (s, 2H, spirocyclic -C$\underline{H}$), 6.92 (d, 2H, aromatic -C$\underline{H}$), 7.01 (d, 2H, aromatic -C$\underline{H}$), 7.06 (s, 2H, aromatic -C$\underline{H}$).

^{13}C-NMR (500 MHz, $CDCl_3$) δ (ppm): 32.49 (-$\underline{C}$-$(CH_2)_4$-, spirocyclic), 55.93 (O$\underline{C}H_3$), 66.37 (CH_2-O, carbonate), 69.34 (CH-O, carbonate), 70.54-71.03 (-$\underline{C}H_2)_4$-O, spirocyclic), 74.34 ($\underline{C}H_2$-OAr), 101.83 (O-$\underline{C}$H-O, spirocyclic), 110.09-118.82 ($\underline{C}$-H, aromatic), 133.28 ($\underline{C}$-CH, aromatic), 147.92-150.26 ($\underline{C}$-O, aromatic), 154.71 (C=O, carbonate).

HRMS (ESI) m/z: $[M + Na]^+$ calculated for $C_{29}H_{32}O_{14}Na$: 627.1689; found: 627.1684.

3.2.3.3 General procedure for the synthesis of PHUs

The PHU polymers were prepared according to the compositions summarized in **Scheme 3.7**. The ratio between the cyclic carbonate (s), and priamine 1074, was maintained at 1:1. In a 50 mL RB flask, the cyclic carbonates, priamine 1074 and TBD (10 mol%) were added and mixed under an inert atmosphere. Next, the freshly distilled N-methyl-2-pyrrolidinone (2 mL per g) was added.[25] The resulting solution was polymerized under continuous stirring at 80 °C for 24 h. The polymers were precipitated in cold water and further purified using dichloromethane

and petroleum ether. The obtained material was named PHU-*x*, the '*x'* represents the mole percentages of the aromatic DVS-DC, with respect to ISO-DC in the polymers.

3.2.3.4 Acid degradability of PHUs

The acid-induced degradation of DVS-DC monomer and PHU polymers was examined in HCl/H_2O solution at room temperature. To carry out the experiment, 10 mg of DVS-DC was dissolved in an acetone/H_2O mixture (9:1, v/v) in NMR tubes. Subsequently, different concentrations of HCl (0.1, 1.0, and 2.0 mol/L) were added and ^{1}H NMR was recorded while Samples treated with acetone/H_2O (9:1, v/v) alone served as the control. Further, the degradation of PHUs was analyzed by subjecting them (200 mg) to acid degradation in a 1 mol/L HCl solution. The degradation was monitored for up to 49 days at 7-day intervals by measuring the percentage mass loss, and for 1, 7, 14, and 21 days using ^{1}H NMR and FTIR spectroscopy.

3.3 Result and Discussion

3.3.1 Preparation of isosorbide-derived cyclic carbonate

The isosorbide-derived dicarbonate was synthesized in three steps. The first step involved the allylation of isosorbide with allyl bromide at 65 °C for 6 h, using NaOH as a base and TBAB as a phase transfer catalyst (**Scheme 3.1**). This was followed by oxidation with Oxone and carbonation with CO_2. Finally, the dicarbonate monomer was obtained with a total yield of 54.43 %. The FTIR, ^{1}H NMR, and ^{13}C NMR spectroscopies have been used to confirm the structure of synthesized compounds.

The FT-IR spectrum is depicted in (**Figure 3.1**). The characteristics band for the allyl group (C=C-C) was observed at 1647 cm^{-1} which corresponds to the unsaturated C=C bonds. This suggested that the diallyl ether of isosorbide was successfully formed. The absorption band was observed at 2980 cm^{-1}, which corresponds to the C-H stretching of the isosorbide ring. Additionally, the ^{1}H NMR spectrum of ISO-DAE is presented in **Figure 3.2** along with assignments. The proton of the isosorbide ring was labeled as 1, 1′, 2, 2′ and the CH_2 protons were marked as 3, 3′ and displayed multiplets in the range of 3.59 to 4.25 ppm. The singlets observed at 4.51, and 4.63 ppm are due to bridgehead protons of the isosorbide ring (represented as 4, 5), respectively. The protons labeled as 6, 6′, and 7, 7′ of the allyl group exhibited multiplets at 5.20-5.32 and 5.90-5.95 ppm, respectively. All the proton signals collectively confirmed the successful formation of ISO-DAE. Nevertheless, the **Figure 3.3**

presents the ^{13}C NMR spectra of ISO-DAE. The NMR signals appeared at 117.3 and 134.1 ppm (labeled as 5, 5′ and 6, 6′) further demonstrating the existence of allyl functionality in the compound.

The diallyl compound was converted into the di-epoxide compound (ISO-DGE) via oxidation in the second step and was then characterized using FTIR, ^{1}H NMR, and ^{13}C NMR spectroscopies (**Scheme 3.2**). **Figure 3.1** shows the FTIR spectra of the ISO-DGE. The characteristic band at 905 and 833 cm^{-1} for the asymmetric C-O stretch and the symmetric C-O stretch of the epoxy ring, respectively, indicated the successful synthesis of ISO-DGE. Further, the C-H stretching vibration is represented by the absorption band seen at 2980 cm^{-1}. After the oxidation of the ISO-DAE compound, the signal of allyl protons in ^{1}H NMR spectra (**Figure 3.4**) disappeared at 5.20-5.32 and 5.90-5.95 ppm and the new signals appeared in the region of 2.58 to 3.60 ppm, suggesting the transformation of allyl groups into epoxy rings. The methylene protons (CH_2) of epoxy rings showed two multiplets: one at 2.58-2.61 (labeled as 1) and another at 2.78-2.80 ppm (labeled as 1′). The methine protons (CH) of epoxy rings also showed multiplets at 3.08-3.18 ppm (labeled as 1). Further, the CH_2 protons which are adjacent to the epoxy rings exhibited multiplets slightly at higher values (at 3.32-3.83 ppm; labeled as 3, 3′) due to the electron-withdrawing effect of the oxygen group. However, the proton of the bicyclic ring labeled as 4, 4′, 5, 5′ displayed multiplets in the range of 3.78 to 4.01 ppm. The bridgehead protons (marked as 6, 7) showed the multiplets at 4.49 and 4.66 ppm. The ^{13}C NMR spectrum of ISO-DGE is presented in **Figure 3.5**. The disappearance of allyl signals at 117.3 and 134.1 ppm (**Figure 3.3**) and the appearance of epoxy signals at 44.02, 50.53, and 69.79 ppm (labeled as 1, 1′, 2, 2′, and 3, 3′) demonstrate the creation of epoxy compounds (ISO-DGE).

The chemical structure of the prepared isosorbide-derived carbonate monomer (ISO-DC) was confirmed by using ^{1}H, ^{13}C, and FTIR spectroscopy (**Scheme 3.3**). FTIR analysis (**Figure 3.1**) revealed absorption bands around 1791 cm^{-1}, indicating the presence of carbonyl groups of carbonate rings.[19,26] Moreover, the absorption band at 2980 was attributed to the C-H stretching vibration. The **Figure 3.6** provides the ^{1}H NMR spectrum of the ISO-DC. According to ^{1}H NMR spectra, the epoxy signals completely disappeared at 2.56, 2.80, 3.18, 3.46, and 3.81 ppm, and the new carbonate signals appeared at 4.05-4.41 (labeled as 4, 4′), 4.32-4.56 (labeled as 5, 5′), and 4.84 ppm (labeled as 6, 6′), demonstrating the complete transformation of isosorbide diglycidyl ether into dicarbonate compound.[10] However, the skeletal protons of the bicyclic ring were obtained in the area of 3.62-3.99 ppm.[26] Along with FTIR and ^{1}H NMR, the ^{13}C NMR spectroscopy also provides essential information on the existence of carbonyl groups.

The ^{13}C NMR spectrum of the ISO-DC (**Figure 3.7**) displayed the additional signal at 155.36, which corresponded to the carbonyl carbon of dicarbonate compounds.[30,31]

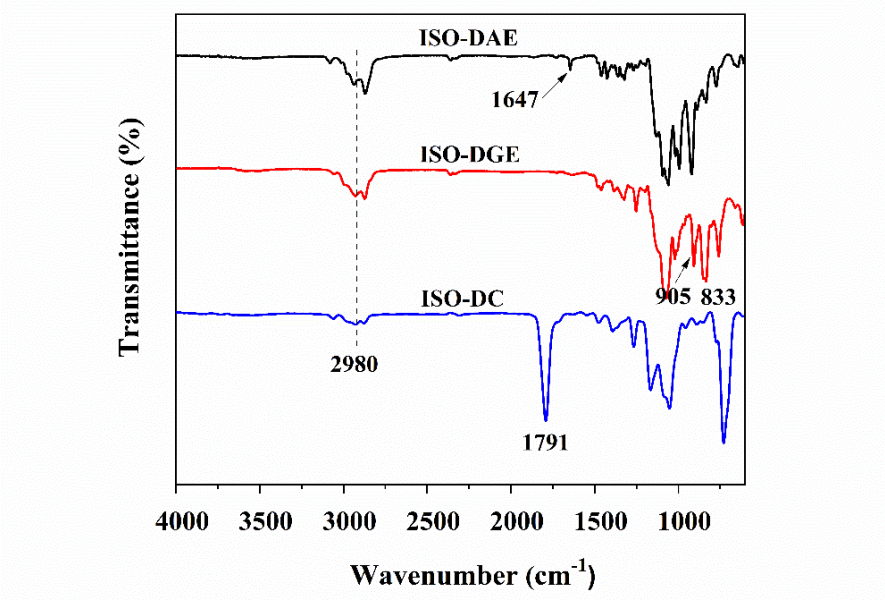

***Figure 3.1**. FTIR spectrum of ISO-DL, ISO-DGE, and ISO-DC compounds.*

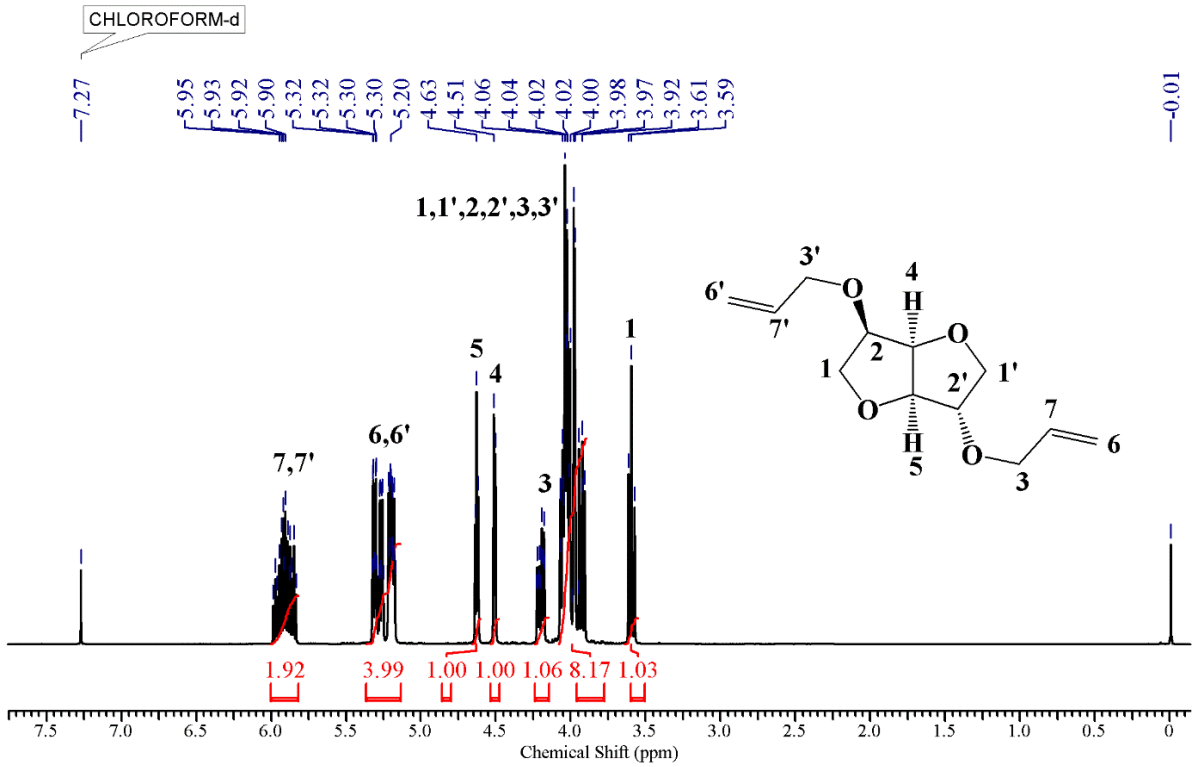

***Figure 3.2.** ^{1}H NMR spectrum of ISO-DAE.*

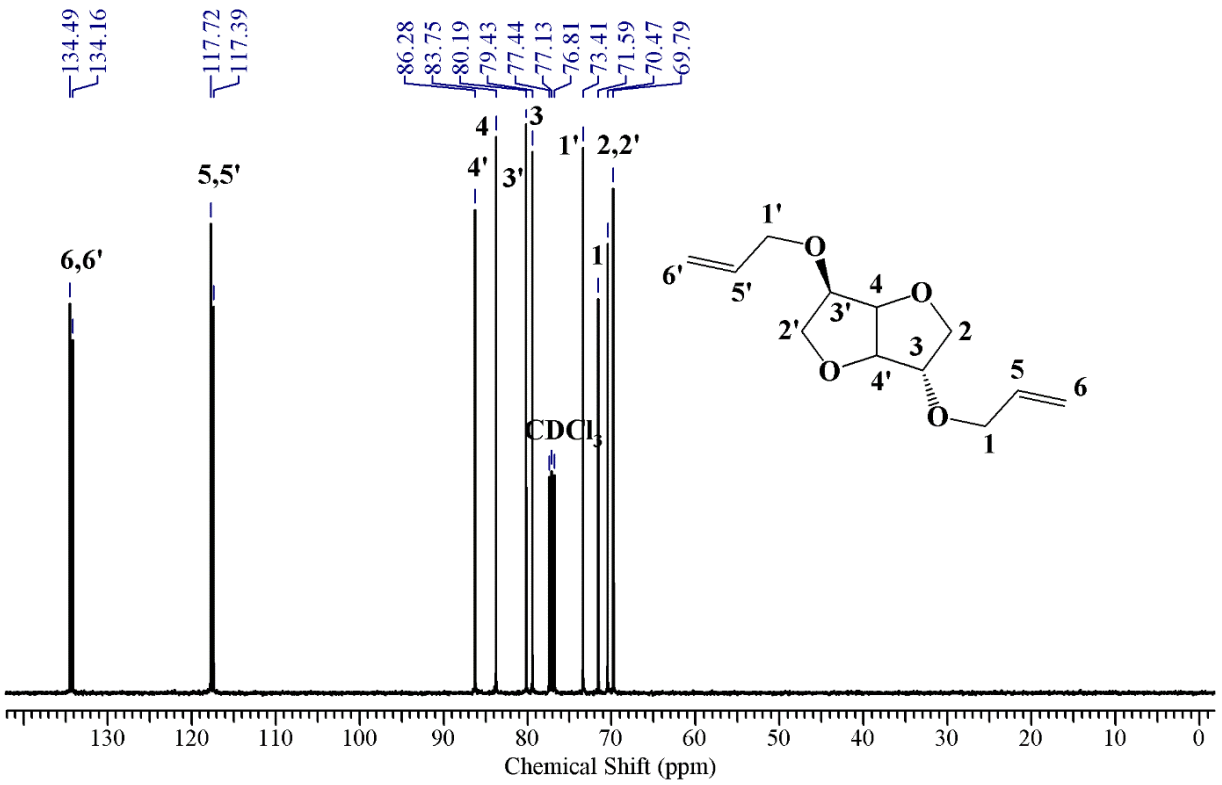

Figure 3.3. *^{13}C NMR spectrum of ISO-DAE.*

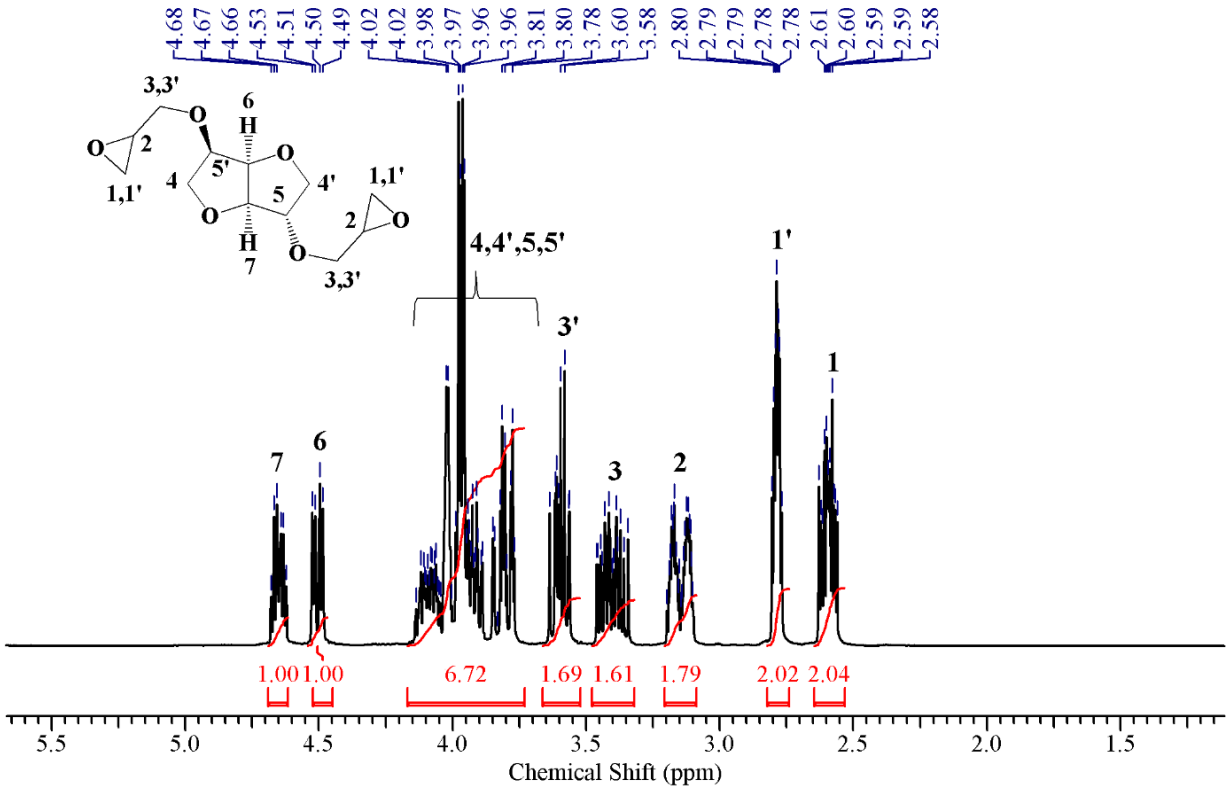

Figure 3.4. *^{1}H NMR spectrum of ISO-DGE.*

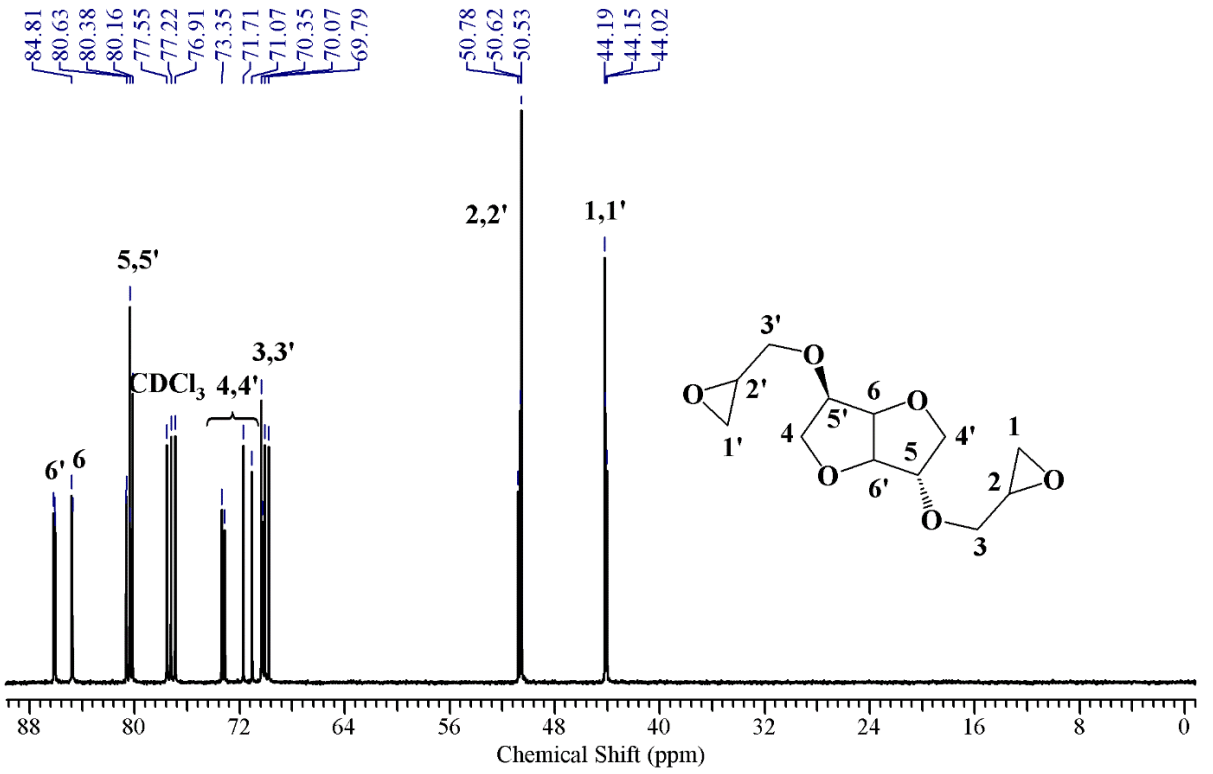

Figure 3.5. *^{13}C NMR spectrum of ISO-DGE.*

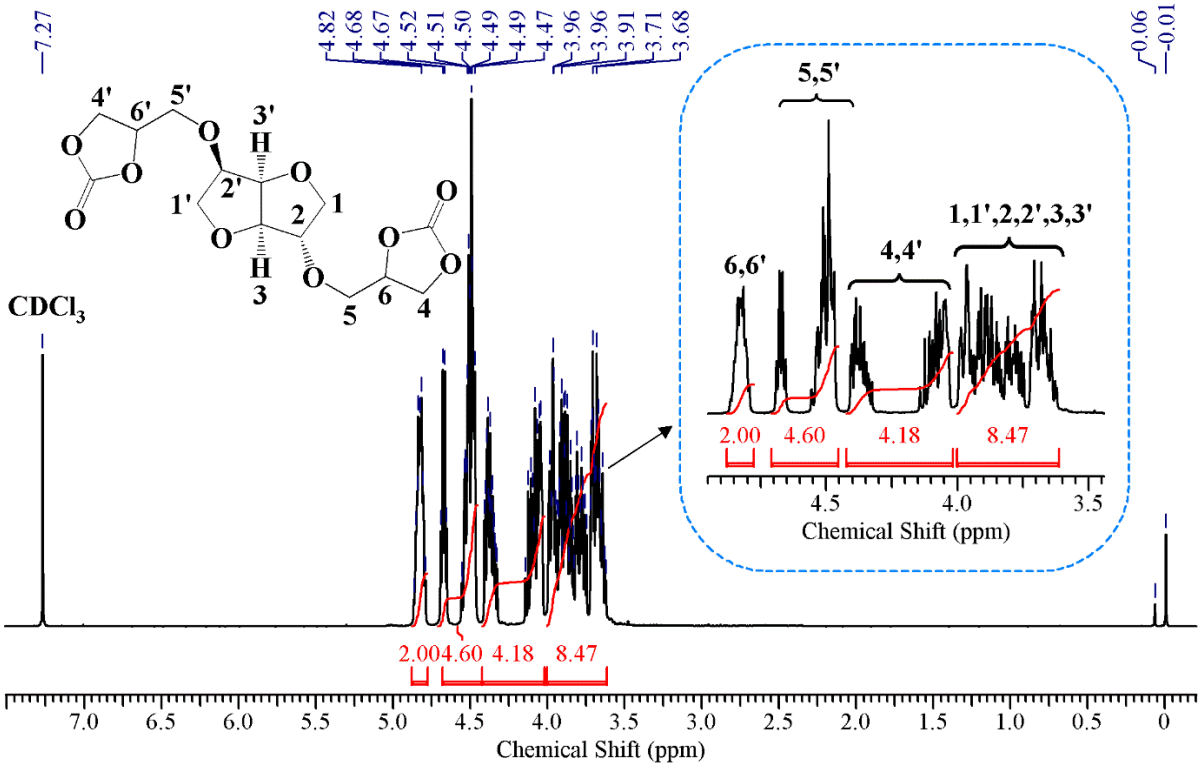

Figure 3.6. *^{1}H NMR spectrum of ISO-DC.*

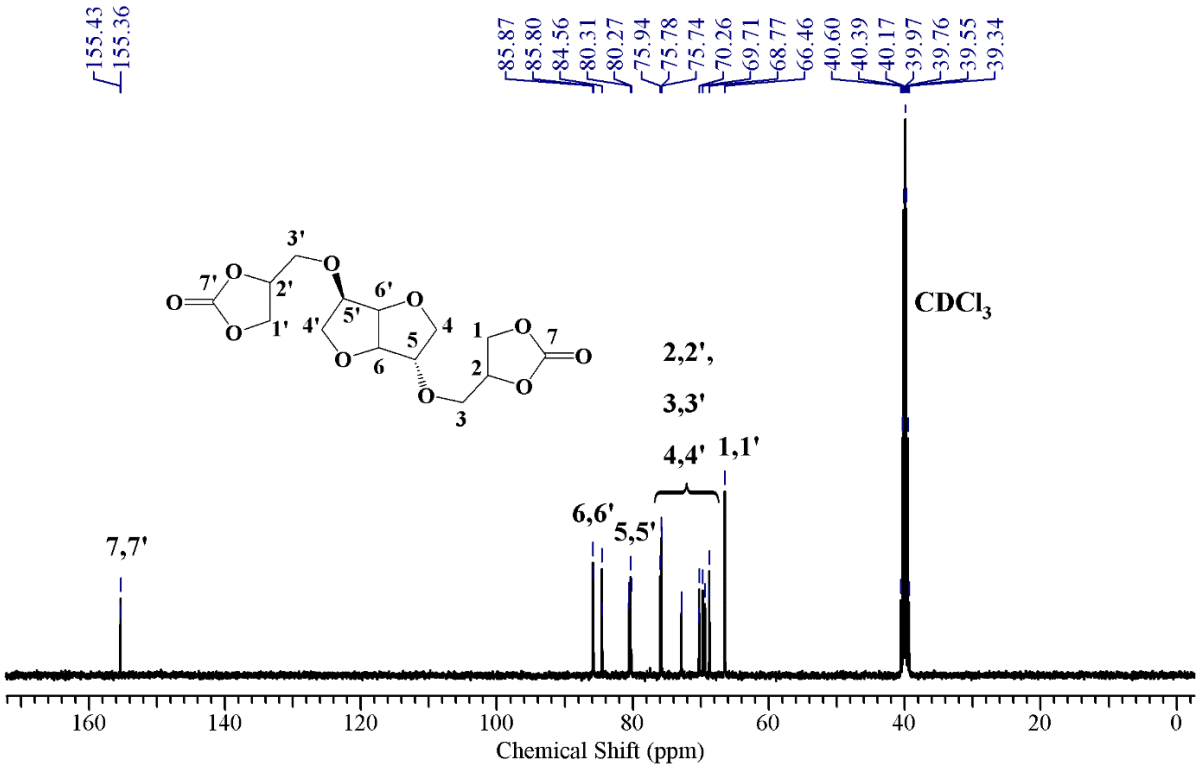

Figure 3.7. *^{13}C NMR spectrum of ISO-DC.*

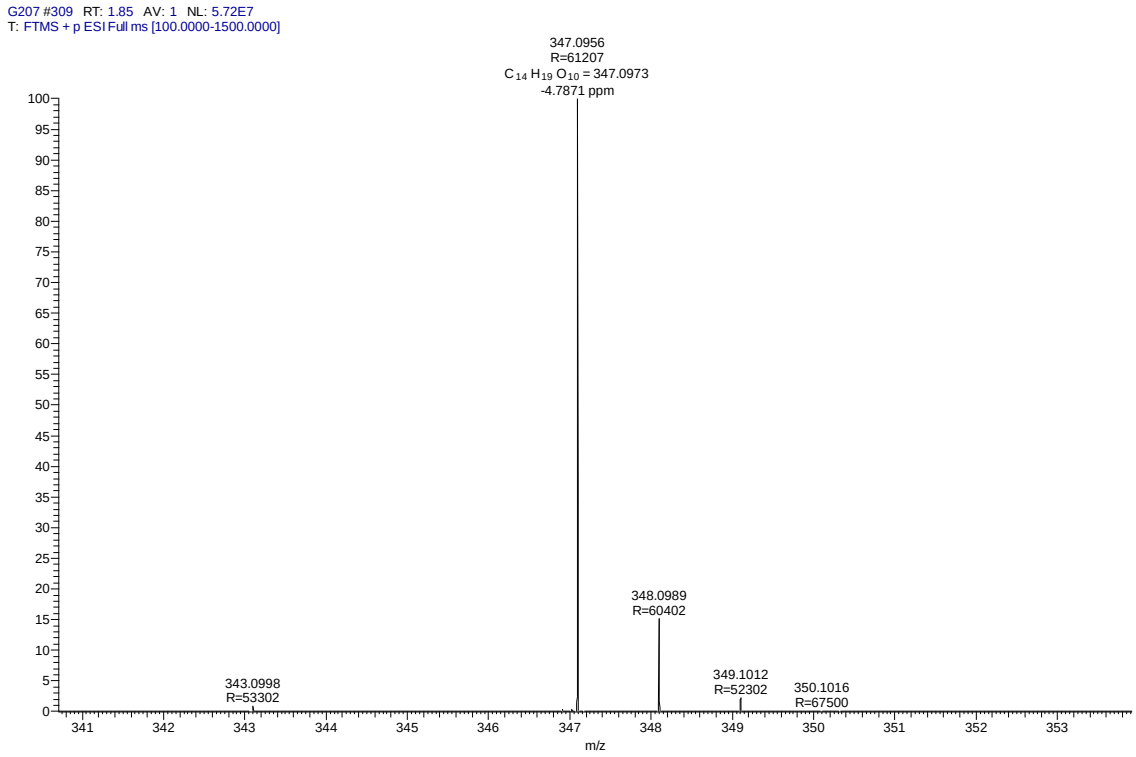

Figure 3.8*. HRMS spectrum of ISO-DC.*

3.3.2 Preparation of vanillin and pentaerythritol-derived cyclic carbonate (DVS-DC)

Vanillin and pentaerythritol have been used to prepare the DVS-DC monomer. The interest in using vanillin and pentaerythritol as starting materials comes from their renewability, diverse functionality, and wide availability. Additionally, pentaerythritol can form acetal groups in polymers after condensation, and these acetal linkages can undergo acid hydrolysis, which aids in developing degradable PHUs. The DVS-DC monomer was synthesized in three steps. First, vanillin was refluxed with pentaerythritol in the presence of p-toluenesulfonic acid monohydrate to obtain the diol compound (DVS-DL) (**Scheme 3.4**). Next, this diol molecule was converted into diglycidyl ether through epoxidation with epichlorohydrin (DVS-DGE) (**Scheme 3.5**). In the final step, the diepoxide reacted with carbon dioxide in a high-pressure reactor in the presence of a TBAB catalyst, resulting in the dicarbonate monomer with a total yield of 36.18 % (**Scheme 3.6**). The chemical structure of all compounds was confirmed by FT-IR, ^{1}H NMR, and ^{13}C NMR spectroscopy.

FTIR spectrum of DVS-DL is shown in **Figure 3.9.** The phenolic group (-OH) appears as a broad absorption band at 3488 cm^{-1}. The C-O-C and C-O stretching bands were noted at 1273 cm^{-1} and 1167 cm^{-1}, respectively. The ^{1}H NMR spectrum of DVS-DL is presented in **Figure 3.10**. The CH_2 protons of the six-membered spiro-acetal rings exhibited doublets at 3.63 ppm, multiplets at 3.80-3.83 ppm, and doublets at 4.86 ppm (labeled as 1, 2, 4 respectively). Additionally, the CH protons of the acetal ring appeared as a singlet at 5.40 ppm (marked as 5). The singlet for the phenolic hydroxyl and methoxy groups (designated as 3 and 6), respectively, was observed at 3.86 and 5.78 ppm. The doublets of aromatic protons (labeled 7, 8, and 9) were seen between 6.90 and 7.05 ppm. **Figure 3.11** displays the ^{13}C NMR spectra of DVS-DL. The peaks at 32.46, 70.59-71.08, and 102.29 ppm could be due to the carbons of the spiro-acetal rings (labeled as 1, 3, and 4). The signals appeared at 108.26, 114.08, 119.51, and 130.15 ppm could be ascribed to the unsubstituted aromatic carbons (labeled as 5, 6, 7, 8) while the signals observed at 146.31 and 146.45 ppm could be attributed to the -OH and -OCH_3 substituted aromatic carbons (labeled as 9, 10).

The FTIR spectra are illustrated in the **Figure 3.9.** The disappearance of a broad absorption band at 3488 cm^{-1}, which corresponds to the phenolic hydroxyl group, and the appearance of two additional vibrations at 921 and 810 cm^{-1}, which belong to the asymmetric and symmetric stretches of the C-O functions (epoxy rings), both have suggested the formation of the DVS-DGE compound. However, the C-O-C and C-O stretching bands for cyclic acetal were detected at 1263 cm^{-1} and 1167 cm^{-1}, respectively. The ^{1}H NMR of DVS-DGE is added in **Figure 3.12**.

After epoxidation, a signal of hydroxyl groups at 5.78 ppm disappeared and additional signals for epoxide protons appeared in the region of 2.74 to 3.86 ppm, demonstrating the complete transformation of phenolic -OH groups into glycidyl ethers. The CH_2 protons of epoxy rings labeled as 1 and 1′ showed doublet at 2.74 and 2.89 ppm, respectively whereas the CH protons of epoxy displayed multiplets at 3.37 ppm (represented by 2). Moreover, the CH_2 protons labeled as 3, and 3′ appeared at 3.66 and 3.85 ppm. The doublet at 3.86, 4.04, 4.22, and 4.84 ppm, (labeled as 4, 6, 7, 8) while a singlet at 5.40 ppm (labeled as 9) could be attributed to the protons of the spirocyclic ring. The remaining signals observed at 3.90 and 6.92-7.02 ppm, could be related to the methoxy and aromatic protons, respectively. The ^{13}C NMR spectrum of DVS-DGE is shown in **Figure 3.13**. The epoxy carbons labeled as 2, 3, and 5 resonated at 45.00, 50.14, and 70.26 respectively. The quaternary carbon of the spirocyclic ring marked as 1 was observed at 32.49 ppm whereas the other methylene carbons, labeled as 1, 6, and 7, appeared at 70.58, 71.07, and 102.09 ppm, respectively. The aromatic carbons appeared as a singlet in the region of 109.51-149.56 ppm. The methoxy carbon, labeled as 4, was observed at 55.94 ppm.

The FTIR of the second dicarbonate monomer (DVS-DC) is included in **Figure 3.9.** The FTIR spectra showed a characteristic band at 1790 cm^{-1}, which is due to the carbonyl stretch of the cyclic carbonate. [19,26] The vibrations at 1263 and 1167 cm^{-1} were respectively assignable to the C-O-C and C-O stretches of the acetal, as well as carbonate rings.

In the ^1H NMR spectrum (**Figure 3.14**), the formation of the dicarbonate precursor is supported by the presence of the carbonate signals at 4.20, 4.60, and 5.01 ppm (labeled as 4, 5, and 7) and the absence of oxirane peaks at 2.74, 2.91, 3.39, 4.05, and 4.25 ppm.[27] The spectra also showed four peaks for the acetal -CH_2 and -CH groups of the spirocyclic backbone at 3.64, 3.84, 4.86, and 5.42 ppm, respectively (labeled as 1, 2, 6, and 8).[28] Furthermore, the methoxy and aromatic protons were identified at 3.87 (marked as 3) and 6.92-7.06 ppm (labeled as 9, 10, 11), respectively.[29] In addition to FTIR and ^1H NMR, ^{13}C NMR spectroscopy is a vital tool for determining the presence of carbonyl groups. The ^{13}C NMR spectra of the DVS-DC (**Figure 3.15**), displayed the additional singlet at 154.71 ppm (labeled as 14), which indicates the existence of the carbonyl carbon of dicarbonate compounds.[30,31]

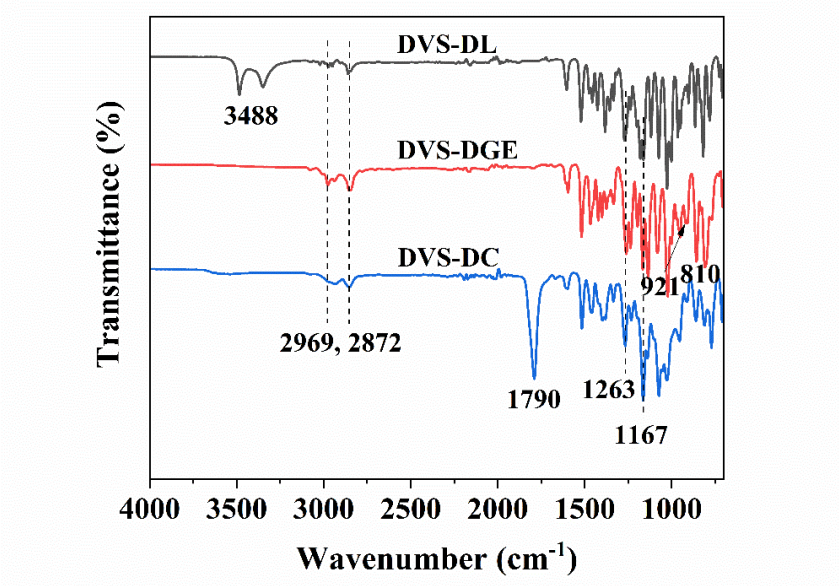

Figure 3.9. *FTIR spectrum of DVS-DL, DVS-DGE, and DVS-DC compounds.*

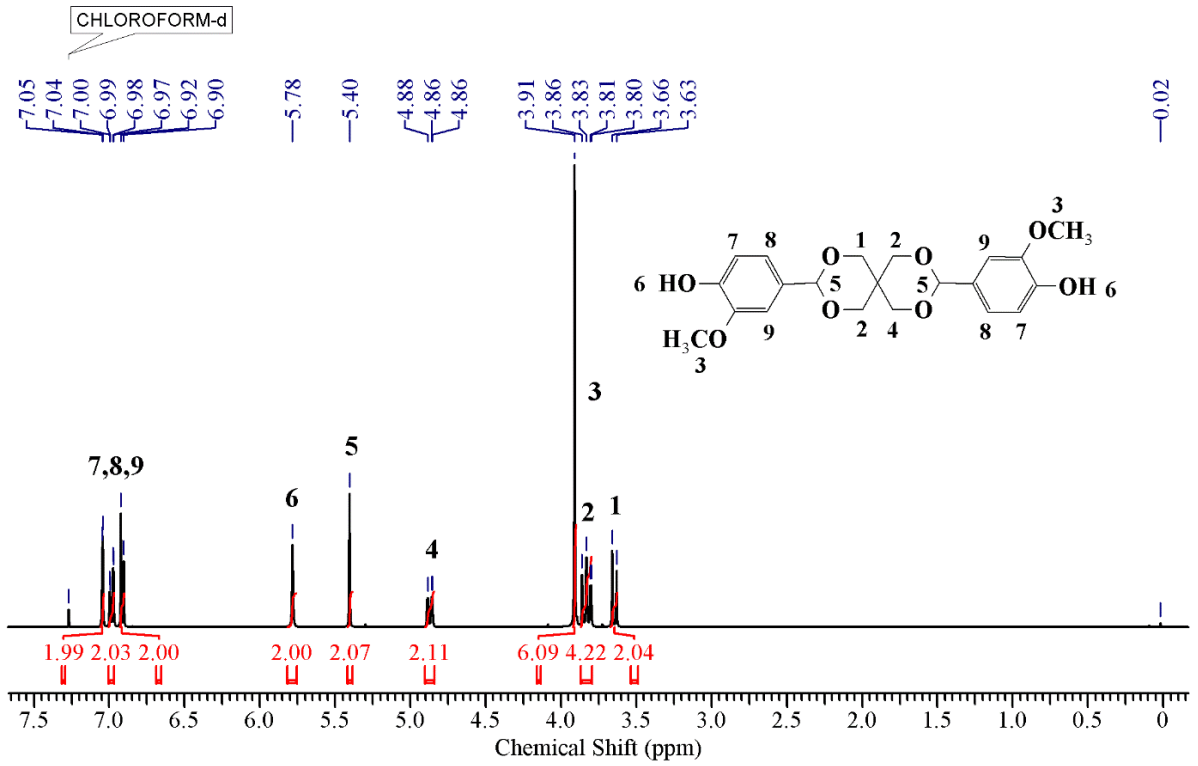

Figure 3.10. *^{1}H NMR spectrum of DVS-DL.*

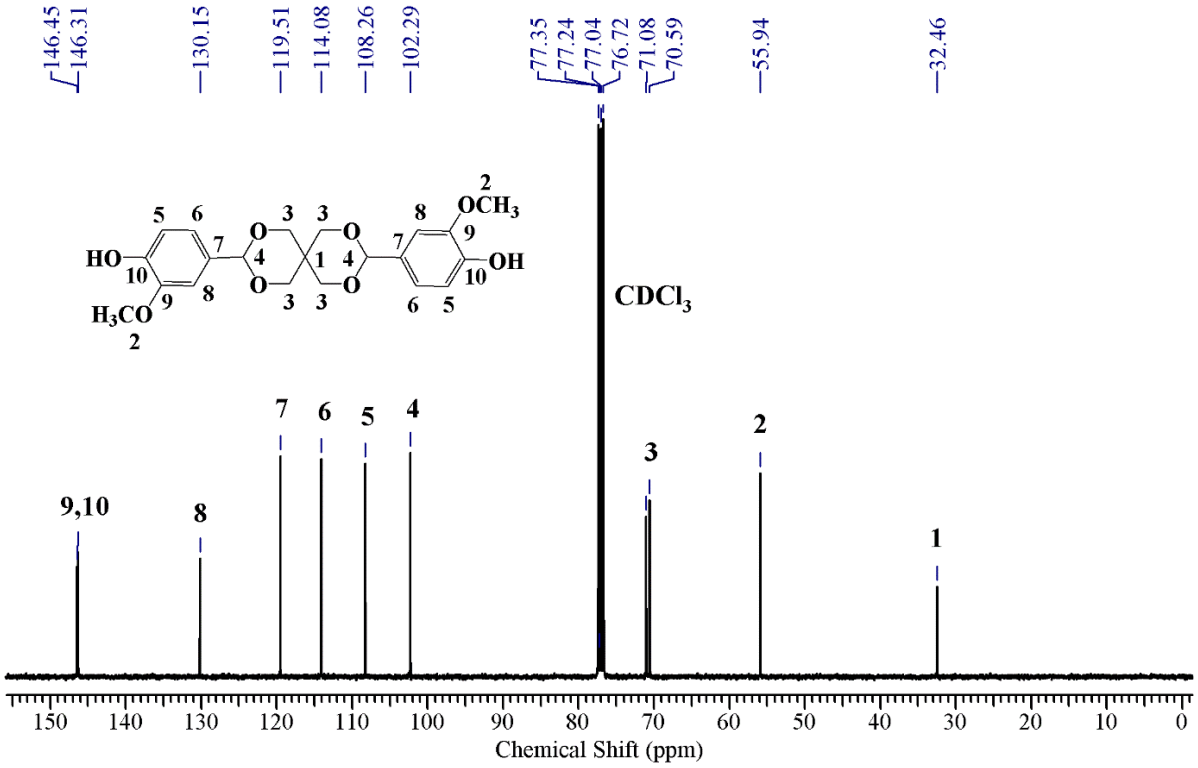

Figure 3.11. *^{13}C NMR spectrum of DVS-DL.*

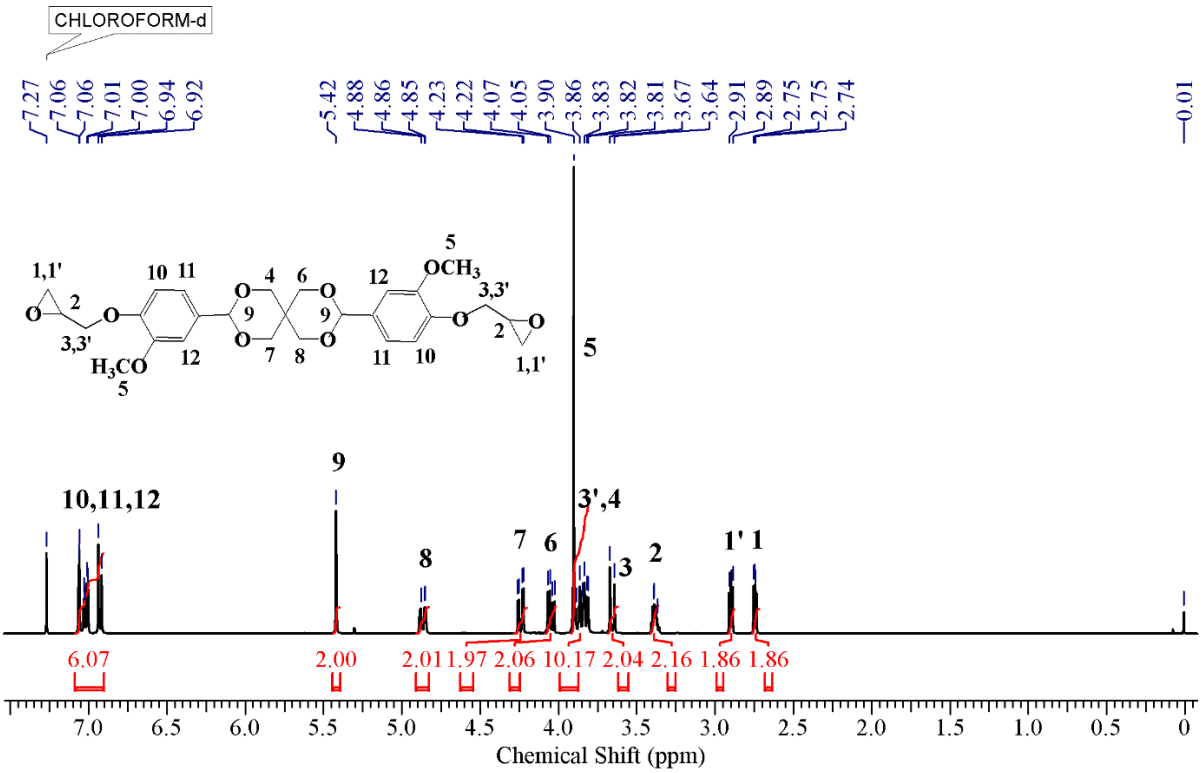

Figure 3.12. *^{1}H NMR spectrum of DVS-DGE.*

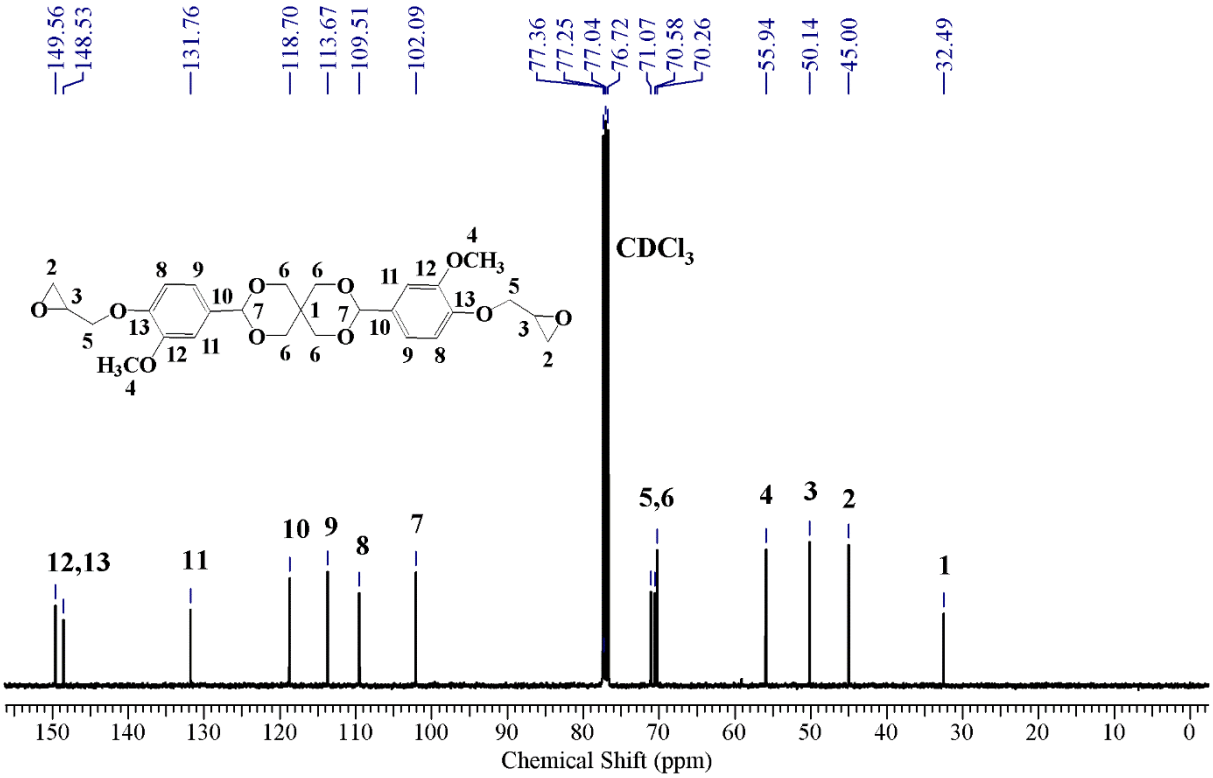

Figure 3.13. *^{13}C NMR spectrum of DVS-DGE.*

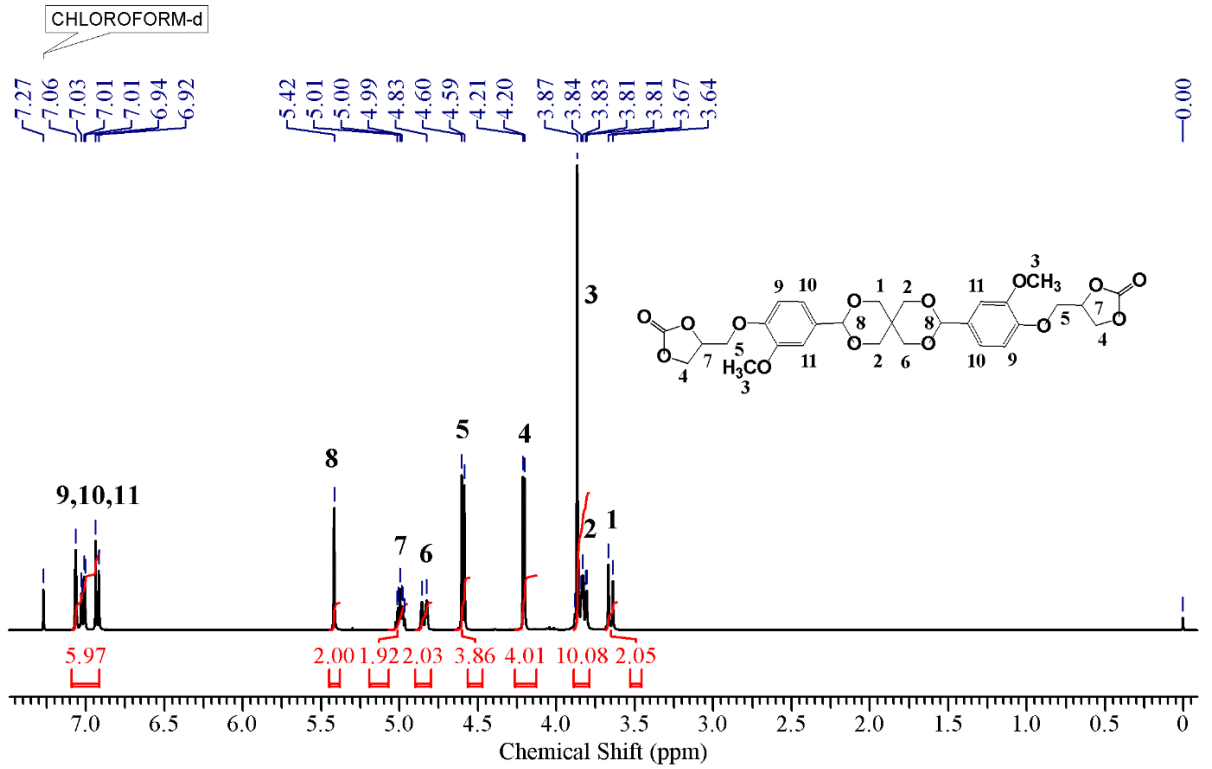

Figure 3.14. *^{1}H NMR spectrum of DVS-DC.*

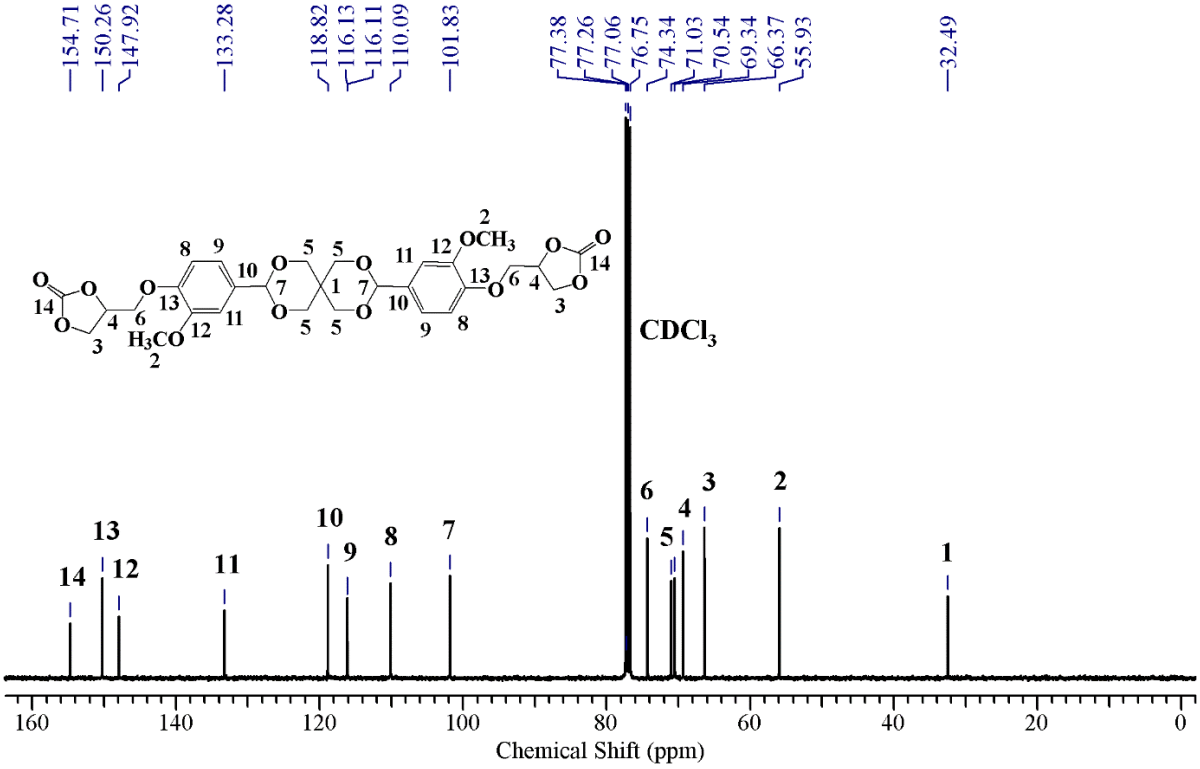

Figure 3.15. *^{13}C NMR spectrum of DVS-DC.*

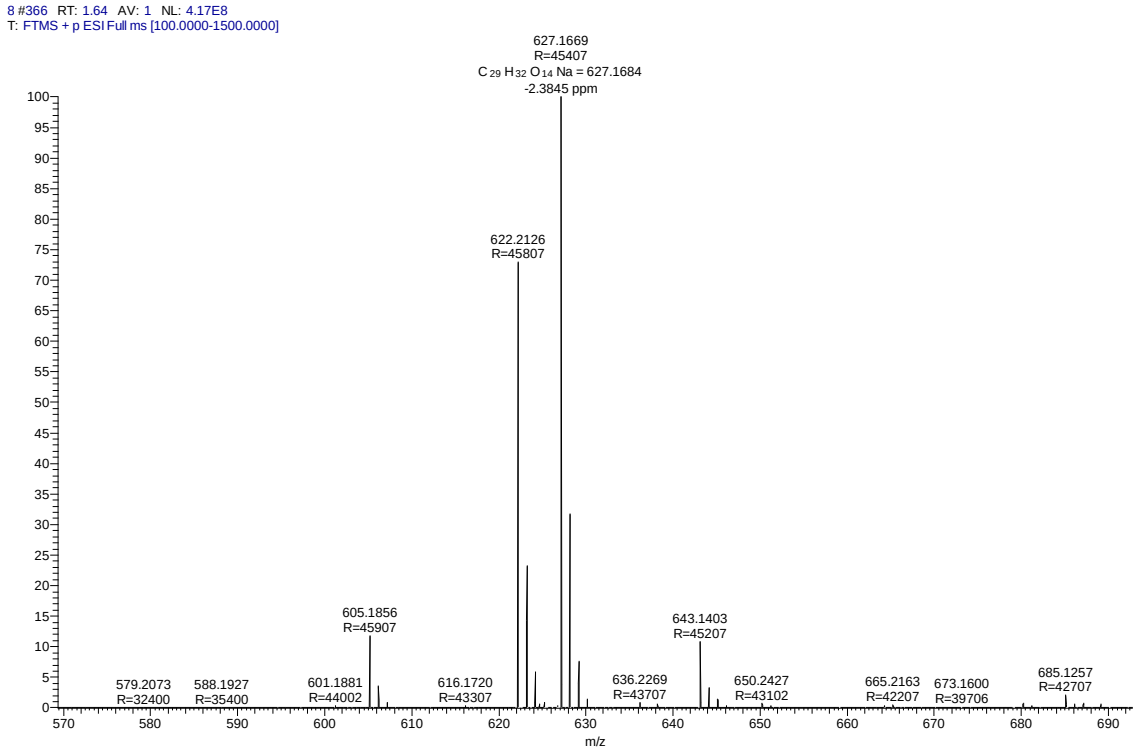

Figure 3.16. *HRMS spectrum of DVS-DC.*

3.3.3 PHU formulations and their structural characterization

Hot-melt adhesives (HMAs) derived from renewable resources are always attractive as they promote less dependence on fossil resources and aid in developing environmentally friendly materials. However, developing sustainable HMAs exhibiting good adhesive performance and biodegradability remains challenging. In this context, a reusable bio-based PHU-HMA with a high bio-content of 88-90 %, biodegradability, and tunable adhesive nature was developed as a possible alternative to conventional petroleum-based hot melt adhesives. Moreover, the structure-property relationship of the product was investigated in detail.

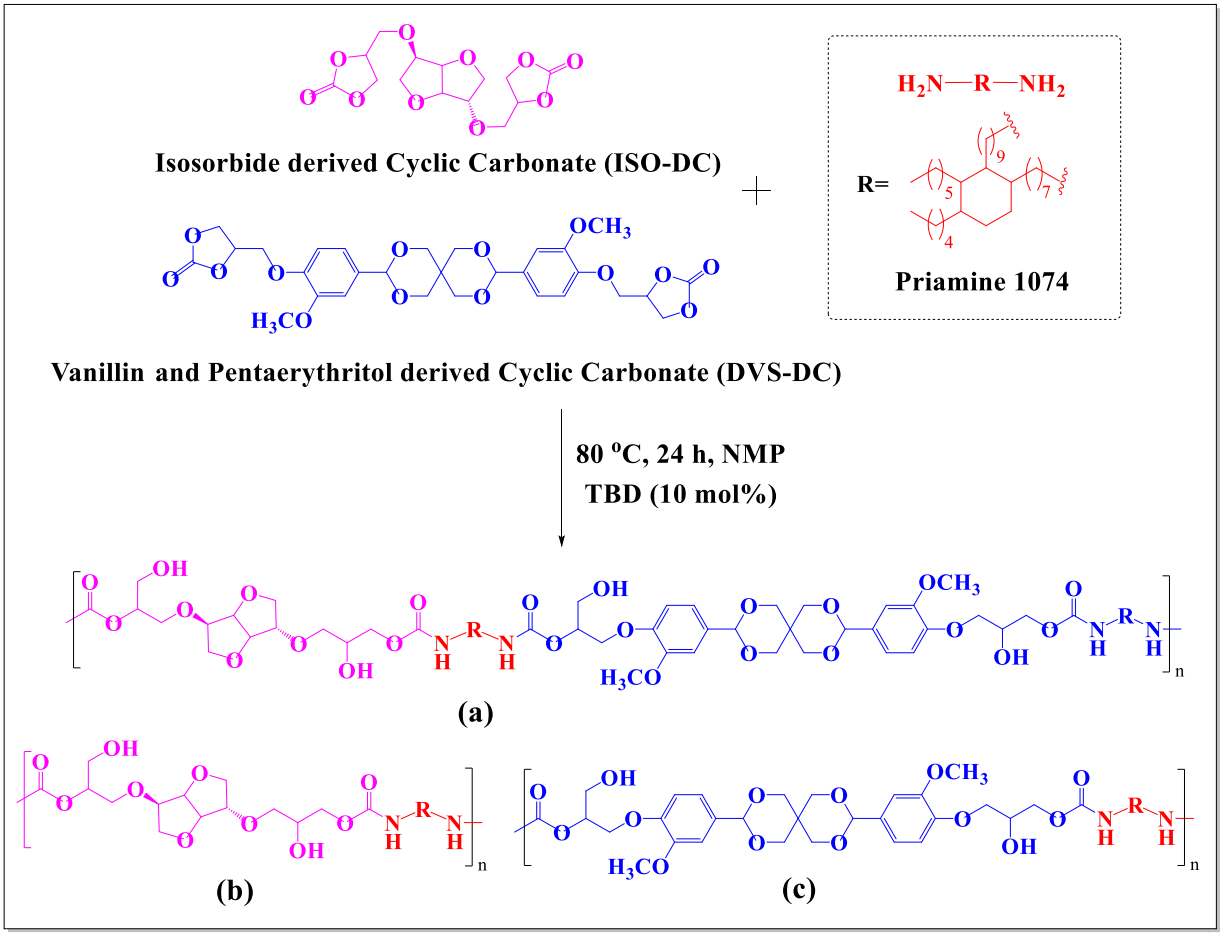

Scheme 3.7. *Preparation of the PHU-based hot melt adhesives from isosorbide and vanillin-derived cyclic carbonates (a) structure of the copolymers when two cyclic carbonates were used, (b, c) structure of homopolymers when individual monomers were used.*

Polymers were synthesized by reacting various molar compositions of ISO-DC and DVS-DC monomers with Priamine 1074 in the presence of TBD catalysts (**Table 3.1**), maintaining a constant molar ratio of 1:1 between dicarbonates and diamine (**Scheme 3.7**). Solution polymerization was employed to ensure sufficient mixing of the components, using a minimum

of 2 mL of NMP as the solvent. The resulting solution was polymerized under continuous stirring at 80 °C for 24 h to produce analogous PHU chains.

All PHUs (except PHU1-0) have formed free-standing films (**Figure 3.17**) when drop-cast from corresponding chloroform solutions. PHU1-0 is sticky, thus we were unable to make a film using it. The films were prepared in plastic Petri dishes and displayed a faint yellow color, which could be ascribed to the presence of amine functionality in the backbone.

Table 3.1*. Molar compositions of the precursors utilized in PHUs preparation.*

Polymers	ISO-DC (mole ratio)	DVS-DC (mole ratio)	Priamine 1074 (mole ratio)
PHU1-0	1.0	0.0	1
PHU2-20	0.8	0.2	1
PHU3-40	0.6	0.4	1
PHU4-60	0.4	0.6	1
PHU5-80	0.2	0.8	1
PHU6-100	0.0	1.0	1

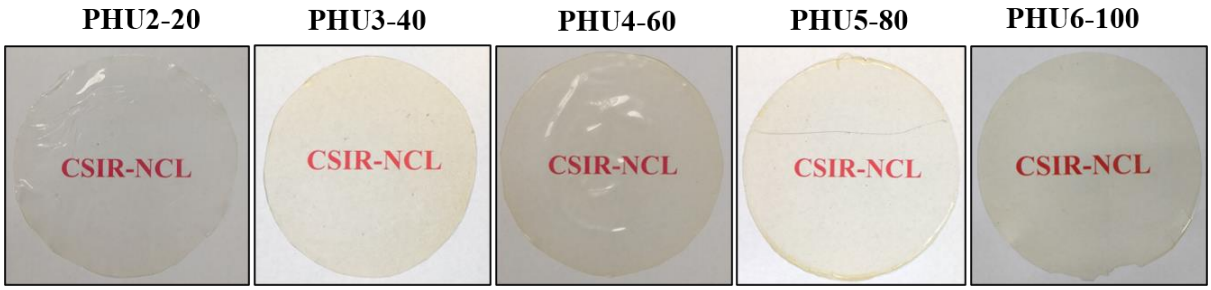

Figure 3.17. *The photographs of PHU polymers.*

The chemical structure and composition of the polymers were confirmed by FTIR, ^{1}H NMR, and ^{13}C NMR spectroscopy. As shown in **Figure 3.18**, the cyclic carbonate carbonyl band for DVS-DC and ISO-DC around 1790-1791 cm^{-1} disappeared in the FTIR spectra of PHU indicating the successful reaction of cyclic carbonate groups with diamine, leading to urethane linkages. Further, PHUs exhibited two characteristic stretching vibrations, one at 1706 cm^{-1} (strong and sharp), which is ascribed to the -C=O stretch [10,32] and the other at 3150-3600 cm^{-1} (broad), for the hydroxyl as well as the -NH stretch which verify the formation of hydroxyurethane groups.[16,32] Additionally, new peaks were observed at 1466 cm^{-1} (N-H bending), at 2856-2934 cm^{-1} (C-H stretches), and at 1592-1638 cm^{-1} (C=C stretching of the aromatic rings, except in the case of PHU1-0.[33] Moreover, the appearance of characteristic

bands at 1036, 1080, 1142 cm^{-1}, and 1210-1260 cm^{-1}, can be assigned to the C-O-C, and C-O stretching respectively.[33,34]

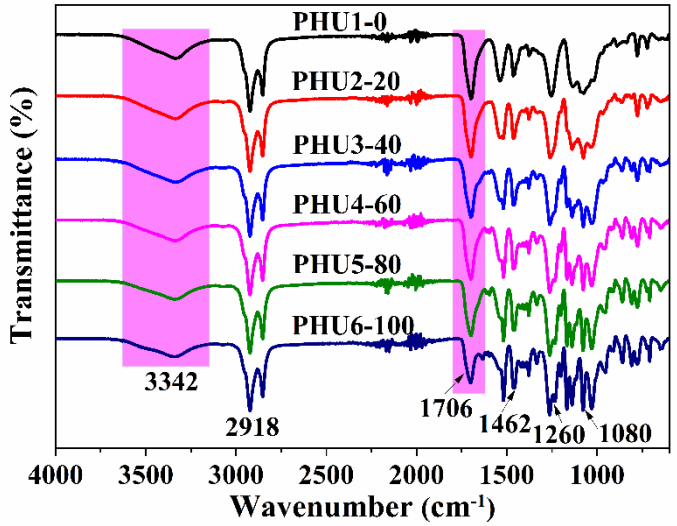

Figure 3.18. *FTIR spectrum of the PHUs.*

The polymer structure was further evaluated by ^{1}H NMR analysis (**Figure 3.19, Figure 3.20, Figure 3.21**), which indicated the emergence of N-H signals at 7.05-7.02 ppm.[26,27] and also observed a chemical shift of the α-methylene group of primary amines from 2.61 ppm (Priamine 1074) to 3.13-3.15 ppm due to the formation of new C-N bonds validating the formation of urethane moieties in the polymer structures.[10] Moreover, the pendant primary and secondary hydroxyl groups generated during the ring-opening reaction were detected at 3.66 ppm and 4.90 ppm, respectively.[27] However, no significant difference in chemical shift for the protons of DVS-DC and ISO-DC was observed on polymerization, indicating the basic chemical structure of the backbones is intact.

^{13}C NMR analysis of polymer (**Figure 3.22, Figure 3.23, and Figure 3.24**) displayed new signals at 156.7 ppm for the carbonyl group of urethane functionality,[35] and the disappearance of the carbonyl peak of the carbonate precursors at 155.4 ppm (ISO-DC) and 154.71 ppm (DVS-DC), which further supported the successful formation of PHU thermoplastics.[30,31]

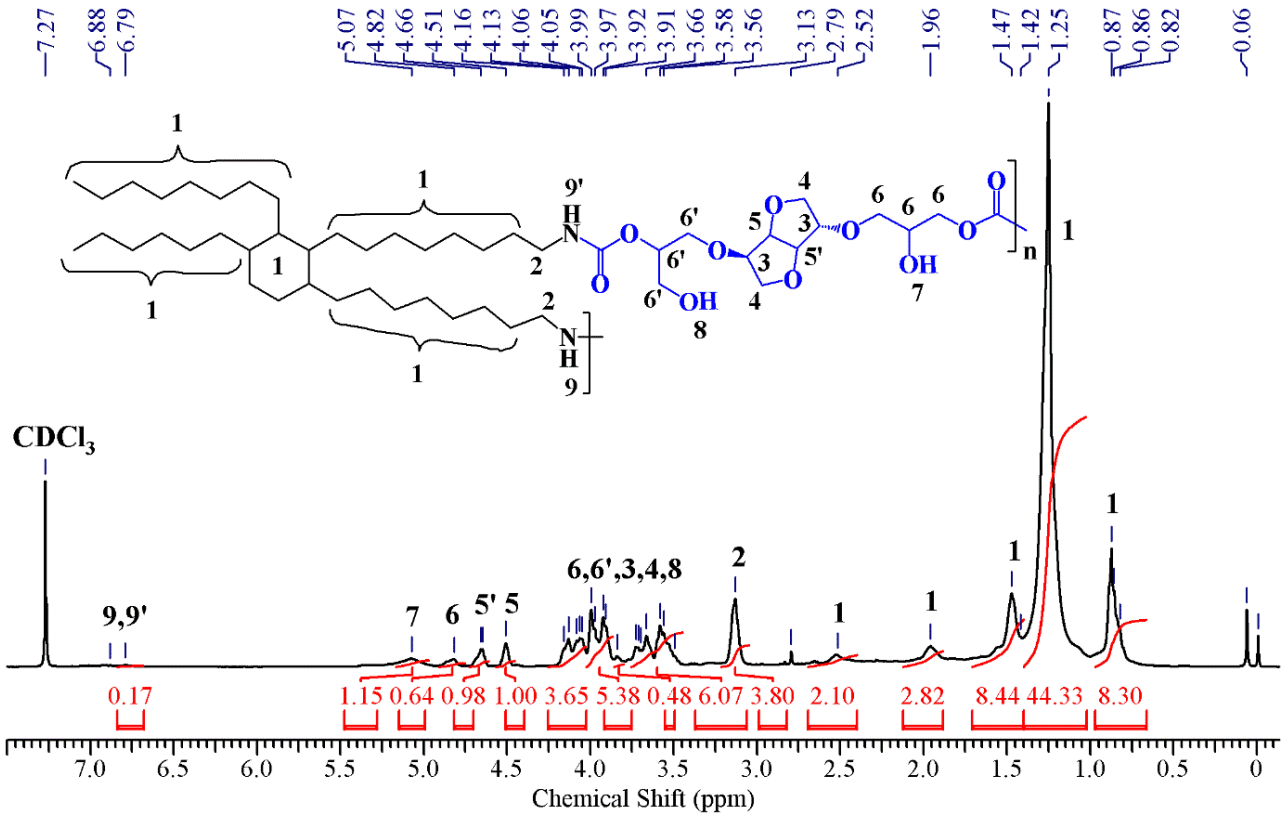

Figure 3.19. *^{1}H NMR spectrum of PHU1-0 (Homo).*

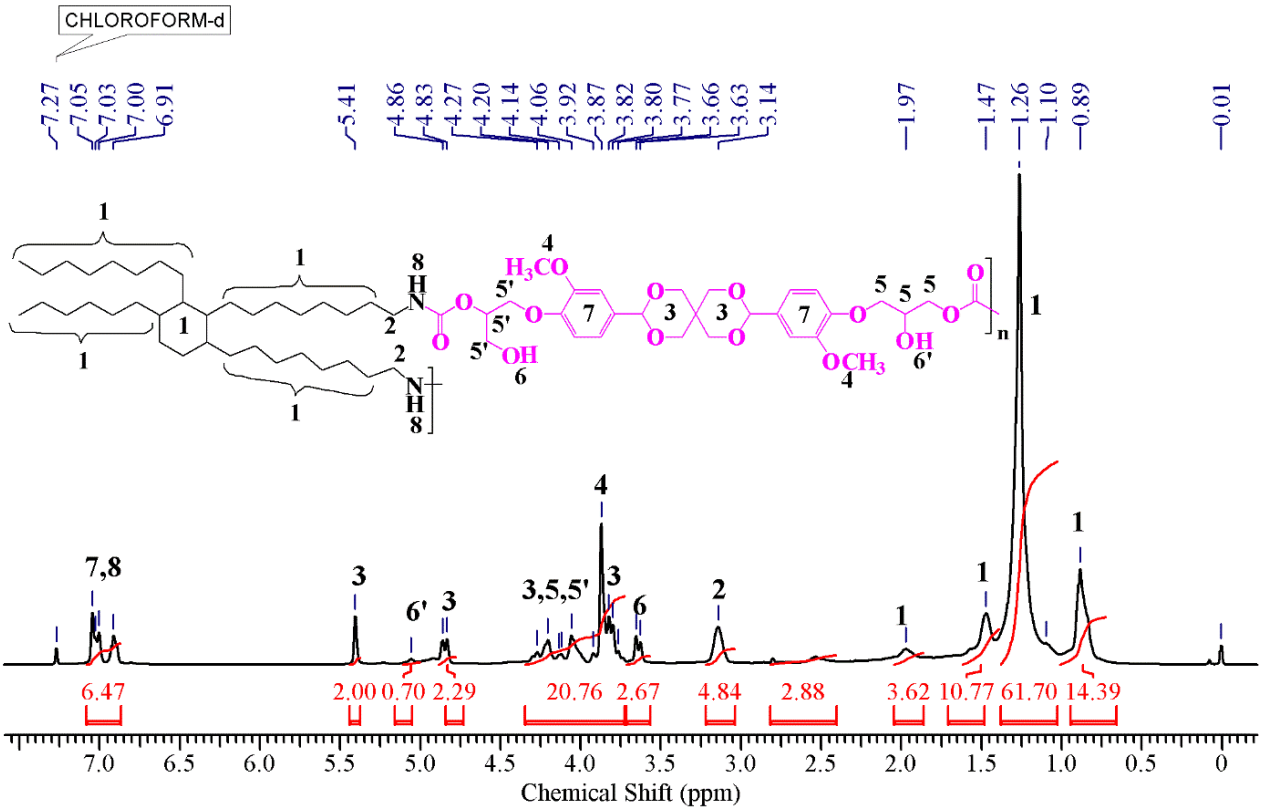

Figure 3.20. *^{1}H NMR spectrum of PHU6-100 (Homo).*

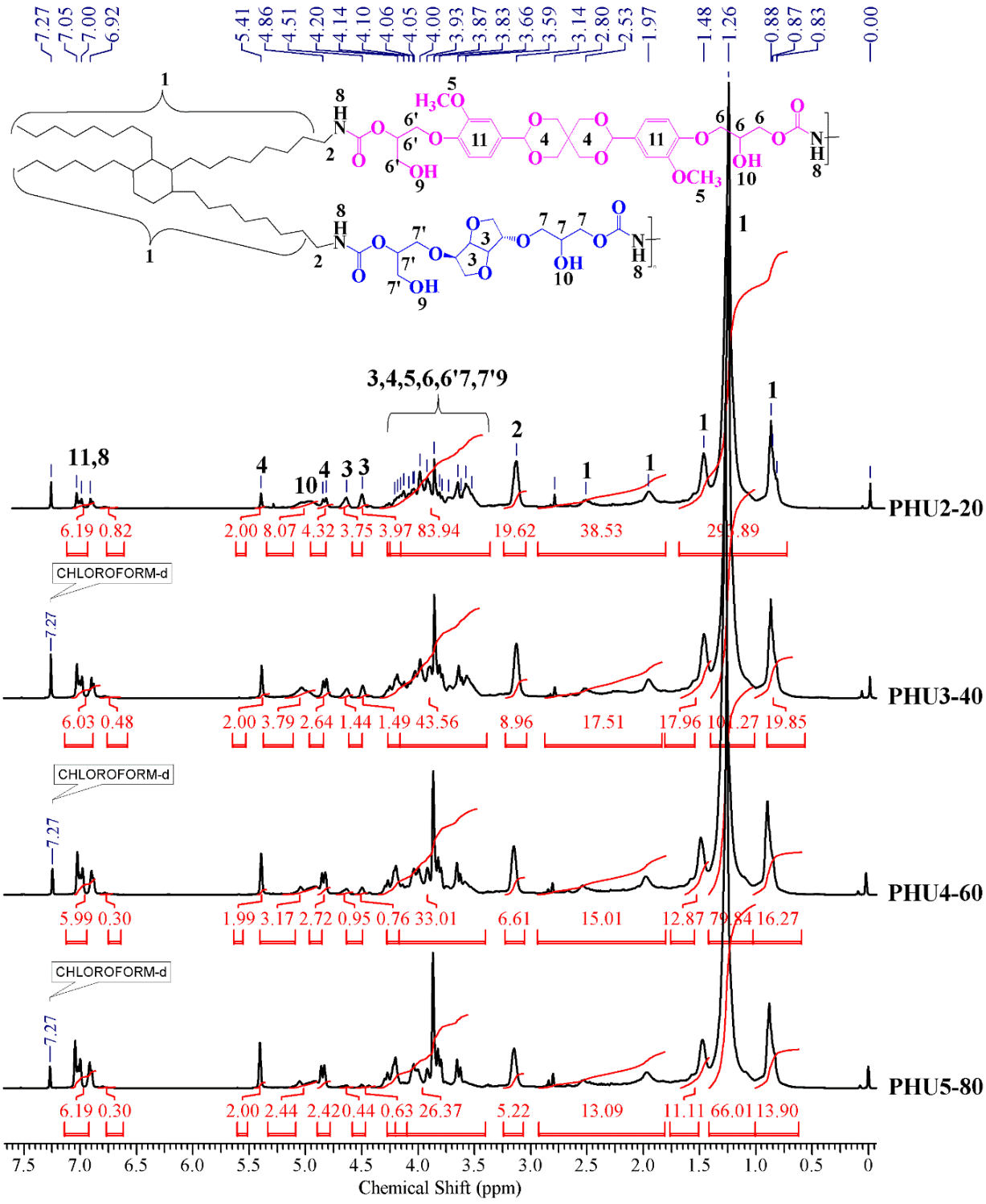

Figure 3.21. *^{1}H NMR spectrum of PHU copolymers.*

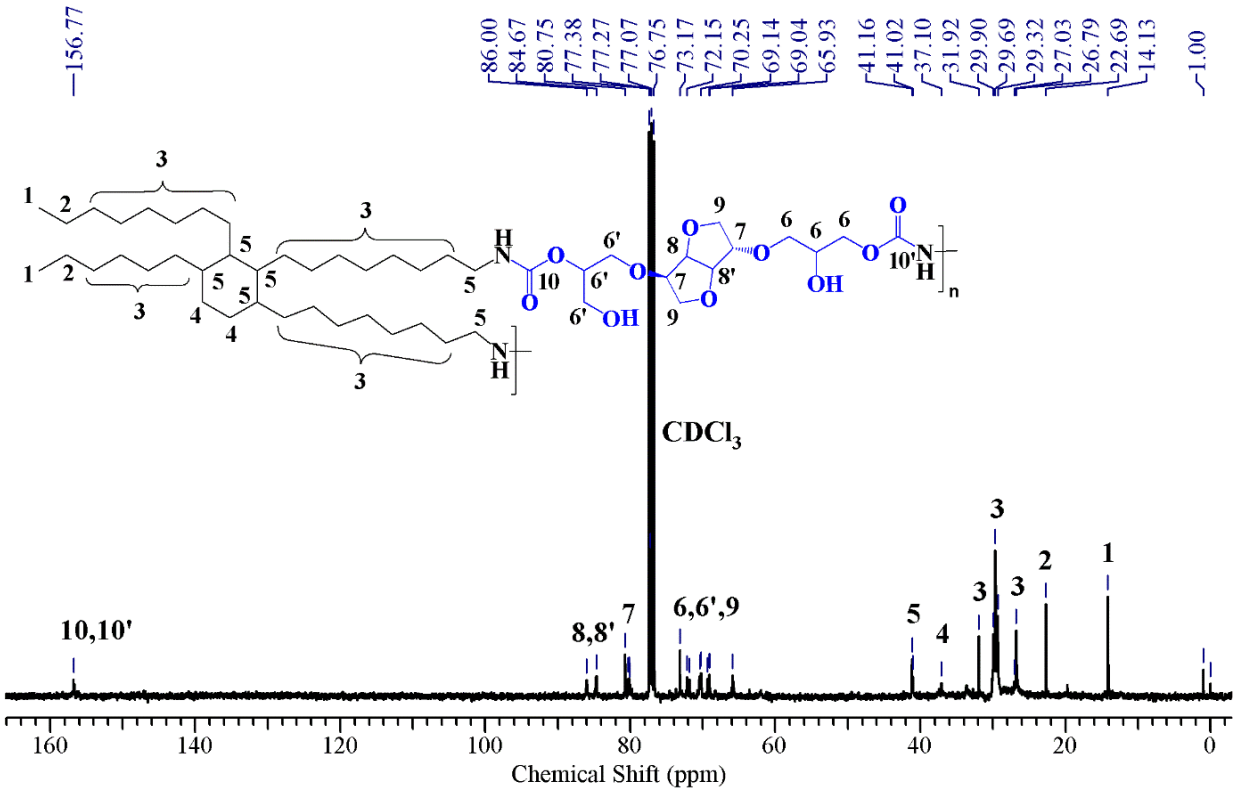

Figure 3.22. *^{13}C NMR spectrum of PHU1-0 (Homo).*

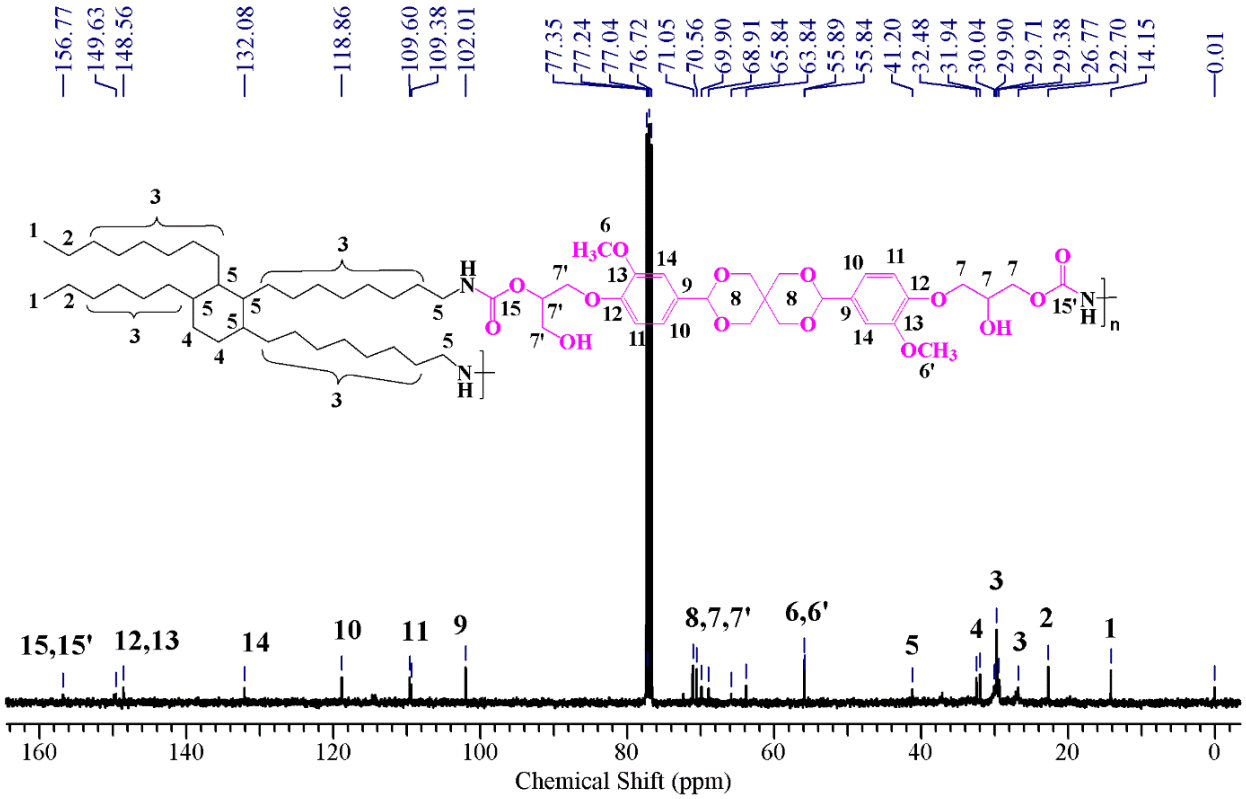

Figure 3.23. *^{13}C NMR spectrum of PHU6-100 (Homo).*

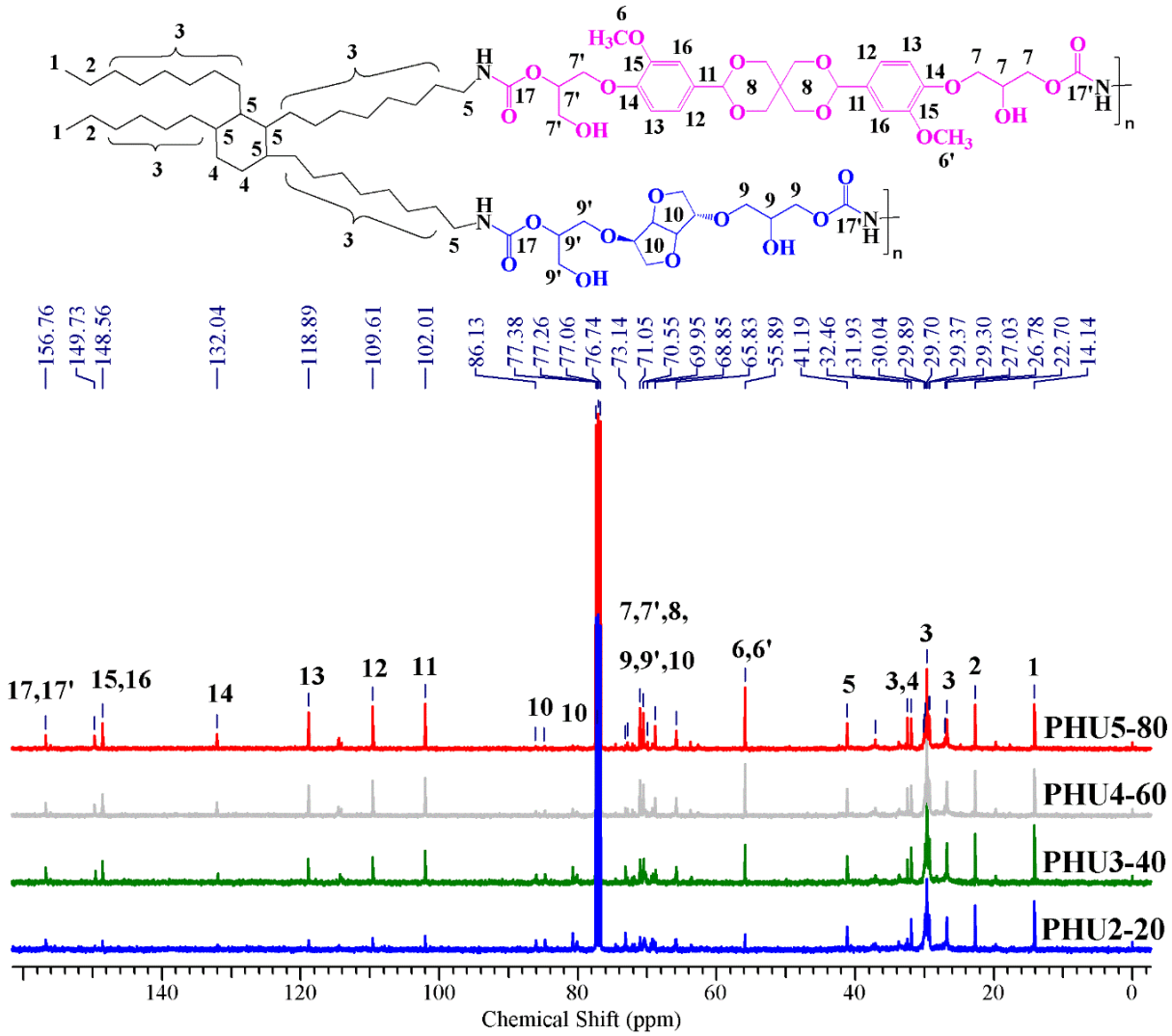

Figure 3.24. *^{13}C NMR spectrum of PHU copolymers.*

Furthermore, based on the monomer composition, the signal intensity corresponding to DVS-DC and ISO-DC showed a consistent variation in the case of copolymers (**Table 3.4**). Moreover, the integral of aromatic protons of DVS-DC (signal c, c'), acetal protons of DVS-DC (signals b, b'), and bridge-head protons of ISO−DC (signal a, a') confirmed the incorporated content of DVS-DC in the polymer varied from 19 to 72 mol% (**Figure 3.25**).[36] These values were consistent with the initial monomer compositions, indicating good reactivity and stability of the monomers under the optimized polymerization conditions. However, the bio-renewable carbon content for both carbonate monomers and their polymers has been calculated as mentioned in **Table 3.2** and **Table 3.3**, and was found to be as high as 88-90 % for polymers.

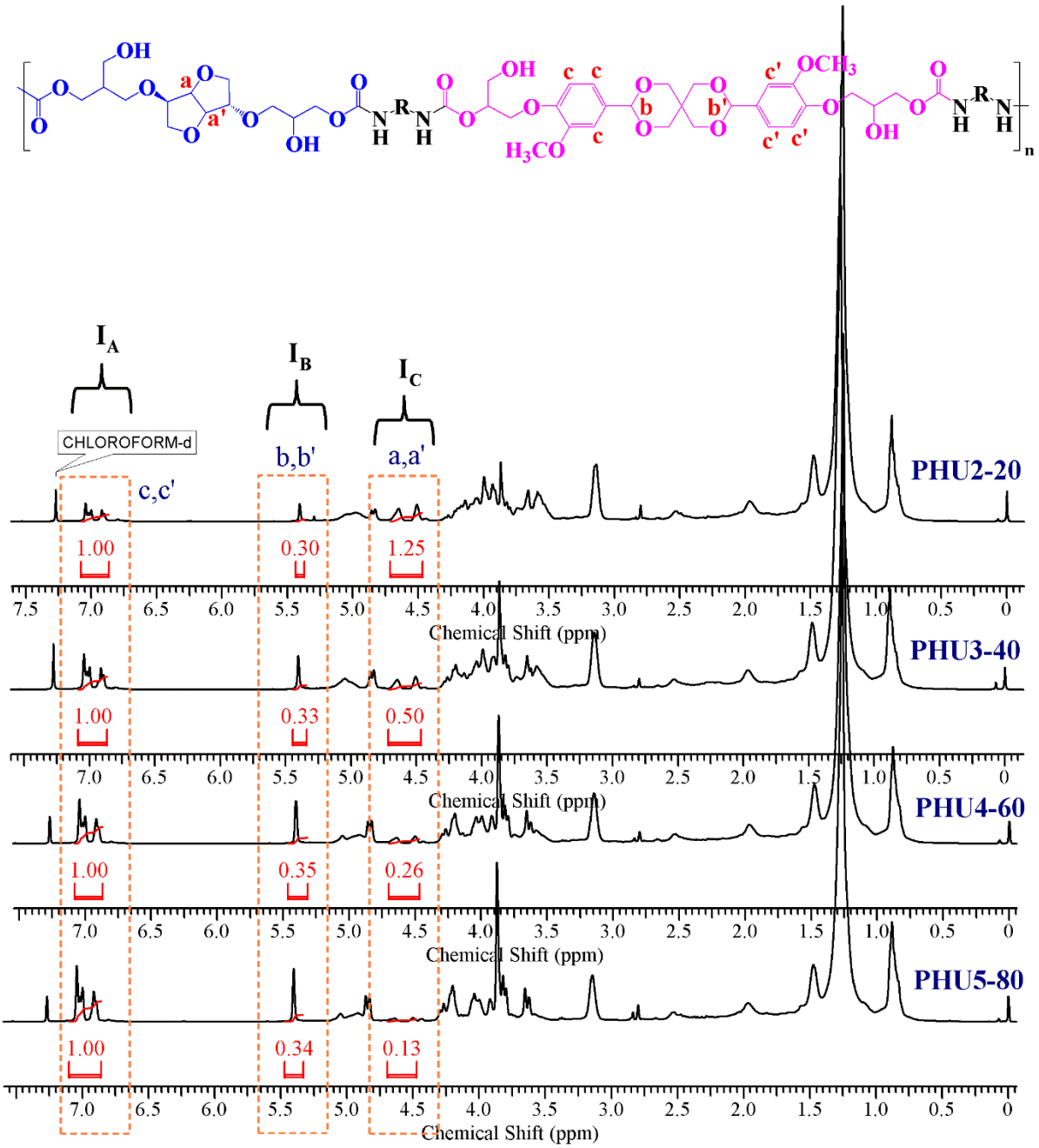

Figure 3.25. *The % molar compositions of PHU copolymers were determined by ^{1}H NMR spectroscopy.*

Table 3.2*. Renewable carbon contents for cyclic dicarbonate monomers developed from the sugar and lignin-derived precursors.*

Dicarbonates	Chemical structure [a]	RCC (%) [b]
ISO-DC	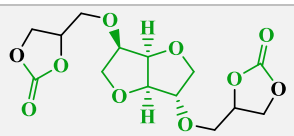	57.15
DVS-DC	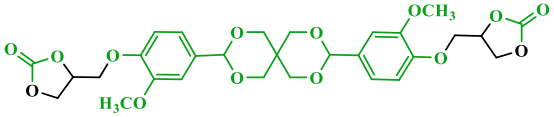	79.31

[a] Green color shows the carbon atoms originating from renewable resources.

[b] RCC: Renewable carbon content is determined ratio of the mass of biobased carbon in the material to the total organic carbon mass, multiplied by 100.

Table 3.3. *Renewable carbon contents of PHU adhesives.*

Polymers	Total Carbon Present in PHUs [a]	Total RC Present in PHUs [b]	RCC (%) [c]
PHU1-0	=C14×1+C29×0+C36 =C14+C0+C36=C50	=C8×1+C23×0+C36 =C8+C0+C36=C44	88.00
PHU2-20	=C14×0.8+C29×0.2+C36 =C11.2+C5.8+C36=C53	=C8×0.8+C23×0.2+C36 =C6.4+C4.6+C36=C47	88.67
PHU3-40	=C14×0.6+C29×0.4+C36 =C8.4+C11.6+C36=C56	=C8×0.6+C23×0.4+C36 =C4.8+C9.2+C36=C50	89.28
PHU4-60	=C14×0.4+C29×0.6+C36 =C5.6+C17.4+C36=C59	=C8×0.4+C23×0.6+C36 =C3.2+C13.8+C36=C53	89.83
PHU5-80	=C14×0.2+C29×0.8+C36 =C2.8+C23.2+C36=C62	=C8×0.2+C23×0.8+C36 =C1.6+C18.4+C36=C56	90.32
PHU6-100	=C14×0+C29×1+C36 =C0+C29+C36=C65	=C8×0+C23×1+C36 =C0+C23+C36=C59	90.76

[a] Total number of carbon present in PHUs was calculated by the formula = (total carbon of ISO-DC × mol% of ISO-DC) + (total carbon of × mol% of DVS-DC) + (total carbon of Priamine 1074).

[b] Total renewable carbon (RC) present in PHUs was determined by the formula = (RC of ISO-DC × mol% of ISO-DC) + (RC of DVS-DC × mol% of DVS-DC) + (RC of Priamine 1074).

[C] Total RC content in final PHUs (%) was calculated by the formula = (Total RC of NIPUs ÷ Total carbon of NIPUs × 100%).

Table 3.4. *Incorporated mole percentage of dicarbonate monomers in the final PHU copolymers, determined using the integrals of ^{1}H NMR signals.*

Copolymers	I_A [a]	I_B [a]	I_C [a]	Feed (mol%)		Observed (mol%)	
				ISO-DC	DVS-DC	ISO-DC	DVS-DC
PHU2-20	1	0.30	1.25	80	20	80.84	19.35
PHU3-40	1	0.33	0.50	60	40	60.24	39.75
PHU4-60	1	0.35	0.26	40	60	42.62	57.37
PHU5-80	1	0.34	0.13	20	80	27.65	72.34

[a] I_A, I_B, and I_C represent the integrals of six aromatic protons of DVS-DC (signal c, c′), two acetal protons of DVS-DC (signals b, b′), and two bridge-head protons of ISO-DC (signal a, a′), respectively.

3.3.3.1 Analysis of the ^{1}H NMR recorded at various temperatures

It is a well-established PHU that can engage in more hydrogen bonds than regular PUs due to the presence of pendant hydroxyl groups.[37] Studies have shown that these interactions are responsible for segmental stability in PHUs, which positively impacts the material properties.[38,39] The presence of hydrogen bonds in synthesized PHUs was investigated using temperature-dependent ^{1}H NMR analysis (**Figure 3.26**) of PHU3-40 at four different temperatures (30, 50, 70, and 90 °C). At room temperature, the signal of the urethane -NH was not visible, as it overlaps with the signals of aromatic protons in the area of 7.02-7.05 ppm. However, as the temperature increased, the signal became completely visible and moved upfield, and on cooling to 30 °C, it eventually returned to its original position. Similar shifting was observed with hydroxyl groups where the signals are observed at 3.66 ppm (primary -OH) and 4.90 ppm (secondary -OH) at 30 °C. As the temperature increased, both signals migrated to a lower chemical shift as hydrogen bonds became labile and then immediately returned to their original positions as the temperature dropped to 30 °C. These shifts of the labile protons as a function of temperature indicate that the urethane -NH and both hydroxyl groups (primary and secondary) of PHUs were involved in the hydrogen bonding.[12]

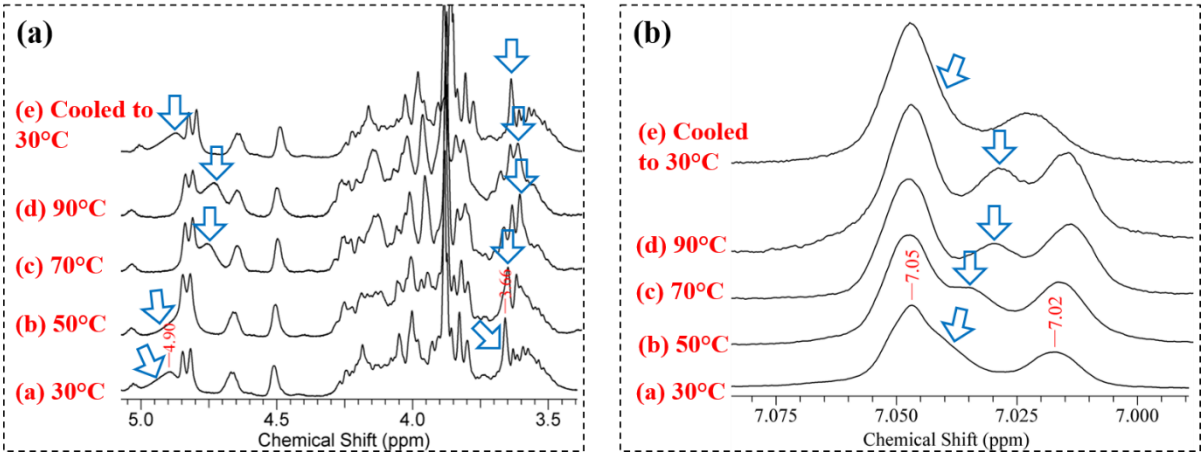

Figure 3.26. *^{1}H NMR spectrum of PHU3-40 taken at different temperatures (a) displaying the shifting of primary and secondary hydroxyl groups, and (b) the shifting of urethane -NH.*

Table 3.5. *Molecular weight distribution and Thermal properties of the PHUs.*

Polymers	**SEC**			**DSC**	**TGA**
	M_n (g/mol)	**M_w (g/mol)**	**Dispersity**	**T_g (°C)**	**T_{d}, 10% (°C)** [a]
PHU1-0	6,000	10,400	1.73	4	293
PHU2-20	4,400	7,800	1.77	10	305
PHU3-40	6,400	10,500	1.64	17	303
PHU4-60	5,100	9,600	1.90	30	315
PHU5-80	6,500	11,800	1.80	36	328
PHU6-100	6,100	10,200	1.58	43	335

[a] $T_{d10\%}$ denotes the temperatures at which polymeric materials have lost respectively, 10% weights of their initial mass.

3.3.3.2 Size Exclusion Chromatography

The molecular weight of the synthesized PHUs was determined employing SEC and tabulated in **Table 3.5**. All PHUs exhibited a monomodal distribution (**Figure 3.27**), and the molecular weight (M_n) of PHUs varied between 4400 and 6500 g.mol^{-1} with dispersity ranging from 1.58 to 1.90, which is usual for the step-growth polyaddition reaction.[8]

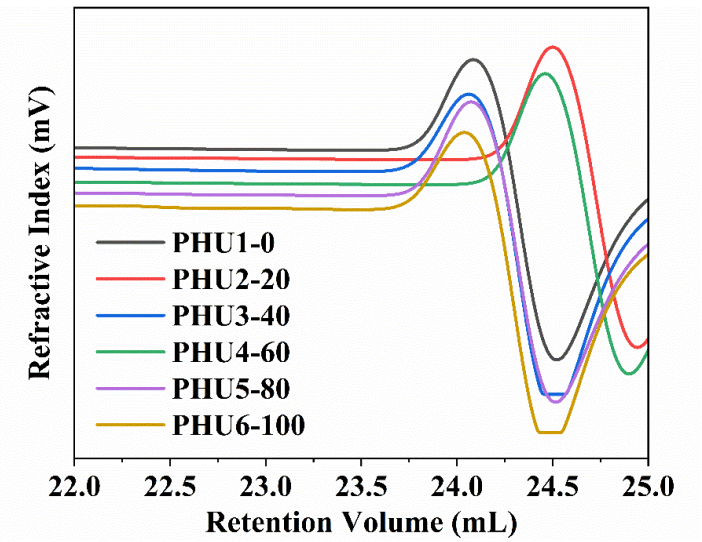

Figure 3.27*. GPC traces of PHUs.*

3.3.3.3 Thermal properties

The thermal transitions of the PHUs were analyzed by differential scanning calorimeter (DSC) and thermogravimetric analysis (TGA). As can be seen from **Figure 3.28**, the second heating curves of all PHUs lack a distinctive melting peak, indicating the amorphous nature. Moreover, only a T_g was observed in DSC for all PHU copolymers, despite their polymeric backbone being composed of two structurally different dicarbonates (DVS-DC and ISO-DC), indicates good uniformity and better phase mixing behavior in all polymers.[12]

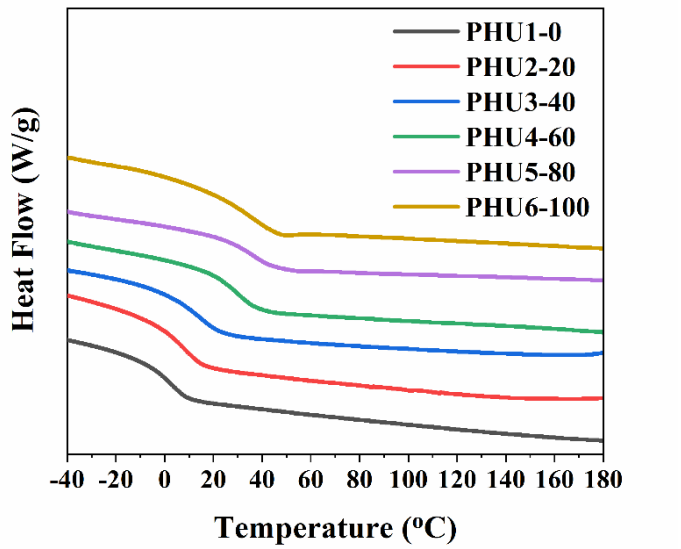

Figure 3.28. *Overlay of the DSC curves (second heating cycles).*

As expected, PHU1-0 exhibited a lower T_g of 4 °C, whereas T_g values increased linearly with spiro-aromatic addition, revealing a maximum value of 43 °C for PHUs 6-100 (**Table 3.5**). The

improvement in T_g on the addition of DVS-DC can be accounted for by the fact that their polymeric matrix comprises less free space due to their backbone's high stiffness, accounting for the restricted mobility of polymer chains.[40,41]

The thermal stability of the prepared PHUs was examined by TGA under a nitrogen atmosphere and their corresponding thermograms and decomposition temperature ($T_{d,10\%}$) of the polymers were displayed in **Figure 3.29a and** (**Table 3.5**)**,** respectively. The PHUs developed from isosorbide and vanillin-derived building blocks showed excellent thermal stability. The $T_{d,10\%}$ values were in the range of 293-335 °C, These $T_{d,10\%}$ values were comparable to or even higher than those of similar PHU system.[10,31,42] Further, the thermal stability of PHUs was found to increase as a DVS-DC content in the polymer chain increased, which in turn can be attributed to the incorporation of the high molar proportion of the rigid aromatic content in the backbone. In DTG curves of PHUs (**Figure 3.29b**) indicated two distinct stages of degradation. The first stage degradation between 295-400 °C can be attributed to the breakdown of urethane linkages,[43,44] while the decomposition of the other hydrocarbon framework.[44,45] was observed in the second stage between 400-500 °C range.

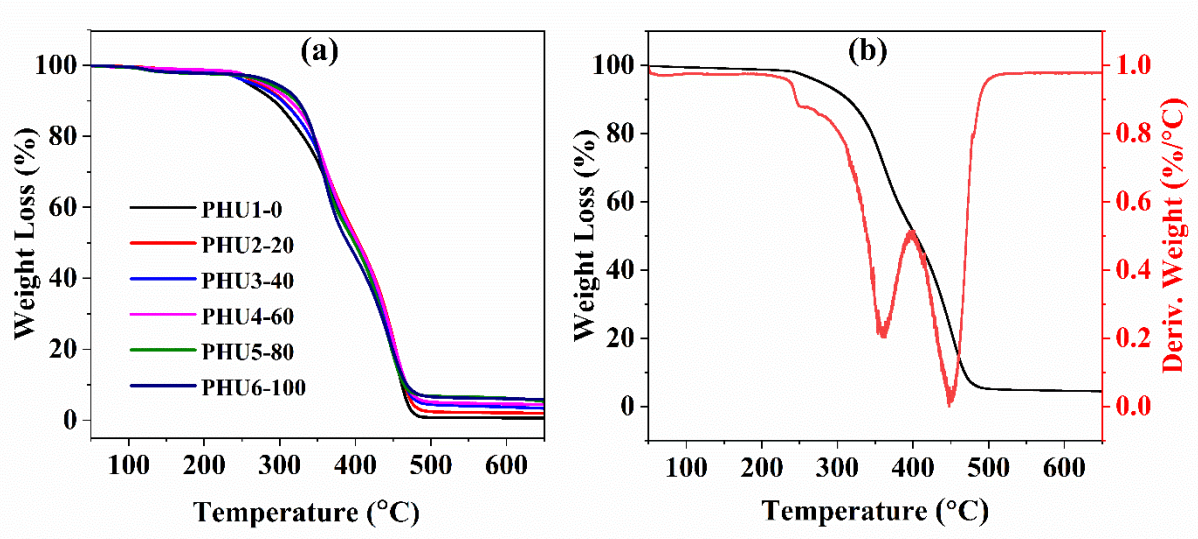

Figure 3.29. *TGA results of PHUs (a) TGA thermograms (b) DTG curve of PHU4-60.*

3.3.3.4 Water contact angle measurements

The surface wettability of the PHU films was analyzed by the water contact angle, and the values obtained are summarized in **Table 3.6** (**Figure 3.30**). The WCA of the PHU polymers varied in the range of 93.9 ± 1.5° to 105.9 ± 0.9°, exhibiting a hydrophobic nature. The hydrophobic nature of these films can be attributed to the strong water-repellence properties of the priamine architecture due to the long aliphatic backbone and two-pendant alkyl chain.[47,48]

Table 3.6. *Water contact angle measurements of PHU polymers.*

Polymer code	Water contact angle (°)
PHU1-0	105.9±0.9
PHU2-20	101.4±1.4
PHU3-40	98.6±1.3
PHU4-60	96.6±0.4
PHU5-80	95.8±0.3
PHU6-100	93.9±1.5

However, the WCA changed from 105.9 ± 0.9° to 93.9 ± 1.5° after increasing the molar composition of DVS-DC in PHUs. The enhanced wettability of films arises from the increase in concentration of the polar methoxy groups in polymer architecture, which raises the surface free energy.[49]

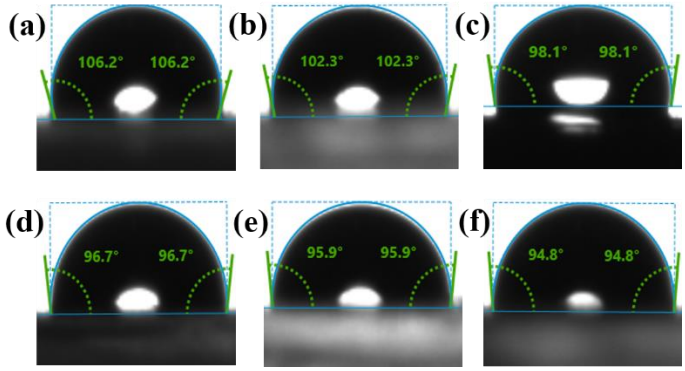

Figure 3.30. *Water contact angle measurement images of PHUs.*

3.3.3.5 X-ray diffraction spectroscopy

To address the molecular structure and chain arrangement of a polymer, a powder X-ray diffraction was performed. The XRD results demonstrate that all samples show a broad diffraction peak located within a 2θ range of 12.5 to 27.5° (**Figure 3.31**), indicating the formation of an amorphous phase.[12,50] The amorphous nature of PHUs can be attributed to the presence of pendant primary and secondary hydroxyl groups, which disrupts the regular packing of polymer chains due to the formation of hydrogen bonds with urethane groups.[39] These results are consistent with DSC findings as they do not exhibit a melting transition due to the absence of long-range order (**Figure 3.28**).

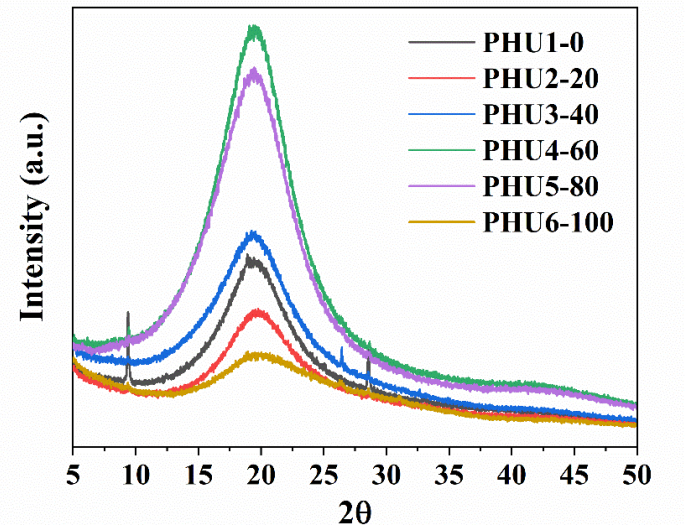

Figure 3.31. *X-ray diffractogram profile of PHUs.*

3.3.3.6 Rheological measurements

To elucidate the effect of molecular composition on the viscoelastic behavior of PHUs, rheological experiments were performed. Strain (2.5 %) within the LVR region was further applied for the frequency sweep and temperature ramp measurements (**Figure 3.32a**). **Figure 3.32b** exhibits the plot of storage (G′) and loss modulus (G″) as a function of frequency for all PHUs. The PHU3-40 had the highest G" value, indicating higher viscosity compared to other compositions, which is in agreement with the plot of complex viscosity presented in **Figure 3.33a**.

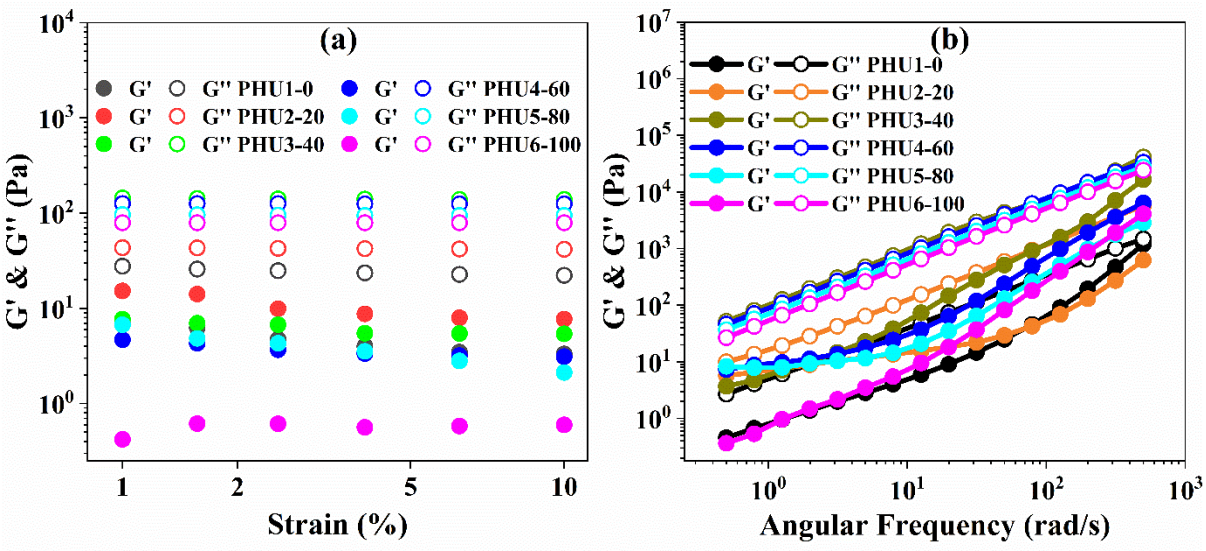

Figure 3.32. *Plot of (a) storage and loss modulus vs strain (b) storage and loss modulus vs angular frequency.*

This enhanced viscosity could be attributed to the synergetic effect of the high density of non-covalent interactions (hydrogen bonds and π-π interactions), as well as the ordered arrangement of the cycloaliphatic and spiro-aromatic segments present in PHU3-40 (**Figure 3.35**).[12,13] As expected, the lowest G″ and complex viscosity were noted for PHU1-0, revealing the absence of or negligible the π-π interactions due to a lower content of aromatic segments. Moreover, the loss modulus of the synthesized samples follows the trend as, PHU3-40 > PHU4-60 > PHU5-80 > PHU6-100 > PHU2-20 > PHU1-0. This may be attributed to the higher segmental stability, supported locally by inter and/or intra-molecular hydrogen bonds, formed between primary and secondary hydroxyl groups and urethane linkages of PHUs.[12] It is interesting to note that except in the case of PHU1-0 cross-over point (G' ≈ G") points of all other compositions are higher than the measured frequency range.

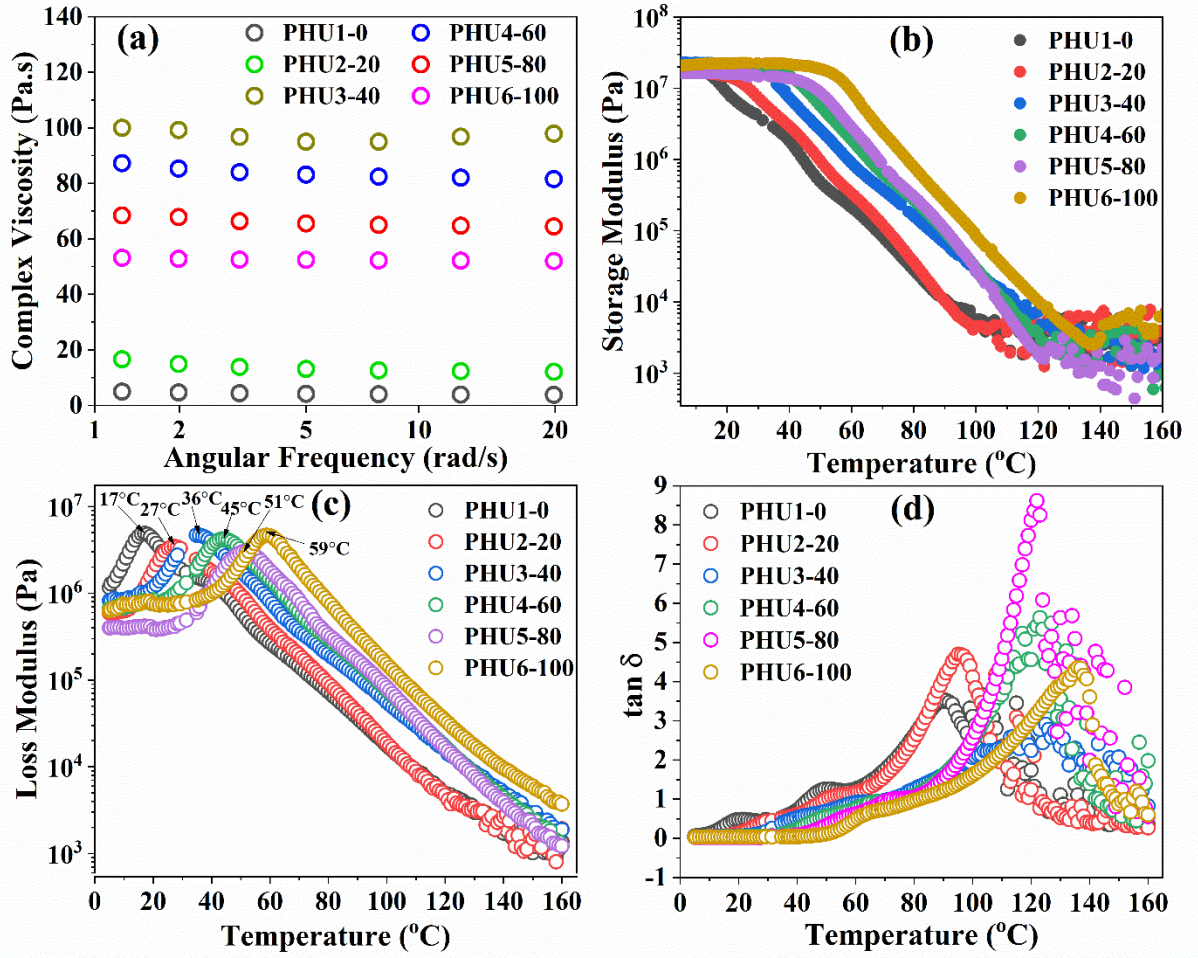

Figure 3.33. *Plot of (a) complex viscosity vs angular frequency. (b) storage modulus vs temperature, (c) loss modulus vs temperature, and (d) tan δ vs temperature, obtained from rheological measurement for PHUs.*

As relaxation time (ω_c) is the reciprocal of the cross-over frequency, PHU1-0 possessing negligible noncovalent interaction exhibited the highest relaxation time as compared with other compositions which is indicative of the lower cohesive force within the polymer chains.[51]

Temperature sweep experiments were conducted to gather more information about the thermal transition of thermoplastic polymers. **Figure 3.33b-d** shows the temperature-dependence of storage modulus (G′), loss modulus (G″), and tan δ of the PHUs. The T_g is determined from G″ curves (range of 16 to 57 °C) and is added in **Table 3.8.** These values are in agreement with DSC results which increased with increasing spiro-aromatic contents. The PHU1-0 exhibited the lowest T_g value (16 °C), while the PHU6-100 displayed the highest T_g value (57 °C).

3.3.3.7 Adhesive properties

The application potential of the developed PHUs as sustainable adhesives was studied by lap shear test according to ASTM D1002 by directly sandwiching PHU films between two aluminum joints by thermal treatment **(Figure 3.34a**).

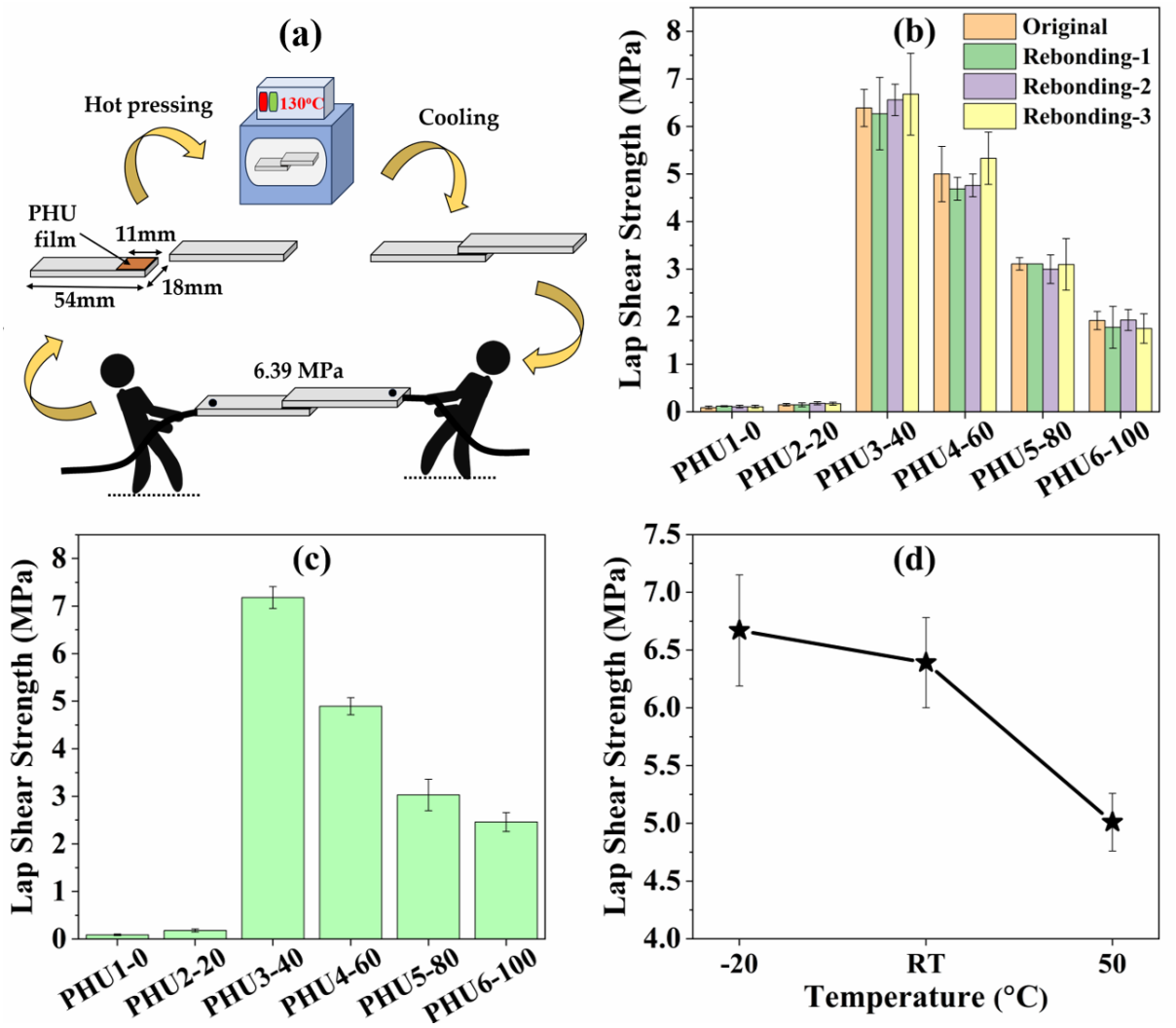

Figure 3.34. *a) Schematic diagram of the bonding of PHU adhesives to aluminum substrate (b) Original and recycled lap shear strength of PHU hot melt adhesives assessed on aluminum (c) Adhesive strength after water soaking for 12 h and (d) Lap shear strength of PHU3-40 at different temperature.*

As displayed in **Figure 3.34b**, (**Figure 3.36, Table 3.7**), the shear strength of PHUs varied between 0.09 to 6.39 MPa based on the monomer composition. A gradual increment in adhesive properties was observed upto 40 mol% of the DVS-DC monomer incorporation in PHU polymers above which the adhesion performances declined on the increment in the DVS-DC content. Interestingly, the PHU3-40 (40 mol% of the DVS-DC monomer) exhibited higher adhesion strength, up to 6.39±0.39 MPa, representing a 71% increment in strength compared to PHU1-0. Moreover, the adhesive strength expressed by PHU3-40 was much higher than previously reported results of biobased hot melt adhesives.[19-21]

The improved adhesion property exhibited by PHU3-40 can be concluded to be a synergetic effect raising from non-covalent interactions (hydrogen bonds and π-π interactions) and also can be accounted to the balanced behavior of the cycloaliphatic and spiro-aromatic segments present in PHU3-40 (**Figure 3.35**).[12,13] Further results analyzed by rheological measurements support the improved adhesion exhibited, as high viscosity was observed in the case of PHU3-40 which supports better non-covalent interactions within the network (**Figure 3.33a**). However, the PHU1-0 and PHU2-20 without or with lower aromatic content exhibited low adhesive strength indicating the absence of or negligible π-π interactions, respectively (Leading to cohesive failure). However, it was observed that increment in the incorporation of spiro-aromatic dicarbonate in PHU4-60, PHU5-80, and PHU6-100 leads to decreased adhesive strength. The reduction in adhesive strength can be accounted for by the increased steric hindrance s by aromatic rings, which leads to the disruption of ordered packing of chain segments and the pattern of non-covalent interactions. Finally, the failure nature of specimens has been examined. It was identified that the mixture of cohesive and adhesive failure occurred in all polymer films except in the case of PHU1-0 and PHU2-20. Particularly, PHU1-0 and PHU2-20 exhibited cohesive failure (**Figure 3.38**).[10]

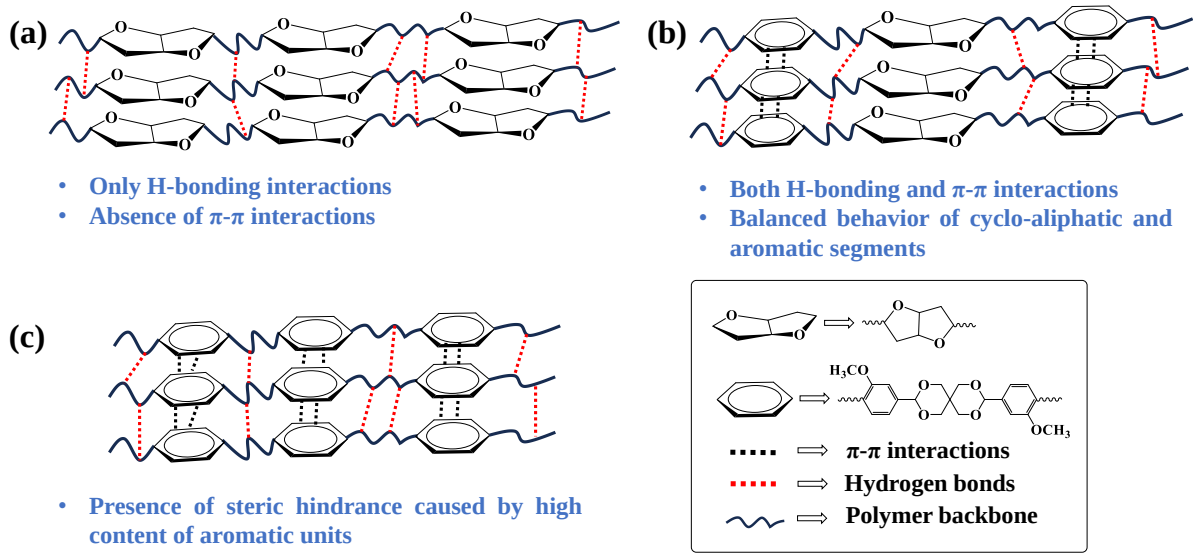

Figure 3.35. *Schematic representation of the possible non-covalent interactions and structural arrangement of cycloaliphatic and aromatic segments in PHU1-0 (a), PHU3-40 (b), and PHU6-100 (c).*

To explore the robustness of the developed PHU adhesives thermo-reversible adhesion properties, the temperature tolerance of adhesives and their adhesion performance under wet conditions was explored. The thermoreversibility adhesion nature of PHUs was investigated

by bonding and debonding repeatedly for three times. The results showed that almost identical adhesive strengths were observed during the consecutive reuses, which indicates the excellent thermo-reversibility of the synthesized adhesives. Upon temperature tolerance adhesion studies, PHU adhesive exhibited excellent adherence at low temperatures (-20°C) and only a slight drop in shear strength (%) at high temperatures (50°C), indicative of the adhesive applicability for a broad range of temperature (**Figure 3.34d)**. The PHUs also exhibited good adhesion properties even after immersing in de-ionized water for 12 h. As shown in **Figure 3.34c** (**Table 3.7**), all PHU samples retained their original strength after soaking in water stating the superior adhesion stability and applicability of the material under different conditions. Moreover, the visualization of the remarkable adhesion strength of PHU3-40 can be observed in **Figure 3.37a** where the bonded aluminum slides held over 100 kg of weight. Further, upon a detailed comparison of reported hot melt adhesives, it was found that the synthesized PHU3-40 showcased notable adhesion properties and had a high bio-content (**Figure 3.37b**). This suggests that it could be a promising candidate for use in various applications that demand robust and environmentally friendly adhesives.

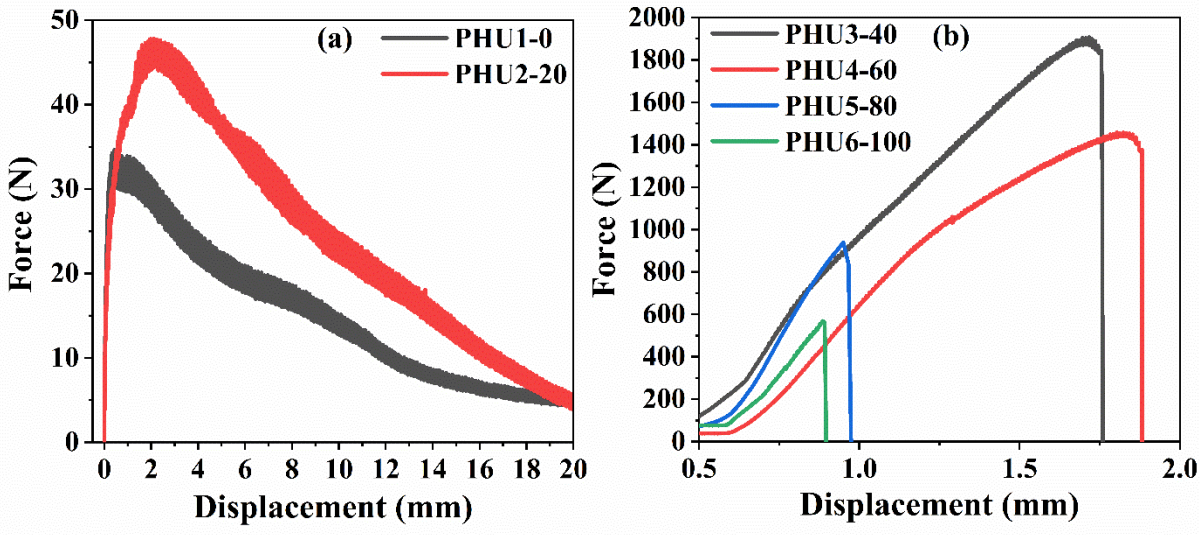

***Figure 3.36**. Force vs. displacement curves of PHU adhesives.*

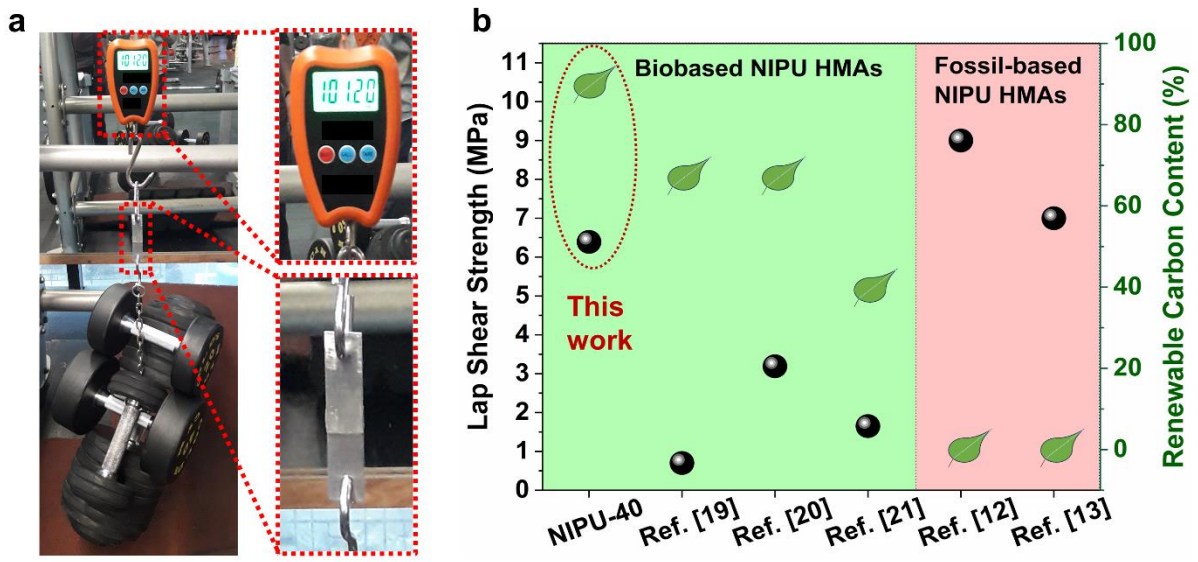

Figure 3.37. *(a) Two aluminum joints bonded by a PHU3-40 held 100 kg of weight. (b) Lap shear strength of PHU3-40 compared against thermoplastic PHU-based hot melt adhesives reported in the literature.*

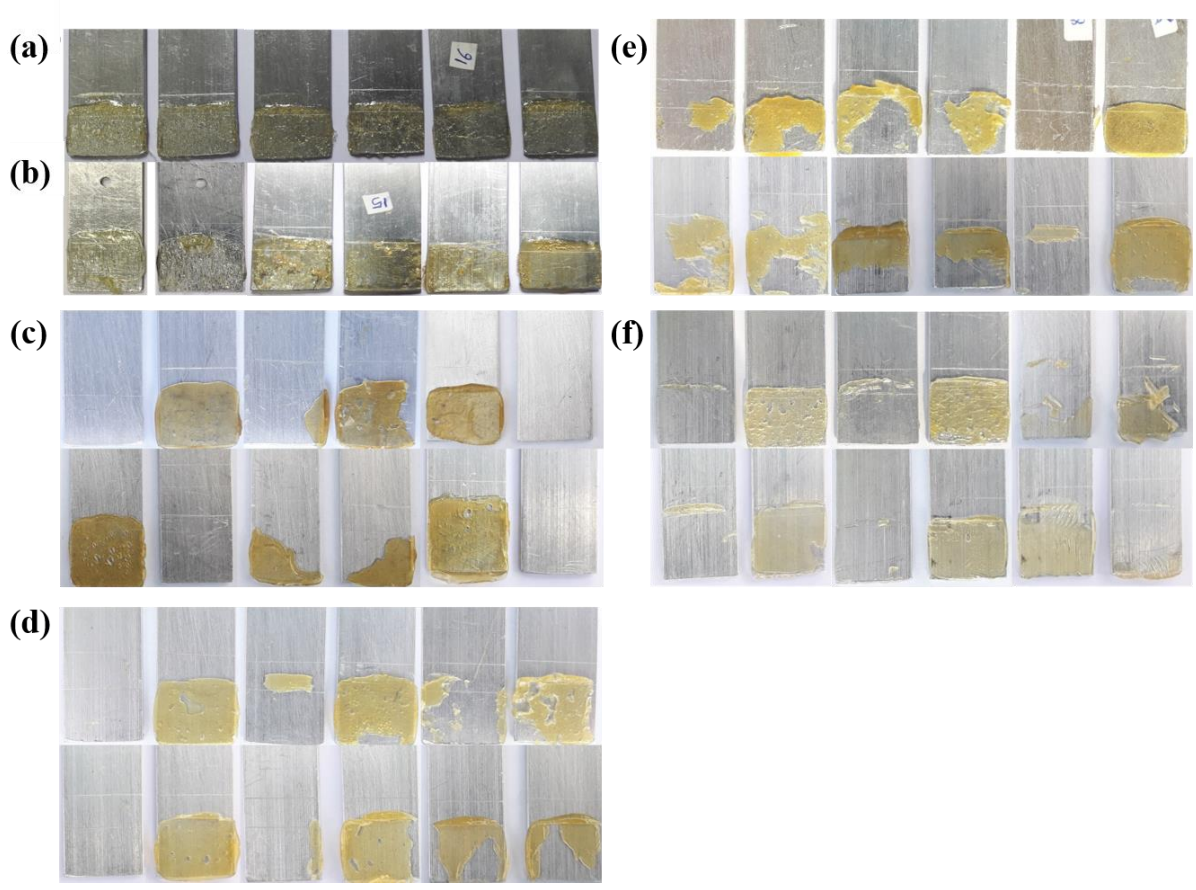

Figure 3.38. *Fracture interfaces of the PHU adhesives (a) PHU1-0 and (b) PHU2-20 (c) PHU3-40 (d) PHU4-60 (e) PHU5-80 (f) PHU6-100.*

Table 3.7. *Lap shear strength of PHUs on the aluminum substrate.*

Polymers	Lap shear strengths (MPa)				
	Original	Rebonding			Underwater
		1	2	3	
PHU1-0	0.09±0.03	0.12±0.01	0.11±0.02	0.11±0.03	0.08±0.01
PHU2-20	0.15±0.02	0.15±0.04	0.18±0.33	0.17±0.03	0.18±0.03
PHU3-40	6.39±0.39	6.27±0.76	6.56±0.33	6.68±0.86	7.18±0.22
PHU4-60	4.71±0.58	4.69±0.24	4.76±0.24	5.33±0.55	4.89±0.18
PHU5-80	3.11±0.13	3.11±0.00	3.00±0.30	3.10±0.54	3.03±0.33
PHU6-100	1.98±0.19	1.78±0.44	1.93±0.22	1.75±0.31	2.46±0.20

3.3.3.8 Mechanical properties

The stress-strain curves of PHUs synthesized by varying the molar composition of dicarbonate/priamine monomers are displayed in **Figure 3.39** and the data are summarized in **Table 3.8.** These developed PHUs were found to have extremely adaptable mechanical properties. PHU1-0 showed considerably inferior modulus, and tensile properties due to the absence of rigid spiro-aromatic moiety.

Table 3.8. *Mechanical properties of the PHU samples.*

Polymers	Tensile Properties			T_g (°C) from rheology
	Young's modulus (MPa)	Tensile strength (MPa)	Elongation at break (%)	
PHU1-0	1.22±0.17	0.21±0.01	>2000	16
PHU2-20	4.76±0.42	0.27±0.02	1493±395	27
PHU3-40	13.54±1.1	1.87±0.30	686±42	36
PHU4-60	51.10±2.4	5.11±0.30	312±37	44
PHU5-80	151.38±8.0	10.48±0.38	148±10	50
PHU6-100	254.07±25	14.56±1.9	59±20	57

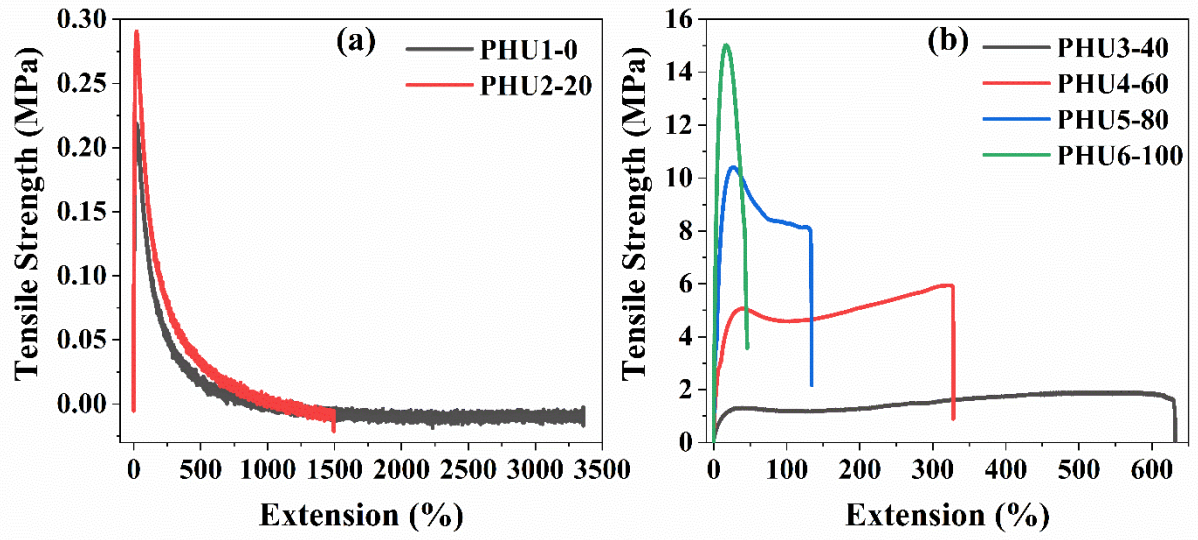

Figure 3.39. *Tensile test curves (stress-strain) of the (a) PHU1-0, PHU2-20, and b) PHU3-40, PHU4-60, PHU5-80, and PHU6-100.*

However, the introduction of DVS-DC in the polymer chain improved the mechanical properties of PHUs. The observed change in mechanical property can be accounted to the incorporation of rigid segments (DVS-DC) leading to restricted mobility of the chains resulting in a positive impact on the modulus as well as, tensile strength values whereas a reduction in elongation.[52,53] These values are considerably higher than those of previously reported thermoplastic PHUs.[38,39,54,55]

3.3.3.9 Acid degradability of PHUs

Degradation profiles of the DVS-DC and PHUs were analyzed as they contained a susceptible acetal group, which is well-known to undergo hydrolysis under acidic conditions.[36,57]

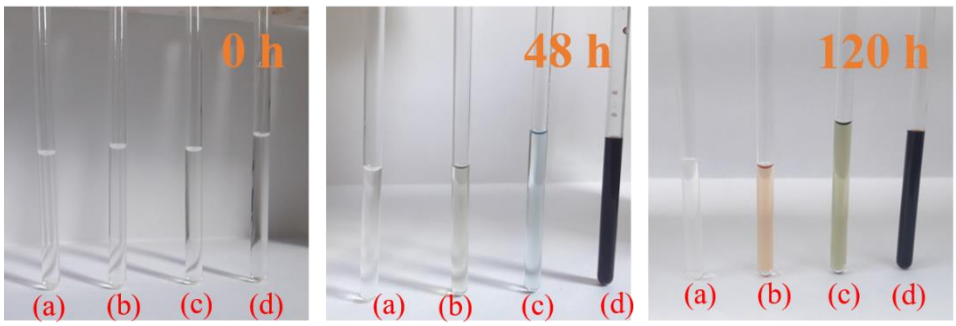

Figure 3.40. *The change in color of DVS-DC solutions in NMR tubes at room temperature (a) 0 mol/L (b) 0.1 mol/L (c) 1.0 mol/L (d) 2.0 mol/L.*

The study initially focused on examining the breakdown of the DVS-DC monomer in the presence of acid at room temperature using ^{1}H NMR. Three different concentrations of HCl (0.1, 1.0, and 2.0 mol/L) were utilized, and the degradation was observed at different time intervals. ^{1}H NMR analysis revealed monomer DVS-DC exhibited faster degradation as HCl concentration increased and afforded a darker solution on degradation (**Figure 3.40**).

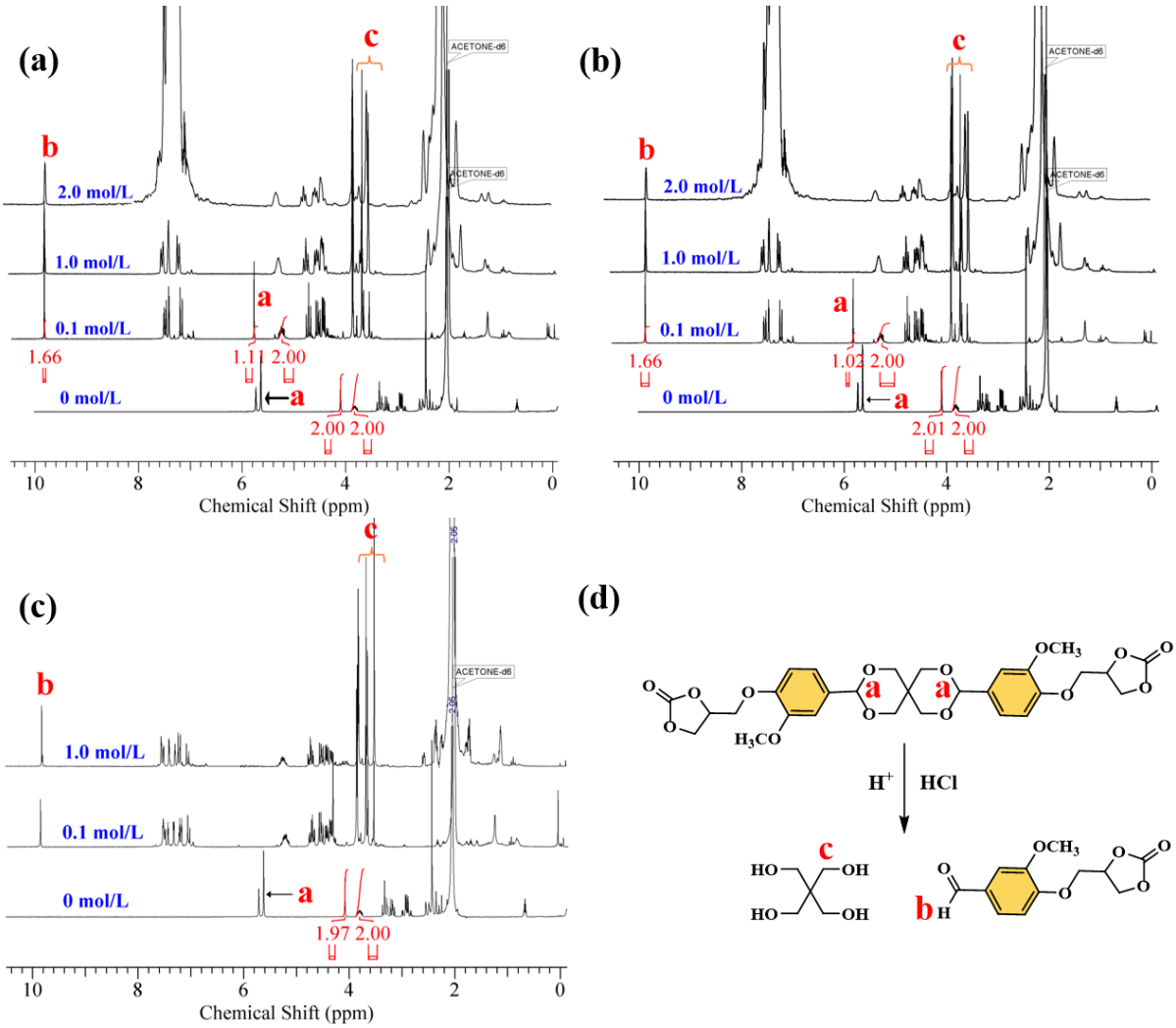

Figure 3.41. *^{1}H NMR spectra of DVS-DC (a) after 5 h (b) after 24 h (c) after 120 h (d) possible degradation mechanism of DVS-DC in HCl solutions.*

Compared to the control, samples treated with HCl expressed a reduction in the integration values of the acetal peak at 5.81 ppm (peak 'a') and new intense signals were observed at 9.88 ppm (peak 'b') [58,59] and 3.53−3.72 ppm (peak 'c'). These observations indicate the decomposition of the characteristic acetal bond into aldehyde and pentaerythritol compounds, respectively (**Figure 3.41**). It took 120 h for the complete hydrolysis of the acetal linkage in DVS-DC when treated with 0.1 mol/L HCl, whereas treatment with 1 and 2 mol/L HCl resulted

in complete hydrolysis of the acetal group within 5 h. Furthermore, the potential breakdown products are vanillin mono-carbonate and pentaerythritol, which was confirmed through ^{1}H NMR of fully decomposed monomer in HCL (1.0 mol/L samples for 5 h) (**Figure 3.42**).

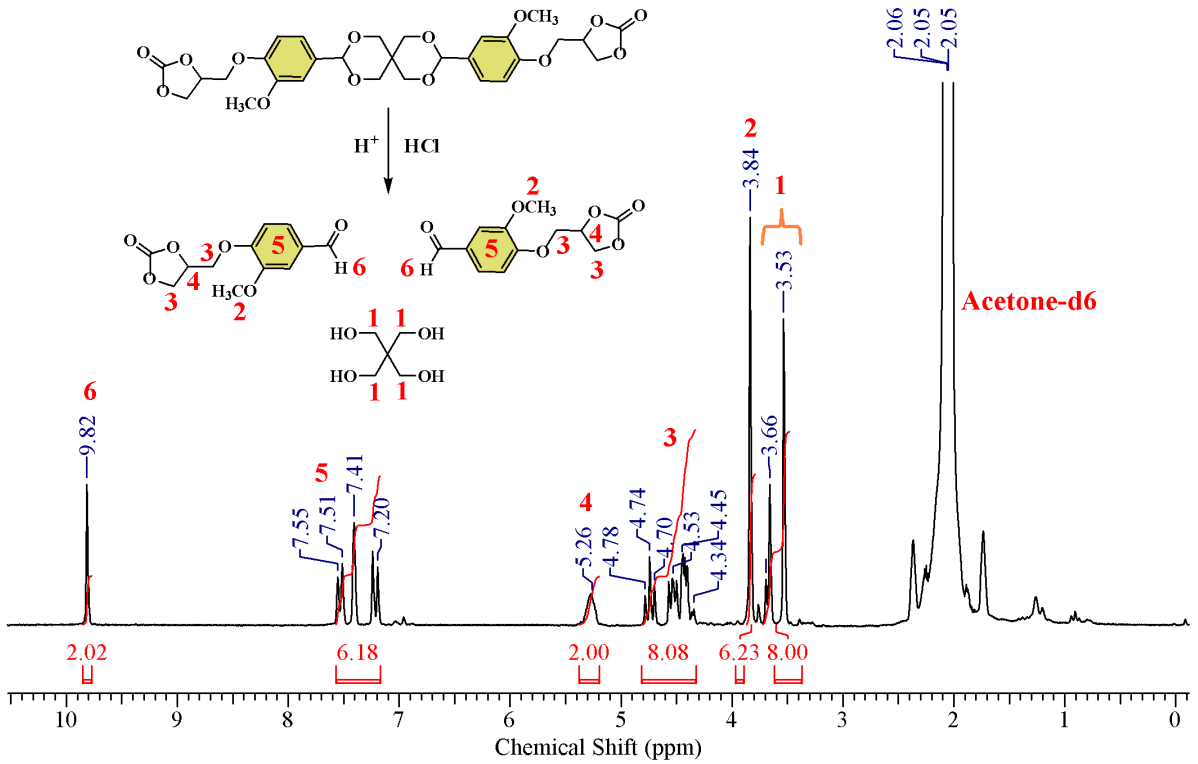

Figure 3.42. *^{1}H NMR spectrum of possible degradation products (1.0 mol/L, 5 h).*

Further, the degradation assessment of PHU1-0, PHU3-40, and PHU6-100 samples was analyzed (**Figure 3.43**) by immersing them in acid solutions (1 mol/L HCl), and their decomposition process was monitored over different periods (1, 7, 14, and 21 days) using ^{1}H NMR and FTIR techniques. PHU3-40 and PHU6-100 samples, which have a significant content of spiro-aromatic monomer, showed complete disappearance of the acetal peak at 5.40 ppm (peak 'a') and the emergence of a new -CHO peak at 9.86 ppm (peak 'b') within 24 hours. (**Figure 3.44b and 3.44c**), This indicates the formation of aldehyde functional oligomers and pentaerythritol as a possible degradation product which demonstrates that PHUs containing acetal linkages are susceptible to degradation in acidic environments. However, PHU1-0 devoid of acetal linkage did not exhibit any signs of degradation even after 21 days of treatment with HCl (**Figure 3.44a**). Further FTIR analysis of samples showed that PHU6-100 had visible absorbance of -CHO groups at 1680 cm^{-1}, but not in the case of PHU1-0 and PHU3-40 due to their lower or lack of spiro-aromatic content (**Figure 3.45**).

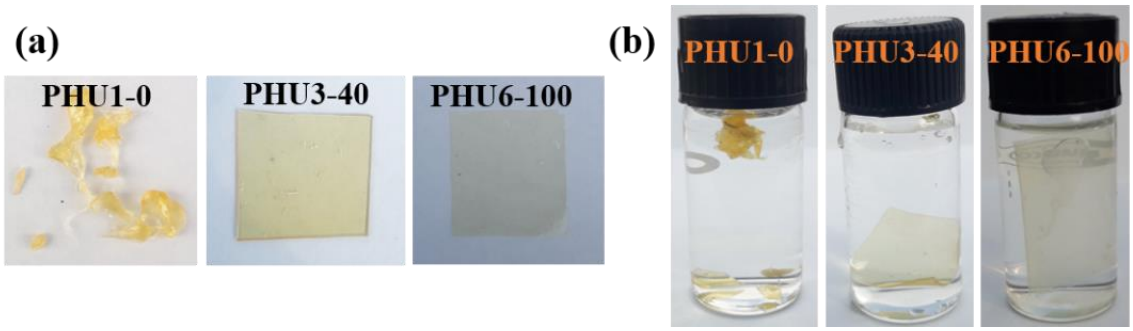

Figure 3.43. *Photographs of the PHU samples before and after adding to 1 mol/L HCl solutions.*

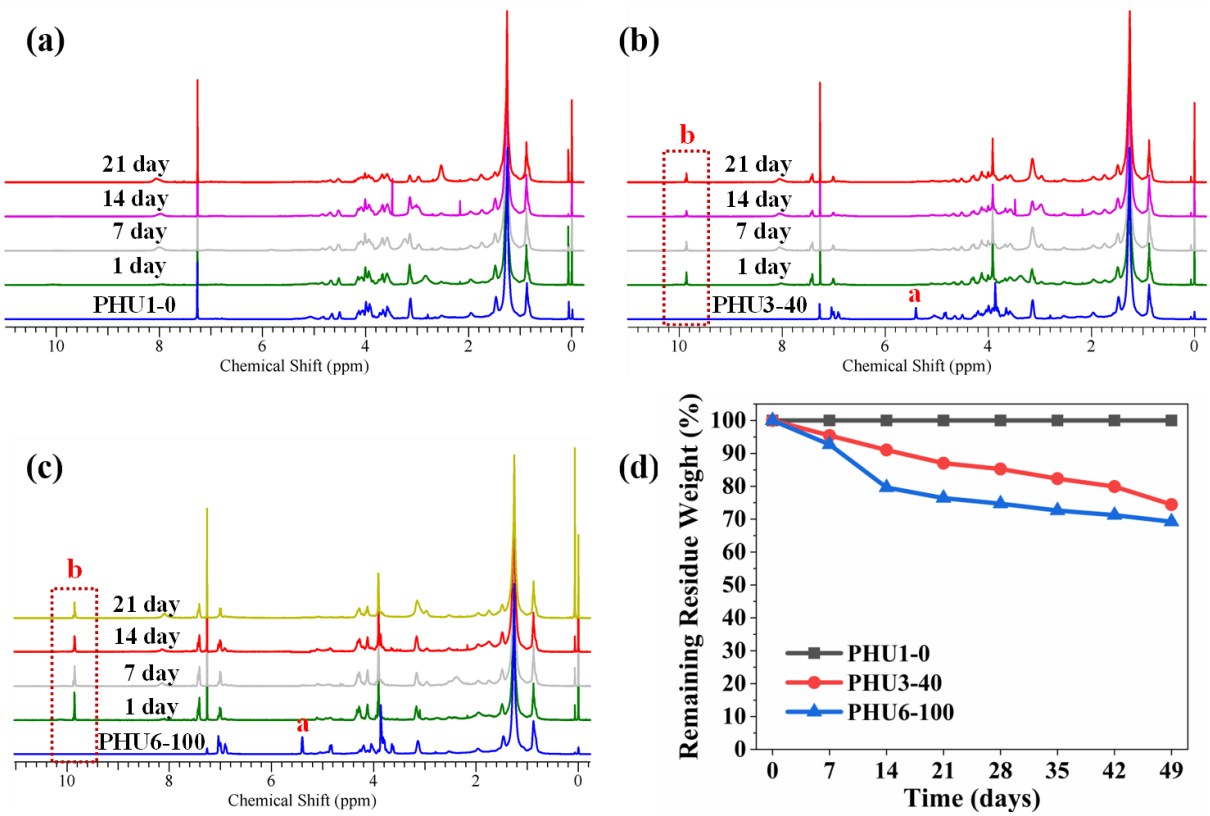

Figure 3.44. *^{1}H NMR spectrum of (a) PHU1-0, (b) PHU3-40, and (c) PHU6-100, before and after degradation (1 mol/L HCl). (d) weight loss of the PHUs with different times (under 1 mol/L HCl).*

To assess the degradation effect in PHU samples, the change in mass was measured under 1 mol/L HCl after a one-week time interval and up to 49 days (**Figure 3.44d)**. PHU6-100 with higher acetal linkages was more prone to weight loss with a percent mass loss of 30.76 % while PHU6-100 with lesser acetal linkages showed a mass loss of 25.56 %. In contrast, PHU1-0, which lacks acetal linkage, did not exhibit any change in mass loss after 49 days of degradation

studies. The results indicated that the percentage of mass loss in the PHU samples corresponded directly to the amount of acetal linkages present in them.

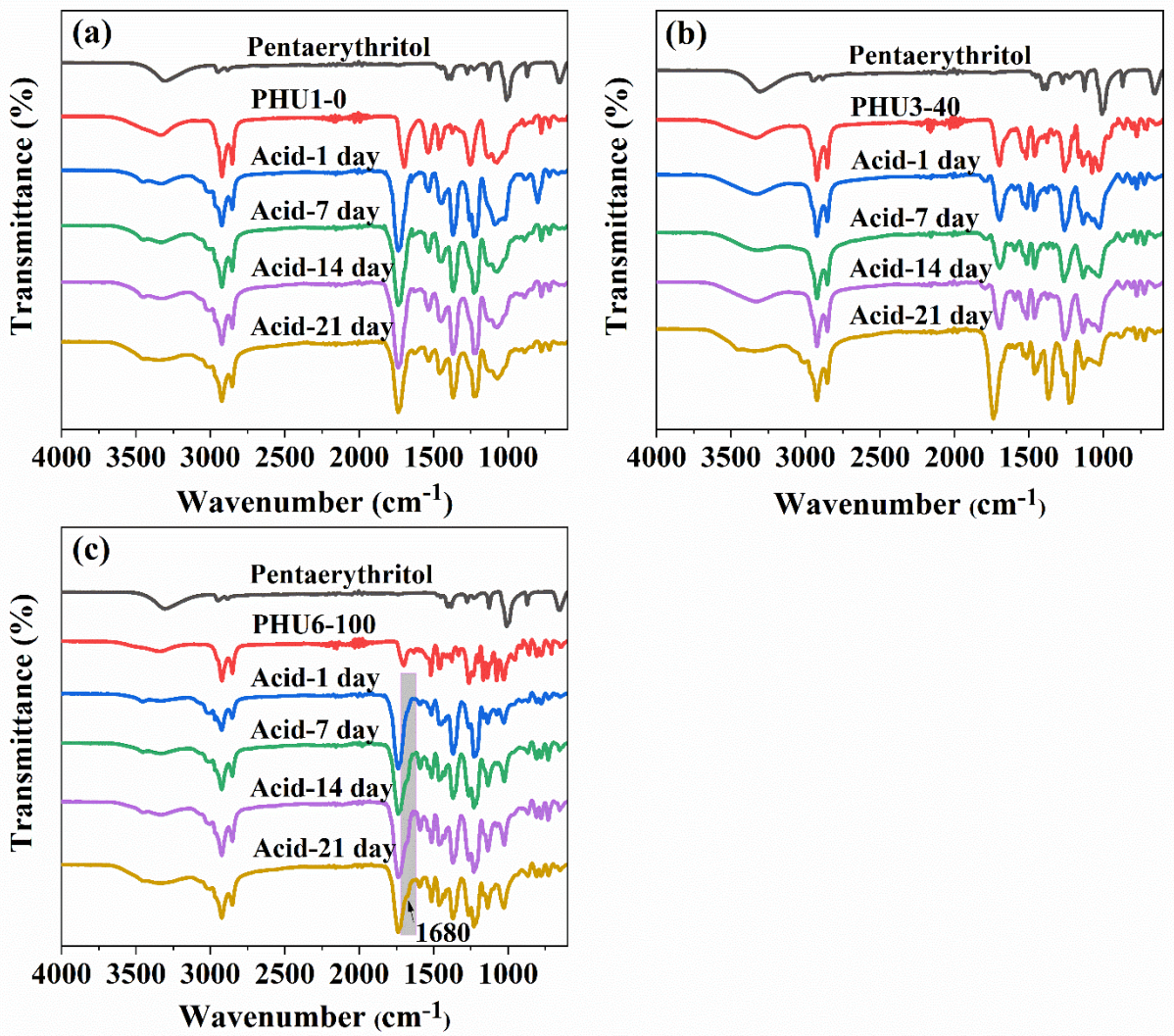

Figure 3.45. *FTIR spectra of (a) PHU1-0, (b) PHU3-40, and (c) PHU6-100 before and after degradation under 1 mol/L HCl.*

3.4 Conclusion

In summary, as a possible alternative to conventional petroleum-based hot melt adhesives, we have successfully constructed a reusable bio-based HMA with a bio-renewable carbon content of >88 %, biodegradability, excellent reusability, and superior adhesive nature was developed. Two biobased cyclic carbonates with high renewable carbon content were synthesized from Vanillin and Isosorbide and these monomers were used to prepare PHU-HMAs with finely tailored physico-mechanical properties by step-growth polyaddition. In addition, the structure-property relationship and influence of the monomer composition on the mechanical and thermal properties of the obtained PHUs were studied in detail. PHU-HMAs presented

excellent mechanical performance including a high adhesion strength, thermo-reversible adhesion properties, good temperature tolerance, and adhesion under wet conditions. The enhanced properties of HMAs were attributed to the synergetic effect of the high density of non-covalent interactions (hydrogen bonds and π-π interactions), as well as the arrangement of the cycloaliphatic and spiro-aromatic segments. Further, the unique rigid spirocyclic acetal molecular architecture of DVS-DC makes them ideal for enabling a facile selective acidic hydrolysis and aiding chemical degradability. Our diligent efforts have paved a pathway in the development of sustainable and environmentally friendly PHUs with good adhesive and potential degradation properties.

3.5 References

(1) Dinte, E.; Sylvester, B. Adhesives: Applications and Recent Advances. *Appl. Adhes. Bond. Sci. Technol.* **2018**, 142-156.

(2) Silva, L. F. M.; Ochsner, A.; Adams, R. D. Handbook of adhesion technology, Springer, Oxford, **2018**, UK.

(3) Vineeth, S. K.; Gadhave, R. V. Sustainable Raw Materials in Hot Melt Adhesives: A Review. *Open J. Polym. Chem.* **2020**, *10*, 49–65.

(4) Hot Melt Adhesives Market Global Forecast (2022-2027) by Type, Application, and Region. https://www.marketsandmarkets.com/Market-Reports/hot-melt-adhesives-market-1088.html (accessed 13 January 2024).

(5) Polyurethane Hot Melt Adhesive Market Size, Share, and Trend Analysis Report By Type, Application, and Region- Forecast, 2020-2030, https://www.straitsresearch.com/report/polyurethane-hot-melt-adhesive-market (accessed 13 January 2024).

(6) Sardon, H.; Pascual, A.; Mecerreyes, D.; Taton, D.; Cramail, H.; Hedrick, J. L. Synthesis of Polyurethanes Using Organocatalysis: A Perspective. *Macromolecules* **2015**, *48* (10), 3153–3165.

(7) Lockey, J. E.; Redlich, C. A.; Streicher, R.; Pfahles-Hutchens, A.; Hakkinen, P. J.; Ellison, G. L.; Harber, P.; Utell, M.; Holland, J.; Comai, A.; White, M. Isocyanates and Human Health: Multistakeholder Information Needs and Research Priorities. *J. Occup. Environ. Med.* **2015**, *57* (1), 44–51.

(8) Maisonneuve, L.; Lamarzelle, O.; Rix, E.; Grau, E.; Cramail, H. Isocyanate-Free Routes to Polyurethanes and Poly(Hydroxy Urethane)S. *Chem. Rev.* **2015**, *115* (22), 12407–12439.

(9) Gomez-Lopez, A.; Grignard, B.; Calvo, I.; Detrembleur, C.; Sardon, H. Accelerating the Curing of Hybrid Poly(Hydroxy Urethane)-Epoxy Adhesives by the Thiol-Epoxy Chemistry. *ACS Appl. Polym. Mater.* **2022**, *4* (12), 8786–8794.

(10) Gomez-Lopez, A.; Grignard, B.; Calvo, I.; Detrembleur, C.; Sardon, H. Monocomponent Non-Isocyanate Polyurethane Adhesives Based on a Sol–Gel Process. *ACS Appl. Polym. Mater.* **2020**, *2* (5), 1839–1847.

(11) Gomez-lopez, A.; Grignard, B.; Calvo, I.; Detrembleur, C.; Sardon, H. Synergetic Effect of Dopamine and Alkoxysilanes in Sustainable Non-Isocyanate Polyurethane Adhesives. *Macromol. Rapid Commun.* **2020**, *42* (3), *2000538*.

(12) Sukumaran Nair, A.; Cherian, S.; Balachandran, N.; Panicker, U. G.; Kalamblayil Sankaranarayanan, S. K. Hybrid Poly(Hydroxy Urethane)s: Folded-Sheet Morphology and Thermoreversible Adhesion. *ACS Omega* **2019**, *4* (8), 13042–13051.

(13) Gomez-Lopez, A.; Ayensa, N.; Grignard, B.; Irusta, L.; Calvo, I.; Müller, A. J.; Detrembleur, C.; Sardon, H. Enhanced and Reusable Poly(Hydroxy Urethane)-Based Low Temperature Hot-Melt Adhesives. *ACS Polym. Au* **2022**, *2* (3), 194–207.

(14) Panchireddy, S.; Grignard, B.; Thomassin, J. M.; Jerome, C.; Detrembleur, C. Bio-Based Poly(Hydroxyurethane) Glues for Metal Substrates. *Polym. Chem.* **2018**, *9* (19), 2650–2659.

(15) Cornille, A.; Michaud, G.; Simon, F.; Fouquay, S.; Auvergne, R.; Boutevin, B.; Caillol, S. Promising Mechanical and Adhesive Properties of Isocyanate-Free Poly(Hydroxyurethane). *Eur. Polym. J.* **2016**, *84*, 404–420.

(16) Panchireddy, S.; Grignard, B.; Thomassin, J.-M.; Jerome, C.; Detrembleur, C. Catechol Containing Polyhydroxyurethanes as High-Performance Coatings and Adhesives. *ACS Sustain. Chem. & Eng.* **2018**, *6* (11), 14936–14944.

(17) Panchireddy, S.; Thomassin, J. M.; Grignard, B.; Damblon, C.; Tatton, A.; Jerome, C.; Detrembleur, C. Reinforced Poly(Hydroxyurethane) Thermosets as High Performance Adhesives for Aluminum Substrates. *Polym. Chem.* **2017**, *8* (38), 5897–5909.

(18) Anitha, S.; Vijayalakshmi, K. P.; Unnikrishnan, G.; Kumar, K. S. S. CO2 Derived Hydrogen Bonding Spacer: Enhanced Toughness, Transparency, Elongation and Non-Covalent Interactions in Epoxy-Hydroxyurethane Networks. *J. Mater. Chem. A* **2017**, *5* (46), 24299–24313.

(19) Tryznowski, M.; Świderska, A.; Gołofit, T.; Zołek-Tryznowska, Z. Wood Adhesive Application of Poly(Hydroxyurethane)s Synthesized with a Dimethyl Succinate-Based Amide Backbone. *RSC Adv.* **2017**, *7* (48), 30385–30391.

(20) Tryznowski, M.; Swiderska, A. Poly (Hydroxyurethane) s with Diethyl Tartrate-Based Amide Backbone by an Isocyanate-Free Route : Use as Adhesives. **2018**, *144*, 1–6.

(21) Ghuge, G. H.; Kambikanam, K. V.; Nair, K. S. Evaluation of the Adhesive Properties of Vanillin-Derived Polyhydroxy Urethanes. *J. Appl. Polym. Sci.* **2023**, *40*, 1–11.

(22) Ukaszczyk, J.; Janicki, B.; López, A.; Skołucka, K.; Wojdyła, H.; Persson, C.; Piaskowski, S.; Śmiga-Matuszowicz, M. Novel Injectable Biomaterials for Bone Augmentation Based on Isosorbide Dimethacrylic Monomers. *Mater. Sci. Eng. C* **2014**, *40*, 76–84.

(23) Lorenzini, C.; Versace, D. L.; Gaillet, C.; Lorthioir, C.; Boileau, S.; Renard, E.; Langlois, V. Hybrid Networks Derived from Isosorbide by Means of Thiol-Ene Photoaddition and Sol-Gel Chemistry. *Polymer,* **2014**, *55* (17), 4432–4440.

(24) Ma, S.; Wei, J.; Jia, Z.; Yu, T.; Yuan, W.; Li, Q.; Wang, S.; You, S.; Liu, R.; Zhu, J. Readily Recyclable, High-Performance Thermosetting Materials Based on a Lignin-Derived Spiro Diacetal Trigger. *J. Mater. Chem. A* **2019**, *7* (3), 1233–1243.

(25) Dong, W.; Yoshida, Y.; Endo, T. Synthesis of Poly(Hydroxyurethane) from 5-Membered Cyclic Carbonate under Mild Conditions in the Presence of Bicyclic Guanidine and Their Reaction Process. *J. Polym. Sci.* **2021**, *59* (6), 502–509.

(26) Besse, V.; Auvergne, R.; Carlotti, S.; Boutevin, G.; Otazaghine, B.; Caillol, S.; Pascault, J. P.; Boutevin, B. Synthesis of Isosorbide Based Polyurethanes: An Isocyanate Free Method. *React. Funct. Polym.* **2013**, *73* (3), 588–594.

(27) Ménard, R.; Caillol, S.; Allais, F. Chemo-Enzymatic Synthesis and Characterization of Renewable Thermoplastic and Thermoset Isocyanate-Free Poly(Hydroxy)Urethanes from Ferulic Acid Derivatives. *ACS Sustain. Chem. Eng.* **2017**, *5* (2), 1446–1456.

(28) Warlin, N.; Garcia Gonzalez, M. N.; Mankar, S.; Valsange, N. G.; Sayed, M.; Pyo, S. H.; Rehnberg, N.; Lundmark, S.; Hatti-Kaul, R.; Jannasch, P.; Zhang, B. A Rigid Spirocyclic Diol from Fructose-Based 5-Hydroxymethylfurfural: Synthesis, Life-Cycle Assessment, and Polymerization for Renewable Polyesters and Poly(Urethane-Urea)S. *Green Chem.* **2019**, *21* (24), 6667–6684.

(29) Zhao, D.; Liang, X.; Wang, J.; Du, J.; Zhu, Y. Vanillin-Based Degradable Polyurethane Thermosets Demonstrating High Bio-Content and Mechanical Properties. *ACS Appl. Polym. Mater.* **2023**, *5* (6), 4536–4545.

(30) Mokhtari, C.; Malek, F.; Manseri, A.; Caillol, S.; Negrell, C. Reactive Jojoba and Castor Oils-Based Cyclic Carbonates for Biobased Polyhydroxyurethanes. *Eur. Polym. J.* **2019**, *113*, 18–28.

(31) Kathalewar, M.; Sabnis, A.; D'Mello, D. Isocyanate Free Polyurethanes from New CNSL Based Bis-Cyclic Carbonate and Its Application in Coatings. *Eur. Polym. J.* **2014**, *57*, 99–108.

(32) Hu, S.; Chen, X.; Torkelson, J. M. Biobased Reprocessable Polyhydroxyurethane Networks: Full Recovery of Crosslink Density with Three Concurrent Dynamic Chemistries. *ACS Sustain. Chem. Eng.* **2019**, *7* (11), 10025–10034.

(33) Ummadisetti, C.; Rachapudi, B. N. P.; Bethala, L. A. P. D. Glycerol-Based SO3H-Carbon Catalyst: A Green Recyclable Catalyst for the Chemoselective Synthesis of Pentaerythritol Diacetals. *Eur. J. Chem.* **2014**, *5* (3), 536–540.

(34) Mankar, S. V.; Garcia Gonzalez, M. N.; Warlin, N.; Valsange, N. G.; Rehnberg, N.; Lundmark, S.; Jannasch, P.; Zhang, B. Synthesis, Life Cycle Assessment, and Polymerization of a Vanillin-Based Spirocyclic Diol toward Polyesters with Increased Glass-Transition Temperature. *ACS Sustain. Chem. Eng.* **2019**, *7* (23), 19090–19103.

(35) Tryznowski, M.; Żołek-Tryznowska, Z. Surface Properties of Poly(Hydroxyurethane)s Based on Five-Membered BIS-Cyclic Carbonate of Diglycidyl Ether of Bisphenol A. *Materials (Basel).* **2020**, *13* (22), 1–14.

(36) Mankar, S. V.; Wahlberg, J.; Warlin, N.; Valsange, N. G.; Rehnberg, N.; Lundmark, S.; Jannasch, P.; Zhang, B. Short-Loop Chemical Recycling via Telechelic Polymers for Biobased Polyesters with Spiroacetal Units. *ACS Sustain. Chem. Eng.* **2023**, *11* (13), 5135–5146.

(37) Blain, M.; Cornille, A.; Boutevin, B.; Auvergne, R.; Benazet, D.; Andrioletti, B.; Caillol, S. Hydrogen Bonds Prevent Obtaining High Molar Mass PHUs. *J. Appl. Polym. Sci.* **2017**, *134* (45), 1–13.

(38) Hu, S.; Chen, X.; Torkelson, J. M. Isocyanate-Free, Thermoplastic Polyhydroxyurethane Elastomers Designed for Cold Temperatures: Influence of PDMS Soft-Segment Chain Length and Hard-Segment Content. *Polymer,* **2022**, *256*, 125251.

(39) Leitsch, E. K.; Beniah, G.; Liu, K.; Lan, T.; Heath, W. H.; Scheidt, K. A.; Torkelson, J. M. Nonisocyanate Thermoplastic Polyhydroxyurethane Elastomers via Cyclic Carbonate Aminolysis: Critical Role of Hydroxyl Groups in Controlling Nanophase Separation. *ACS Macro Lett.* **2016**, *5* (4), 424–429.

(40) Chantawansri, T. L.; Yeh, I. C.; Hsieh, A. J. Investigating the Glass Transition Temperature at the Atom-Level in Select Model Polyamides: A Molecular Dynamics Study. *Polymer,* **2015**, *81*, 50–61.

(41) Aharoni, S. M. Molecular Stiffness and Thermal Properties of Polymers. *J. Appl. Polym.*

Sci. **1976**, *20* (10), 2863–2869.

(42) Sheng, X.; Ren, G.; Qin, Y.; Chen, X.; Wang, X.; Wang, F. Quantitative Synthesis of Bis(Cyclic Carbonate)s by Iron Catalyst for Non-Isocyanate Polyurethane Synthesis. *Green Chem.* **2015**, *17* (1), 373–379.

(43) Farhadian, A.; Ahmadi, A.; Omrani, I.; Miyardan, A. B.; Varfolomeev, M. A.; Nabid, M. R. Synthesis of Fully Bio-Based and Solvent Free Non-Isocyanate Poly (Ester Amide/Urethane) Networks with Improved Thermal Stability on the Basis of Vegetable Oils. *Polym. Degrad. Stab.* **2018**, *155*, 111–121.

(44) Ling, Z.; Zhang, C.; Zhou, Q. Synthesis and Characterization of 1 K Waterborne Non-Isocyanate Polyurethane Epoxy Hybrid Coating. *Prog. Org. Coatings* **2022**, *169*, 106915.

(45) Duval, C.; Kébir, N.; Jauseau, R.; Burel, F. Organocatalytic Synthesis of Novel Renewable Non-Isocyanate Polyhydroxyurethanes. *J. Polym. Sci. Part A Polym. Chem.* **2016**, *54* (6), 758–764.

(46) Ecochard, Y.; Leroux, J.; Boutevin, B.; Auvergne, R.; Caillol, S. From Multi-Functional Siloxane-Based Cyclic Carbonates to Hybrid Polyhydroxyurethane Thermosets. *Eur. Polym. J.* **2019**, *120*, 109280.

(47) Wołosz, D.; Fage, A. M.; Parzuchowski, P. G.; Świderska, A.; Brüll, R. Reactive Extrusion Synthesis of Biobased Isocyanate-Free Hydrophobically Modified Ethoxylated Urethanes with Pendant Hydrophobic Groups. *ACS Sustain. Chem. Eng.* **2022**, *10* (35), 11627–11640.

(48) Younes, G. R.; Maric, M. Increasing the Hydrophobicity of Hybrid Poly(Propylene Glycol)-Based Polyhydroxyurethanes by Capping with Hydrophobic Diamine. *Ind. Eng. Chem. Res.* **2021**, *60* (22), 8159–8171.

(49) Wenzl, I.; Yam, C. M.; Barriet, D.; Lee, T. R. Structure and Wettability of Methoxy-Terminated Self-Assembled Monolayers on Gold. *Langmuir* **2003**, *19* (24), 10217–10224.

(50) Ke, J.; Li, X.; Wang, F.; Jiang, S.; Kang, M.; Wang, J.; Li, Q.; Wang, Z. Non-Isocyanate Polyurethane/Epoxy Hybrid Materials with Different and Controlled Architectures Prepared from a CO2-Sourced Monomer and Epoxy via an Environmentally-Friendly Route. *RSC Adv.* **2017**, *7* (46), 28841–28852.

(51) Novikov, M. B.; Gdalin, B. E.; Anosova, J. V.; Feldstein, M. M. Stress Relaxation during Bond Formation and Adhesion of Pressure-Sensitive Adhesives. *J. Adhes.* **2008**, *84* (2), 164–190.

(52) Xu, X.; Ma, S.; Wu, J.; Yang, J.; Wang, B.; Wang, S.; Li, Q.; Feng, J.; You, S.; Zhu, J. High-Performance, Command-Degradable, Antibacterial Schiff Base Epoxy Thermosets: Synthesis and Properties. *J. Mater. Chem. A* **2019**, *7* (25), 15420–15431.

(53) Türel, T.; Tomović, Ž. Chemically Recyclable and Upcyclable Epoxy Resins Derived from Vanillin. *ACS Sustain. Chem. Eng.* **2023**, *11* (22), 8308–8316.

(54) Beniah, G.; Chen, X.; Uno, B. E.; Liu, K.; Leitsch, E. K.; Jeon, J.; Heath, W. H.; Scheidt, K. A.; Torkelson, J. M. Combined Effects of Carbonate and Soft-Segment Molecular Structures on the Nanophase Separation and Properties of Segmented Polyhydroxyurethane. *Macromolecules* **2017**, *50* (8), 3193–3203.

(55) Beniah, G.; Fortman, D. J.; Heath, W. H.; Dichtel, W. R.; Torkelson, J. M. Non-Isocyanate Polyurethane Thermoplastic Elastomer: Amide-Based Chain Extender Yields Enhanced Nanophase Separation and Properties in Polyhydroxyurethane. *Macromolecules* **2017**, *50* (11), 4425–4434.

(56) Miao, J. T.; Yuan, L.; Guan, Q.; Liang, G.; Gu, A. Biobased Epoxy Resin Derived from Eugenol with Excellent Integrated Performance and High Renewable Carbon Content. *Polym. Int.* **2018**, *67* (9), 1194–1202.

(57) Zhang, W.; Gao, F.; Chen, X.; Shen, L.; Chen, Y.; Lin, Y. Recyclable, Degradable, and Fully Bio-Based Covalent Adaptable Polymer Networks Enabled by a Dynamic Diacetal Motif. *ACS Sustain. Chem. Eng.* **2023**, *11* (7), 3065–3073.

(58) Hu, H.; Tian, Y.; Kong, Z.; Ying, W. Bin; Chen, C.; Li, F.; Zhang, R.; Zhu, J. A High Performance Copolyester with "Locked" Biodegradability: Solid Stability and Controlled Degradation Enabled by Acid-Labile Acetal. *ACS Sustain. Chem. Eng.* **2021**, *9* (5), 2280–2290.

(59) Miao, P.; Liu, J.; He, M.; Leng, X.; Li, Y. Bio-Based Non-Isocyanate Polyurethane with Closed-Loop Recyclability and Its Potential Application. *Chem. Eng. J.* **2023**, *475*, 146398.

Chapter 4

Post-Functionalizable and Reusable Biobased Polyhydroxyurethane Adhesives with Pendant Furyl Groups

4.1 Introduction

Hot melt adhesives are a type of thermoplastic adhesive that is applied in a molten state and solidifies as it cools. These adhesives are popular in various industries, such as packaging, woodworking, automotive, and textiles, due to their fast bonding, ease of use, and versatility.[1] Additionally, HMAs are solvent-free, making them non-toxic and safer with fewer environmental concerns compared to adhesives that release volatile organic compounds.[2] HMA formulations include several key components designed to enhance specific properties such as wetting, flexibility, setting time, and bonding performance. The primary ingredients are polymers, tackifiers, waxes, and additives like plasticizers and stabilizers.[1,2] However, there are various types of HMAs available, each formulated for specific applications, including polyurethane, ethylene-vinyl acetate, polyolefin, polyamide, polyethylene acrylic acid copolymer, and other copolymer variants.[3] Among these, PU hot melt adhesives are particularly popular due to their superior bonding strength, flexibility, biocompatibility, and resistance to extreme conditions.[4] These adhesives are especially used in industries where high performance and durability are critical. Furthermore, the mechanical properties of these adhesives can be tailored by modifying the molecular structure, allowing customization of strength and elasticity through polymer chemical reactions, making them versatile for various applications.[3]

Despite the strong performance of PU-HMAs in many areas, the growing concerns about the use of toxic isocyanates in PU synthesis have led to the exploration of greener alternative approaches that avoid the use of these harmful substances while achieving similar properties.[5] Among the different approaches, one of the widely adopted alternatives for PU production is the step-growth polyaddition of cyclic carbonates and diamines, as it eliminates the need for toxic isocyanates, making the method safer and more eco-friendly. Additionally, the monomers can be produced on a large scale by coupling biosourced CO_2 with epoxides, and the polymerization has 100 % atom economy, meaning no by-products are generated, making the process highly efficient and reducing waste.[6]

In recent years, significant research has been conducted on PHU adhesives, particularly by Sardon,[6–8], Sylvain,[9,10], Detrembleur,[5,11,12] and Figovsky.[13] After reviewing these reports, it can be concluded that some limitations still exist with PHU adhesives, including wet delamination, slow curing, poor thermo-mechanical properties, and limited reversibility, which hinder their commercialization. To address these issues, several approaches have been developed, where PHUs are combined with other functionalities such as epoxy, sol-gel, or composites, creating hybrid systems that have been shown to enhance PHU performance.[8] However, to the best of

our knowledge, monomers bearing furyl clickable groups have not yet been studied as precursors in the synthesis of PHU adhesives, which could later be modified to enhance the properties of PHU adhesives through post-polymerization modification approach, such as the Diels-Alder reaction (DA). Moreover, a preliminary study on the reversibility of PHUs using DA click chemistry was first conducted by the team of Sylvain Caillol.[14] In fact, the DA reaction is a type of cycloaddition reaction that occurs between a conjugated diene and a dienophile to form a six-membered DA adduct. It is one of the most important and widely used reactions in organic, materials, and polymer chemistry, and has already demonstrated its utility in various systems, such as self-healing materials, thermo-reversible macromolecules, and polymers with controlled cross-linking processes.[14] We hypothesized that reacting the pendant furyl groups of the developed PHU-HMAs with a BMI crosslinker through the DA reaction may improve the thermo-mechanical and adhesion properties.

Due to growing environmental concerns and the push to reduce dependence on petroleum-based materials, there has been a significant interest in exploring bio-based resources to produce sustainable adhesives.[15] Despite this, the biobased thermoplastic PHU adhesives have not been extensively studied, and there are only a few reports available in this area.[16,17] In this regard, the lignin-derived vanillin, and guaiacol, as well as sugar-derived furfural molecules, which are eco-friendly, cost-effective, and commercially available on a large scale, have been used as renewable precursors in the development of thermoplastic PHU adhesives.[18–20] In this work, we aimed to develop bio-based high-performance PHU hot melt adhesives (PHU-HMAs), by preparing a range of PHU-HMAs using bio-based Priamine 1074, varying contents of vanillin-guaiacol-derived dicarbonate (BGF-DC), and guaiacol-furfural dicarbonate with pendant furyl groups (BGF-PF-DC). Furthermore, the effect of the molar composition of cyclic dicarbonate blends on thermal, rheological, water uptake, and adhesion properties was investigated. Additionally, post-modification of PHUs with pendant furyl groups was carried out using a bismaleimide crosslinker via a DA reaction, and its impact on adhesion properties was assessed. Renewable carbon content was also measured to evaluate the environmental friendliness and sustainability of the developed HMAs.

4.2 Experimental section

4.2.1 Materials

Vanillin (>98%), tetrabutylammonium bromide (TBAB, >98%), and 1,5,7- triazabicyclo-[4.4.0] dec-5-ene (TBD, >98%) was purchased from the TCI Chemicals. Priamine 1074 was

provided by the Croda, Netherlands. Epichlorohydrin (>99%), and sulfuric acid (98%) were procured from Sigma Aldrich, and sodium. Guaiacol (99%), furfural (99%), 1, 1′-(methylenedi-1, 4-phenylene) bismaleimide, sodium bicarbonate ($NaHCO_3$), were procured from SRL chemicals. Sodium hydroxide pellets (NaOH, 98%), hydrochloric acid (HCl, 35-38%), and pet ether were supplied by the S. D. fine chemical. Sodium borohydride ($NaBH_4$, 98%), sodium sulfate (anhydrous, >99.5%), ethyl acetate, and dichloromethane (DCM), were delivered by Leonid Chemicals. Dimethyl sulfoxide (DMSO-d6, 99.80% D), 1, 1, 2, 2-tetrachloroethane-d_2 (99.5% D), and chloroform (99.80% D) were purchased from Eurisotop. Carbon dioxide cylinder (CO_2, 99.99%) was obtained from Sandesh Gases. Absolute ethanol (99.90%) was procured from Changshu Hongsheng Fine Chemical. Calcium hydride (CaH_2, 95%) was collected from Chempure. N-methyl pyrrolidinone (NMP), N, N-dimethyl acetamide (DMAc), acetone, and dimethylformamide (DMF) were procured from Sigma Aldrich, further distilled over CaH_2, and stored over molecular sieves (4 Å). All chemicals were used as received unless specified.

4.2.2 Characterization techniques

The procedure and conditions described in Chapter 2 (Section 2.2.2) were similarly followed in this chapter for the structural, molecular weight, and thermal analysis of the synthesized compounds and polymers. These analyses were conducted using ^{1}H NMR, ^{13}C NMR, FTIR, HRMS, GPC, DSC, and TGA. Similarly, the rheological analysis (melting temperature: 100 °C), water contact angle measurement, and X-ray diffraction analysis were performed following the procedure and conditions detailed in Chapter 3 (Section 3.2.2). Additionally, a lap shear test was conducted on two substrates, aluminum, and stainless steel, using a displacement rate of 5 mm·min^{-1}. For this test, 200 mg of polymer film was applied to stainless steel with an adhesive contact area of 300 mm², and 134 mg was applied to aluminum with an adhesive contact area of 200 mm². The adhesive specimens were prepared by melting at 100 °C under gentle pressure. All other conditions were consistent with those described in Chapter 2 (Section 2.2.2).

4.2.3 Methods

4.2.3.1 Preparation of vanillin and guaiacol-derived cyclic carbonate

4.2.3.1.1 Synthesis of vanillyl alcohol

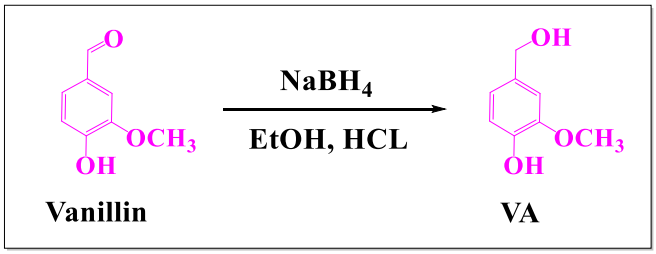

Scheme 4.1. *Reduction of vanillin to VA using $NaBH_4$ as a reducing agent.*

Vanillin (10 g, 6.57 mmol) was dissolved in a 5 wt% aqueous solution of NaOH (2.92 g, 7.29 mmol) at 15 °C in a 250 ml of two necked-round bottom flask. After that, $NaBH_4$ (2.76 g, 7.29 mmol) was added and the mixture was stirred for 3h. The pH of the reaction solution was adjusted to acidic using 2M HCl (2M) to obtain a white solid powder. The resulting VA was purified using column chromatography with ethyl acetate and petroleum ether (yield: 55 %; m. p.: 80-82 ºC).

^{1}H-NMR (500 MHz, DMSO-d6) δ (ppm): 3.56 (2H, OH), 3.74 (s, 3H, -OC$\underline{H_3}$), 4.36 (s, 2H, C$\underline{H_2}$-OH), 6.70 (dd, 2H, aromatic -C$\underline{H}$), 6.87 (s, 1H, aromatic -C$\underline{H}$).
^{13}C-NMR (500 MHz, DMSO-d6) δ (ppm): 55.94 (-O$\underline{C}H_3$), 63.45 (-$\underline{C}H_2$-OH), 111.50 ($\underline{C}$-H, aromatic), 115.50 ($\underline{C}$-H, aromatic), 119.57 ($\underline{C}$-H, aromatic), 133.76 ($\underline{C}$-CH_2, aromatic), 145.87 ($\underline{C}$-OH, aromatic), 147.83 ($\underline{C}$-OCH_3, aromatic).
FTIR (cm^{-1}): 3401 (OH), 2925 (C-H stretch).
HRMS (ESI) m/z: $[M + H]^+$ calculated for $C_8H_{10}O_3$: 154.0630; found:154.0624.

4.2.3.1.2 Synthesis of bisguaiacol diol

To synthesize the BGF-DL compound, vanillyl alcohol (20 g, 0.130 mol) and guaiacol (16.10 g, 0.130 mol) were weighed into a 1 L two-neck round-bottom flask, connected with a reflux condenser.[21] Following this, 600 mL of ethanol and 30 mL of diluted H_2SO_4 (0.5 N) were added to the flask and the solution was stirred at room temperature. The reaction mixture was then heated to 100 °C for 24 h. After completion of the reaction, the excess ethanol was evaporated on the rotary evaporator, and the resulting product was extracted with the ethyl acetate. The crude product, appearing as a reddish-brown liquid was subjected to further purification via

column chromatography, employing ethyl acetate and petroleum ether as eluent (yield: 50-52 %, m. p.:112 °C).

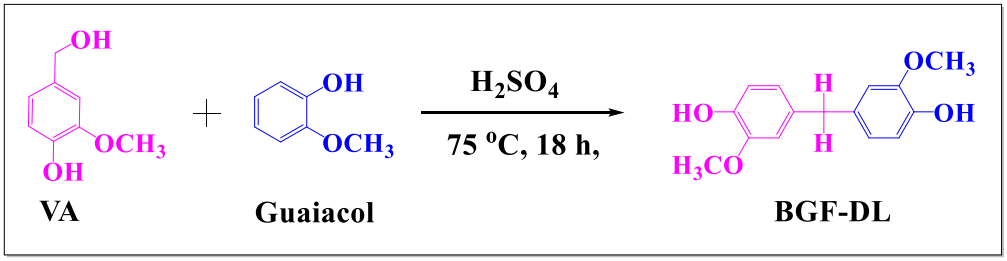

Scheme 4.2. *Preparation of BGF-DL by condensation of vanillyl alcohol with guaiacol.*

^{1}H-NMR (500 MHz, CDCl$_3$) δ (ppm): 3.84 (s, 6H, -OC<u>H</u>$_3$), 3.85 (s, 2H, bridge -C<u>H</u>$_2$), 5.50 (s, 2H, -O<u>H</u>), 6.67 (dd, 4H, aromatic -C<u>H</u>), 6.84 (d, 2H, aromatic -C<u>H</u>).

^{13}C-NMR (500 MHz, CDCl3) δ (ppm): 40.97 (-<u>C</u>H$_2$, bridge), 55.89 (-O<u>C</u>H$_3$), 111.36 (<u>C</u>-H, aromatic), 114.22 (<u>C</u>-H, aromatic), 121.50 (<u>C</u>-H, aromatic), 133.37 (<u>C</u>-CH$_2$, aromatic), 143.91 (<u>C</u>-OH, aromatic), 146.51 (<u>C</u>-OCH$_3$, aromatic).

FTIR (cm^{-1}): 3440 (OH), 2925 (C-H stretch).

HRMS (ESI) m/z: $[M + H]^+$ calculated for $C_{15}H_{16}O_4$: 260.1049; found: 260.1041.

4.2.3.2 Preparation of guaiacol and furfural-derived cyclic carbonate

4.2.3.2.1 Synthesis of bisguaiacol diol bearing pendant furyl group

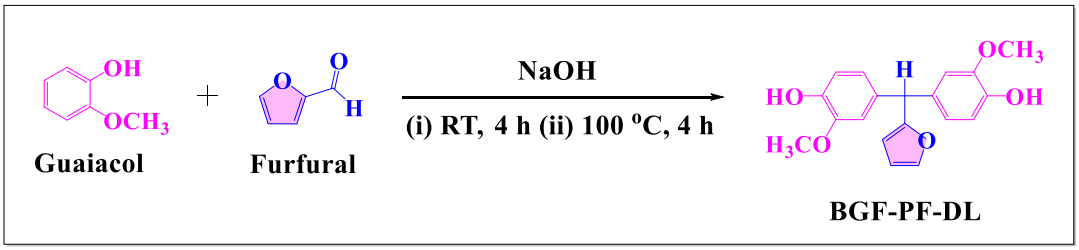

Scheme 4.3. *Synthesis of BGF-PF-DL from the reaction of guaiacol with furfural.*

Guaiacol (60 g, 0.484 mol), along with 20 % aqueous NaOH (6 g, 10 wt%) were added into a 500 mL two-necked round bottom flask that was equipped with a reflux condenser.[22] 23.22 g (0.242 mol) of furfural was added dropwise to the mixture and stirred at room temperature for 4 h, followed by heating at 100 °C for an additional 4 h. The reaction mixture was further heated to 100 °C for an additional 4 h. The resulting product was received by precipitating into the cold water. Next, the product was dissolved in dichloromethane and the solution was washed with water. The organic layer was collected, dried over anhydrous sodium sulfate, and

concentrated on the rotary evaporator. The crude product obtained was further purified by column chromatography (using ethyl acetate and petroleum ether as an eluent), and followed by recrystallization using ethanol and water (1:1) (yield: 54-55 %, m. p.: 145 °C).

^{1}H-NMR (500 MHz, CDCl$_3$) δ (ppm): 3.82 (s, 6H, -OC<u>H</u>$_3$), 5.34 (s, 1H, bridge -C<u>H</u>), 5.60 (s, 2H, -O<u>H</u>), 5.93 (s, 1H, furyl -C<u>H</u>), 6.32 (s, 1H, furyl -C<u>H</u>), 6.65 (dd, 4H, aromatic -C<u>H</u>), 6.86 (d, 2H, aromatic -C<u>H</u>), 7.39 (s, 1H, furyl -C<u>H</u>).

^{13}C-NMR (500 MHz, CDCl3) δ (ppm): 50.10 (-<u>C</u>H, bridge), 55.88 (-O<u>C</u>H$_3$), 108.09 (-<u>C</u>H=C, furyl), 110.10 (-<u>C</u>H=C, furyl), 111.29 (<u>C</u>-H, aromatic), 114.22 (<u>C</u>-H, aromatic), 121.41 (<u>C</u>-H, aromatic), 133.95 (C=<u>C</u>H-O, furyl), 141.85 (<u>C</u>-CH, aromatic), 144.38 (<u>C</u>-OH, aromatic), 146.46 (<u>C</u>-OCH$_3$, aromatic), 157.30 (-<u>C</u>-, furyl).

FTIR (cm^{-1}): 3456 (OH), 2963 (C-H stretch).

HRMS (ESI) m/z*:* $[M - H]^+$ calculated for $C_{19}H_{18}O_5$: 325.1047; found: 325.1087.

4.2.3.3 General procedure for diglycidyl ether preparation

Bisguaiacol diglycidyl ethers were prepared following the procedure outlined by Nicastro et al.[23,24] In a typical synthesis, 0.01 mol of bisguaiacol (BGF-DL and BGF-PF-DL), 0.20 mol of epichlorohydrin, and 0.001 mol of TBAB were carefully measured and added into a 500 mL two-neck round-bottom flask equipped with a reflux condenser. The mixture was stirred and heated at 80 °C for 3 h. Following this, the solution was allowed to cool to room temperature (maintained at 16-20 °C), and a 20 wt% aqueous solution of NaOH (0.04 mol) was added dropwise to the mixture. The reaction proceeded for an additional 3 h. Upon completion of the reaction, excess epichlorohydrin was removed using a rotary evaporator. The resulting aqueous solution was then extracted with ethyl acetate, and the organic phases were collected, washed with brine, and dried over anhydrous sodium sulfate. Solvents were evaporated using a rotary evaporator, and further purification of the crude product was achieved through column chromatography employing ethyl acetate and petroleum ether as eluents (BGF-DGE: 92 % yield, and BGF-PF-DGE: 97 % yield).

The reaction scheme and characterizations data for BGF-DGE and BGF-PF-DGE compounds are provided below.

4.2.3.3.1 Bisguaiacol diglycidyl ether

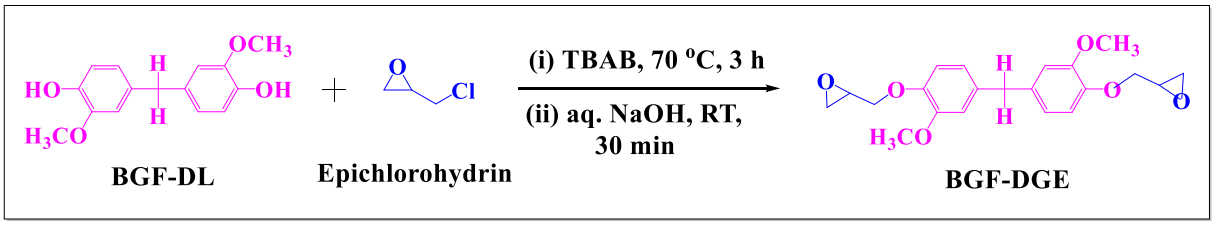

Scheme 4.4. *Method for synthesizing the BGF-DGE using glycidation.*

^{1}H-NMR (500 MHz, CDCl$_3$) δ (ppm): 2.71 (dd, 2H, epoxy -C$\underline{H}_2$), 2.87 (t, 2H, epoxy -C$\underline{H}_2$), 3.35 (m, 2H, epoxy -C$\underline{H}$), 3.81 (s, 6H, -O$\underline{CH}_3$), 3.87 (s, 2H, bridge -C$\underline{H}_2$), 4.01 (dd, 2H, epoxy -C$\underline{H}_2$), 4.19 (dd, 2H, epoxy -C$\underline{H}_2$), 6.68 (dd, 4H, aromatic -C$\underline{H}$), 6.84 (d, 2H, aromatic -C$\underline{H}$).

^{13}C-NMR (500 MHz, CDCl3) δ (ppm): 40.91 (-$\underline{C}H_2$, bridge), 44.94 ($\underline{C}H_2$-O, epoxy), 50.21 ($\underline{C}H_2$-O, epoxy), 55.92 (-O$\underline{C}H_3$), 70.26 ($\underline{C}$H-O, epoxy), 112.77 ($\underline{C}$-H, aromatic), 114.34 ($\underline{C}$-H, aromatic), 120.89 ($\underline{C}$-H, aromatic), 135.01 ($\underline{C}$-CH_2, aromatic), 146.40 ($\underline{C}$-O-C, aromatic), 149.61 ($\underline{C}$-OCH_3, aromatic).

FTIR (cm^{-1}): 2925 (C-H stretch), 914 (C-O, epoxy ring), 860 (C-O, epoxy ring).

HRMS (ESI) m/z: $[M + H]^+$ calculated for $C_{21}H_{25}O_6$: 373.1651; found: 373.1641.

4.2.3.3.2 2 Bisguaiacol diglycidyl ether bearing pendant furyl group

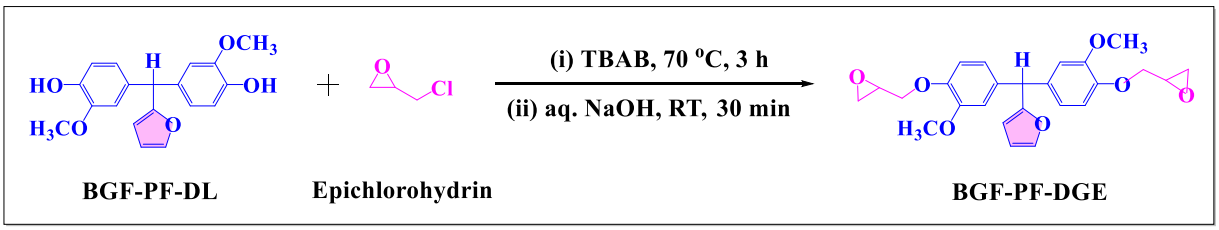

Scheme 4.5. *Synthetic scheme for BGF-PF-DGE compound.*

^{1}H-NMR (500 MHz, CDCl3) δ (ppm): 2.71 (dd, 2H, epoxy -C$\underline{H}_2$), 2.86 (t, 2H, epoxy -C$\underline{H}_2$), 3.36 (m, 2H, epoxy -C$\underline{H}$), 3.77 (s, 6H, -O$\underline{CH}_3$), 3.97 (dd, 2H, epoxy -C$\underline{H}_2$), 4.20 (dd, 2H, epoxy -C$\underline{H}_2$), 5.33 (s, 1H, bridge -C$\underline{H}$), 5.90 (s, 1H, furyl -C$\underline{H}$), 6.30 (s, 1H, furyl -C$\underline{H}$), 6.64 (dd, 4H, aromatic -C$\underline{H}$), 6.84 (d, 2H, aromatic -C$\underline{H}$), 7.36 (s, 1H, furyl -C$\underline{H}$).

^{13}C-NMR (500 MHz, CDCl3) δ (ppm): 44.90 ($\underline{C}H_2$-O, epoxy), 50.21 (-$\underline{C}$H, bridge), 55.92 (-O$\underline{C}H_3$), 60.37 ($\underline{C}$H-O, epoxy), 70.29 ($\underline{C}H_2$-O, epoxy), 108.14 (-$\underline{C}$H=C, furyl), 110.13 (-$\underline{C}$H=C, furyl), 112.70 ($\underline{C}$-H, aromatic), 113.93($\underline{C}$-H, aromatic), 120.80 ($\underline{C}$-H, aromatic), 135.52 (C=$\underline{C}$H-O, furyl), 141.88 ($\underline{C}$-CH, aromatic), 146.85 ($\underline{C}$-O-C, aromatic), 149.50 ($\underline{C}$-OCH_3, aromatic), 156.95 (-$\underline{C}$-, furyl).

FTIR (cm^{-1}): 2963 (C-H stretch), 916 (C-O, epoxy ring), 863 (C-O, epoxy ring).

HRMS (ESI) m/z: $[M + H]^+$ calculated for $C_{25}H_{26}O_7$: 439.1757; found: 439.1749.

4.2.3.4 General procedure for dicarbonate preparation

The synthesis of bisguaiacol-based cyclic carbonates proceeded as follows:[23,25] Initially, 0.1 mol of diglycidyl ethers (BGF-DGE and BGF-PF-DGE), along with 5 mol% of TBAB, were dissolved in dry acetone (1 mL g^{-1}). Subsequently, the resulting solution was introduced into an autoclave, and the reactor was pressurized with CO_2 gas (30 bar) at ambient temperature after being purged 2-3 times with CO_2 gas to remove the moisture. The solution was then heated at 100 °C with continuous stirring for 24 h. Upon completion of the reaction, the autoclave was allowed to cool to room temperature and subsequently depressurized. The resulting mixture was then collected and precipitated into ice-cold water (BGF-DC: 86 % yield, and BGF-PF-DC: 91 % yield).

The reaction scheme and characterizations data for BGF-DC and BGF-PF-DC monomers are provided below.

4.2.3.4.1 Bisguaiacol dicarbonate

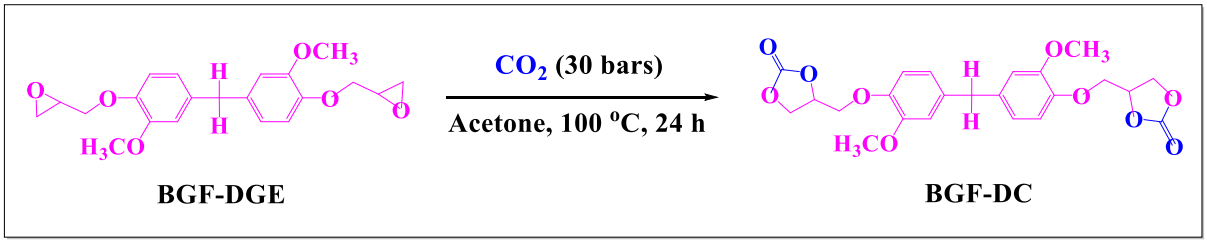

Scheme 4.6. *Preparation of BGF-DC monomer using carbonation.*

^{1}H-NMR (500 MHz, $CDCl_3$) δ (ppm): 3.79 (s, 6H, -OC<u>H</u>$_3$), 3.86 (s, 2H, bridge -C<u>H</u>$_2$), 4.18 (m, 4H, carbonate -C<u>H</u>$_2$), 4.58 (m, 4H, carbonate -C<u>H</u>$_2$), 4.97 (m, 2H, carbonate -C<u>H</u>), 6.67 (dd, 4H, aromatic -C<u>H</u>), 6.82 (dd, 2H, aromatic -C<u>H</u>).

^{13}C-NMR (500 MHz, $CDCl_3$) δ (ppm): 41.14 (-<u>C</u>H$_2$, bridge), 55.93 (-O<u>C</u>H$_3$), 66.35 (<u>C</u>H$_2$-O, carbonate), 69.35 (<u>C</u>H$_2$-O, carbonate), 74.28 (<u>C</u>H-O, carbonate), 113.22 (<u>C</u>-H, aromatic), 116.76 (<u>C</u>-H, aromatic), 121.08 (<u>C</u>-H, aromatic), 136.41 (<u>C</u>-CH$_2$, aromatic), 145.87 (<u>C</u>-O-C, aromatic), 150.34 (<u>C</u>-OCH$_3$, aromatic), 154.83 (<u>C</u>=O, carbonate).

FTIR (cm^{-1}): 2925 (C-H stretch), 1787 (O-CO-O).

HRMS (ESI) m/z: $[M + Na]^+$ calculated for $C_{23}H_{24}O_{10}Na$: 483.1266 ; found: 483.1252.

4.2.3.4.2 Bisguaiacol dicarbonate bearing pendant furyl group

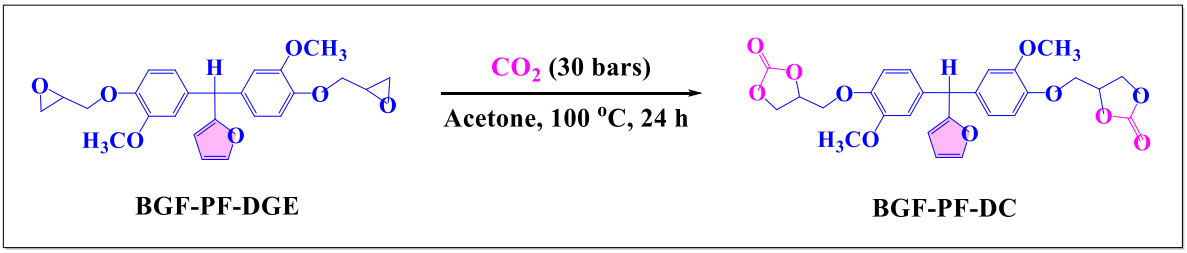

Scheme 4.7. *Carbonation process for synthesizing the BGF-PF-DC monomer.*

^{1}H-NMR (500 MHz, CDCl3) δ (ppm): 3.76 (s, 6H, -OC$\underline{H}_3$), 4.19 (m, 4H, carbonate -C$\underline{H}_2$), 4.58 (m, 4H, carbonate -C$\underline{H}_2$), 4.98 (m, 2H, carbonate -C$\underline{H}$), 5.34 (s, 1H, bridge -C$\underline{H}$), 5.93 (s, 1H, furyl -C$\underline{H}$), 6.31 (s, 1H, furyl -C$\underline{H}$), 6.64 (dd, 4H, aromatic -C$\underline{H}$), 6.85 (d, 2H, aromatic -C$\underline{H}$), 7.38 (s, 1H, furyl -C$\underline{H}$).

^{13}C-NMR (500 MHz, CDCl3) δ (ppm): 50.04 (-$\underline{C}$H, bridge), 55.94 (-O$\underline{C}H_3$), 66.34 ($\underline{C}H_2$-O, carbonate), 69.32 ($\underline{C}H_2$-O, carbonate), 74.23 ($\underline{C}$H-O, carbonate), 108.30 (-$\underline{C}$H=C, furyl), 110.20 (-$\underline{C}$H=C, furyl), 113.14 ($\underline{C}$-H, aromatic), 116.33($\underline{C}$-H, aromatic), 120.96 ($\underline{C}$-H, aromatic), 136.93 (C=$\underline{C}$H-O, furyl), 142.01 ($\underline{C}$-CH, aromatic), 146.29 ($\underline{C}$-O-C, aromatic), 150.24 ($\underline{C}$-OCH_3, aromatic), 156.48 (-$\underline{C}$-, furyl), 154.74 ($\underline{C}$=O, carbonate).

FTIR (cm^{-1}): 2963 (C-H stretch), 1788 (O-CO-O).

HRMS (ESI) m/z: $[M + Na]^+$ calculated for $C_{27}H_{26}O_{11}Na$: 549.1372 ; found:549.1354

4.2.3.5 A typical procedure for the synthesis of PHU polymers

The process of polymerizing PHU adhesives involves the addition of reacting cyclic carbonates, priamine 1074, and a TBD catalyst (10 mol%) into a 50 mL two-necked round bottom flask. Subsequently, dry N-methyl-2-pyrrolidinone (NMP) is introduced as the solvent, and the resulting solution is heated at 80 °C for 24 h in an oil bath under an inert atmosphere, while being stirred. Afterward, the reaction was allowed to cool down and the resulting polymers were precipitated out in ice-cold water. The obtained polymers were then purified using dichloromethane and petroleum ether to remove the unreacted diamine. The resultant brownish material was named PHU-PF-x, where 'PF-x' represents the mole percentages of the bisguaiacol-F dicarbonate-bearing pendant furyl group (BGF-PF-DC). The dicarbonate compositions utilized in the preparation of the PHUs are detailed in **Table 4.1.**

***Table 4.1**. Molar compositions and molecular weight of the PHUs.*

Polymers	BGF-DC (Mole ratio)	BGF-PF-DC (Mole ratio)	Priamine 1074 (Mole ratio)	RCC (%) [a]
PHU1-PF0	1	0	1	89.83
PHU2-PF20	0.8	0.2	1	89.96
PHU3-PF40	0.6	0.4	1	90.09
PHU4-PF60	0.4	0.6	1	90.22
PHU5-PF80	0.2	0.8	1	90.35
PHU6-PF100	0	1	1	90.47

[a] Renewable carbon content

4.2.3.6 Preparation of the cross-linked PHU/BMI networks

To prepare the film, PHUs bearing pendant furyl groups (2.00 g, PHU6PF100) and various concentrations of BMI crosslinker (Bismaleimide, 1, 5, 10, and 20 wt%) were dissolved in dry chloroform (30 mL) and stirred at room temperature for 24 h. The resulting solution was poured into a teflon petri dish, and the chloroform was allowed to evaporate at room temperature, forming a free-standing film. The film was then dried in a vacuum oven at 40 °C for 24 h. The resulting cross-linked polymer film was used for further analysis.

To study the thermo-reversibility of the polymer network, PHU6-PF100 (200 mg) and BMI crosslinker (10 wt%) were added to a 5 mL vial and dissolved in DMAc (1 mL). Diels-Alder crosslinking was performed at 80 °C for 24 h to allow gel formation while decrosslinking of the gel was carried out at 120 °C for 24 h.

4.3 Result and Discussion

4.3.1 Preparation of vanillin and guaiacol-derived cyclic carbonate

The BGF-DC monomer was synthesized from biobased vanillin and guaiacol molecules in four steps, and its structure was validated using FTIR and NMR spectroscopy. However, the FTIR spectrum of vanillyl alcohol (**Scheme 4.1**) showed a broad peak around 3401 cm^{-1}, indicating diol formation (**Figure 4.1**). The ^{1}H NMR further supported the reduction of the aldehyde group to an alcohol, as the peak at 9.85 ppm disappeared and a new broad peak appeared around 3.56 ppm (**Figure 4.2**). In the ^{13}C NMR, an additional signal appeared at 63.45 ppm after the reduction of vanillin, corresponding to the methylene group attached to the benzene ring and the hydroxyl group (**Figure 4.3**). However, the vanillyl alcohol further reacted with guaiacol

in the presence of sulfuric acid to produce bisguaiacol diglycidyl ether (**Scheme 4.2**). The disappearance of the broad peak at 3401 cm^{-1} and the appearance of a sharp signal in the FTIR spectrum confirmed the formation of BGF-DL (**Figure 4.1**). Additionally, the absence of a broad signal around 3.56 ppm in the ^{1}H NMR spectrum and the emergence of an intense signal at 5.50 ppm, related to the aromatic hydroxyl groups of BGF-DL, further supported the structure (**Figure 4.4**). The shift of the signal corresponding to CH_2 protons from 4.36 ppm to 3.85 ppm also confirmed the formation of the compound. This upfield shift of the CH_2 protons after the condensation reaction is likely due to the electron-donating effect of the aromatic rings. In the ^{13}C NMR spectrum, the bridging CH_2 protons show a signal at 41.19 ppm, while the OCH_3 and aromatic protons appear at 55.89 ppm and in the range of 111.36–146.51 ppm, respectively (**Figure 4.5**). After refluxing BGF-DL with epichlorohydrin, bisguaiacol diglycidyl ether (BGF-DGE) was obtained (**Scheme 4.4**). The compound showed characteristic signals of epoxy rings at 914 and 860 cm^{-1} in the FTIR spectrum (**Figure 4.1**), and signals in the range of 2.71 to 4.19 ppm in the ^{1}H NMR spectrum (**Figure 4.6**), validating the structure of BGF-DGE. In the ^{13}C NMR spectrum (**Figure 4.7**), additional peaks were observed at 44.94, 50.21, and 70.26 ppm, corresponding to the epoxy carbons. In the final step, the carbonation of BGF-DGE was carried out, and the structure of the resulting bisguaiacol dicarbonate monomer was confirmed by various spectroscopy techniques (**Scheme 4.6**). The FTIR spectrum showed an intense peak at 1787 cm^{-1} corresponding to the carbonyl group of the carbonate ring (**Figure 4.1**).[26] In the ^{1}H NMR spectrum, the epoxy peaks at 2.71–4.19 ppm disappeared, and new carbonate peaks appeared at slightly higher shifts (4.18, 4.58, 4.97 ppm) due to the electron-withdrawing effect of the carbonyl group (**Figure 4.8**).[27] Additionally, the characteristic peak of the carbonyl carbon was observed at 154.83 ppm in the ^{13}C NMR spectrum (**Figure 4.9**).[28,29]

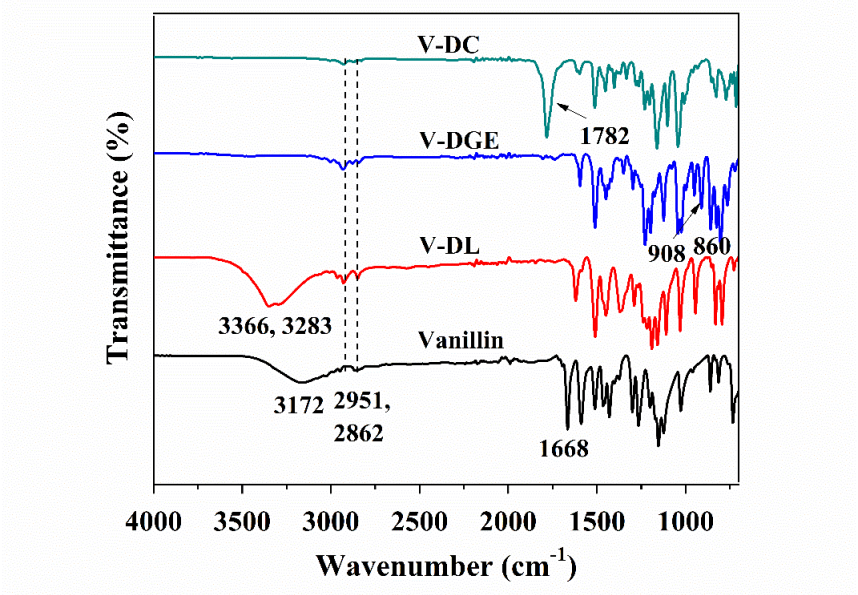

Figure 4.1. *FTIR spectrum of Vanillin, BGF-DL, BGF-DGE, and BGF-DC compounds*

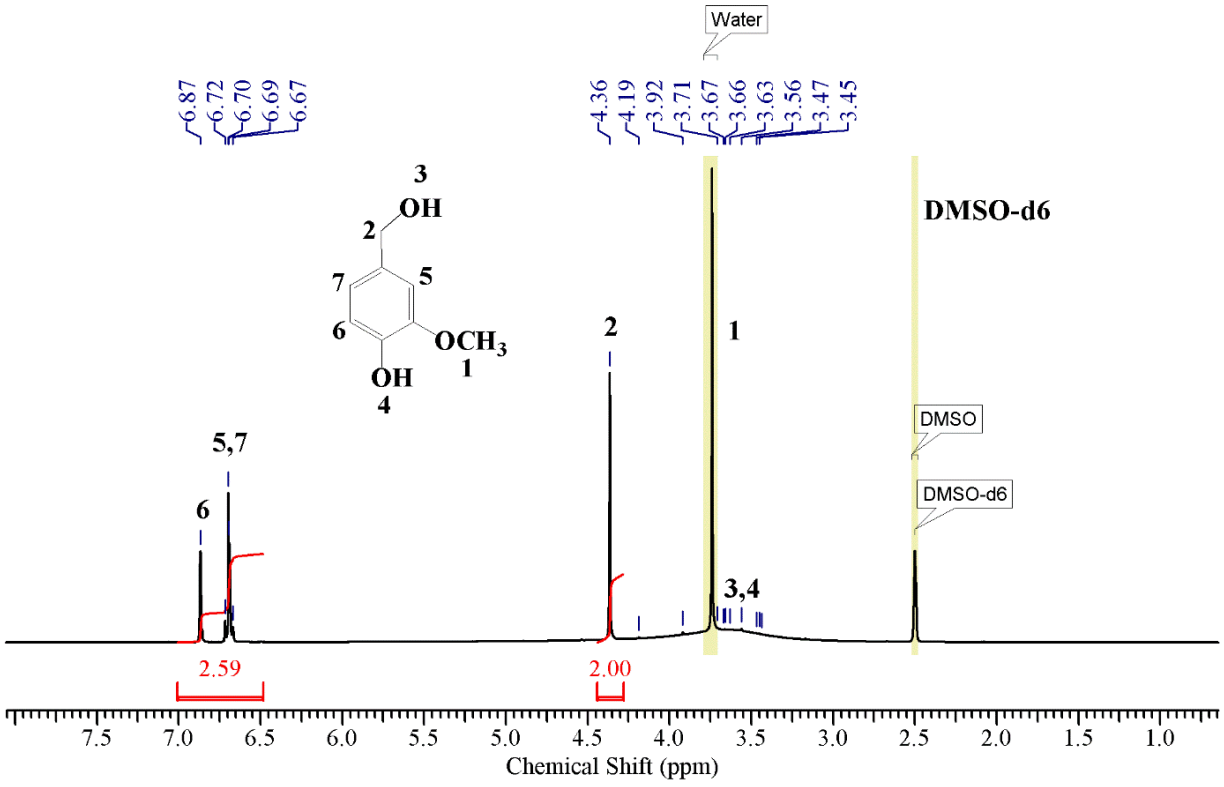

Figure 4.2. *^{1}H NMR spectrum of VA.*

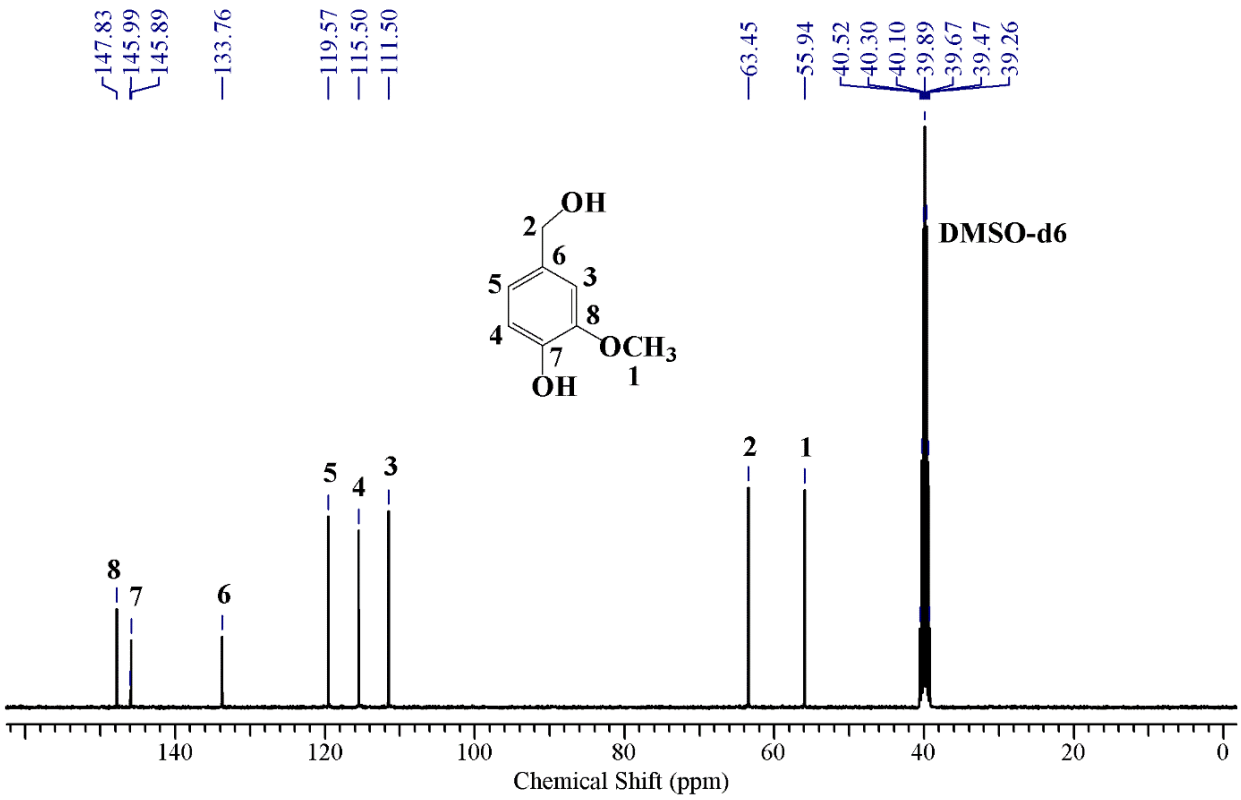

Figure 4.3. *^{13}C NMR spectrum of VA.*

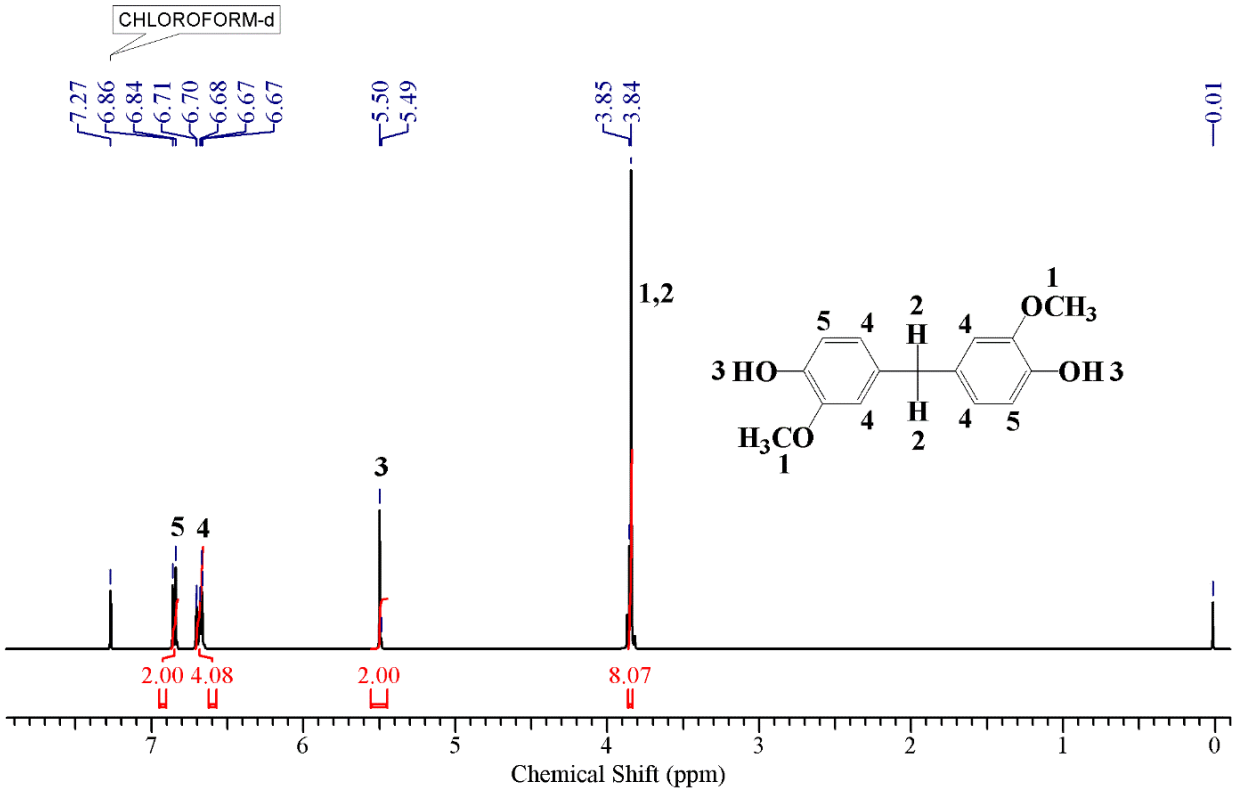

Figure 4.4. *^{1}H NMR spectrum of BGF-DL.*

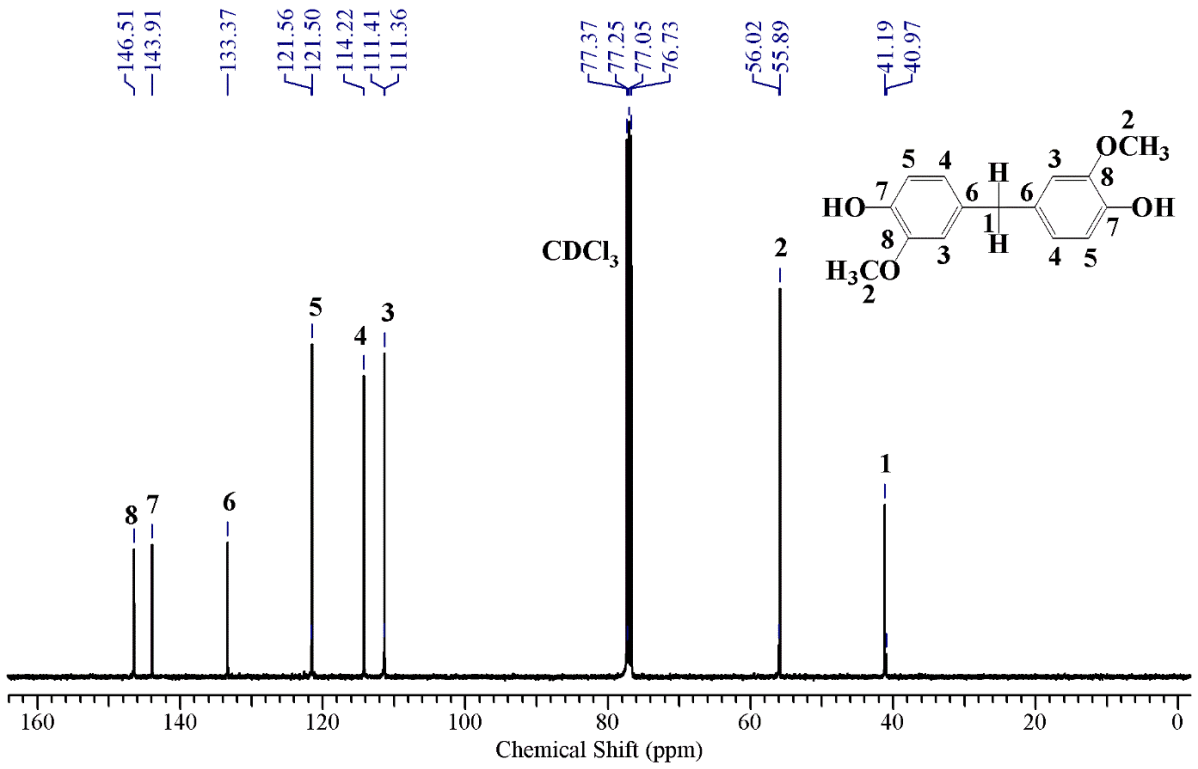

Figure 4.5. *^{13}C NMR spectrum of BGF-DL.*

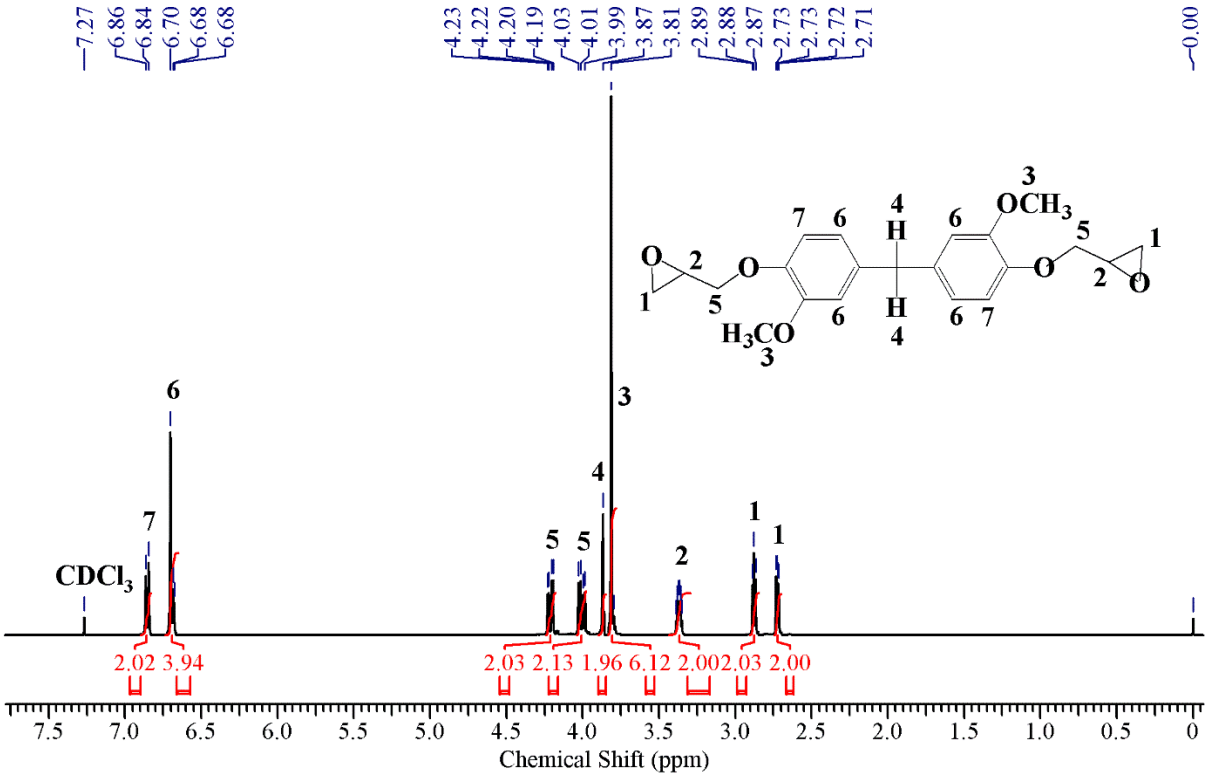

Figure 4.6. *^{1}H NMR spectrum of BGF- DGE.*

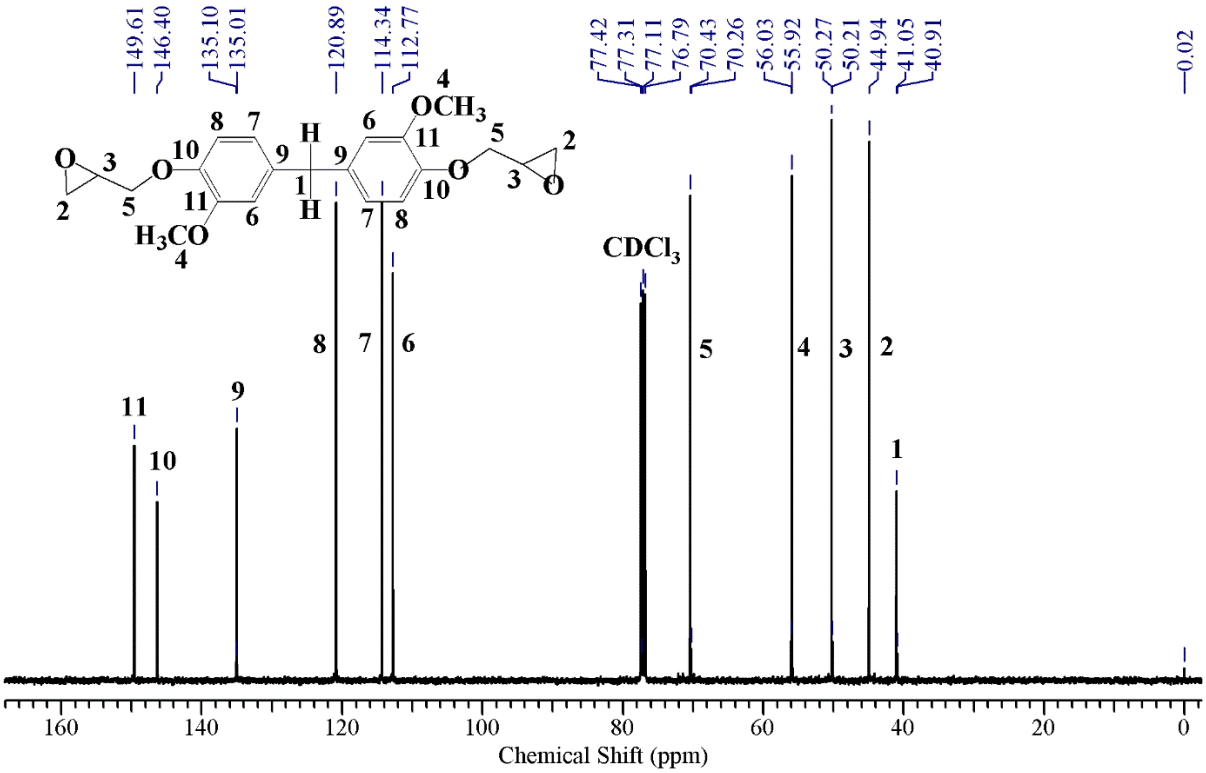

Figure 4.7. *^{13}C NMR spectrum of BGF- DGE.*

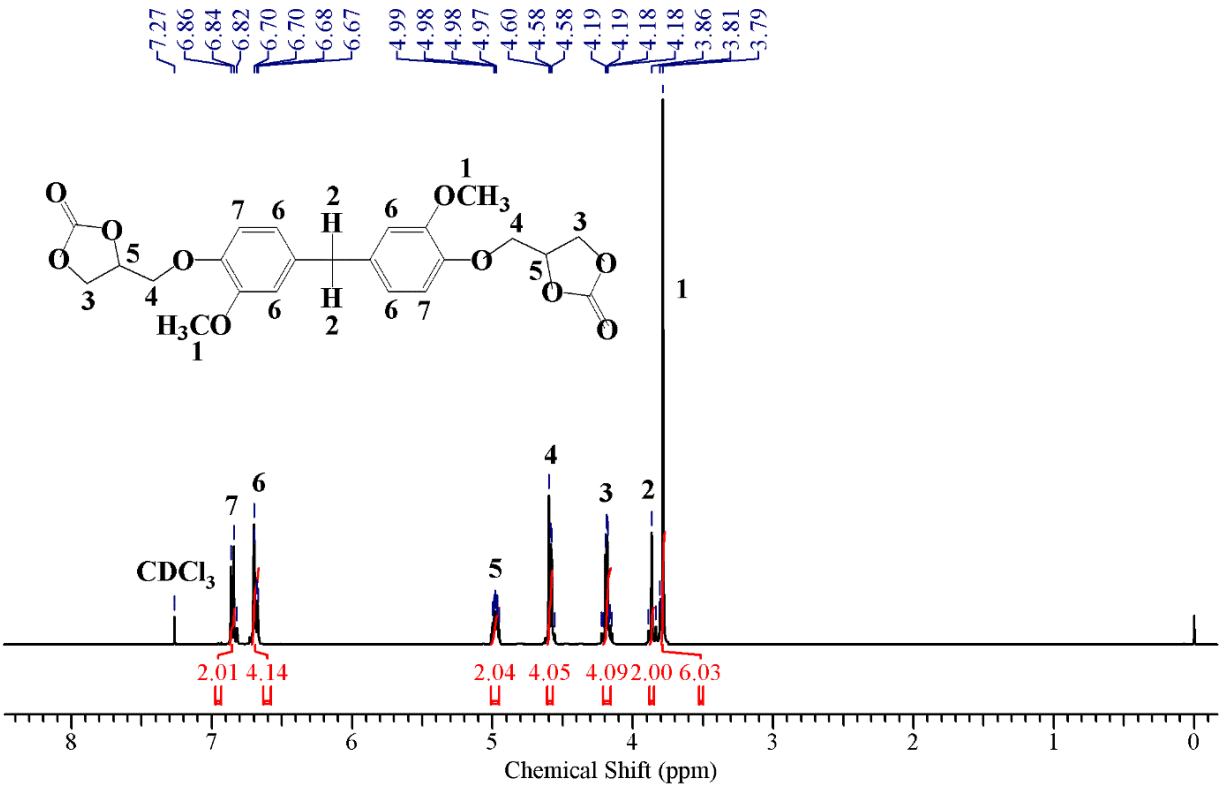

Figure 4.8. *^{1}H NMR spectrum of BGF-DC.*

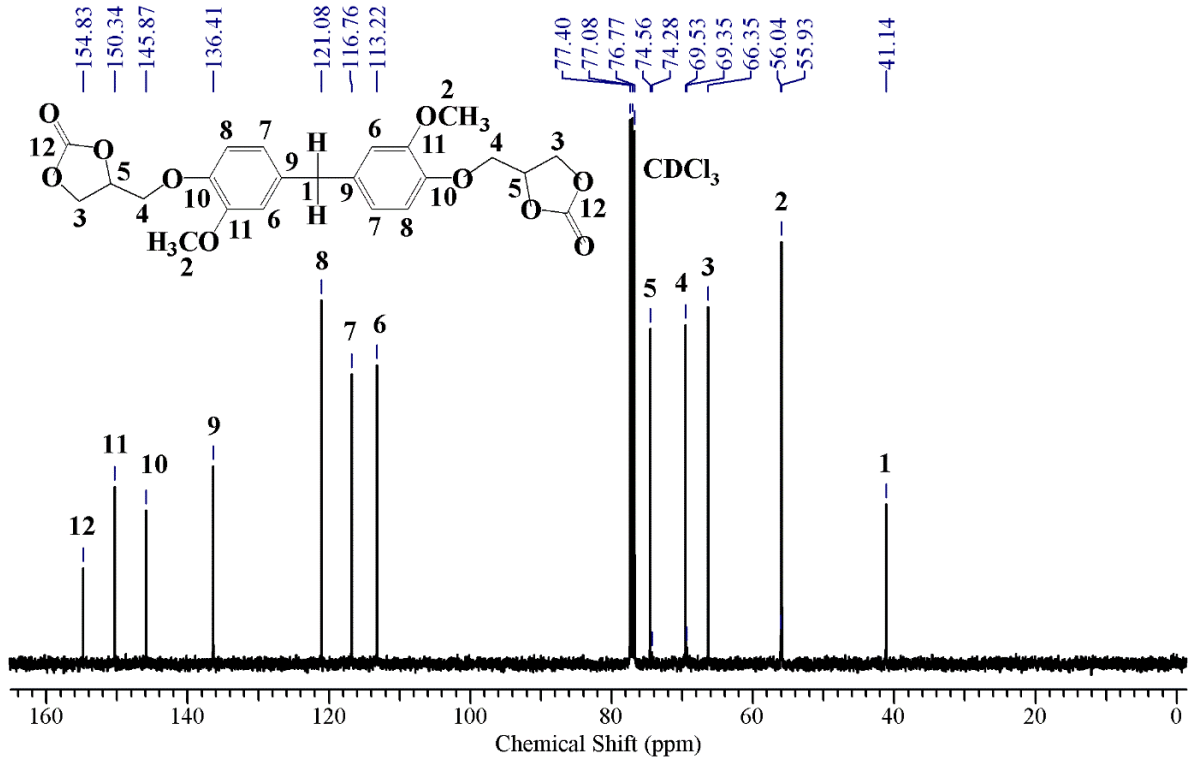

Figure 4.9. *^{13}C NMR spectrum of BGF-DC.*

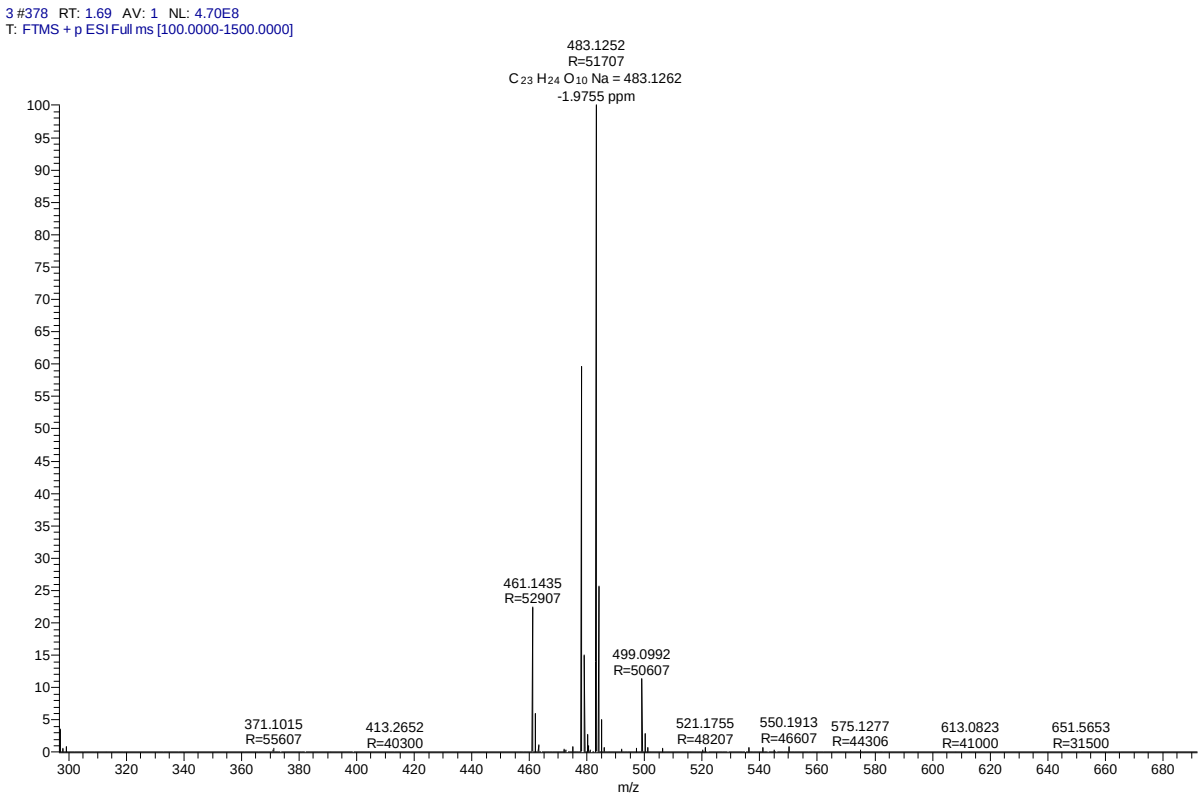

Figure 4.10. *HRMS spectrum of BGF-DC.*

4.3.2 Preparation of guaiacol and furfural-derived cyclic carbonate (BGD-PF-DC)

The BGD-PF-DC monomer was synthesized in three steps from renewable bisguaiacol and furfural molecules, with a total yield of 48.55 %. The unique aspect of this monomer is its ability to undergo post-modification via a Diels-Alder reaction, enhancing the properties of polymers. In the first step, guaiacol was reacted with furfural in aqueous NaOH, and the resulting product was analyzed using FTIR and NMR techniques (**Scheme 4.3**). The FTIR spectrum of the bisguaiacol diol molecule containing a furyl group is shown in the **Figure 4.11**. The band at 3456 cm^{-1} corresponds to the hydroxyl groups, while the bands at 1510 cm^{-1} and at 1010, 1076 cm^{-1} are attributed to the C=C groups and the breathing modes of the furan ring, respectively.[22] In the ^{1}H NMR spectrum, the aromatic hydroxyl protons appeared at 5.60 ppm, furyl protons showed signals at 5.93, 6.32, and 7.39 ppm,[22] and the bridging CH_2 group was observed at 5.60 ppm (**Figure 4.12)**.[22] These observations confirm the successful formation of the diol compound with a pendant furyl group. The ^{13}C NMR spectrum also supports the incorporation of the furyl group, showing carbon signals at 108.09, 110.10, 133.95, and 157.30 ppm (**Figure 4.13**). The diol molecule was further used to produce the diepoxide compound, and its structure was validated by FTIR and ^{1}H NMR spectroscopy (**Scheme 4.5**). The disappearance of the -OH band at 3456 cm^{-1} in the FTIR spectrum (**Figure 4.11**), along with the disappearance of aromatic -OH protons at 5.60 ppm and the appearance of epoxy signals in the range of 2.71–4.23 ppm in the ^{1}H NMR spectrum (**Figure 4.14**), confirm the formation of the glycidated molecule (BGF-DGE). The ^{13}C NMR spectrum is displayed in the (**Figure 4.15**).

The final dicarbonate monomer, prepared from BGF-DGE via carbonation (**Scheme 4.7**), showed a characteristic band at 1788 cm^{-1} in the FTIR spectrum **Figure 4.11**).[26] In the ^{1}H NMR spectrum, the carbonate protons appeared at 4.19, 4.58, and 4.98 ppm (**Figure 4.16**),[27] while in the ^{13}C NMR spectrum, the characteristic signal of the carbonyl group appeared at 154.74 ppm (**Figure 4.17**). These observations confirm the structure of the carbonate monomer.[28,29]

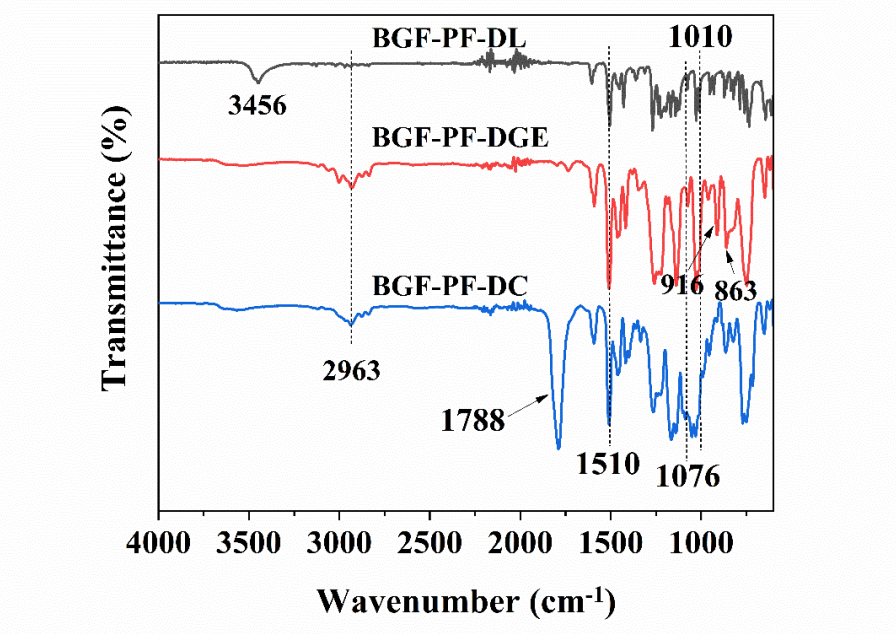

Figure 4.11. *FTIR spectrum of BGF-PF-DL, BGF-PF-DGE, and BGF-PF-DC compounds bearing pendant furyl groups.*

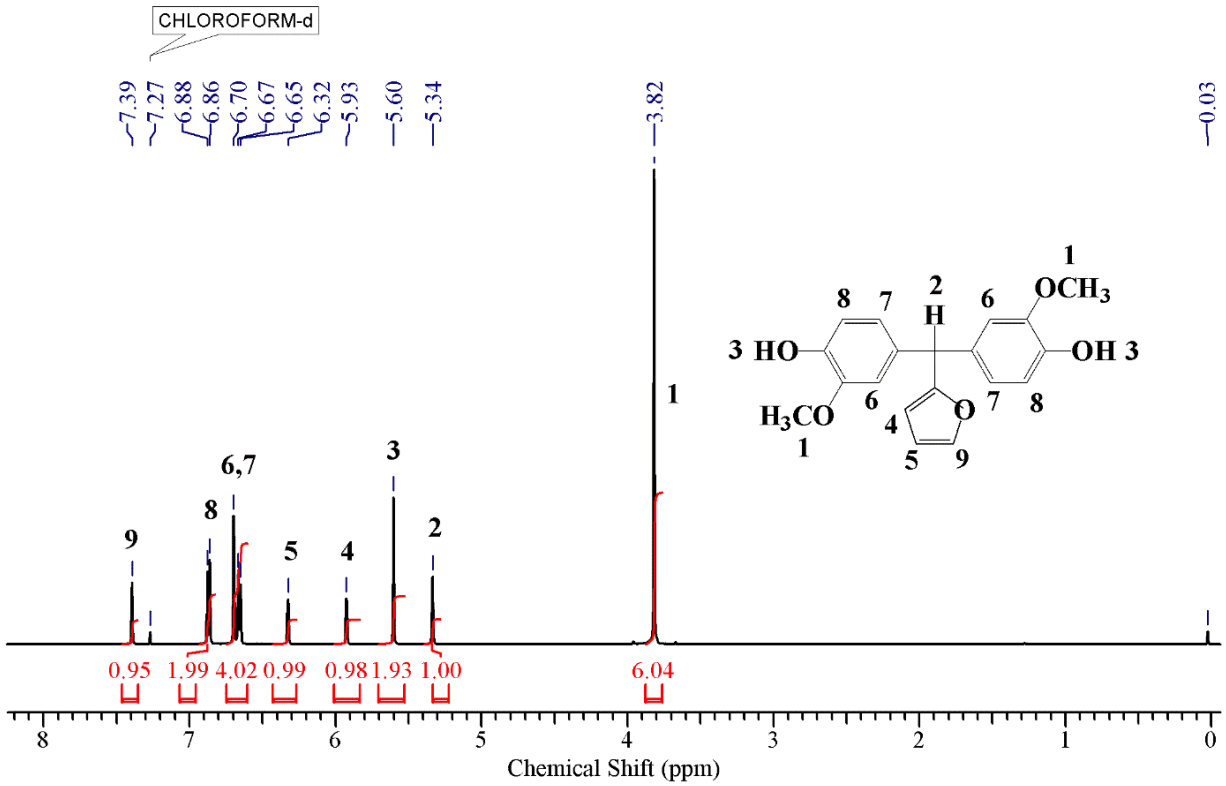

Figure 4.12. *^{1}H NMR spectrum of BGF-PF-DL.*

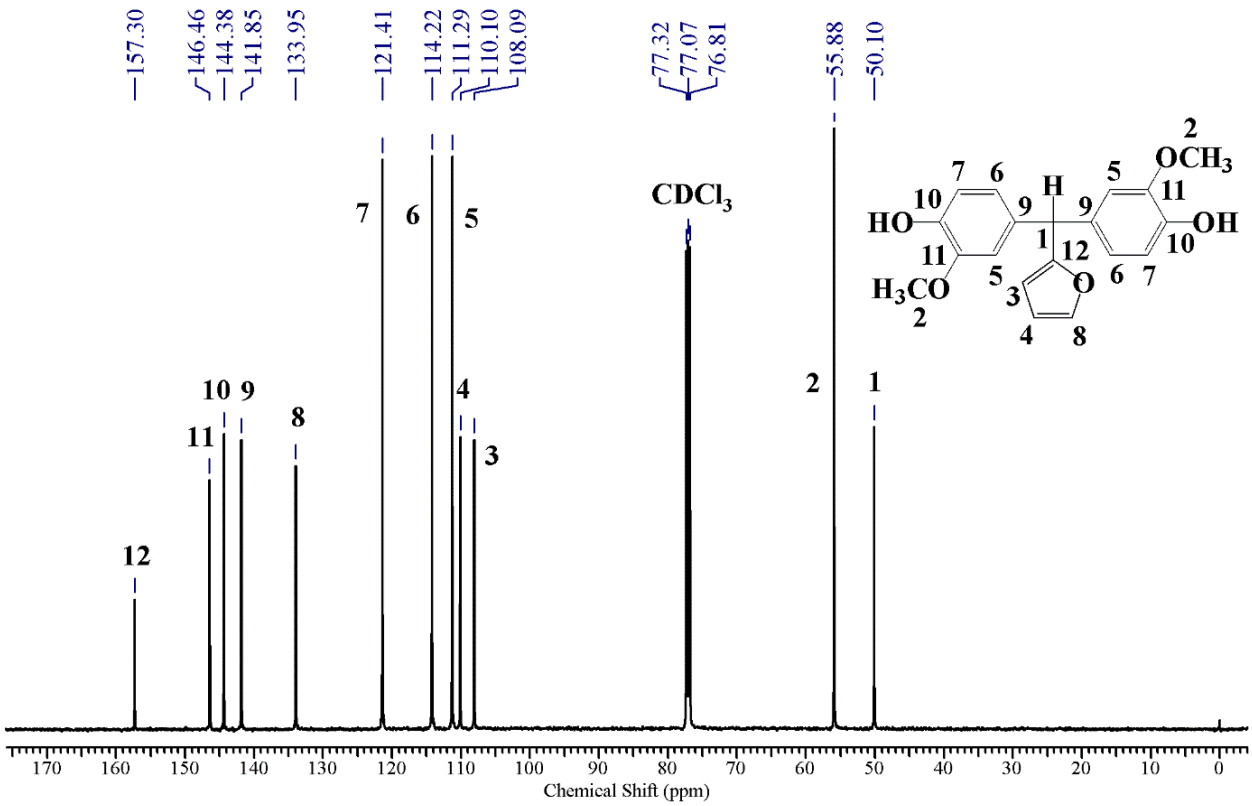

Figure 4.13. *^{13}C NMR spectrum of BGF-PF-DL.*

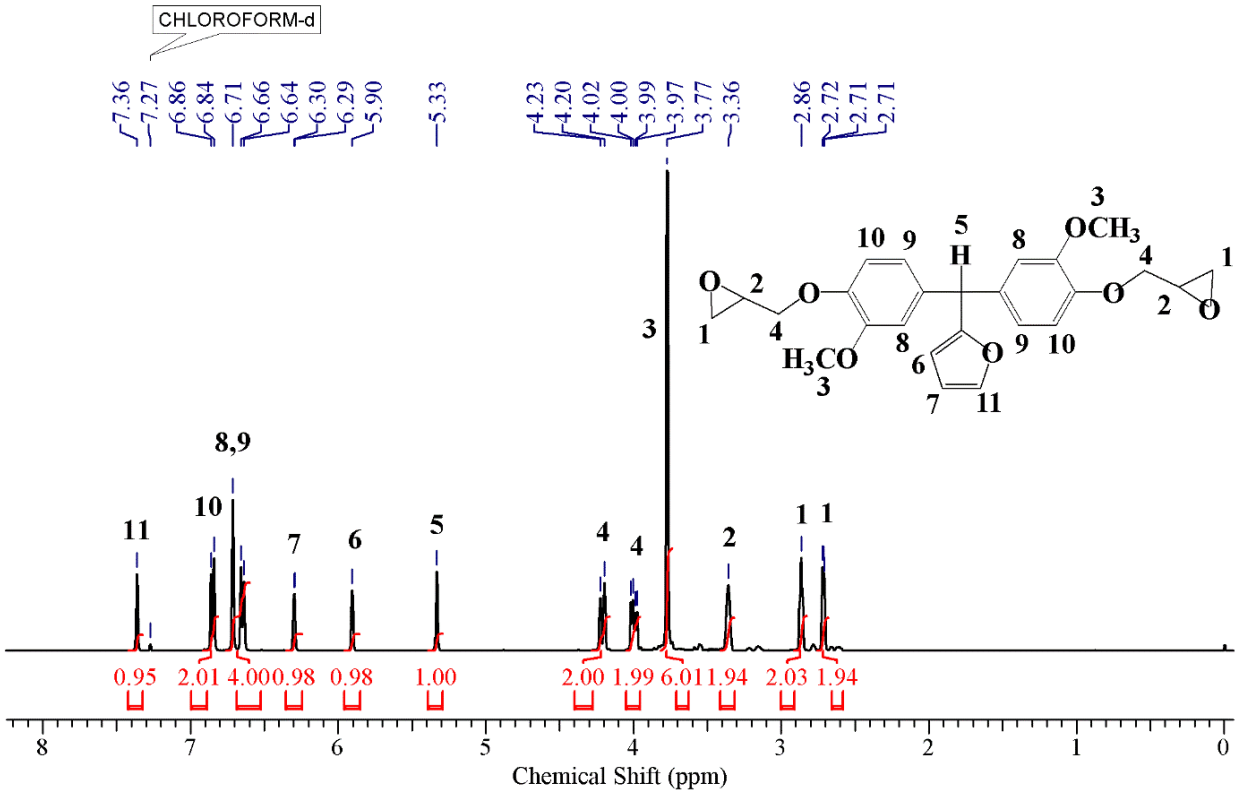

Figure 4.14. *^{1}H NMR spectrum of BGF-PF-DGE.*

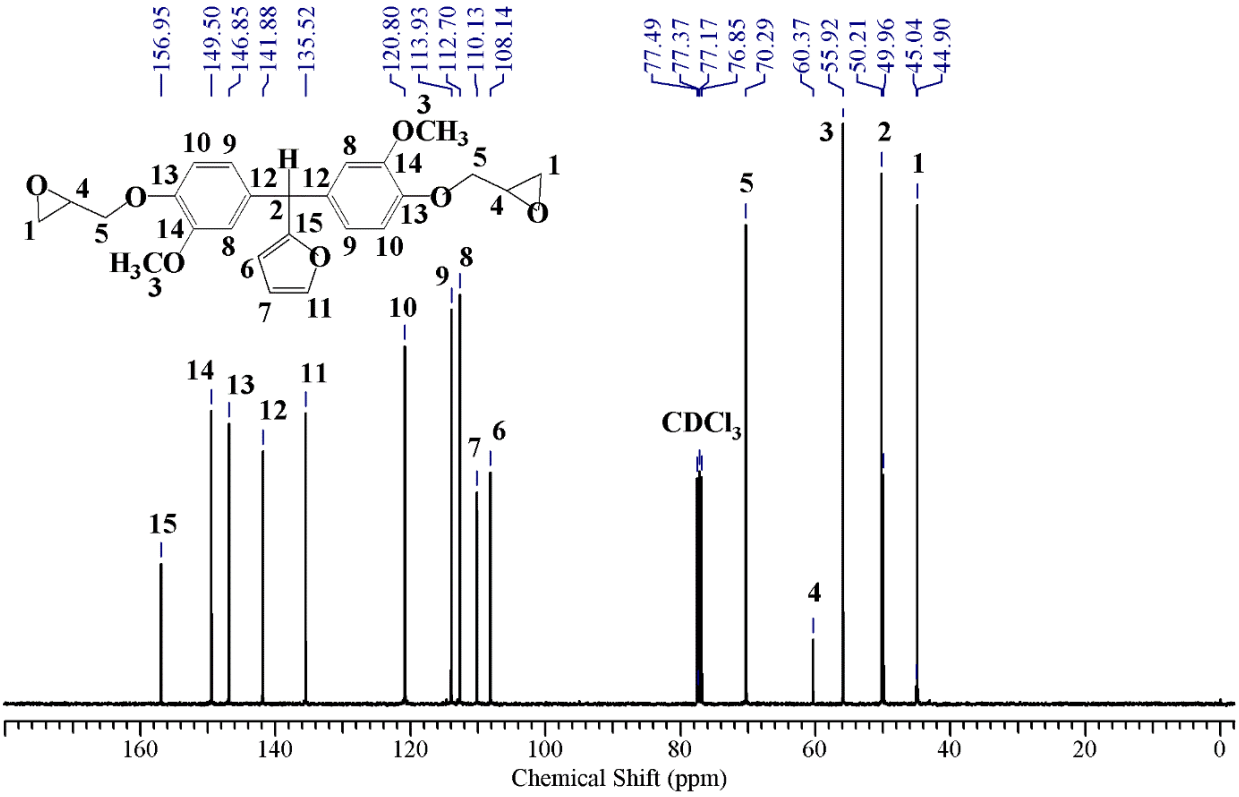

Figure 4.15. *^{13}C NMR spectrum of BGF-PF-DGE.*

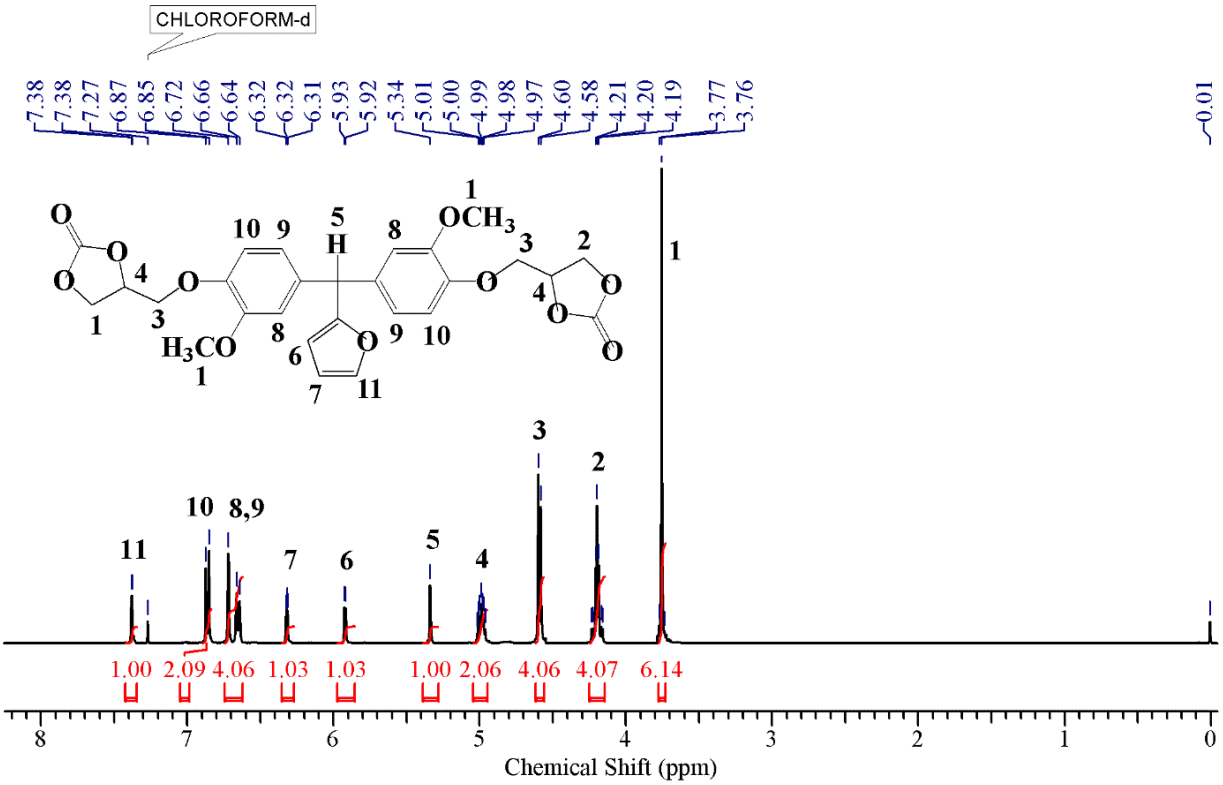

Figure 4.16*. ^{1}H NMR spectrum of BGF-PF-DC.*

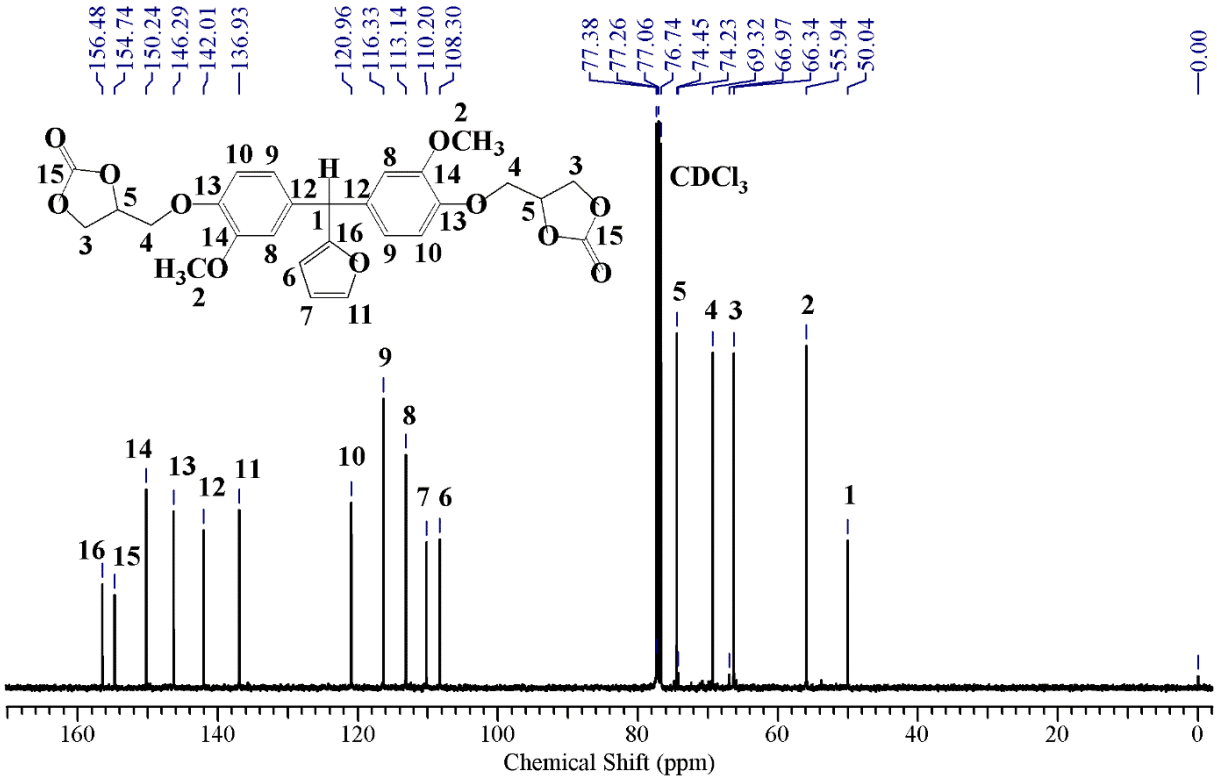

Figure 4.17. *^{13}C NMR spectrum of BGF-PF-DC.*

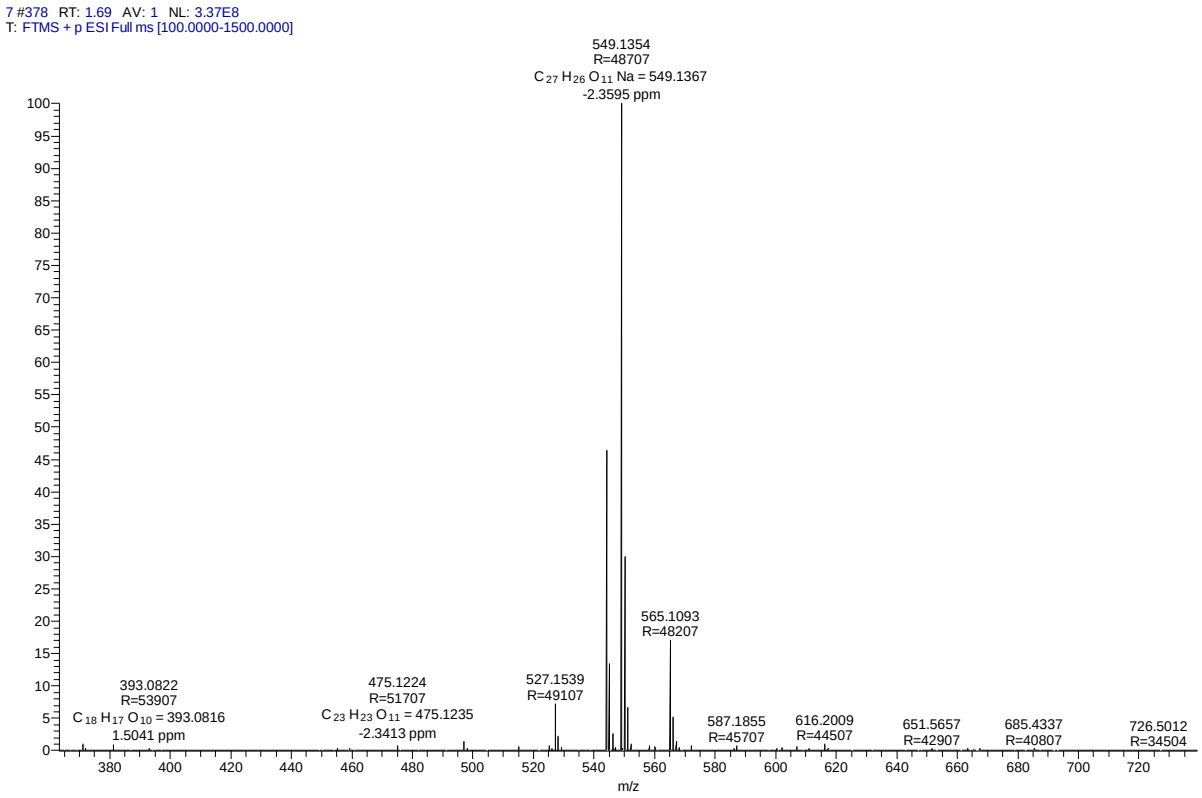

Figure 4.18. *HRMS spectrum of BGF-PF-DC.*

4.3.3 Synthesis and Characterization of PHUs.

In this work, the biobased PHU sustainable adhesives with increased adhesion strength, as well as higher renewable carbon content were formulated, by varying the molar amount between the two structurally different biobased dicarbonates, which were reacted with priamine in the presence of TBD catalysts and NMP solvent (**Scheme 4.8**). The resulting solution was polymerized under continuous stirring at 80 °C for 24 h, and the complete transformation of dicarbonate precursors into PHU polymers was analyzed by FTIR, and NMR (^{1}H, ^{13}C) spectroscopies. However, the biosourced carbon content for PHUs ranged from 89 % to 90 % (**Table 4.1**). **Figure 4.19** shows the FTIR spectrum of developed polymeric materials. The disappearance of carbonyl stretches of BGF-DC and BGF-PF-DC at 1788 cm^{-1} (**Figure 4.1 and Figure 4.11**) and the appearance of two new characteristic peaks around 3360 (due to -OH and N-H stretching from hydroxyl and urethane groups) and at 1702 cm^{-1} (due to C=O stretching from urethane groups) indicating the successful synthesis of all PHUs.[5] Furthermore, the additional peaks appeared at 1515, 1076, and 1012 cm^{-1}, are attributed to the C=C groups and the breathing modes of the furan ring.

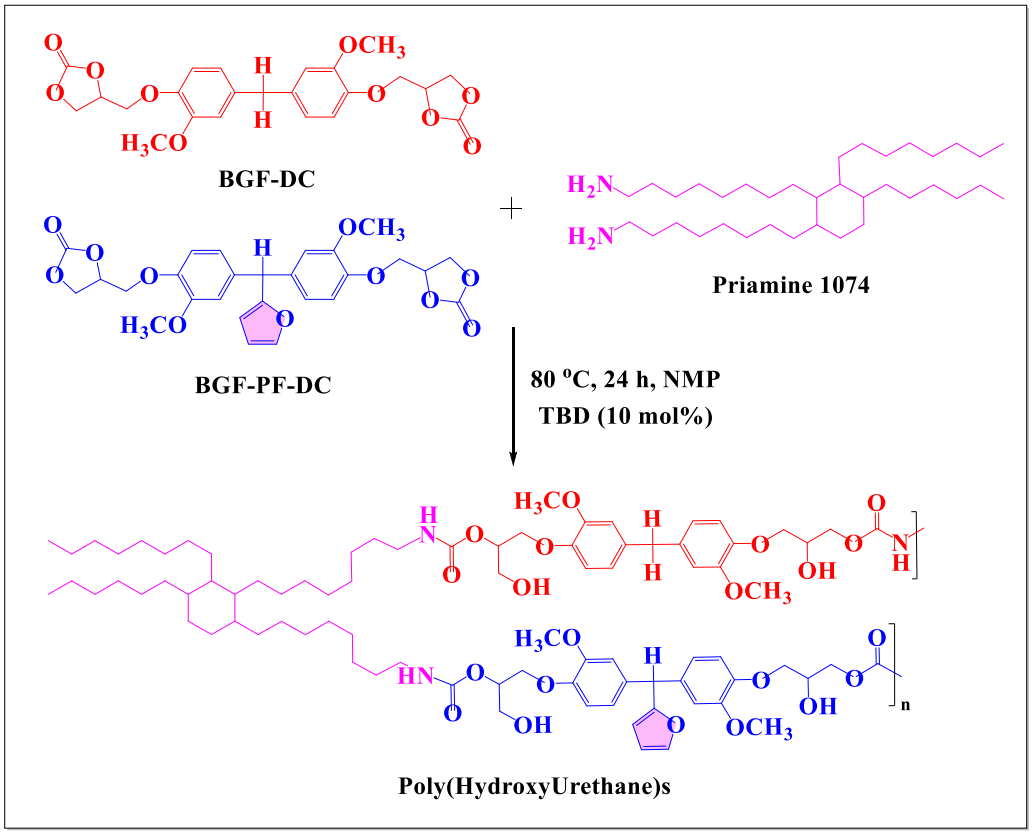

Scheme 4.8. *Design and synthesis of PHU-derived hot melt adhesives bearing pendant furyl groups.*

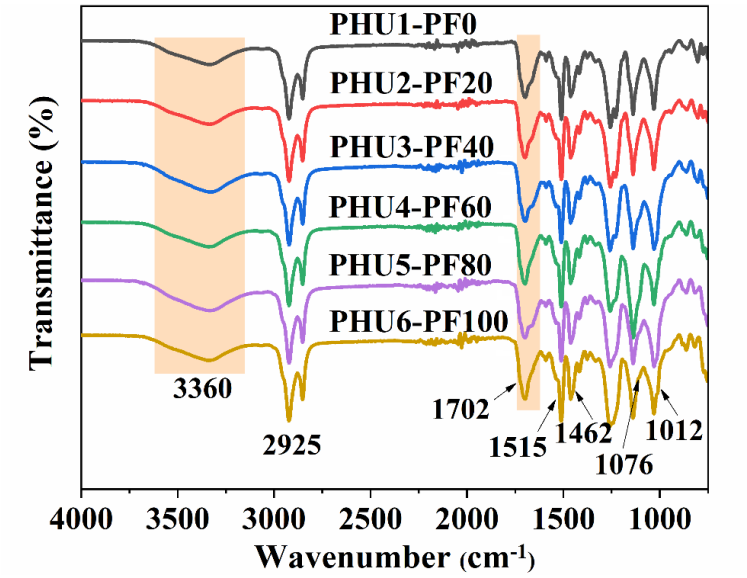

Figure 4.19. *FTIR spectrum of PHUs bearing pendant furyl groups.*

The structure of PHUs was further validated by ^{1}H NMR (**Figure 4.20, Figure 4.21,** and **Figure 4.22**). It was challenging to identify the NMR signals of the hydroxyl and urethane groups present in the polymers since they overlapped with other signals. In order to identify them, we first recorded ^{1}H NMR of one sample (PHU4-PF60, **Figure 4.23**) at high temperatures (50 and 80 °C), and based on this, we assigned the signals for all other compositions. However, the successful preparation of all PHUs is indicated by the emergence of the signals at 6.68 ppm (due to the N-H group of urethane linkages),[27] at 3.80 and 4.89 ppm (due to the primary and secondary hydroxyl groups, respectively),[27] and the shifting of carbonate protons from downfield (4.18-4.19, 4.18, and 4.97-4.98 ppm) to upfield (3.99-4.27 ppm) after the polymerization.[27] Additional evidence of the effective production of PHUs comes from the shifting of the α-methylene group of primary amines from 2.61 ppm (Priamine 1074) to 3.14-3.16 ppm due to the formation of electron-withdrawing carbamate groups.[6] The analysis of the ^{13}C NMR spectrum also supports the existence of urethane linkages in the backbone of PHUs **(Figure 4.24, Figure 4.25,** and **Figure 4.27)**. It revealed the disappearance of the carbonyl peak at 154.83 (BGF-DC) and 154.74 ppm (BGF-PF-DC), and the emergence of new signals at 156.75-156.80 ppm, corresponding to the carbonyl group of the carbamate moiety.[33] These results showed that the PHU materials have been successfully prepared from biobased precursors. The incorporation ratio of dicarbonate monomers in final polymers was determined by ^{1}H NMR (**Figure 4.43**) and values are added in **Table 4.4**.

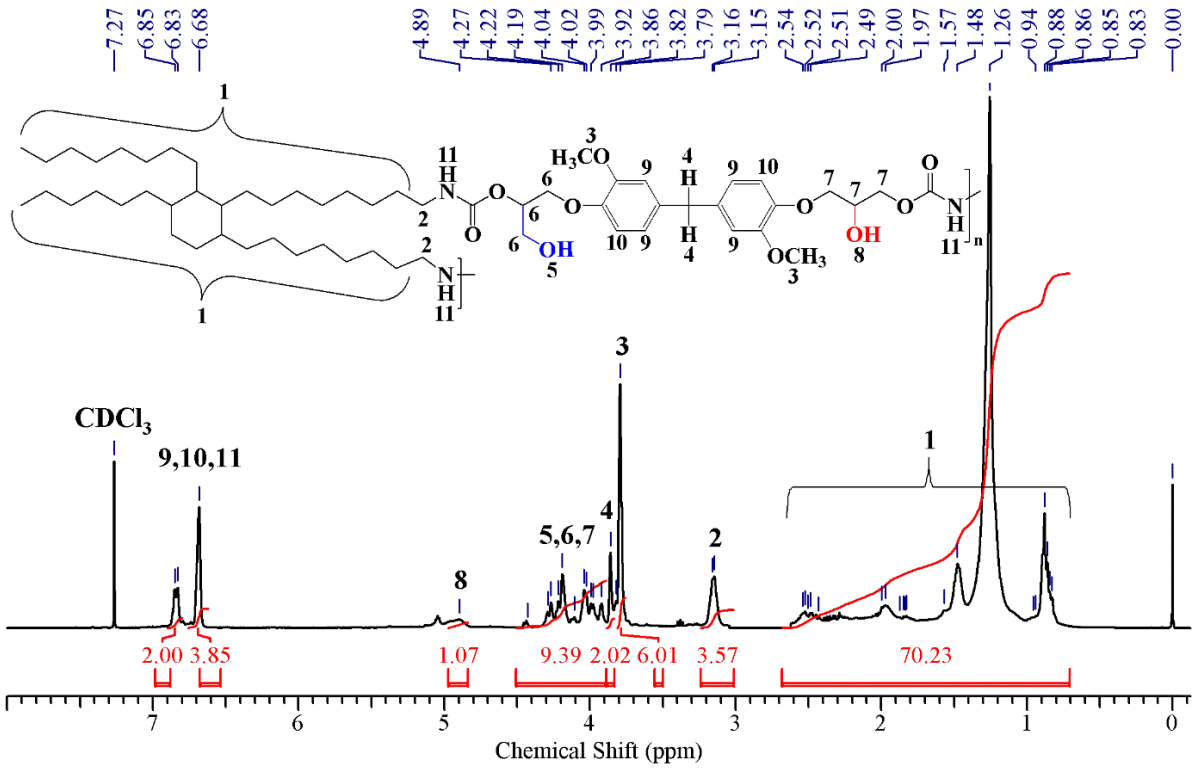

Figure 4.20. *^{1}H NMR spectrum of PHU1-PF0 (Homo).*

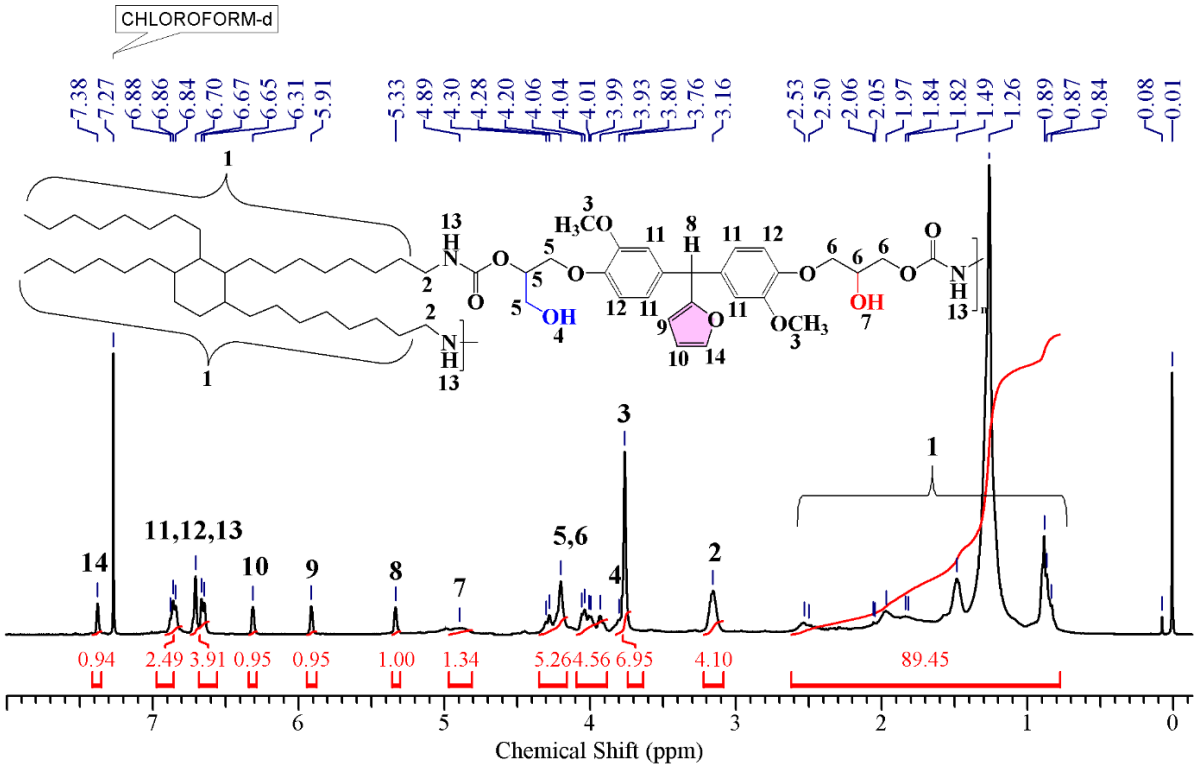

Figure 4.21. *^{1}H NMR spectrum of PHU6-PF100 (Homo).*

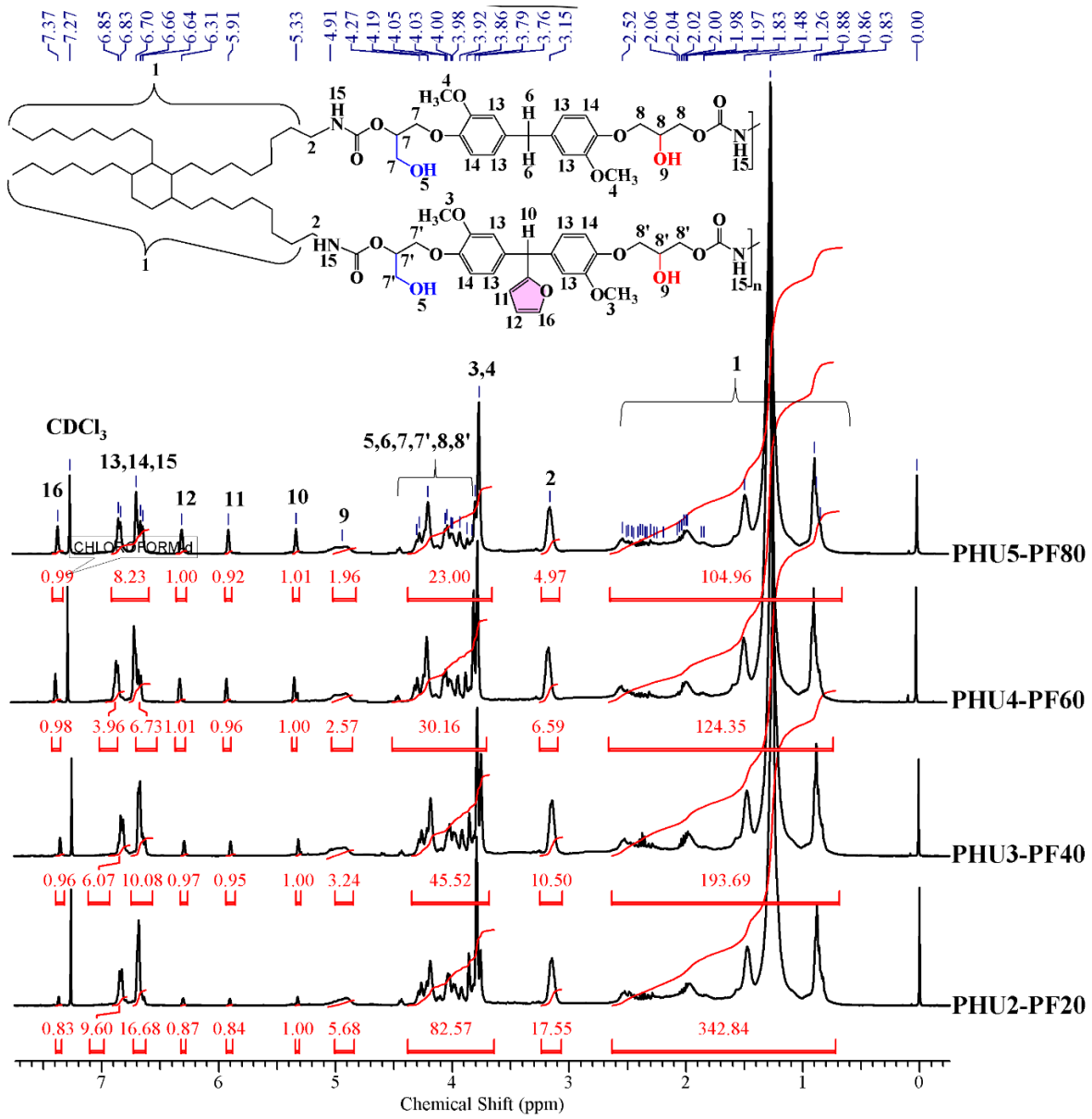

Figure 4.22. *^{1}H NMR spectrum of PHUs (Copolymers).*

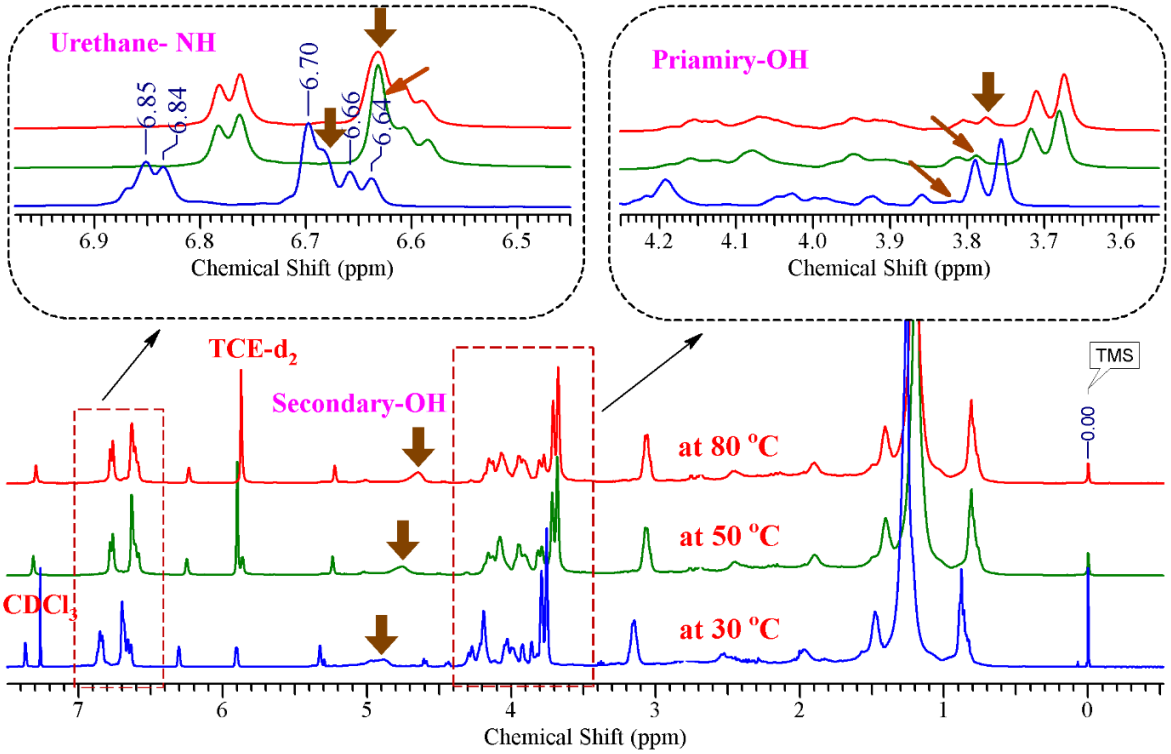

Figure 4.23. *^{1}H NMR spectrum of PHU4-PF60 recorded at different temperatures.*

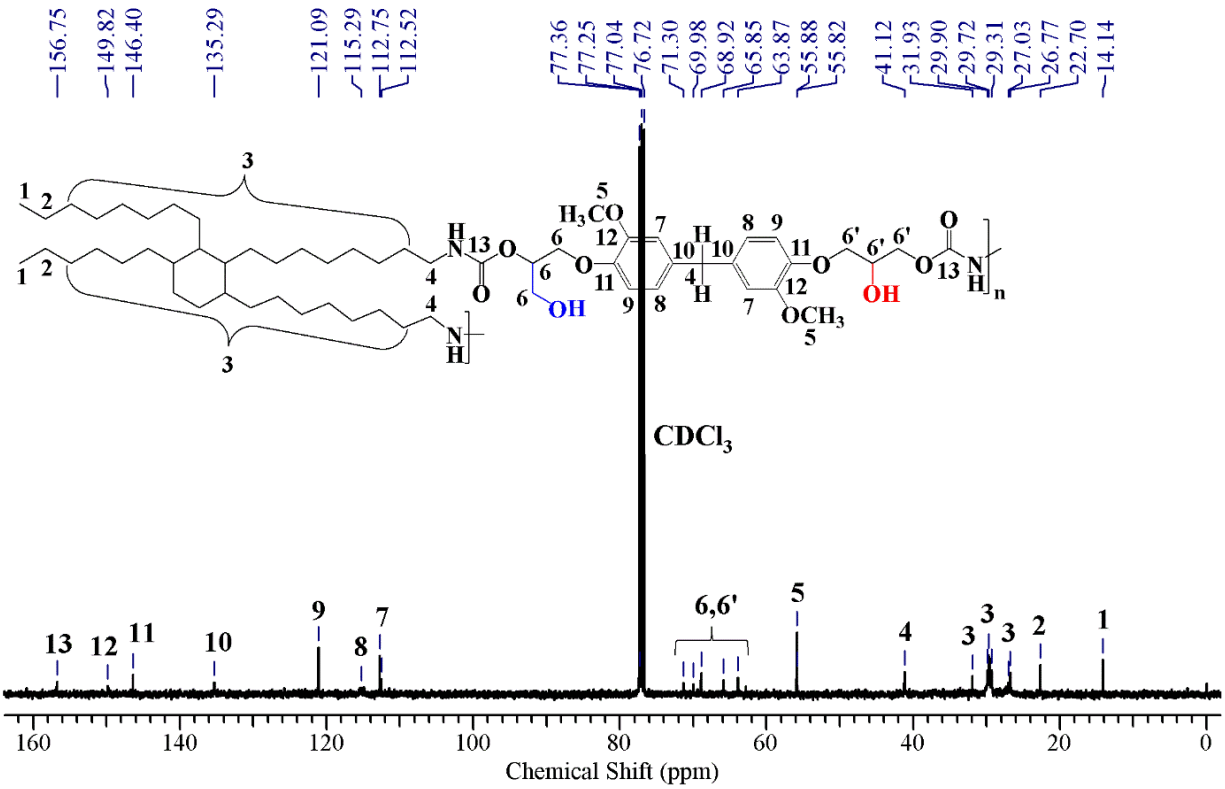

Figure 4.24. *^{13}C NMR spectrum of PHU1-PF0 (Homo).*

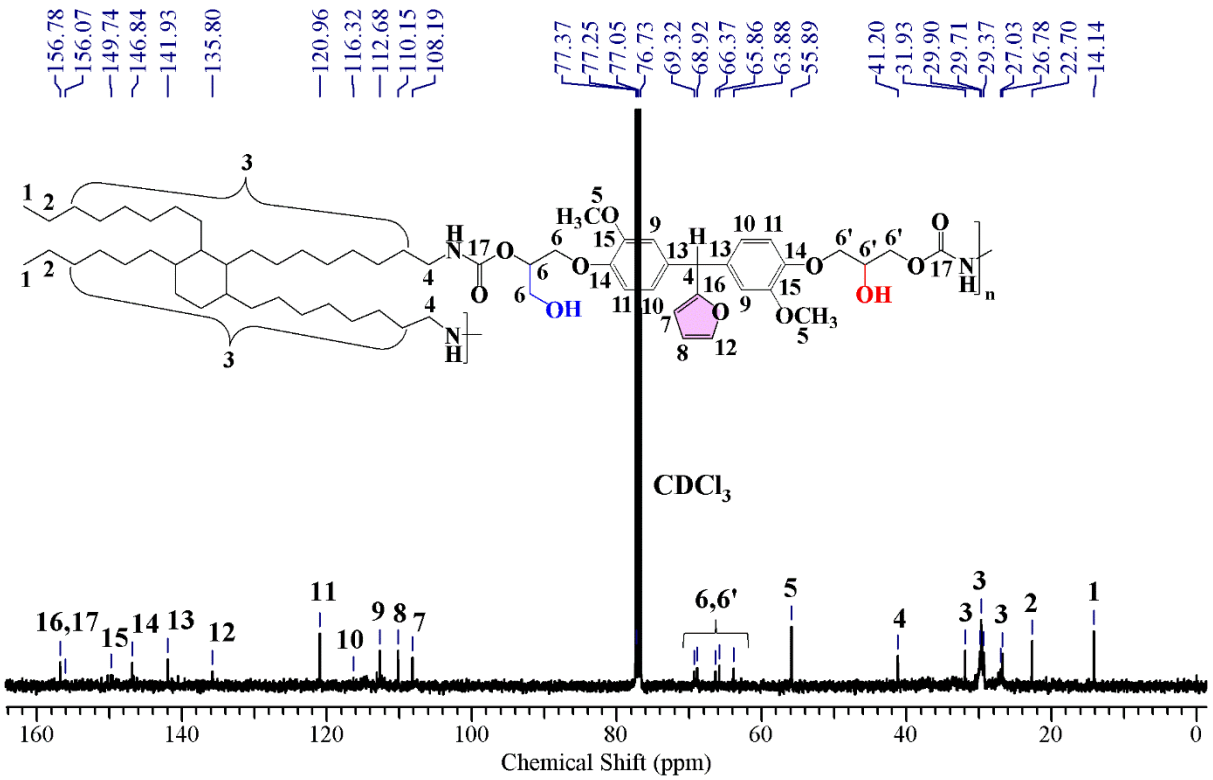

Figure 4.25. *^{13}C NMR spectrum of PHU6-PF100 (Homo).*

4.3.3.1 Size Exclusion Chromatography

The molecular weight and polymer dispersity index (PDI) of prepared PHUs were determined by SEC. The values are shown in **Table 4.2** and SEC curves are displayed in **Figure 4.26.**

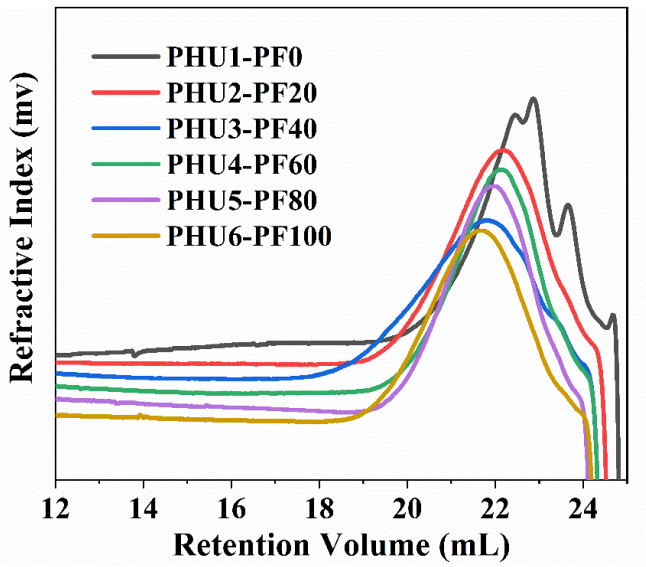

Figure 4.26. *SEC curves for PHUs bearing pendant furyl group.*

All samples demonstrate moderate molecular weights within the range of M_n = 9,300-13,800 g/mol, with corresponding polydispersity indices (M_w/M_n) ranging from 1.35 to 1.81. These values are in agreement with the previously published results of the PHUs, synthesized through step-growth polymerization.[26,34,35]

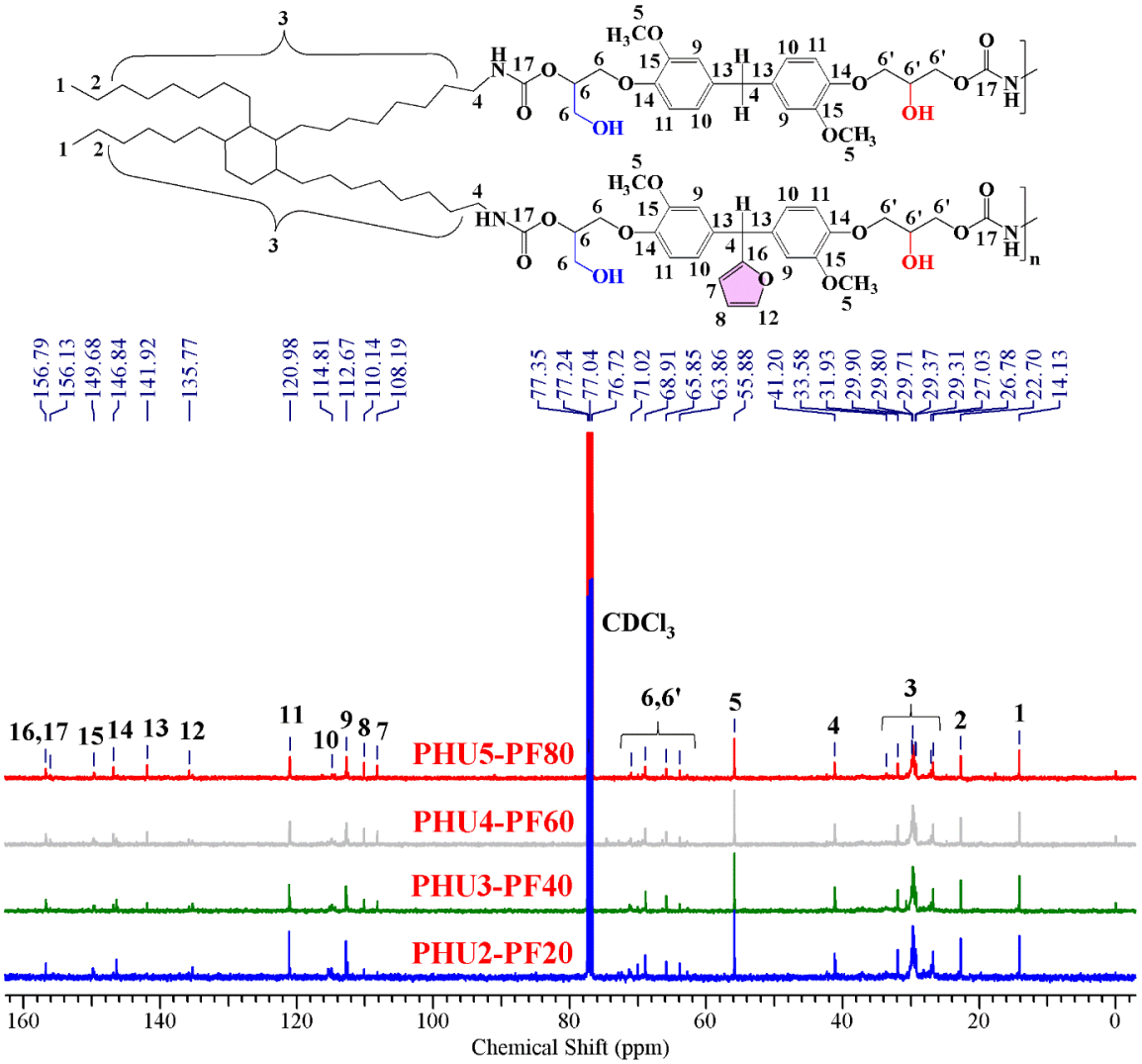

Figure 4.27. *^{13}C NMR spectrum of PHUs (Copolymers).*

4.3.3.2 Thermal properties

The thermal properties of bisguaiacol-based PHUs were examined using DSC over a temperature range of 40 to 180 °C in a nitrogen atmosphere, with a heating rate of 10°C min^{-1}. The second heating curves obtained from DSC are added in **Figure 4.28**, and corresponding values are summarized in **Table 4.2**. The T_g of synthesized PHUs was observed to fall between 14 and 24 °C as the content of BGF-PF-DC monomer increased from 0 to 100 mol%. Interestingly, the presence of the bulky furyl substituents at the bridging carbon of the BGF-

PF-DC influences the T_g of PHU materials. For example, in the case of PHU1-PF0, where no substituent is present at the bridging carbon, a lower T_g (14 °C) is noted, possibly due to greater rotational freedom. whereas, in PHU6-PF100, with a bulky furyl group at the bridging carbon, a higher T_g (24 °C) is observed, which could be due to reduced rotational freedom. These findings comparable with previous studies, which reported that PHUs derived from monomers with dimethyl-substituted bridging carbons showed higher T_g compared to their unsubstituted counterparts.[25,31] Further, no melting transition was noticed in any of the samples demonstrating the amorphous nature of all PHUs.[36,37]

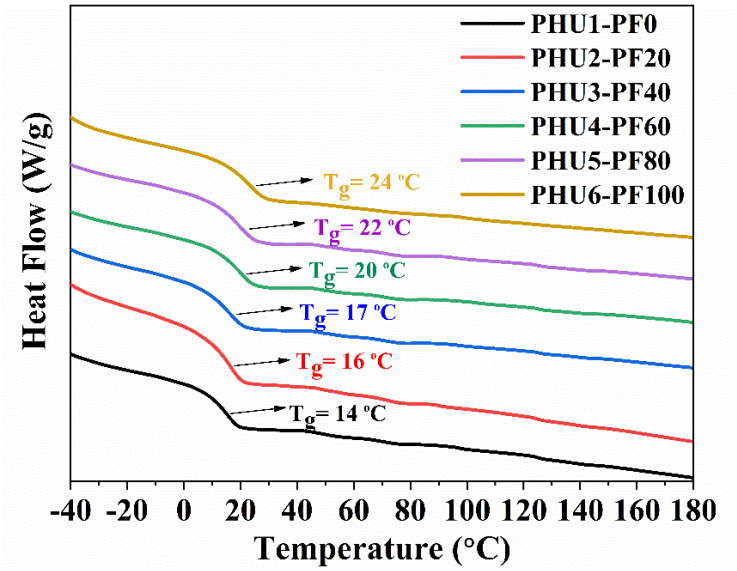

Figure 4.28. *DSC thermograms of PHUs bearing pendant furyl groups.*

The TGA thermograms are illustrated in **Figure 4.29a**, and the corresponding data are presented in **Table 4.2**. The $T_{d,10\%}$ was in the range of 290–323 °C, indicative of the excellent thermal stability exhibited by the PHU polymers. However, the TGA thermogram reveals that the degradation temperatures of PHU6-PF100 ($T_{d,10\%}$ = 323 °C) are higher than those of PHU1-PF0 ($T_{d,10\%}$ = 290 °C). This higher thermal stability observed in PHU6-PF100 may be ascribed to the presence of a pendant furyl ring at the bridging carbon. The furyl group is relatively bulky and could hinder the movement of polymer chains, thereby reducing their susceptibility to thermal decomposition. Additionally, the aromatic nature of the furyl groups contributes to the polymer stability, which could lead to increased delocalization of π-electrons and make the polymer more resistant to thermal degradation.[22,38]

Furthermore, the DTG curves of the PHU6-PF100 are depicted in **Figure 4.29b**, illustrating the two stages of the decomposition mechanism.[39] The first stage occurs within the temperature range of 287-405 °C, attributed to the breakage of hydroxyurethane linkages, while the second

stage occurs between the temperature range of 405-497 °C, possibly due to the decomposition of aliphatic or soft segments.

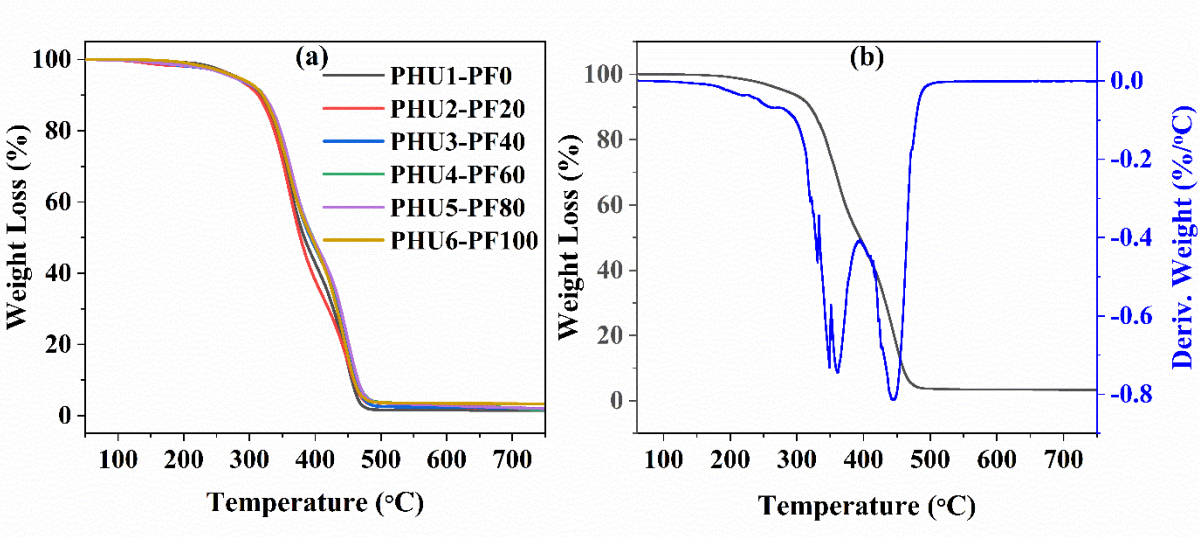

Figure 4.29. *TGA results of PHUs bearing furyl groups (a) TGA thermograms (b) DTG curve of PHU6-PF100.*

Table 4.2. *Thermal properties and molecular weights distribution of the PHUs.*

Polymers	TGA	DSC	SEC [c]		
	$T_{d10\%}$ (°C) [a]	T_g (°C) [b]	M_n (g/mol)	M_w (g/mol)	Dispersity
PHU1-PF0	290	14	9,300	12,500	1.35
PHU2-PF20	313	16	11,600	16,300	1.41
PHU3-PF40	317	17	11,350	14,950	1.32
PHU4-PF60	319	20	13,800	24,900	1.81
PHU5-PF80	320	22	12,200	19,400	1.59
PHU6-PF100	323	24	11,100	32,600	2.93

[a] Determined by TGA in an N_2 atmosphere at a heating rate of 10 °C min^{-1}. [b] Determined from the second heating curves of DSC experiments at a heating rate of 10 °C min^{-1}. [c] Measured by GPC in DMF solvent using polymethyl methacrylate as calibration standards.

4.3.3.3 X-ray diffraction

The XRD technique was employed to analyze the crystallization behavior of bisguaiacol-based PHUs. The obtained XRD patterns for all samples, as illustrated in **Figure 4.30**, show a broad diffraction peak in the 2θ region from ~10° to 30°, caused by the scattering of PHU materials,

indicating that the polymers are predominantly amorphous in nature.[40,41] This is consistent with previously reported values for PHUs,[42,43] which showed that the PHUs exhibit only glass transition curves (T_g), which are typically found in amorphous polymers, and there was no melting transition was observed in any of the samples, a phenomenon commonly observed in crystalline polymers.

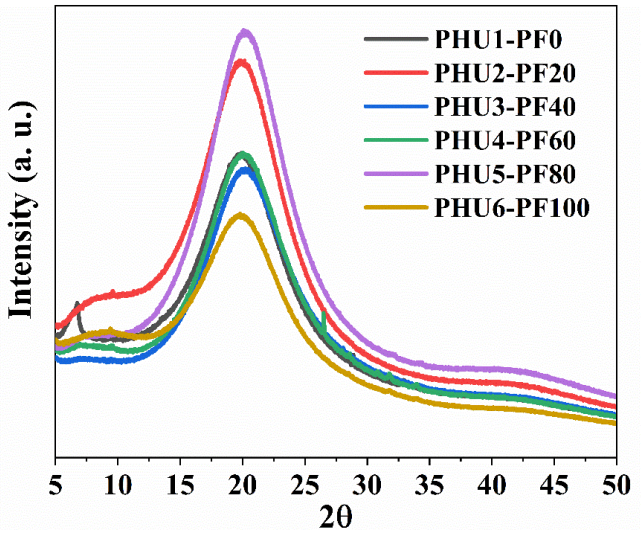

Figure 4.30. *XRD pattern of PHUs bearing pendant furyl group.*

4.3.3.4 Water contact angle

The surface wettability of the prepared adhesives was assessed through water contact angle experiments. As illustrated in **Figure 4.31 and**

Table 4.3, indicate that the water contact angles for the synthesized PHUs are consistently greater than 90°, ranging from 96.0 ± 0.15° to 99.4 ± 0.87°.

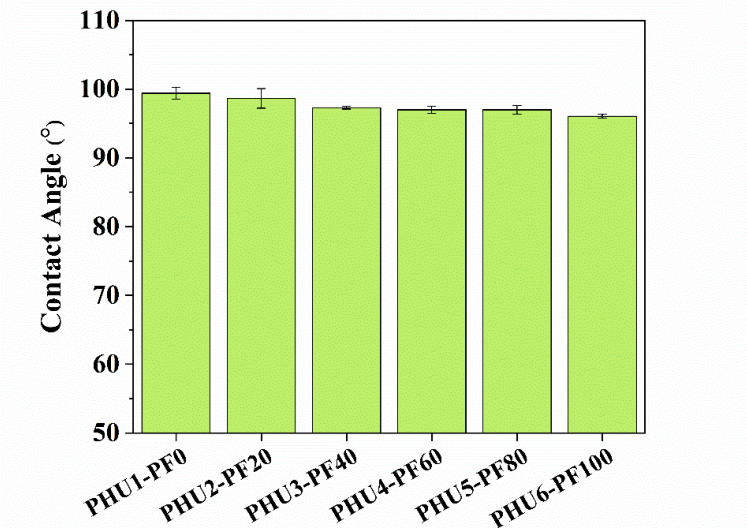

Figure 4.31. *Contact angle measurements of PHUs bearing pendant furyl groups.*

This suggests that these polymer surfaces exhibit hydrophobic properties. This hydrophobicity can be attributed to the presence of hydrophobic groups like aliphatic priamine 1074 and aromatic moieties within the polymer backbone.[44,45] Additionally, as the molar content of the BGF-PF-DC monomer bearing pendant furyl group increases, a very slight decrease in the water contact angle was observed, from 99.4 ± 0.87° to 96.0 ± 0.15°, This phenomenon could be explained by an increase in the amount of polar furyl groups.[46,47]

4.3.3.5 Rheological behavior of PHU materials

The viscoelastic behavior of the synthesized polymeric materials at 100 °C was studied using rheological measurements on a stress-controlled rheometer (MCR 301, Anton Paar). An amplitude sweep test was performed to determine the linear viscoelastic (LVE) region of the PHUs (**Figure 4.32a**), from which a 2 % strain was selected and further applied for the frequency and temperature sweep measurements.

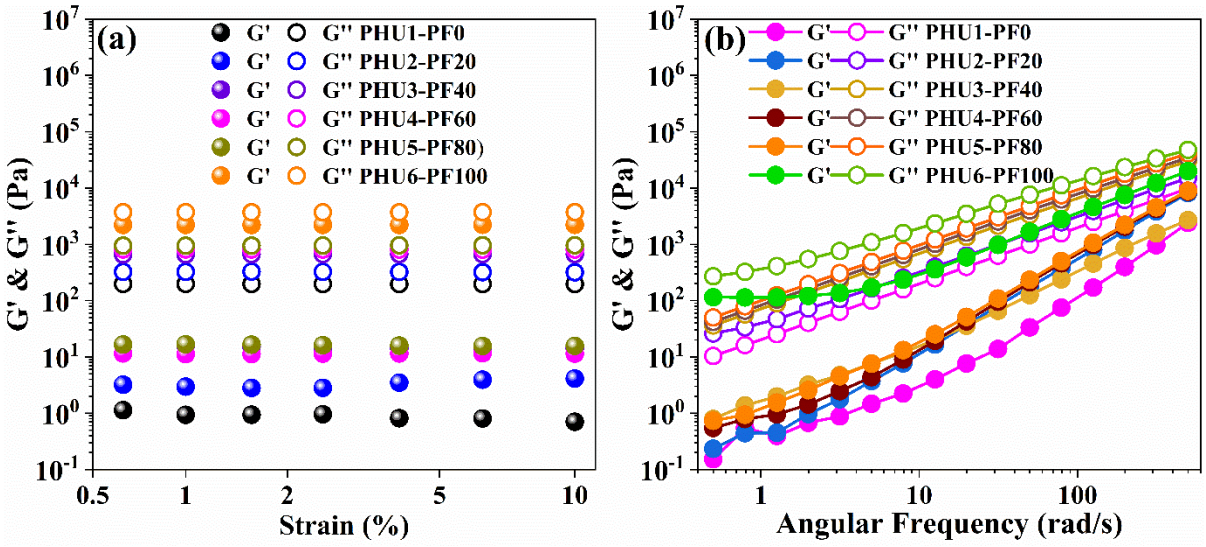

Figure 4.32. *Plot of (a) storage and loss modulus vs strain (b) storage and loss modulus vs angular frequency for PHUs bearing pendant furyl group.*

The storage (G′) and loss (G") modulus were studied as a function of frequencies ranging from 0.5 to 500 rad/s (**Figure 4.32b**). Across all samples, the G″ was consistently observed to be dominant over G′, indicating the predominant viscous behavior of the polymers.[48,49] Moreover, both G′ and G" of all materials exhibited a significant increase with increasing frequency, suggesting a strong dependence of viscoelastic properties on frequency. However, a remarkable increase in the G″ of PHU formulations was observed with the increase in the molar concentration of the BGF-PF-DC monomer from 0 to 100 %, and following the trend of G″ as PHU1-PF0 < PHU2-PF20 < PHU3-PF40 < PHU4-PF60 < PHU5-PF80 < PHU6-PF100. This

trend indicates that PHU6-PF100 exhibit high viscous in nature, while PHU1-PF0 demonstrate low viscous in nature. This enhanced viscosity might be attributed to the synergetic effect of a high density of non-covalent interactions (including hydrogen bonds and π-π interactions), along with the ordered arrangement of the soft segments (aliphatic backbone of the priamine) and hard segments (backbone of the rigid BGF-PF-DC monomer with pendant furyl substituents).

In order to acquire more information regarding the thermal transition of prepared materials, temperature sweep experiments were performed. **Figure 4.33a-c** shows the plots of storage modulus (G′), loss modulus (G″), and tan δ against the temperature. The glass transition is determined from loss modulus curves (

Table 4.3), and it falls within the range of 24 to 40 °C. These values correspond to the trend observed in the DSC results, showing an increase in the content of BGF-PF-DC monomers bearing stiff furyl groups. PHU1-PF0 exhibited the lowest T_g (24 °C), whereas PHU6-100 displayed the highest T_g (40 °C).

However, in all compositions, there are two well-defined drops in the curves of the G′ can be visible with increasing temperature (**Figure 4.33a**). The first onset occurred exactly near the glass transition hump and thereafter it shows a log-range rubbery plateau region, followed by another drop in the range of 80 to 129 °C (different for all samples) which indicates the transition of rubbery elastic state to a fluid state. Additionally, all PHUs showed a crossover (G′ = G″) in the temperature range of 36 to 53 °C, indicating a shift from a solid-like (glassy) state to a rubbery state. Below this range, the PHUs exhibit an elastic response due to the rigidity of the polymer chains and their limited mobility. Above the crossover, but below the second transition temperature, the loss modulus (G″) becomes dominant, signaling a rubbery state where the polymer chains gain increased mobility.

Table 4.3. Experimental values from rheological measurements and water contact angle.

Polymers	**T_g from G″ curves (°C)**	**G′ = G″ (°C)**	**2nd transition from Tan δ (°C)**	**Water contact angle (°)**
PHU1-PF0	24	36	99	99.4 ± 0.8
PHU2-PF20	25	37	93	98.6 ± 1.4
PHU3-PF40	27	42	82	97.3 ± 0.2
PHU4-PF60	30	49	114	97.0 ± 0.5

PHU5-PF80	35	44	80	97.0 ± 0.6
PHU6-PF100	40	53	129	96.0 ± 0.1

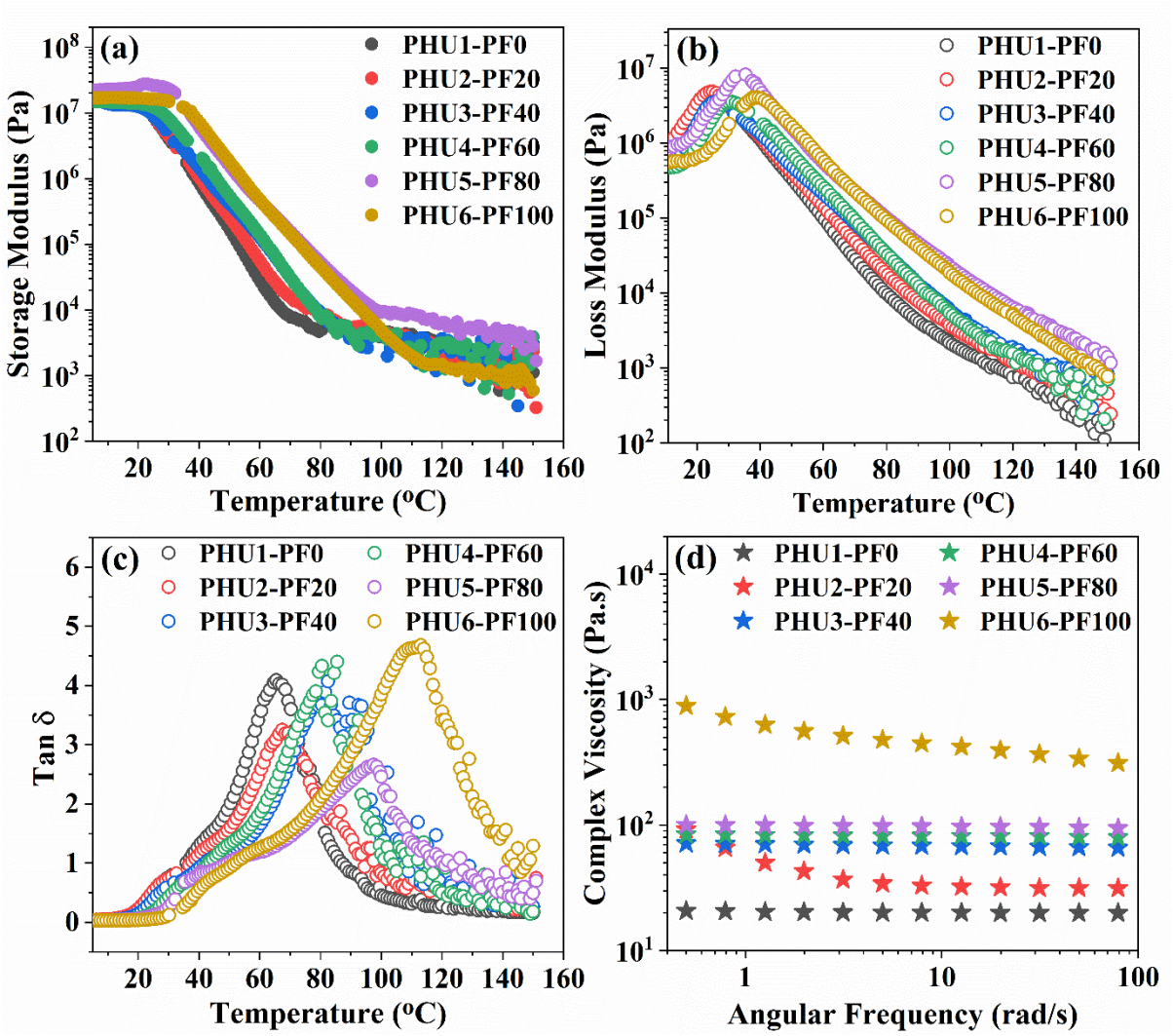

Figure 4.33. *A plot of (a) storage modulus vs temperature (b) loss modulus vs temperature (c) tan δ vs temperature (d) complex viscosity vs angular frequency acquired from rheological measurement for PHUs bearing pendant furyl group.*

4.3.3.6 Adhesive Properties

Hot melt adhesive is an environmentally friendly adhesive that does not require the use of curing agents or solvents during the bonding process.[2] This adhesive has been extensively used in several industries such as furniture manufacturing, the automotive industry, footwear manufacturing, and wood processing.[2] In this work, the developed PHUs exhibited a structure containing several urethane bonds and pendant hydroxyl groups distributed along the polymer chain. These functional groups facilitated the formation of both intra- and intermolecular

hydrogen bonds. Moreover, the bonding interactions, such as covalent or non-covalent with the substrate, also increased adhesion forces, making it suitable for various adhesive applications.[8] The application of biobased PHUs as hot-melt adhesives was investigated. The specimen of signal-lap shear joints was prepared according to ASTM standard D1002 by placing the PHU films on the overlap areas of substrates (aluminum and stainless steel). Then hot pressing was conducted at 100 °C for 20 minutes with applying light pressure.

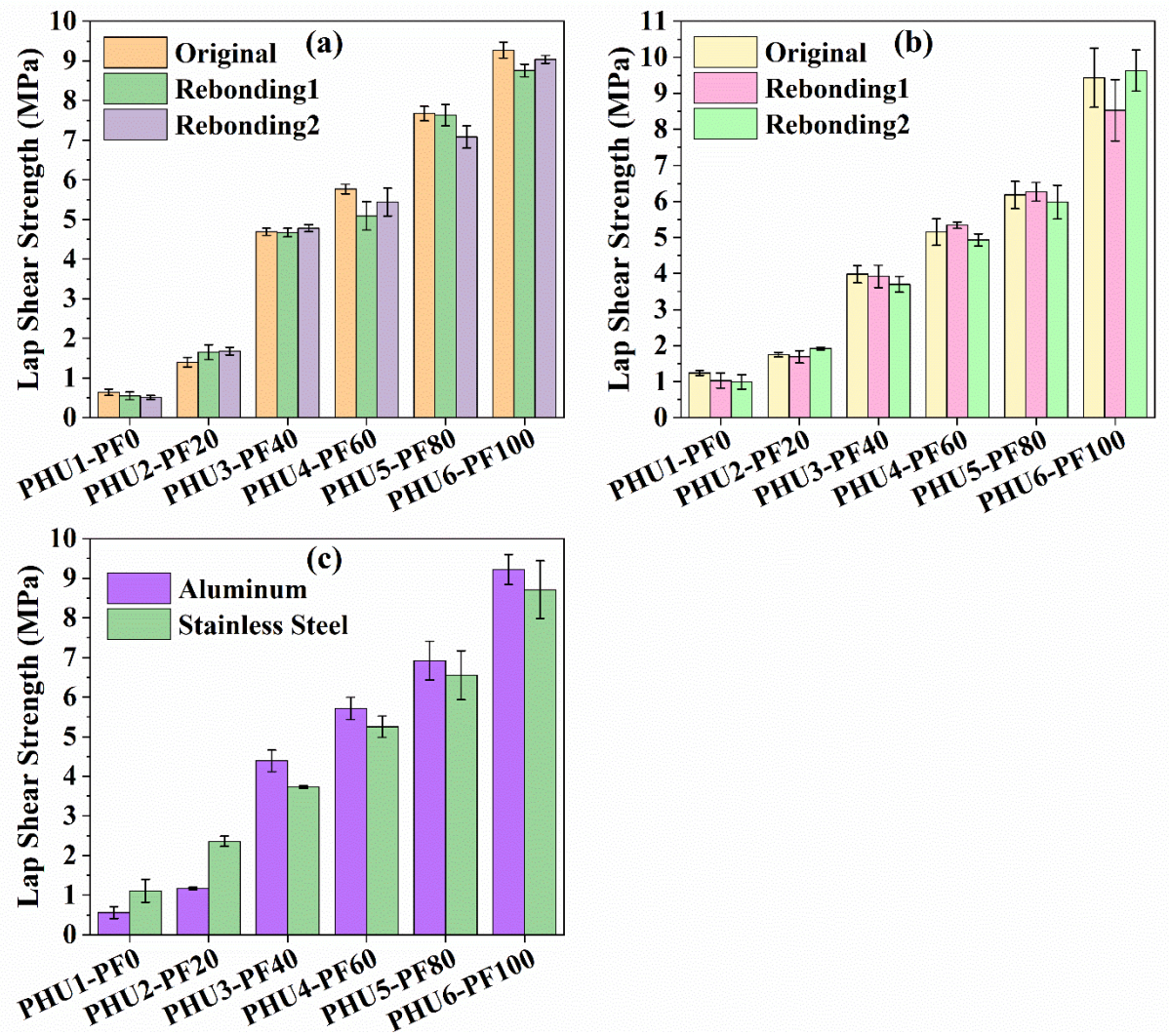

Figure 4.34. *The lap shear strength of PHUs bearing pendant furyl groups (a) evaluated on the aluminum (b) evaluated on the stainless steel and (c) evaluated under the water environment.*

The adhesive strength of the prepared formulations is shown in **Figure 4.34**. In the case of aluminum substrates (**Figure 4.34a**), the lap shear strength increased to approximately 9.27 ± 0.20 MPa by the rise in the molar concentration of BGF-PF-DC from 0 to 100 %. The PHU1-PF0, with an absence of rigid pendant furyl groups, has achieved a lower adhesion strength of

0.64 ± 0.08 MPa, whereas PHU6-PF100, having the highest concentration of furyl groups, demonstrated a higher value of 9.27 ± 0.20 MPa. When the substrates are stainless steel, almost similar values and trends of the adhesion strengths were noted. PHU1-PF0 and PHU6-PF100 respectively exhibited shear strength of 1.24±0.07 and 9.43±0.82 MPa (**Figure 4.34b**). However, the superior adhesive strength of PHU6-PF100 can be attributed to two main factors (i) the presence of non-covalent interactions, such as hydrogen bonding and π-π interactions, and (ii) the balance behavior between the hard and soft domains.[7,50] Interestingly, in this formulation, the backbone of the BGF-PF-DC could act as hard segments due to furyl substituents at the bridging carbon, making it more rigid and stiff, thereby restricting the rotational freedom.[25] whereas the long aliphatic flexible chains of the Priamine could act as the soft segment. As a result, the PHU6-PF100 has exhibited greater adhesion compared to other formations. Furthermore, an observed reduction in adhesive strength was documented for additional PHU samples as the quantity of BGF-DC (without furyl) increased. This could be related to its unsubstituted bridging carbon, which may give it relatively more rotational freedom,[25] and disrupt the balance behavior by incorporating more flexibility in the matrix.[51] To explore the reusability of the PHU-based hot melt adhesive, the bonded substrates were separated, then rejoined simply by hot-pressing under the same conditions, and their adhesion strength was analyzed. **Figure 4.34a-b** illustrates a minimal variation in the adhesion strength of all compositions after two consecutive reuses. However, in most of the formulations, a decrease in adhesive strength was noted after two reuses. This phenomenon may be attributed to the gradual flow of some samples between the substrate plates out of the bonding area during the bonding and debonding cycles.[52]

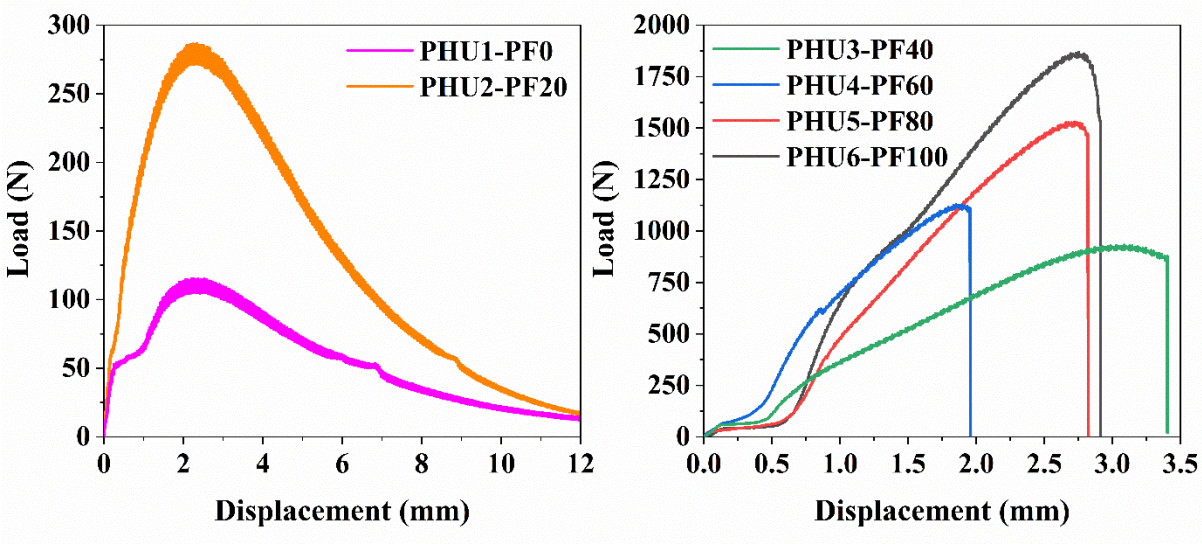

Figure 4.35. *Force vs. displacement curves of PHUs bearing pendant furyl group (an aluminum substrate).*

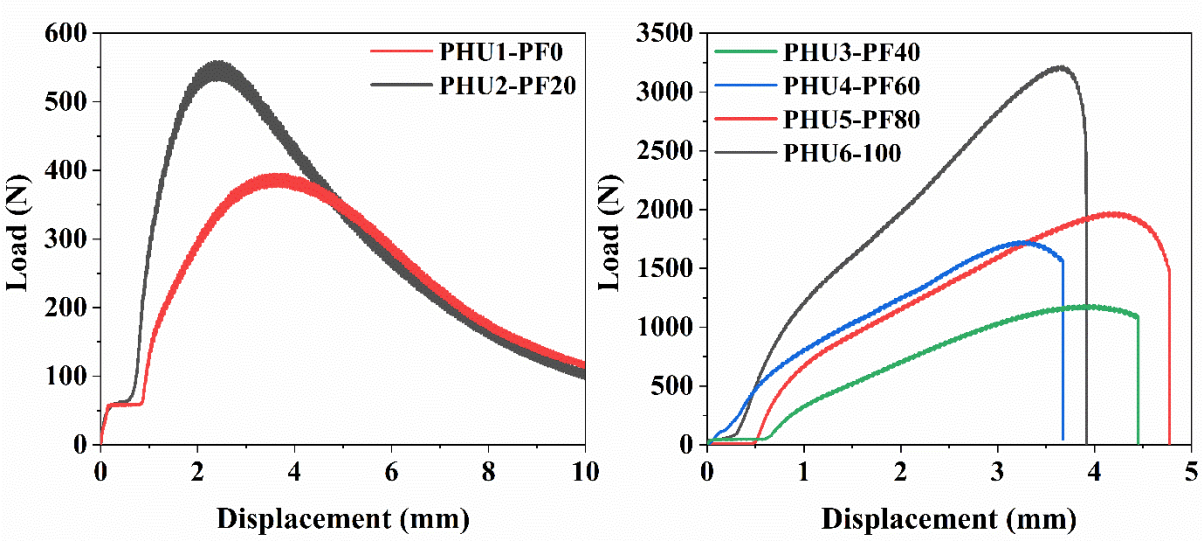

Figure 4.36. *Force vs. displacement curves of PHUs bearing pendant furyl group (stainless-steel substrate).*

Moreover, the analysis of the shear strength of PHU6-PF100 after two cycles reveals that its lap shear strength remains stable at approximately 9.04 ± 0.10 MPa (aluminum) and 9.68 ± 0.57 MPa (stainless steel), highlighting its remarkable reusability as a hot melt adhesive. Furthermore, to study the potential of PHU-based adhesive for use as an underwater glue, the bonded specimens were immersed in water at room temperature and after 12 h, the lap shear strength was investigated and the values are provided in **Figure 4.34c**. However, a slight reduction in the adhesion strength was observed in most of the samples. These results demonstrated that the PHU-based hot melt adhesive can withstand water after bonding under

the specified conditions. Nevertheless, the failure mode of joints was examined after the test based on visual inspection, and digital photographs of both substrates (Al and SS) were depicted in **Figure 4.37a-f, and Figure 4.38a-f,** respectively. The four samples (PHU1-PF0 to PHU4-PF60) exhibited cohesive failure while the remaining two (PHU5-PF80 and PHU6-PF100) showed a mixture of cohesive and adhesive failure. The force vs. displacement curves of PHUs are added in **Figure 4.35** (AL) and **Figure 4.36** (SS).

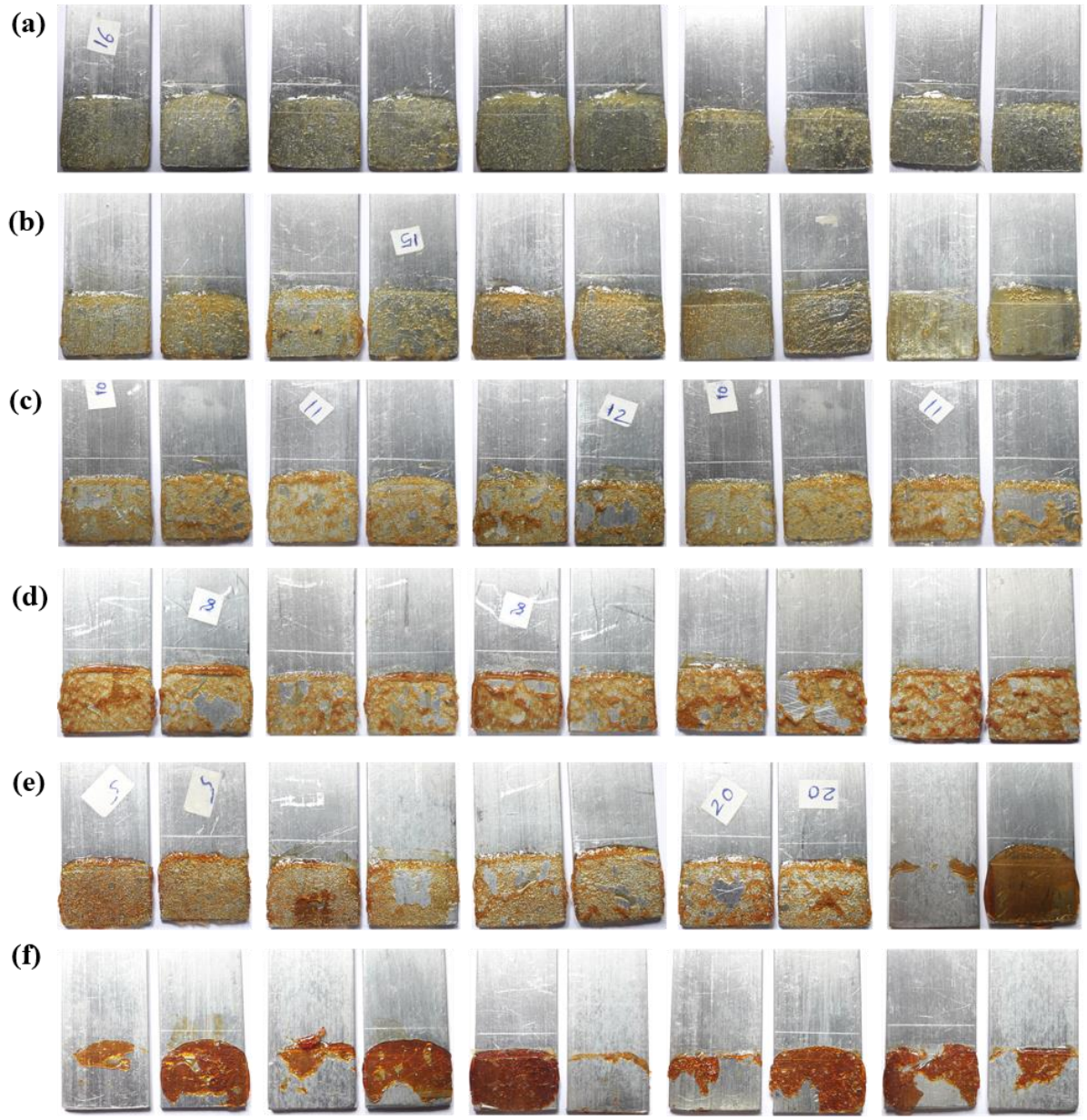

Figure 4.37*. Photos of the representative cohesive failure for (a) PHU1-PF0 (b) PHU2-PF20 (c) PHU3-PF40 (d) PHU4-PF60, and the mixture of cohesive/adhesive failure for (e) PHU5-PF80 (f) PHU6-PF100, after the lap shear test assessed on an aluminum substrate.*

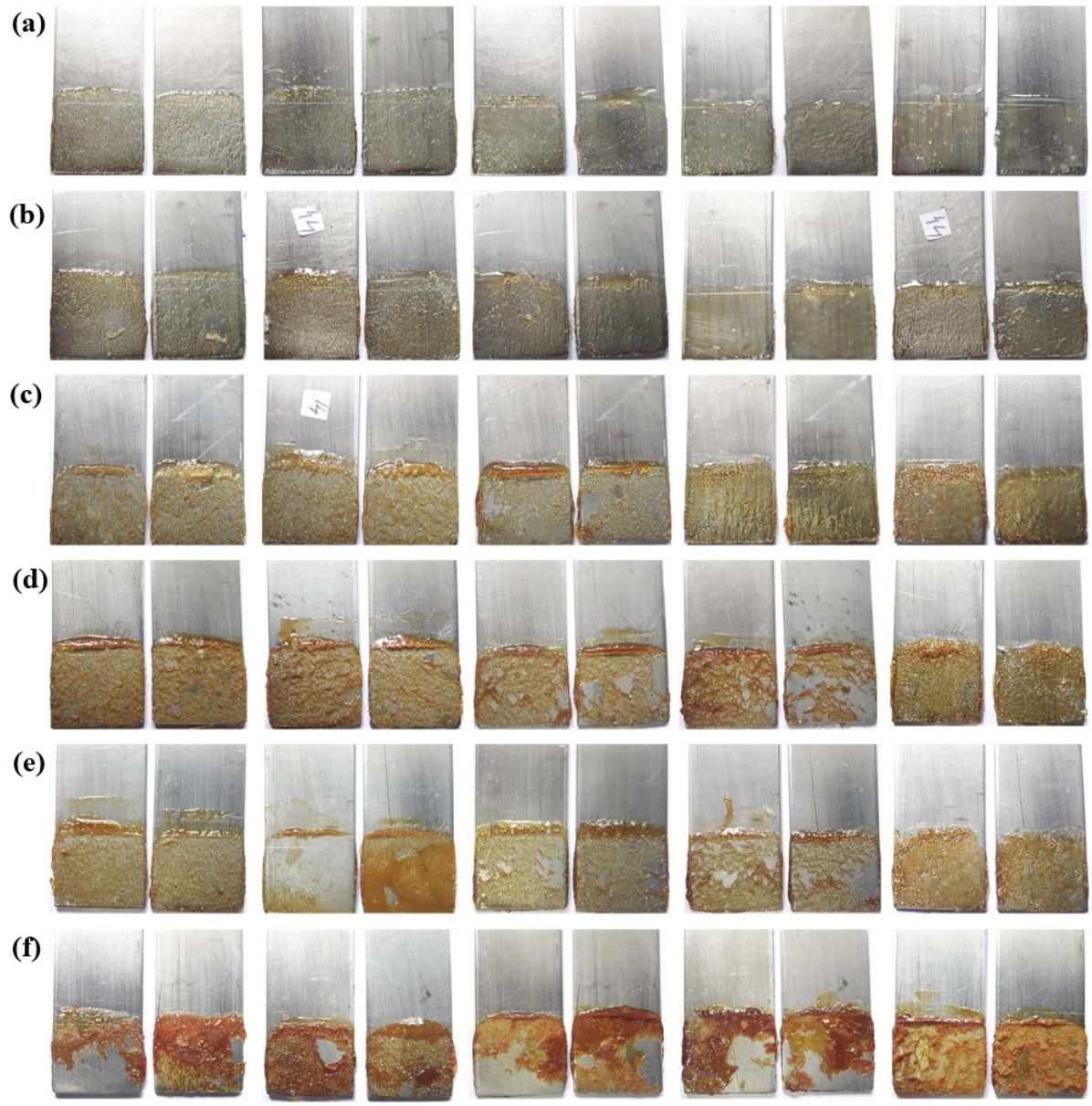

Figure 4.38. *Photos of the representative cohesive failure for (a) PHU1-PF0 (b) PHU2-PF20 (c) PHU3-PF40 (d) PHU4-PF60, and the mixture of cohesive/adhesive failure for (e) PHU5-PF80 (f) PHU6-PF100, after the lap shear test assessed on stainless-steel.*

4.3.4 Thermal and adhesive properties of cross-linked PHU/BMI networks

As previously indicated, the incorporation of pendant furyl groups on the backbone of the developed PHU adhesives offers an opportunity to augment their thermo-mechanical properties through the Diels-Alder reaction (DA).[22] Subsequently, a postmodification investigation was conducted on PHU6- PF100, which is distinguished by its significant content of pendant furyl groups. A crosslinked polymer network was then synthesized through a DA reaction involving PHU6-PF100 and varying concentrations of Bismaleimide (BMI). Subsequently, an

assessment of its thermoreversibility and adhesive properties was conducted. The reversibility of the DA reaction was assessed through DSC analysis, and the corresponding first and second heating curves are presented in **Figure 4.39a**, and **Figure 4.39b**, respectively. In **Figure 4.39b**, it is evident that the crosslinked polymers exhibited elevated T_g values following the DA reaction when compared to the reference PHU6-PF100. This substantiates the successful formation of the D-A adduct.[53]

The T_g increase might correspond to greater rigidity and crosslinking density of the polymeric network due to the addition of the BMI crosslinker. Furthermore, the first heating curves of all crosslinked polymers showed two endothermic peaks, which were attributed to the Retro Diels-Alder (rDA) reaction of the endo and exo isomers, respectively.[53-55] Moreover, these rDA peaks were absent in the second heating curves of all polymer samples (**Figure 4.39b**), indicating the complete dissociation of the DA adducts.[22,53]

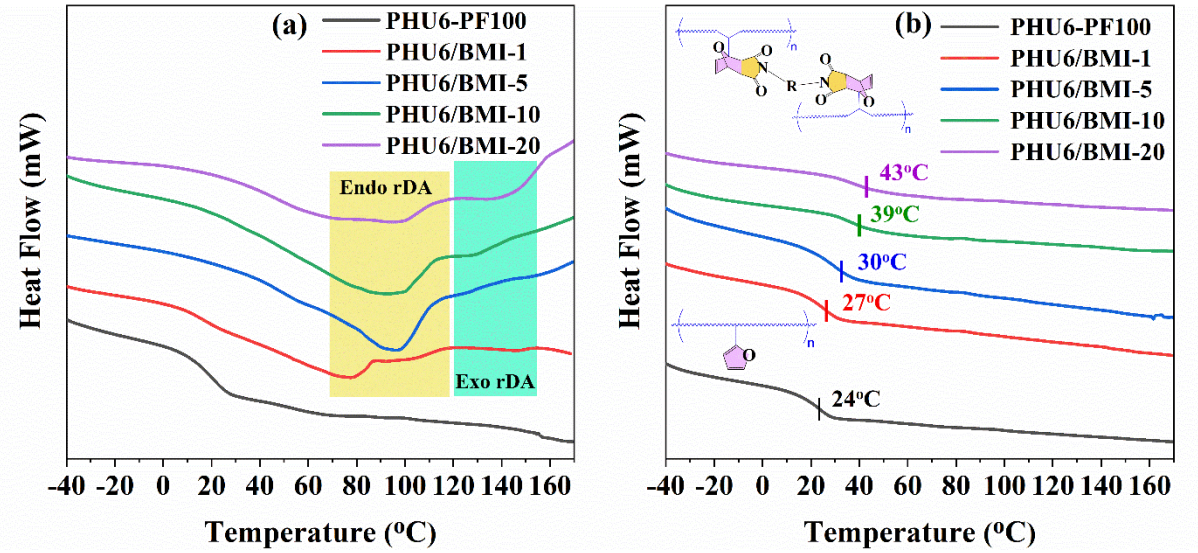

Figure 4.39. *DSC curves of the cross-linked PHU/BMI polymers (a) first heating curves (b) second heating curves.*

Furthermore, gel formation experiments were conducted in the laboratory to validate the above results. PHU6-PF100 and BMI were dissolved in DMAc, and the solution was agitated at 60 °C. The formation of the DA adduct was indicated by a significant rise in solution viscosity after 24 h, making it non-flowable even when the vial was inverted (**Figure 4.40**).[22] After heating this gel-containing vial at 120 °C, a low-viscous, flowable solution appeared, demonstrating the cleavage of the DA adduct through the decrosslinking reaction.

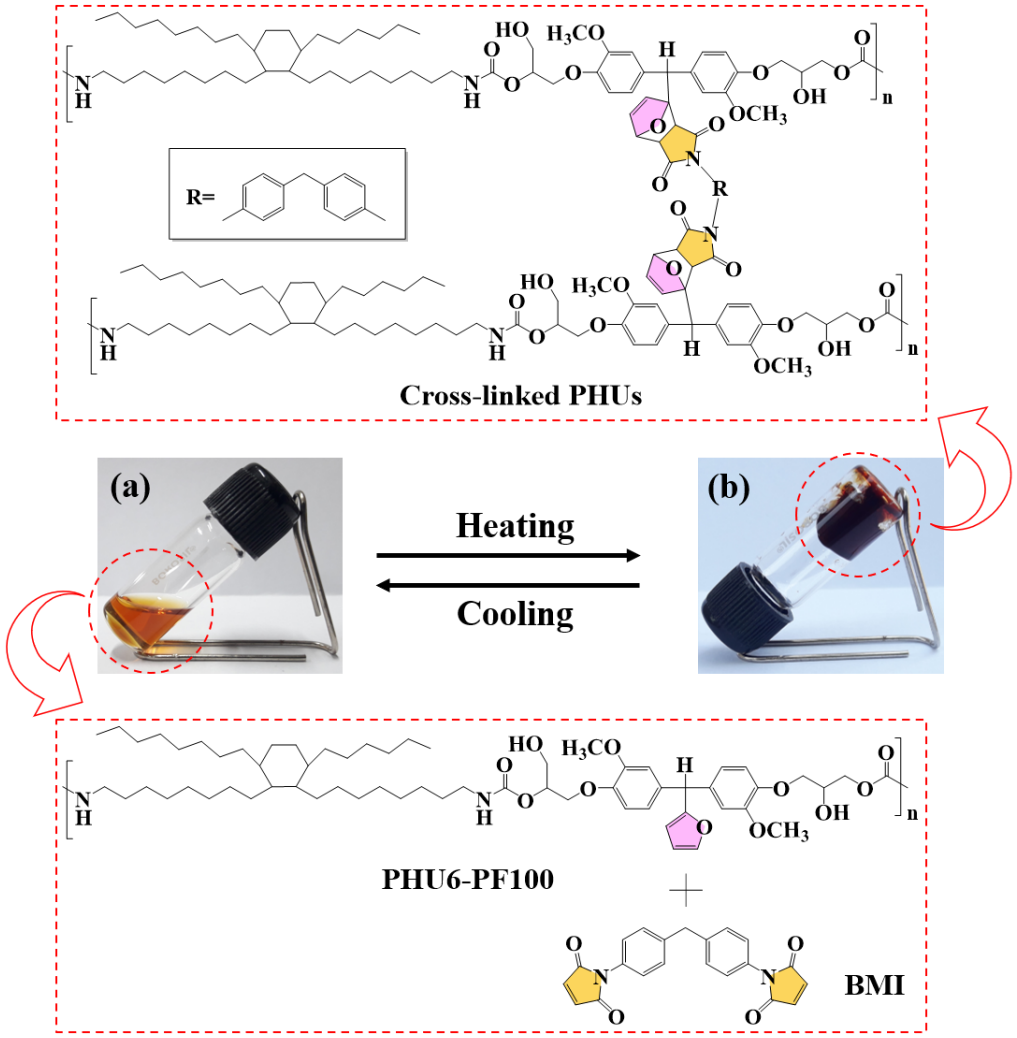

Figure 4.40. *Preparation of crosslinked PHU/BMI network via Diels-Alder reaction.*

To study how different concentrations of BMI crosslinkers influence the adhesive properties of crosslinked PHU adhesives, the shear strength on the aluminum substrate was analyzed and illustrated in **Figure 4.41**. It was found that the crosslinked systems exhibited a reduction in adhesion strength compared to the reference PHU6-PF100 (**Figure 4.41a**). Nevertheless, in previous studies, various crosslinking agents were used to produce thermoset PHU adhesives, which initially showed an increase in adhesive strength due to higher crosslinking density but beyond a certain point, it began to decrease due to increased brittleness, as optimal crosslinking density led to increased brittleness.[5,56,57] In our study, we expected a similar trend in adhesion strength of the developed crosslinked PHUs, but the results were the opposite. We have not observed any increase in adhesion strength with the addition of different BMI crosslinker concentrations. This could be due to the high brittleness of the crosslinked PHUs, which is supported by the increase in T_g values compared to the original PHU6-PF100 (**Figure 4.41a**).[11] Furthermore, the failure images of the crosslinked PHU adhesives show cohesive/adhesive

failure for PHU6/BMI-1 and PHU6/BMI-5, while adhesive failure was observed for PHU6/BMI-10 and PHU6/BMI-20 (**Figure 4.42**). The force vs. displacement curves for crosslinked PHUs are added in **Figure 41b**.

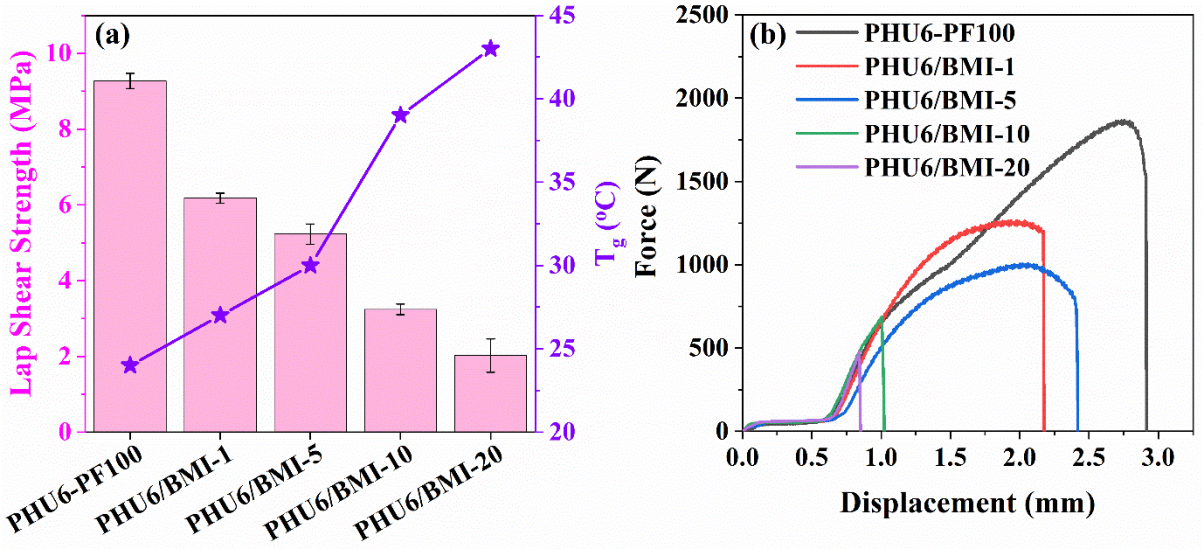

Figure 4.41. *(a) Comparison of adhesion strength (aluminum) and glass transition temperature, and (b) force-displacement curves of the crosslinked PHU/BMI network.*

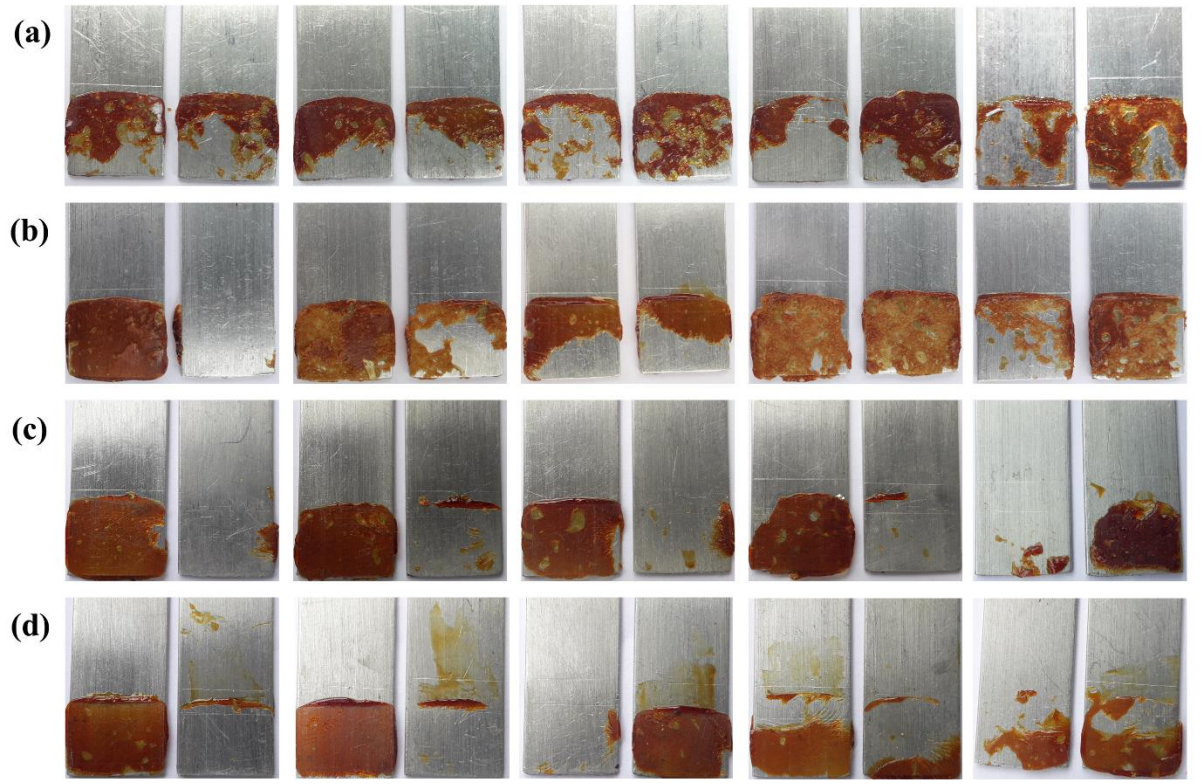

Figure 4.42. *Failure images of crosslinked PHU/BMI network (a) PHU6/BMI-1, (b) PHU6/BMI-5, (c) PHU6/BMI-10, and (d) (a) PHU6/BMI-20.*

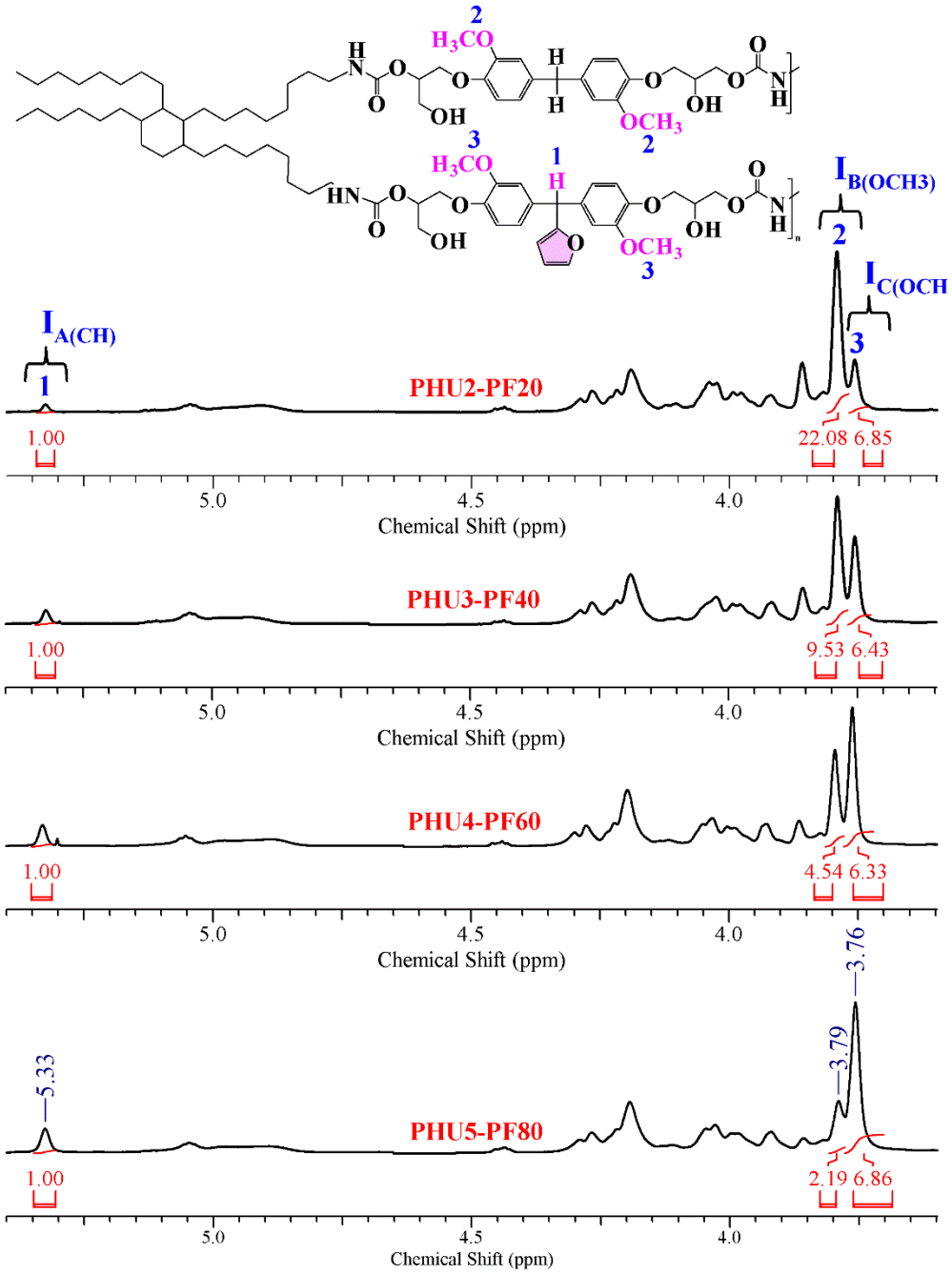

Figure 4.43. *Incorporated mole percentage of dicarbonate monomers in the final PHU copolymers, were determined using the integrals of ^{1}H NMR signals. The $I_{A(CH)}$, $I_{B(OCH3)}$, and $I_{C(OCH3)}$ represent the integrals of one bridge-head proton of BGF-PF-DC (signal 1), six methoxy protons of BGF-DC (signals 2), and six methoxy protons of BGF-PF-DC (signal 3), respectively.*

Table 4.4. *Incorporated mole percentage of dicarbonate monomers in the final PHU copolymers, were determined using the integrals of ^1H NMR signals.*

Polymers	$I_{A(CH)}$ [a]	$I_{B(OCH3)}$ [a]	$I_{C(OCH3)}$ [a]	BGF-DC (mol%)	BGF-PF-DC (mol%)	Total DC (mol%)
PHU1-PF0	-	-	-	-	-	-
PHU2-PF20	1.00	22.08	6.85	76.32	23.68	99.99
PHU3-PF40	1.00	9.53	6.43	59.71	40.29	99.99
PHU4-PF60	1.00	4.54	6.33	41.76	58.24	100
PHU5-PF80	1.00	2.19	6.86	24.19	75.81	100
PHU6-PF100	-	-	-	-	-	-

[a] The $I_{A(CH)}$, $I_{B(OCH3)}$, and $I_{C(OCH3)}$ represent the integrals of one bridge-head proton of BGF-PF-DC (signal 1), six methoxy protons of BGF-DC (signals 2), and six methoxy protons of BGF-PF-DC (signal 3), respectively.

4.4 Conclusion

In this study in addition to the goal of enhancing adhesion and renewable carbon content, we studied the impact of the Diels-Alder network on the adhesive properties of sustainable PHUs. Two biobased dicarbonate monomers were synthesized and fully characterized. One of the monomers with a pendant furyl group was synthesized from guaiacol and furfural (BGF-PF-DC), while another monomer without the pendant group (BGF-DC) was synthesized from vanillin and guaiacol. Further, a series of PHU-HMAs containing pendant furyl groups with varying amounts of two dicarbonates (BGF-DC and BGF-PF-DC), in combination with Priamine 1074, were formulated. The resulting polymers exhibited a renewable carbon content (RCC) in the range of 89-90 %. Subsequently, it was observed that the thermal and adhesive properties, including T_g, exhibited an increase as the concentration of the monomer with pendant groups (BGF-PF-DC) rose from 0 to 100 mol%. Concurrently, adhesion properties exhibited a similar correlation. The highest adhesion strength was evident in PHU6-PF100, with approximately 9.27 ± 0.20 MPa on aluminum and 9.43 ± 0.82 MPa on stainless steel. These values markedly surpass previously reported adhesion strengths for biobased monomers.

4.5 References

(1) Gharde, S.; Sharma, G.; Kandasubramanian, B. Hot-Melt Adhesives: Fundamentals,

Formulations, and Applications: A Critical Review. *Rev. Adhes. Adhes.* **2020**, *8* (1), 1–28.

(2) Vineeth, S. K.; Gadhave, R. V. Sustainable Raw Materials in Hot Melt Adhesives: A Review. *Open J. Polym. Chem.* **2020**, *10* (August), 49–65.

(3) Yang, J.; Liu, K.; Wang, Z.; Rao, L.; Fu, L.; Tang, D.; Yang, X.; Li, Y.; Chen, H.; Liu, Y. Electron Beam Radiation Constructed and Improved Bone Repairing Performance Based on Hierarchical Thermoplastic Polyurethane/Graphene Oxide/Hydroxyapatite Hot Melt Adhesive with High Flow Ductility. *Polym. Compos.* **2024**, *45* (6), 4961–4972.

(4) Sun, L.; Zhang, W.; Xue, W.; Zeng, Z. Reactive Polyurethane Hot Melt Adhesives Based on Polycarbonate and Sebacic Acid-Based Polyester Polyols. *J. Adhes. Sci. Technol.* **2023**, *37* (4), 663–682.

(5) Panchireddy, S.; Grignard, B.; Thomassin, J. M.; Jerome, C.; Detrembleur, C. Catechol Containing Polyhydroxyurethanes as High-Performance Coatings and Adhesives. *ACS Sustain. Chem. Eng.* **2018**, *6* (11), 14936–14944.

(6) Gomez-Lopez, A.; Grignard, B.; Calvo, I.; Detrembleur, C.; Sardon, H. Monocomponent Non-Isocyanate Polyurethane Adhesives Based on a Sol–Gel Process. *ACS Appl. Polym. Mater.* **2020**, *2* (5), 1839–1847.

(7) Gomez-Lopez, A.; Ayensa, N.; Grignard, B.; Irusta, L.; Calvo, I.; Müller, A. J.; Detrembleur, C.; Sardon, H. Enhanced and Reusable Poly(Hydroxy Urethane)-Based Low Temperature Hot-Melt Adhesives. *ACS Polym. Au* **2022**, *2* (3), 194–207.

(8) Gomez-Lopez, A.; Panchireddy, S.; Grignard, B.; Calvo, I.; Jerome, C.; Detrembleur, C.; Sardon, H. Poly(Hydroxyurethane) Adhesives and Coatings: State-of-the-Art and Future Directions. *ACS Sustain. Chem. Eng.* **2021**, *9* (29), 9541–9562.

(9) Cornille, A.; Michaud, G.; Simon, F.; Fouquay, S.; Auvergne, R.; Boutevin, B.; Caillol, S. Promising Mechanical and Adhesive Properties of Isocyanate-Free Poly(Hydroxyurethane). *Eur. Polym. J.* **2016**, *84*, 404–420.

(10) Delliere, P.; Laborie, D.; Caillol, S.; Bakkali-Hassani, C. Controlling Hybrid Polyhydroxyurethane Adhesive and Rheological Properties by Partial Carbonation of Biobased Epoxy Monomer. *Macromol. Rapid Commun.* **2024**, *2400542*, 1–9.

(11) Panchireddy, S.; Grignard, B.; Thomassin, J. M.; Jerome, C.; Detrembleur, C. Bio-Based Poly(Hydroxyurethane) Glues for Metal Substrates. *Polym. Chem.* **2018**, *9* (19), 2650–2659.

(12) Panchireddy, S.; Thomassin, J. M.; Grignard, B.; Damblon, C.; Tatton, A.; Jerome, C.; Detrembleur, C. Reinforced Poly(Hydroxyurethane) Thermosets as High Performance

Adhesives for Aluminum Substrates. *Polym. Chem.* **2017**, *8* (38), 5897–5909.

(13) Figovsky, O.; Shapovalov, L.; Birukova, O.; Leykin, A. Modification of Epoxy Adhesives by Hydroxyurethane Components on the Basis of Renewable Raw Materials 1. **2013**, *6* (4), 271–274.

(14) Dolci, E.; Michaud, G.; Simon, F.; Boutevin, B.; Fouquay, S.; Caillol, S. Remendable Thermosetting Polymers for Isocyanate-Free Adhesives: A Preliminary Study. *Polym. Chem.* **2015**, *6* (45), 7851–7861.

(15) Heinrich, L. A. Future Opportunities for Bio-Based Adhesives-Advantages beyond Renewability. *Green Chem.* **2019**, *21* (8), 1866–1888.

(16) Tryznowski, M.; Świderska, A.; Gołofit, T.; Zołek-Tryznowska, Z. Wood Adhesive Application of Poly(Hydroxyurethane)s Synthesized with a Dimethyl Succinate-Based Amide Backbone. *RSC Adv.* **2017**, *7* (48), 30385–30391.

(17) Tryznowski, M.; Gołofit, T.; Świderska, A. Poly(Hydroxyurethane)s with Diethyl Tartrate-Based Amide Backbone by an Isocyanate-Free Route: Use as Adhesives. *Polymer (Guildf).* **2018**, *144*, 1–6.

(18) Yue, X.; Queneau, Y. 5-Hydroxymethylfurfural and Furfural Chemistry Toward Biobased Surfactants. *ChemSusChem* **2022**, *15* (13), e202102660.

(19) Upton, B. M.; Kasko, A. M. Strategies for the Conversion of Lignin to High-Value Polymeric Materials: Review and Perspective. *Chem. Rev.* **2016**, *116* (4), 2275–2306.

(20) Araújo, J. D. P.; Grande, C. A.; Rodrigues, A. E. Vanillin Production from Lignin Oxidation in a Batch Reactor. *Chem. Eng. Res. Des.* **2010**, *88* (8), 1024–1032.

(21) Periyasamy, T.; Asrafali, S. P.; Muthusamy, S.; Kim, S. C. Replacing Bisphenol-A with Bisguaiacol-F to Synthesize Polybenzoxazines for a Pollution-Free Environment. *New J. Chem.* **2016**, *40* (11), 9313–9319.

(22) Nagane, S. S.; Kuhire, S. S.; Mane, S. R.; Wadgaonkar, P. P. Partially Bio-Based Aromatic Poly(Ether Sulfone)s Bearing Pendant Furyl Groups: Synthesis, Characterization and Thermo-Reversible Cross-Linking with a Bismaleimide. *Polym. Chem.* **2019**, *10* (9), 1089–1098.

(23) Fache, M.; Darroman, E.; Besse, V.; Auvergne, R.; Caillol, S.; Boutevin, B. Vanillin, a Promising Biobased Building-Block for Monomer Synthesis. *Green Chem.* **2014**, *16* (4), 1987–1998.

(24) Nicastro, K. H.; Kloxin, C. J.; Epps, T. H. Potential Lignin-Derived Alternatives to Bisphenol A in Diamine-Hardened Epoxy Resins. *ACS Sustain. Chem. Eng.* **2018**, *6* (11), 14812–14819.

(25) Mhatre, S. V.; Mahajan, J. S.; Epps, T. H.; Korley, L. S. T. J. Lignin-Derivable Alternatives to Petroleum-Derived Non-Isocyanate Polyurethane Thermosets with Enhanced Toughness. *Mater. Adv.* **2022**, *4* (1).

(26) Ghuge, G. H.; Kambikanam, K. V.; Nair, K. S. Evaluation of the Adhesive Properties of Vanillin-Derived Polyhydroxy Urethanes. *J. Appl. Polym. Sci.* **2023**, No. May, 1–11.

(27) Ménard, R.; Caillol, S.; Allais, F. Chemo-Enzymatic Synthesis and Characterization of Renewable Thermoplastic and Thermoset Isocyanate-Free Poly(Hydroxy)Urethanes from Ferulic Acid Derivatives. *ACS Sustain. Chem. Eng.* **2017**, *5* (2), 1446–1456.

(28) Mokhtari, C.; Malek, F.; Manseri, A.; Caillol, S.; Negrell, C. Reactive Jojoba and Castor Oils-Based Cyclic Carbonates for Biobased Polyhydroxyurethanes. *Eur. Polym. J.* **2019**, *113* (December 2018), 18–28.

(29) Kathalewar, M.; Sabnis, A.; D'Mello, D. Isocyanate Free Polyurethanes from New CNSL Based Bis-Cyclic Carbonate and Its Application in Coatings. *Eur. Polym. J.* **2014**, *57*, 99–108.

(30) Zhao, D.; Liang, X.; Wang, J.; Du, J.; Zhu, Y. Vanillin-Based Degradable Polyurethane Thermosets Demonstrating High Bio-Content and Mechanical Properties. *ACS Appl. Polym. Mater.* **2023**, *5* (6), 4536–4545.

(31) Mahajan, J. S.; Hinton, Z. R.; Nombera Bueno, E.; Epps, T. H.; Korley, L. S. T. J. Lignin-Derivable, Thermoplastic, Non-Isocyanate Polyurethanes with Increased Hydrogen-Bonding Content and Toughness vs. Petroleum-Derived Analogues. *Mater. Adv.* **2024**, *5* (9), 3950–3964.

(32) Saha, P.; Goswami, L.; Kim, B. S. Novel Biobased Non-Isocyanate Polyurethanes from Microbially Produced 7,10-Dihydroxy-8(E)-Octadecenoic Acid for Potential Packaging and Coating Applications. *ACS Sustain. Chem. Eng.* **2022**, *10* (14), 4623–4633.

(33) Tryznowski, M.; Żołek-Tryznowska, Z. Surface Properties of Poly(Hydroxyurethane)s Based on Five-Membered BIS-Cyclic Carbonate of Diglycidyl Ether of Bisphenol A. *Materials (Basel).* **2020**, *13* (22), 1–14.

(34) Fanjul-Mosteirín, N.; Fonseca, L. P.; Dove, A. P.; Sardon, H. Bio-Based Non-Isocyanate Poly(Hydroxy Urethane)s (PHU) Derived from Vanillin and CO2. *Mater. Adv.* **2023**, *4* (11), 2437–2448.

(35) Quienne, B.; Pinaud, J.; Caillol, S. Synthesis of Hydrophobically Modified Ethoxylated Non-Isocyanate Urethanes (HENIURs) and Their Use as Rheology Additives. *Eur. Polym. J.* **2022**, *175* (May), 111384.

(36) Jiang, S.; Liu, L. Novel Carbon Dioxide Based Poly(Hydroxyurethane-Urea)s:

Synthesis and Properties. *Polymer (Guildf).* **2022**, *244* (December 2021).

(37) Van Velthoven, J. L. J.; Gootjes, L.; Van Es, D. S.; Noordover, B. A. J.; Meuldijk, J. Poly(Hydroxy Urethane)s Based on Renewable Diglycerol Dicarbonate. *Eur. Polym. J.* **2015**, *70*, 125–135.

(38) Wang, H. M.; Hsiao, S. H. Electrochemically and Electrochromically Stable Polyimides Bearing Tert-Butyl-Blocked N,N,N′,N′-Tetraphenyl-1,4-Phenylenediamine Units. *Polymer (Guildf).* **2009**, *50* (7), 1692–1699.

(39) Parcheta-Szwindowska, P.; Rohde, K.; Datta, J. Bio-Derived Polyurethanes Obtained by Non-Isocyanate Route Using Polyol-Based Bis(Cyclic Carbonate)s—Studies on Thermal Decomposition Behavior. *J. Therm. Anal. Calorim.* **2022**, *147* (23), 13329–13339.

(40) He, X.; Xu, X.; Wan, Q.; Bo, G.; Yan, Y. Solvent- and Catalyst-Free Synthesis, Hybridization and Characterization of Biobased Nonisocyanate Polyurethane (NIPU). *Polymers (Basel).* **2019**, *11* (6).

(41) Ke, J.; Li, X.; Wang, F.; Jiang, S.; Kang, M.; Wang, J.; Li, Q.; Wang, Z. Non-Isocyanate Polyurethane/Epoxy Hybrid Materials with Different and Controlled Architectures Prepared from a CO2-Sourced Monomer and Epoxy via an Environmentally-Friendly Route. *RSC Adv.* **2017**, *7* (46), 28841–28852.

(42) Beniah, G.; Chen, X.; Uno, B. E.; Liu, K.; Leitsch, E. K.; Jeon, J.; Heath, W. H.; Scheidt, K. A.; Torkelson, J. M. Combined Effects of Carbonate and Soft-Segment Molecular Structures on the Nanophase Separation and Properties of Segmented Polyhydroxyurethane. *Macromolecules* **2017**, *50* (8), 3193–3203.

(43) Schimpf, V.; Max, J. B.; Stolz, B.; Heck, B.; Mülhaupt, R. Semicrystalline Non-Isocyanate Polyhydroxyurethanes as Thermoplastics and Thermoplastic Elastomers and Their Use in 3D Printing by Fused Filament Fabrication. *Macromolecules* **2019**, *52* (1), 320–331.

(44) Wołosz, D.; Fage, A. M.; Parzuchowski, P. G.; Świderska, A.; Brüll, R. Reactive Extrusion Synthesis of Biobased Isocyanate-Free Hydrophobically Modified Ethoxylated Urethanes with Pendant Hydrophobic Groups. *ACS Sustain. Chem. Eng.* **2022**, *10* (35), 11627–11640.

(45) Younes, G. R.; Maric, M. Increasing the Hydrophobicity of Hybrid Poly(Propylene Glycol)-Based Polyhydroxyurethanes by Capping with Hydrophobic Diamine. *Ind. Eng. Chem. Res.* **2021**, *60* (22), 8159–8171.

(46) Appasamy, S.; M, G.; Krishnasamy, B.; Ramachandran, S.; Muthukaruppan, A. Vanillin

Derived Partially Bio-Based Benzoxazine Resins for Hydrophobic Coating and Anticorrosion Applications: Studies on Syntheses and Thermal Behavior. *Polym. Technol. Mater.* **2024**, *63* (3), 287–298.

(47) Xiangjun, W.; Li, X.; Lin, Q.; Xia, J.; Xue, H. A Thermoreversible Crosslinking Hot-Melt Adhesive: Reversibility and Performance. *RSC Adv.* **2021**, *11* (52), 32565–32572.

(48) Kadam, P.; Vaidya, P.; Mhaske, S. Correlation between Rheological and Adhesion Properties of Polyamide Hot Melt Adhesive Synthesized from Dimer Acid (Dilinoleic Acid) and Ethylene Diamine. *Indian J. Adv. Chem. Sci.* **2014**, *2* (2), 124–133.

(49) Younes, G. R.; Marić, M. Bio-Based Thermoplastic Polyhydroxyurethanes Synthesized from the Terpolymerization of a Dicarbonate and Two Diamines: Design, Rheology, and Application in Melt Blending. *Macromolecules* **2021**, *54* (21), 10189–10202.

(50) Sukumaran Nair, A.; Cherian, S.; Balachandran, N.; Panicker, U. G.; Kalamblayil Sankaranarayanan, S. K. Hybrid Poly(Hydroxy Urethane)s: Folded-Sheet Morphology and Thermoreversible Adhesion. *ACS Omega* **2019**, *4* (8), 13042–13051.

(51) Anitha, S.; Vijayalakshmi, K. P.; Unnikrishnan, G.; Kumar, K. S. S. CO2 Derived Hydrogen Bonding Spacer: Enhanced Toughness, Transparency, Elongation and Non-Covalent Interactions in Epoxy-Hydroxyurethane Networks. *J. Mater. Chem. A* **2017**, *5* (46), 24299–24313.

(52) Bao, C.; Yin, Y.; Ding, Y.; Liu, J.; Xu, Y.; Miao, R.; Liu, Z.; Duan, B.; Qin, Y.; Xin, Z. Chemically Recyclable Supramolecular Thermosets toward Strong and Reusable Hot-Melt Adhesives. *Macromolecules* **2023**, *56* (17), 6633–6643.

(53) Platonova, E.; Chechenov, I.; Pavlov, A.; Solodilov, V.; Afanasyev, E.; Shapagin, A.; Polezhaev, A. Thermally Remendable Polyurethane Network Cross-Linked via Reversible Diels–Alder Reaction. *Polymers (Basel).* **2021**, *13* (12), 1–15.

(54) Froidevaux, V.; Borne, M.; Laborbe, E.; Auvergne, R.; Gandini, A.; Boutevin, B. Study of the Diels-Alder and Retro-Diels-Alder Reaction between Furan Derivatives and Maleimide for the Creation of New Materials. *RSC Adv.* **2015**, *5* (47), 37742–37754.

(55) Cuvellier, A.; Verhelle, R.; Brancart, J.; Vanderborght, B.; Van Assche, G.; Rahier, H. The Influence of Stereochemistry on the Reactivity of the Diels-Alder Cycloaddition and the Implications for Reversible Network Polymerization. *Polym. Chem.* **2019**, *10* (4), 473–485.

(56) Gomez-Lopez, A.; Grignard, B.; Calvo, I.; Detrembleur, C.; Sardon, H. Synergetic Effect of Dopamine and Alkoxysilanes in Sustainable Non-Isocyanate Polyurethane Adhesives. *Macromol. Rapid Commun.* **2021**, *42* (3), 1–9.

(57) Gomez-Lopez, A.; Grignard, B.; Calvo, I.; Detrembleur, C.; Sardon, H. Accelerating the Curing of Hybrid Poly(Hydroxy Urethane)-Epoxy Adhesives by the Thiol-Epoxy Chemistry. *ACS Appl. Polym. Mater.* **2022**, *4* (12), 8786–8794.

Chapter 5

Conclusion and Future Outlook

5.1 Conclusion

This thesis, titled "**Design and Synthesis of Poly(HydroxyUrethane) Hot-Melt Adhesives from CO_2 and Bio-Based Monomers**," focuses on developing poly(hydroxyurethane) based adhesives for hot-melt applications by non-isocyanate route from renewable sources. Hot-melt adhesives are a green alternative to traditional adhesives, offering solvent-free application, user-friendly characteristics, and cost efficiency. Polyurethane hot melt adhesives are particularly popular due to their superior bonding, strength, flexibility, and resistance to extreme conditions. Presently, the production of these adhesives relies heavily on toxic precursors and fossil fuels, giving rise to notable safety and environmental concerns.

Therefore, this thesis was devoted to addressing a multitude of challenges, encompassing sustainability, the applicability of non-hazardous and non-volatile compounds, enhanced adhesion, biodegradability, improved performance under extreme conditions, durability, and cost-effectiveness in order to compete with existing commercial materials. To achieve this goal, the thesis is centered on meeting these demands through the design and implementation of highly efficient sustainable formulations in a green approach. This entails the transformation of CO_2 and the utilization of bio-sourced monomers to enhance the performance and broaden the application of the materials by designing sustainable polyurethanes.

In the first working chapter (**Chapter 2**), an exploration of the potential development of PHUs from renewable resources is undertaken. The pursuit of a sustainable PHUs involves the investigation of vanillin utilization due to its environmentally friendly nature, economic viability, sustainability, and industrial-scale production. The initial stage involves the synthesis of a dicarbonate monomer derived from bio-sourced vanillin and CO_2. Subsequently, there is an investigation into the potential utilization of vanillin dicarbonate for the synthesis of PHUs, followed by the optimization of this process. A series of PHUs was synthesized through step-growth polyaddition involving the dicarbonate monomer and six aliphatic diamines with varying chain lengths, resulting in the synthesis of PHUs with renewable carbon content ranging from 33 % to 68 %. Notably, the chemical structure of the diamines was found to exert a pronounced influence on the physico-thermal properties exhibited by the resulting PHUs. To assess their potential application, the adhesion performance of the PHUs was tested on Al-Al and SS-SS substrates using lap shear strength tests. The adhesives showed strength values ranging from 0.0025 to 1.65 MPa for Al and 0.0025 to 2.24 MPa for SS. These observations underscore the potential of utilizing vanillin-based monomers for developing PHU adhesives

with favorable properties, thereby substantiating the sustainability concept outlined in the thesis.

Seeking advancements in sustainability and lap-shear strengths, the potential of integrating rigid and flexible segments in the synthesis of PHU adhesives was investigated (**Chapter 3**). This involved a deliberate design of dicarbonate monomers to enhance adhesion strength, elevate bio-renewable carbon content, and facilitate the degradability of the PHU adhesives. Two biobased cyclic carbonates characterized by high renewable carbon content were synthesized from vanillin and isosorbide. Subsequently, these monomers, in conjunction with Priamine 1074, were utilized to develop a series of PHU-HMAs featuring a bio-renewable carbon content exceeding 88%. The molecular composition of PHUs, significantly influenced their mechanical, thermal, and adhesive properties. Notably, PHUs, containing 40 mol% of the DVS-DC monomer, demonstrated the highest adhesion strength, reaching 6.39 ± 0.39 MPa. This heightened adhesion can be attributed to the synergistic effect of the high density of non-covalent interactions, such as hydrogen bonds and π-π interactions, as well as the ordered arrangement of the cycloaliphatic and spiro-aromatic segments present in PHU3-40, as evidenced by the rheological properties. Further, the PHU-HMAs exhibit remarkable reusability, maintaining consistent strength throughout repeated applications. Moreover, the distinctive rigid spirocyclic acetal molecular architecture of DVS-DC renders it well-suited for facilitating selective acidic hydrolysis and enhancing chemical degradability. Consequently, this feature has facilitated the advancement of sustainable and eco-friendly PHUs.

In the third working chapter (**Chapter 4)**, in addition to the goal of enhancing adhesion and renewable carbon content, we studied the impact of the Diels-Alder network on the adhesive properties of sustainable PHUs. Two biobased dicarbonate monomers were synthesized: one with a pendant furyl group, synthesized from guaiacol and furfural (BGF-PF-DC), and another without the pendant group (BGF-DC), synthesized from vanillin and guaiacol and fully characterized. A series of (PHU-HMAs) containing pendant furyl groups with varying amounts of two dicarbonates (BGF-DC and BGF-PF-DC), in combination with Priamine 1074, were formulated. The resulting polymers exhibited a renewable carbon content (RCC) in the range of 89-90%. Subsequently, it was observed that the thermal and adhesive properties, including T_g, exhibited an increase as the concentration of the monomer with pendant groups (BGF-PF-DC) rose from 0 to 100 mol%. Concurrently, adhesion properties exhibited a similar correlation. The highest adhesion strength was evident in PHU6-PF100, with approximately 9.27 ± 0.20 MPa on aluminum and 9.43 ± 0.82 MPa on stainless steel. These values markedly surpass previously reported adhesion strengths for biobased monomers.

Further post-modification study between the furyl group of PHUs alongside with conventional BMI was explored to evaluate the impact of thermoreversible cross-links on the physical, thermal and adhesive property of PHUs. The dynamicity solely between the BGF-PF-DC and BMI was first studied and proved by different means. The incorporation of BMI into BGF-PF-DC resulted in enhanced thermal properties of the polymer attributed to the formation of a crosslinked network. However, this enhancement was accompanied by a decrease in adhesion strength relative to the reference polymers, likely attributable to the heightened network stiffness. In summary, this study validated the primary thesis objective and introduced an innovative design approach for the development of bio-derived PHU-HMAs, thereby contributing to the advancement of more sustainable and environmentally friendly adhesive materials.



Figure 5.1. *Schematic representation illustrating the chapter-wise (working) improvements in renewable carbon content (RCC) and lap shear strength (LSS) of PHU hot melt adhesives.*

5.2 Future Outlook

The current development represents a significant advancement in the field of biobased reusable PHU hot melt adhesives. However, looking ahead, the polyaddition of cyclic carbonates with amines to produce poly(hydroxy urethane)s emerges as the most compelling alternative to conventional polyurethanes. Nonetheless, the commercialization of PHU-based adhesives faces significant challenges, including slower curing, limited availability of cyclic carbonate

precursors on a large scale, and the irreversibility of thermoset adhesives. In contrast to conventional polyurethanes, which can cure at room temperature, the aminolysis of five-membered cyclic carbonates in PHUs is slow and requires higher curing temperatures (60-120 °C). However, studies show that incorporating reactive groups, such as epoxy or sol-gel systems, or adding nanofillers can enhance curing and improve the final properties of PHUs. Despite improvement in room-temperature curing, the reaction times remain too long, limiting their industrial applications. Future studies should concentrate on using larger seven- or eight-membered carbonates to enhance the curing process that can be polymerized more easily at room temperature. Efficient synthesis and enhanced yield of poly(cyclic carbonate)s are paramount for the development of cost-effective adhesives capable of competing with traditional PUs. The current lack of large-scale manufacturing of poly(cyclic carbonate)s results in reduced cost-effectiveness compared to isocyanates. To encourage practical applications of PHUs, it is imperative to devise optimized synthesis methods capable of yielding a broader spectrum of poly(cyclic carbonate)s. Furthermore, the irreversibility of thermoset PHU adhesives renders them non-recyclable, leading to waste generation. Addressing this limitation requires the integration of dynamic bonding into the polymer backbone to augment reversibility and facilitate repeated use. This aspect remains relatively unexplored in PHU adhesives, warranting future research to concentrate on amalgamating dynamic chemistry, such as the Diels-Alder reaction, with PHU adhesives while optimizing their reversibility. Numerous investigations into PHU adhesives have predominantly relied on petroleum-based precursors. In order to diminish environmental impact and advance sustainable production, the utilization of biobased precursors is imperative. Nonetheless, the current market availability of biobased poly(amine)s is limited. Consequently, many studies resort to the use of bio-derived carbonates, while the poly(amine) comonomers continue to be derived from fossil-based sources. To advance the creation of biobased adhesives with a heightened renewable carbon content, the incorporation of both biobased monomers is indispensable. This underscores the necessity for the expansion of the repertoire of biobased poly(amine)s.

Abstract

Name of the Student: Ghuge Gorakh Hiraman
Registration No.: 10CC19J26028
Faculty of Study: Chemical Sciences
Year of Submission: 2024
AcSIR academic centre/CSIR Lab: CSIR-NCL, Pune
Name of the Supervisor: Dr. S. Kiran

Title of the thesis: Design and Synthesis of Poly(HydroxyUrethane) Hot-Melt Adhesives from CO_2 and Bio-Based Monomers

Polyurethane-based hot melt adhesives are widely employed across diverse industries such as packaging, automotive, bookbinding, footwear, healthcare, and textiles due to their superior adhesion, flexibility, biocompatibility, and resilience in challenging environmental conditions. In fact, the reliance on fossil fuels for production and the use of harmful isocyanates in their manufacturing have prompted the development of eco-friendly polyhydroxyurethane hot melt adhesives (PHU-HMAs) as safer alternatives. In light of heightened environmental consciousness and the imperative to diminish reliance on petroleum-based resources, this thesis is dedicated to the development of isocyanate-free PHU-HMAs derived from renewable sources. This endeavor aims to offer sustainable adhesive solutions, thus contributing to environmental conservation efforts. **Chapter 1** offers a comprehensive overview of adhesives, encompassing the market status of HMAs, alternative methods for producing isocyanate-free PUs, the current state of the art in PHU adhesives, based on available studies in the open literature, and the objectives of the thesis. In **Chapter 2**, the study delves into the design and synthesis of a series of PHU-HMAs via a step-growth polyaddition process involving renewable vanillin-derived dicarbonate and six distinct aliphatic diamines of varying chain lengths. Additionally, the study investigates how the length of the diamine chain impacts the thermo-mechanical and adhesive properties. **Chapter 3** focuses on the development of reusable bio-based PHU-HMAs with improved bio-content, presenting biodegradability and adjustable adhesive properties as a potential substitute for conventional HMAs from nonrenewable resources. This involved the preparation of a series of PHU-HMAs by reacting varying proportions of renewable vanillin and isosorbide carbonates with bio-based Priamine 1074. The study delved into the impact of structural variations on the thermal, mechanical, and adhesive characteristics of the PHUs. **Chapter 4** delineates the successful synthesis of bio-based, high-performance PHU-HMAs incorporating pendant furyl groups, derived from renewable vanillin, guaiacol, and furfural-based dicarbonates. Furthermore, the study investigates the effects of post-modification on the adhesion, physio-mechanical, and thermal properties of the modified PHU-HMAs. **Chapter 5** provides a comprehensive overview of the findings from the preceding chapters and offers an in-depth analysis of the overall outcomes of the thesis. Additionally, it outlines future perspectives pertaining to the field of PHU adhesives

List of Publications

List of Publications Emanating from Ph.D. Work

(1) **Ghuge, G. H.**; Kambikanam, K. V.; Nair, K. S. Evaluation of the Adhesive Properties of Vanillin-Derived Polyhydroxy Urethanes. *J. Appl. Polym. Sci.* **2023**, No. May, 1–11. https://doi.org/10.1002/app.54647.

(2) **Ghuge, G. H.**; Torris, A.; Nair, K. S. Biobased Reusable Nonisocyanate Polyurethane Hot-Melt Adhesives with Potential Chemical Degradability. *ACS Appl. Polym. Mater.* **2024**, *6*, 11180−11192. https://doi.org/10.1021/acsapm.4c01526.

Patents

(1) **Ghuge, G. H.**; Kiran S. N. Bio-Derived Cyclic Bicarbonate Monomers and Isocyanate-Free Poly (Hydroxy Urethane)-Based Hot-Melt Adhesives/Polymers Thereof. (Provisional Application No – 202311042903).

Other Publications

(1) **Ghuge, G. H.**; Niphadkar, P.; Rathod, S.; Bokade, V. V. Effect of Rice Husk Particle Size on ZSM-5 Physico-Chemical Properties for Selective Formation of 1,3,5-Trimethyl-2-Benzylbenzene (Pharmaceutical Intermediate). *ChemistrySelect* **2021**, *6* (6), 1255–1262. https://doi.org/10.1002/slct.202004802.

(2) Karthika, V. K.; **Gorakh, G. H.**; Sonali S. N.; Joseph R.; Nair K. S. Synthesis and Characterization of Non-Invasively Traceable Poly (Ether Urethane)s for Biomedical Applications Synthesis and Characterization of Non-Invasively Traceable Poly (Ether Urethane) s for Biomedical Applications. *Biomed. Phys. Eng. Express* **2023**, 9, 045001. https://doi.org/10.1088/2057-1976/acd05e.

List of Papers with Abstract Presented (Oral/Poster) at National/ International Conferences/Seminars

(1) Poster Presentation at the *National Symposium on Polymer Science and Technology*, organized by Somaiya Vidyavihar University, Mumbai; The Society for Polymer Science, India – Mumbai; Department of Polymer Science, S K Somaiya College K J Somaiya College of Engineering, Somaiya Vidyavihar University, Ghatkopar East, Mumbai – 400077, MH, India, during 6-7th May, 2022.

Title: Isocyanate-Free Poly(hydroxyurethane)s from Vanillin-CO_2 derived Cyclic Carbonates.

Abstract: Polyurethanes are an important class of polymers that finds numerous applications in various sectors. The synthesis of these polymers entirely depends on fossil fuel and involves using hazardous chemicals such as isocyanates. Herein, we report the synthesis of a series of polyhydroxyurethane (PHUs) via the polymerization of fully renewable cyclic dicarbonates derived from biomass and CO_2 with a series of diamine compounds. Kinetics of polymerization was studied and the chemical structure of synthesized cyclic dicarbonate and PHUs was confirmed by FTIR and NMR spectroscopy (1H, 13C). Further, the molecular weights of the developed system were determined by gel permeation chromatography (GPC), and we have observed the highest molecular weight of Mn is 5500 g/mol. Moreover, the thermal properties of PHUs were analyzed by differential scanning calorimeter (DSC) and thermogravimetric analysis (TGA) and found out all PHUs are thermally stable above 210 °C. The current methodology, avoiding toxic reagents and using renewable resources from biomass and CO_2, makes this approach an attractive and greener pathway to developing PHUs networks.

(2) Oral Presentation by Virtual Mode at the *International Conference on Novel Swings in Chemical Sciences (NSCS-2022),* organized by the Thakur College of Science and College, Thakur Village, Kandivali (East), Mumbai - 400101, MH, India, on 23th December, 2022.

Title: Isocyanate-Free Poly(hydroxyurethane)s from Vanillin-CO_2 derived Cyclic Carbonates.

Abstract: Polyurethanes are an important class of polymers that finds numerous applications in various sectors. The synthesis of these polymers entirely depends on fossil fuel and involves using hazardous chemicals such as isocyanates. Herein, we report the synthesis of a series of polyhydroxyurethane (PHUs) via the polymerization of fully renewable cyclic dicarbonates derived from biomass and CO_2 with a series of diamine compounds. Kinetics of polymerization was studied and the chemical structure of synthesized cyclic dicarbonate and PHUs was confirmed by FTIR and NMR spectroscopy (^{1}H, ^{13}C). Further, the molecular weights of the developed system were determined by gel permeation chromatography (GPC), and we have observed the highest molecular weight of Mn is 5500 g/mol. Moreover, the thermal properties of PHUs were analyzed by differential scanning calorimeter (DSC) and thermogravimetric analysis (TGA) and found out all PHUs are thermally stable above 210 °C. The current methodology, avoiding toxic reagents and using renewable resources from biomass and CO_2, makes this approach an attractive and greener pathway to developing PHUs networks.

(3) Oral Presentation at the *17th International Conference on Polymer Science and Technology (SPSI-MACRO-2023),* organized by the Department of Chemical Engineering, Indian Institute of Technology Guwahati, Guwahati - 781039, Assam, India, during 10-13th December, 2023.

Title: Isocyanate-Free Poly(hydroxyurethane)s from Vanillin-CO_2 derived Cyclic Carbonates.

Abstract: Polyurethanes are an important class of polymers that finds numerous applications in various sectors. The synthesis of these polymers entirely depends on fossil fuel and involves using hazardous chemicals such as isocyanates. Herein, we report the synthesis of a series of polyhydroxyurethane (PHUs) via the polymerization of fully renewable cyclic dicarbonates derived from biomass and CO_2 with a series of diamine compounds. Kinetics of polymerization was studied and the chemical structure of synthesized cyclic dicarbonate and PHUs was confirmed by FTIR and NMR spectroscopy (^1H, ^{13}C). Further, the molecular weights of the developed system were determined by gel permeation chromatography (GPC), and we have observed the highest molecular weight of Mn is 5500 g/mol. Moreover, the thermal properties of PHUs were analyzed by differential scanning calorimeter (DSC) and thermogravimetric analysis (TGA) and found out all PHUs are thermally stable above 210 °C. The current methodology, avoiding toxic reagents and using renewable resources from biomass and CO_2, makes this approach an attractive and greener pathway to developing PHUs networks.

(4) Poster Presentation at the *NCL-RF Student Annual Conference* at organized by CSIR-National Chemical Laboratory, Pune - 411008 (November 2022).

Title: Isocyanate-Free Poly(hydroxyurethane)s from Vanillin-CO_2 derived Cyclic Carbonates.

Abstract: Polyurethanes are an important class of polymers that finds numerous applications in various sectors. The synthesis of these polymers entirely depends on fossil fuel and involves using hazardous chemicals such as isocyanates. Herein, we report the synthesis of a series of polyhydroxyurethane (PHUs) via the polymerization of fully renewable cyclic dicarbonates derived from biomass and CO_2 with a series of diamine compounds. Kinetics of polymerization was studied and the chemical structure of synthesized cyclic dicarbonate and PHUs was confirmed by FTIR and NMR spectroscopy (^1H, ^{13}C). Further, the molecular weights of the developed system were determined by gel permeation chromatography (GPC), and we have observed the highest molecular weight of M_n is 5500 g/mol. Moreover, the thermal properties of PHUs were analyzed by differential scanning calorimeter (DSC) and thermogravimetric analysis (TGA) and found out all PHUs are thermally stable above 210 °C. The current

methodology, avoiding toxic reagents and using renewable resources from biomass and CO_2, makes this approach an attractive and greener pathway to developing PHU network.

Check for updates

Received: 27 May 2023 | Revised: 17 August 2023 | Accepted: 20 August 2023

DOI: 10.1002/app.54647

RESEARCH ARTICLE

Applied Polymer SCIENCE WILEY

Evaluation of the adhesive properties of vanillin-derived polyhydroxy urethanes

Gorakh Hiraman Ghuge[1,2] | **Karthika Vayalachery Kambikanam**[1] | **Kiran Sukumaran Nair**[1,2]

[1]Polymer Science and Engineering Division, CSIR-National Chemical Laboratory, Pune, India

[2]Academy of Scientific and Innovative Research (AcSIR), Ghaziabad, India

Correspondence
Kiran Sukumaran Nair, Polymer Science and Engineering Division, CSIR-National Chemical Laboratory, Dr. Homi Bhabha Road, Pune, Maharashtra 411008, India.
Email: s.kiran@ncl.res.in

Funding information
CSIR Council of Scientific & Industrial Research (CSIR), New Delhi for the senior research fellowship (SRF), Grant/Award Number: (31/011[1116]/2019-EMR-1); SERB, SERB for the research grant under SRG Scheme, Grant/Award Number: SRG/2020/000954

Abstract

Poly(hydroxy urethanes) (PHUs) have been considered attractive and safer variants of conventional polyurethanes (PUs). To improve the prerequisites of green and sustainable chemistry herein, we propose the synthesis and utilization of cyclic carbonate monomers majorly derived from vanillin, a lignin derivative, and CO_2 for the development of PHUs. Kinetic evaluation on the polymerization temperature ascertained 80°C as the optimum condition for PHU synthesis. The structural evaluation of PHUs was carried out by various spectroscopic techniques, such as FTIR, ^{1}HNMR, and ^{13}C-NMR, molar masses were determined by gel permeation chromatography (Mn varied between 2500 and 11,100 g/mol), and thermal properties evaluated by differential scanning calorimeter (T_g in the ranges of 28–42°C), and thermogravimetric analysis (stable above 180°C). Since the PHUs are enriched with pendant hydroxyl groups on their backbone which can promote adhesion, lap shear studies on the aluminum substrate exhibited a maximum shear strength of 1.65 ± 0.37 MPa. This study demonstrates an attractive and environment-friendly pathway for developing novel PHUs network using renewable biobased resources and further explores its applicability as adhesives.

KEYWORDS

adhesive, biobased cyclic dicarbonate, diamines, poly(hydroxyurethane)s, vanillin

1 | INTRODUCTION

Synthetic polymers have occupied almost every extent of modern life, and their use and production are increasing exponentially and are expected to exceed 500 million metric tons by 2050.[1] Among them, polyurethanes (PUs) have found numerous applications in various sectors (transportation, health, construction, etc.).[2–5] It is also ranked as the sixth most-produced polymer globally, with a market size of about USD 81.3 billion in 2022.[6] However, the precursors for their synthesis depend on fossil fuels and involve using hazardous chemicals.[7] Since PUs are extensively used in various sectors, it would be highly advantageous if these polymeric materials could be developed from renewable biomass and by using non-toxic precursors. Intensive studies in this area have aided in the development of alternate methods such as (a) copolymerization of aziridines with carbon dioxide,[8] (b) rearrangement of acyl azide followed by its polycondensation with alcohol,[8] (c) transurethanization reaction between a bis-carbamate and a diol,[9] and (d) polyaddition between cyclic carbonates and amines,[10,11] for the development of PUs. The latter method, the polyaddition between cyclic carbonates and amines, is considered as one of the most studied and promising routes for developing poly(hydroxy urethane)s (PHUs) since it involves the

 © 2023 Wiley Periodicals LLC.

usage of much safer precursors. However, the structure of PHUs differs from conventional PUs due to the presence of both primary and secondary hydroxyl groups in the main chain of polymers providing additional benefits such as post-functionalization, improved hydrogen bonding, enhanced adhesion forces,[12–14] and miscibility between phases.[15,16] Furthermore, PHUs designed from bis-5-membered cyclic carbonates are considered more viable than PHUs developed from higher cyclic carbonates since it bypasses toxic precursors making the process safer and further involve the utilization of renewable and sustainable resources such as CO_2 as feedstock.[17,18]

However, in most current studies on the development of PHUs, the molecules for cyclic carbonate synthesis mainly depended on fossil fuel. It will be highly feasible if CO_2 can be coupled to molecules derived from renewable biomass since it can improve the sustainability and aid in developing polymers with a low carbon footprint compared to traditional routes. Vanillin is one such molecule derived from lignin, which is of great interest because of its bioactivity and can represent an inexhaustible resource of monomers for developing sustainable polymers.[19,20] Despite the ease in the availability of vanillin, there are hardly very few reports concerning its utilization in developing PHU.[21,22] Furthermore, the applicability of these polymers as adhesives is yet to be explored.

Herein, we elaborate on the potential of bio-renewable vanillin as a dicarbonate precursor for synthesizing novel thermoplastic PHUs suitable for adhesive application. First, a vanillin-derived dicarbonate was developed and further optimization of polymerization conditions based on molecular weights was carried out. We then prepared a series of PHUs via step-growth polyaddition reaction between dicarbonate monomer with six aliphatic diamines of various chain lengths, and their effect on thermo-mechanical properties has been investigated. Finally, adhesion studies were performed to evaluate the application potential of the above synthesized PHUs.

2 | MATERIALS AND METHODS

2.1 | Materials

Vanillin (>98%), tetrabutylammonium bromide (TBAB, >98%), ethylenediamine (anhydrous, >98%), 1,10-diamino decane (>97%), and 1,5,7-triazabicyclo-[4.4.0] dec-5-ene (TBD, >98%) was purchased from the TCI Chemicals, India. Sodium percarbonate (13%–14% active oxygen, $Na_2CO_3.1.5H_2O_2$) was provided by the Alfa Aesar. Epichlorohydrin (≥99%) and hexamethylene diamine (98%) were procured from Sigma Aldrich. Sodium hydroxide pellets (NaOH, 98%), hydrochloric acid (HCl, 35%–38%), ethyl acetate, and petroleum ether were supplied from the S D fine chemical. Sodium sulfate (anhydrous, ≥99.5%, AR) was delivered by Leonid chemicals. Dimethyl sulfoxide (DMSO-d_6, 99.80% D) and chloroform (99.80% D) were purchased from Eurisotop. CO_2 gas cylinder (99.5%) was obtained from the Vadilal chemical. 1, 8-Diaminooctane (98%) and 1, 12-diaminododecane (99%) were received from the Chempure. 1, 4-Diaminobutane (99%), and isopropanol (99.5%) was procured from SRL chemicals. N-Methyl pyrrolidinone (NMP), and dimethylformamide (DMF) were distilled over CaH_2 under a nitrogen atmosphere and stored over molecular sieves (4 Å). All chemicals were used as received unless specified.

2.2 | Methods

2.2.1 | Characterization

The chemical structure of the molecules was determined by ^1H and ^{13}C NMR spectroscopy using a Bruker Advance 500 MHz spectrometer equipped with a QNP z-gradient probe at room temperature. The infrared spectra (IR) were recorded on Bruker alpha Fourier transform infrared spectroscopy (FTIR) spectrometer, where 48 scans were recorded in a frequency range of 4000–500 cm^{-1} at a resolution of 4 cm^{-1}. The high-resolution mass spectrometer (ThermoFisher Scientific) was used to detect the molecular weight of compounds and the data was acquired from a hybrid Quadrapole Q-Exactive orbitrap fitted with an ACCELA PDA detector. Gel permeation chromatography was employed to analyze the molecular weight of PHUs using viscotek GPC max (VE 2001) with a refractive index as a detector. The measurements were done in DMF (DMF plus lithium bromide 1gL^{-1}) as an eluent at 1 mL/min. and using the DT6000M column at 50°C. Molecular weights were estimated relative to polymethyl methacrylate standards. The glass transition temperature (T_g) was analyzed on a DSC-Q10 system from TA instruments. For each sample, two cycles were performed in the range between −70 and 150°C at 10°C/min under a nitrogen atmosphere. The T_g was determined from a second heating cycle. Thermogravimetric studies were performed using a TGA-STA 6000 (Perkin Elmer) at a heating rate of 10°C/min from 50°C to 900°C under a nitrogen atmosphere. The adhesive properties of synthesized PHUs were investigated at room temperature using an Instron 5943 with a displacement rate of 1 mm.min^{-1}. The lap shear test was performed on aluminum substrates having dimensions of 54 mm × 20 mm × 1.55 mm (L*W*T). Aluminum plates were repeatedly washed three to four times using a 50:50

10974628, 2023, 45, Downloaded from https://onlinelibrary.wiley.com/doi/10.1002/app.54647 by Csir-National Chemical, Wiley Online Library on [22/12/2024]. See the Terms and Conditions (https://onlinelibrary.wiley.com/terms-and-conditions) on Wiley Online Library for rules of use; OA articles are governed by the applicable Creative Commons License

combination of acetone and isopropanol, followed by water, and then dried in an oven before using it for adhesion studies. 200 mg of polymer materials were applied on the substrate surface by maintaining the adhesive contact area of 300 mm^2 (20 mm × 15 mm). Further, the adhesive specimen was prepared by melting PHU-2, PHU-3, and PHU-6 at 80°C, while the PHU-4, and PHU-5 at 120°C for 30 min and to enhance the wetting and shaping of adhesive with the substrate 250 g weight were placed on the aluminum substarate during the bonding process. The measurements of each sample were repeated at least five times. The type of failure was also reported after the test on the basis of visual inspection. The lap shear strength was determined by the following formula,

$$\tau = F/A,$$

where:

τ = lap-shear strength ($N.mm^{-2}$ or MPa), F = maximum shear force (N), and A = contact area of the adhesive joints (300 mm^2).

2.2.2 | Synthesis of vanillin-CO_2 derived cyclic dicarbonate

Synthesis of 2-methoxybenzene-1,4-diol

Vanillin (30 g, 0.197 mol) was dissolved in tetrahydrofuran (THF) (220 mL) to this, deionized water (80 mL) was added followed by the addition of sodium percarbonate ($Na_2CO_3.1.5H_2O_2$, 46.43 g, 0.295 mol). The reaction was continuously stirred for another 24 h at room temperature under N_2 atmosphere, followed by quenching the reaction mixture by adding HCl solution (0.1 mol L^{-1}, maintained pH = 3), and the THF was distilled off on a rotary evaporator at 40°C. The above attained crude product was extracted with ethyl acetate, dried over anhydrous Na_2SO_4, and concentrated. Further purified by column chromatography using ethyl acetate and petroleum ether to give a brown-colored powder of 2-methoxybenzene-1,4-diol (MBD) (23 g, yield: 83%; m.p. 88°C).

^{1}H-NMR (500 MHz, DMSO-d_6, δ): 3.69 (s, 3H, OCH_3), 6.16 (dd, 1H, Ar-H), 6.36 (d, 1H, Ar-H), 6.54 (dd, 1H, Ar-H), 8.12 (s, 1H, Ar-OH), 8.72 (s, 1H, Ar-OH).

FTIR (ATR) cm^{-1}: 3366 (OH), 2819–2995 (CH stretches), 1612 (C═C), 1510 (C—O).

HRMS (ESI) *m/z*: $[M + H]^+$ calculated for $C_7H_8O_3$: 140.0473; found: 140.0468 (Figure S7).

Synthesis of 2,2′-(((2-methoxy-1,4-phenylene)bis(oxy))bis (methylene))bis(oxirane)

In a typical synthesis, MBD (20 g, 0.143 mol.), and TBAB (2.65 g, 0.014 mol.) was initially charged into a round bottom flask followed by the addition of epichlorohydrin (145 g, 1.57 mol), and the reaction mixture was stirred for 4 h at 80°C under inert conditions. The reaction medium was further allowed to cool down to room temperature followed by the dropwise addition of aqueous NaOH (22.84 g, 0.570 mol.). The reaction was further continued for another 2 h at 16°C followed by the removal of excess epichlorohydrin by vacuum distillation. The product thus obtained was extracted with ethyl acetate and the crude product was further purified by column chromatography, using petroleum ether and ethyl acetate as eluent to give glycidated-MBD (DGE) (32 g, yield: 88%, m.p. 87°C).

^{1}H-NMR (500 MHz, $CDCl_3$, δ): 2.75 (dd, 2H, CH_2-epoxy), 2.90 (dd, 2H, CH_2-epoxy), 3.34 (m, 2H, CH-epoxy), 3.84 (s, 3H, OCH_3), 3.95 (qq, 2H, CH_2—O), 4.20 (qq, 2H, CH_2—O), 6.39 (dd, 1H, Ar-H), 6.56 (s, 1H, Ar-H), 6.86 (dd, 1H, Ar-H).

FTIR (ATR) cm^{-1}: 2819–2995 (CH stretches), 1612 (C═C), 1510 (C—O), 860, 912 (C—O, epoxy ring).

HRMS (ESI) *m/z*: $[M + H]^+$ calculated for $C_{13}H_{16}O_5$: calculated: 253.0998; found: 253.1071 (Figure S8).

Synthesis of 4,4′-(((2-methoxy-1,4-phenylene)bis(oxy))bis (methylene))bis(1,3-dioxolan-2-one)

A solution of DGE compound (10 g, 0.039 mol), and TBAB (5 mol%) in DMF (40 mL) was prepared and added to a 100 mL autoclave. The reactor was filled with carbon dioxide gas, and the reaction was conducted at 100°C for 24 h. Thus, obtained reaction mixture was collected and precipitated in cold water. The crude product was then dried on anhydrous Na_2SO_4, purified by column chromatography, and recrystallized in isopropanol to obtain carbonated-DGE (DC) (9.71 g, yield: 82%, mp.: 110–112°C).

^{1}H-NMR (500 MHz, $CDCl_3$, δ): 3.76 (s, 3H, OCH_3), 4.17 (m, 4H, carbonate CH_2), 4.40 (dd, 2H, CH_2), 4.61 (dd, 2H, CH_2), 5.13 (m, 2H, carbonate CH), 6.46 (dd, 1H, Ar-H), 6.63 (s, 1H, Ar-H), 6.92 (dd, 1H, Ar-H).

FTIR (ATR) cm^{-1}: 2819–2995 (CH stretches), 1787 (C═O, cyclic carbonate), 1612 (C═C), 1510 (symmetric, C—O stretch).

HRMS (ESI) *m/z*: $[M + H]^+$ calculated for $C_{15}H_{16}O_9$: 341.0794; found: 341.0867 (Figure S9).

2.2.3 | Synthesis of PHUs series

Cyclic dicarbonate (1 eq.) was mixed with respective diamines (1 eq.), followed by the addition of 1,5,7-Triazabicyclo-[4.4.0]-dec-5-ene (10 mol%). Next, the freshly distilled N-methyl-2-pyrrolidinone (5 mL/1 g) was added, and the polyaddition reaction was carried out at

10974628, 2023, 45, Downloaded from https://onlinelibrary.wiley.com/doi/10.1002/app.54647 by Csir-National Chemical, Wiley Online Library on [22/12/2024]. See the Terms and Conditions (https://onlinelibrary.wiley.com/terms-and-conditions) on Wiley Online Library for rules of use; OA articles are governed by the applicable Creative Commons License

Code	Diamine used	SEC			^{1}H NMR	
		M_n (g/Mol)	M_w (g/Mol)	PDI	$R_{P/S}$[a]	$R_{P/S}$[b]
PHU-1	1,2-diamino ethane	2500	2600	1.03	–	–
PHU-2	1,4-diamino butane	4000	8100	2.03	28/72	25/75
PHU-3	1,6-diamino hexane	4900	8800	1.77	19/81	24/76
PHU-4	1,8-diamino octane	11,100	23,200	2.08	22/78	24/76
PHU-5	1,10-diamino decane	6000	9100	1.50	19/81	24/76
PHU-6	1,12-diamino dodecane	5000	7600	1.50	22/78	25/74

[a]Calculated from the primary and secondary hydroxyl group signals.
[b]Calculated from the urethane signals.

TABLE 1 Experimental data from SEC, and ^{1}H NMR

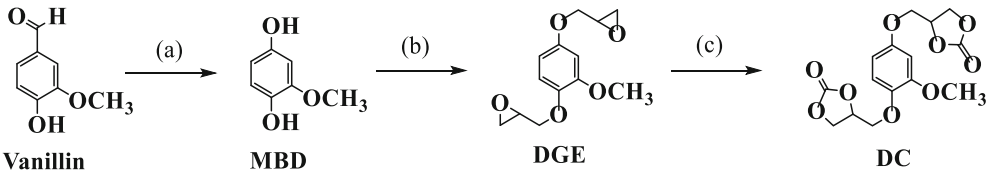

SCHEME 1 Syntheses of bicyclic dicarbonate from vanillin and CO_2 source.

80°C for 24 h under an inert atmosphere.[10] The obtained polymers were then further purified by precipitation in diethyl ether. The nomenclature of the obtained polymers is depicted in Table 1.

3 | RESULT AND DISCUSSION

3.1 | Synthesis and characterization of vanillin-CO_2 derived cyclic dicarbonate

The preparation of cyclic dicarbonate was carried out in three stages with an overall yield of 59.77% (Scheme 1).[21] The first stage is the Dakin reaction, which leads to the product MBD with one carbon loss in the presence of sodium percarbonate as an oxidizing agent. NMR (^{1}H, ^{13}C) and FTIR spectroscopy were used to validate their structure. As anticipated, the FTIR spectrum (Figure S1) of MBD showed a broad peak at 3366 cm^{-1}, which is attributed to the aromatic hydroxyl groups, while the peak at 1668 cm^{-1}, has completely disappeared, which was the characteristic peak of the aldehyde functionality.[23] In ^{1}H NMR spectra (Figure S2), signals were observed at 8.14 ppm and 8.74 ppm, corresponding to the two hydroxyl protons, and the protons attributed to the aldehyde function disappeared at 9.83 ppm.[24] MBD thus obtained was then glycidylated in the second step using epichlorohydrin as a reagent and TBAB as a phase transfer catalyst. The NMR spectra of glycidated-MBD (DGE) (Figure S3) exhibited new signals in the area of 2.73 ppm and 4.18 ppm, which corresponds to the epoxy ring, and signals corresponding to hydroxyl groups at 8.14 ppm and 8.74 ppm disappeared,[25,26] revealing that the complete conversion of hydroxyl groups into glycidyl rings. The FTIR analyses also validated the formation of DGE (Figure S1), where the characteristic absorption peak of hydroxyl groups vanished at 3366 cm^{-1}, and the distinct absorption peak of the epoxy rings appeared at 912 and 860 cm^{-1}.[26–28] In the final step, DGE was converted into its cyclic carbonate (DC) by TBAB-catalyzed CO_2 insertion reaction. The chemical structure of DC was analyzed by FTIR (Figure S1) and NMR (^{1}H, ^{13}C) spectroscopy (Figure 1, Figure S6). FTIR and ^{13}C analysis indicated the presence of a new absorbance band at 1782 cm^{-1} and 155.35 ppm, respectively, attributed to the C═O of five-membered cyclic carbonate rings.[29,30] Moreover, the evaluation of ^{1}H NMR spectra of DC confirmed the formation of cyclic carbonates where the signal associated with protons of the cyclic carbonate appeared in the region of 4.10 ppm to 5.15 ppm. Further, the disappearance of epoxide signals from 2.73 to 4.18 ppm range was noted, indicating the oxirane ring has transformed into carbonate rings.[29–31] In addition, it has been observed that the peaks associated with the protons of the carbonate ring shifted toward the high field in comparison to the epoxide protons, this is probably due to the electron-withdrawing effect of the carbonyl group (C═O) (Figure 1) indicative of the formation of pure DC product.[32]

3.2 | Optimisation of polymerization conditions

To optimize the polymerization conditions, we performed a series of polyaddition reactions between cyclic

10974628, 2023, 45, Downloaded from https://onlinelibrary.wiley.com/doi/10.1002/app.54647 by Csir-National Chemical, Wiley Online Library on [22/12/2024]. See the Terms and Conditions (https://onlinelibrary.wiley.com/terms-and-conditions) on Wiley Online Library for rules of use; OA articles are governed by the applicable Creative Commons License

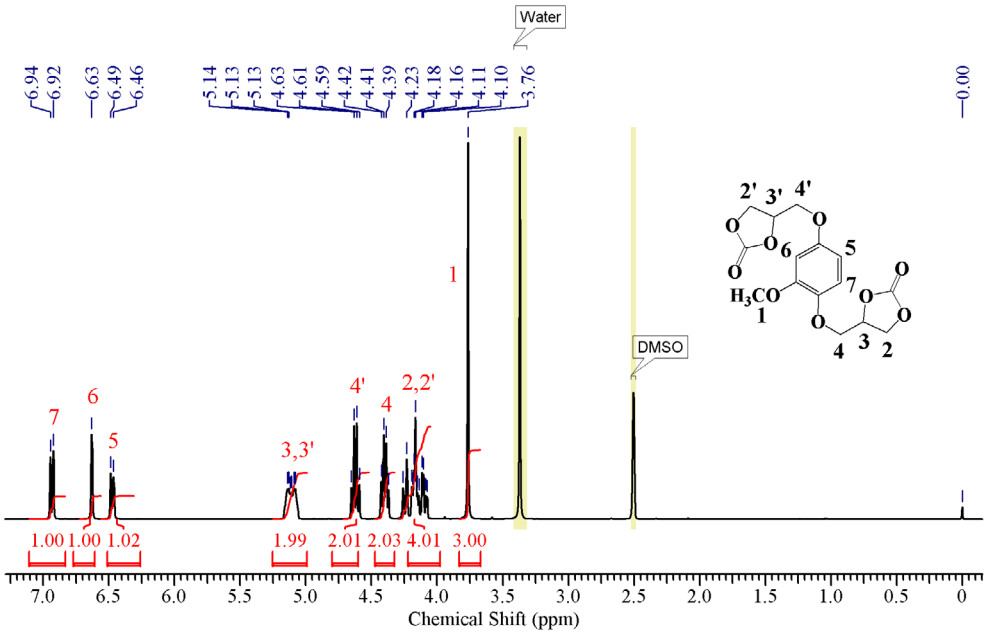

FIGURE 1 ^{1}H NMR spectrum of DC. [Color figure can be viewed at wileyonlinelibrary.com]

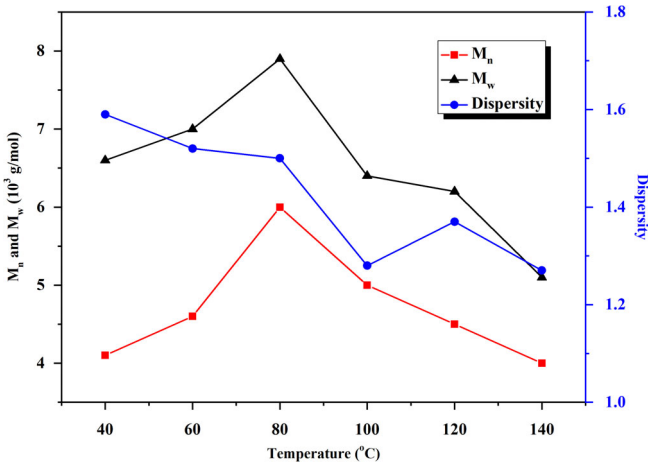

FIGURE 2 Molecular weight distribution of poly(hydroxy urethanes) (PHUs) synthesized at different temperatures. [Color figure can be viewed at wileyonlinelibrary.com]

dicarbonate and 1,10-decane diamine at different temperatures from 40°C to 140°C, and their molecular weight was analyzed by gel permeation chromatography (Table S1, Figure 2 and Figure S10). The molecular weight of PHUs was intially found to increase with a rise in reaction temperature and a maximum molecular weight was attained at 80°C (6000 g/mol). The molecular weight increase can be associated with the increased reactivity of cyclic dicarbonate with temperatures.[33] Further, the molecular weight of PHUs was found to decrease as the reaction temperature was raised above 80°C.[13] ^{1}HNMR evaluation of PHUs synthesized at higher temperatures stated the presence of an additional peak at 5.71 ppm (Figure 3) indicative of urea formation.[11,13] The occurrence of these side reactions could be the probable reason for the reduction in molecular weights of PHUs at higher temperatures. Therefore, the preferred condition for the polyaddition reaction between DC and diamine was chosen as 80°C.[34]

3.3 | Synthesis and characterization of PHUs

3.3.1 | Spectral analysis of PHUs

PHUs were synthesized by reacting DC with a series of different chain length diamines, as shown in Scheme 2 and Table 1. The chemical structure of developed PHUs has been evaluated by FTIR and NMR (^{13}C, ^{1}H) spectroscopy. FTIR spectrum (Figure 4b.) indicated the existence of signals at 1703 cm^{-1} and 1468 cm^{-1}, which correlates to the C═O stretching and N—H bending of urethane linkages, respectively, while the broad signal at 3375 cm^{-1}, relates to the —OH and —NH stretch.[31] Moreover, the lack of the absorption band of the carbonyl of the carbonate group at 1787 cm^{-1} reveals the conversion of DC monomer, indicating the formation of PHUs. The ^{1}H NMR spectra of synthesized materials are displayed in Figure S11–S16, confirming the successful synthesis of PHUs. The formation of urethane bonds (N—H signal) by ring-opening polymerization of cyclic dicarbonate and amine was confirmed by the appearance of signals between 7.10 and 7.21 ppm.[29,31] In fact, the ring opening of cyclic dicarbonates often occurs in two pathways giving two signals, due to the formation of both primary and secondary hydroxyl groups.[35,36] The ratio of the primary to secondary hydroxyl

10974628, 2023, 45, Downloaded from https://onlinelibrary.wiley.com/doi/10.1002/app.54647 by Csir-National Chemical, Wiley Online Library on [22/12/2024]. See the Terms and Conditions (https://onlinelibrary.wiley.com/terms-and-conditions) on Wiley Online Library for rules of use; OA articles are governed by the applicable Creative Commons License

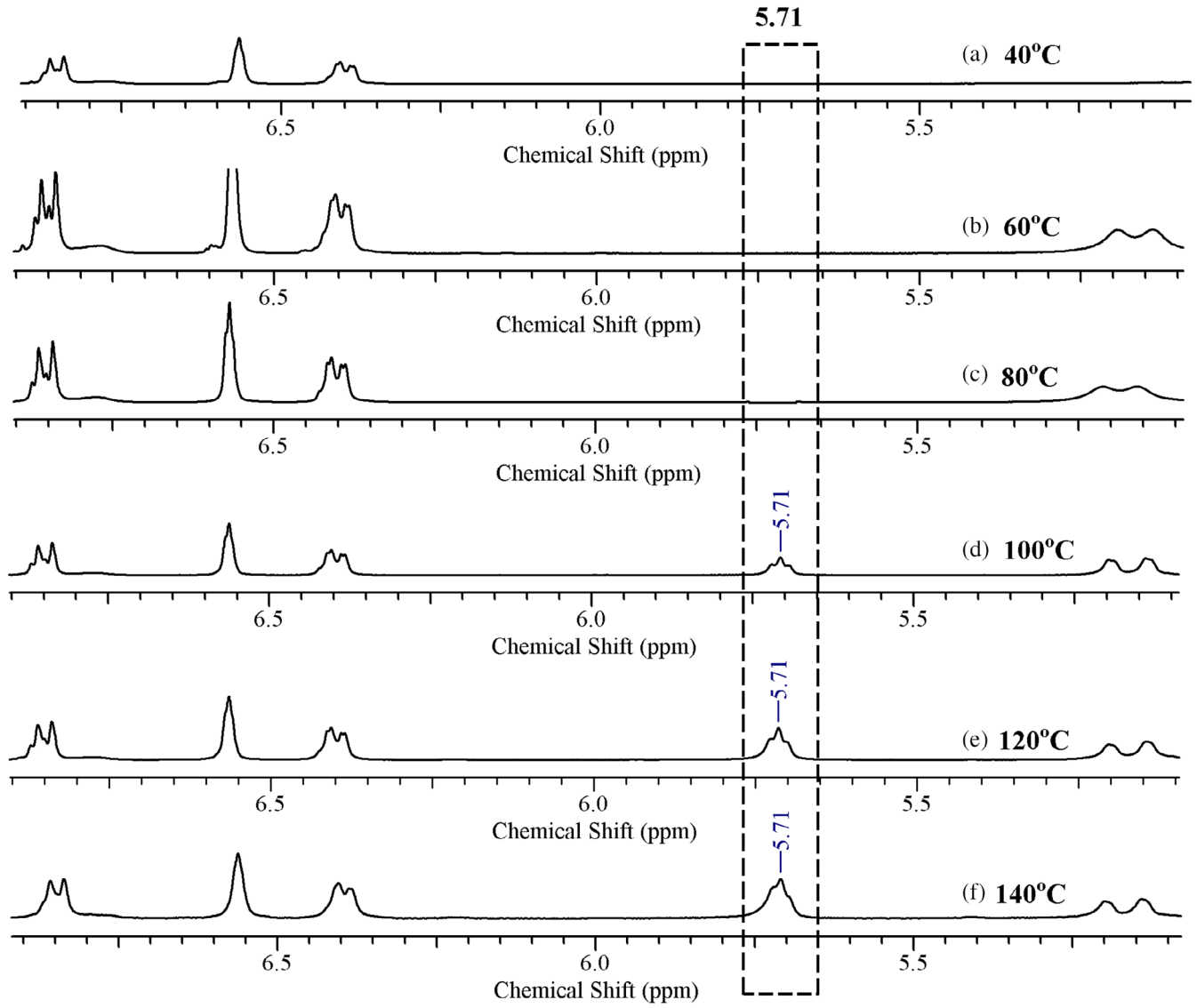

FIGURE 3 ^{1}H NMR spectrum of poly(hydroxy urethanes) (PHUs) developed at different temperatures. [Color figure can be viewed at wileyonlinelibrary.com]

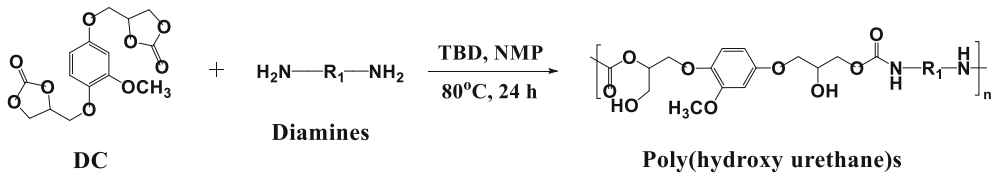

DC

Diamines

Poly(hydroxy urethane)s

R_1= -$(CH_2)_2$- , -$(CH_2)_4$- , -$(CH_2)_6$- , -$(CH_2)_8$- , -$(CH_2)_{10}$- , -$(CH_2)_{12}$-

SCHEME 2 Syntheses of bio-based poly(hydroxy urethanes) (PHUs) from vanillin-derived dicarbonate and diamines of different chain lengths.

groups ($R_{P/S}$) has been calculated from the ^{1}H NMR by integrating the protons of the urethane —NH (i.e., $R_{P/S}$ for PHU-2 obtained 0.32/0.98 = 25/75, Figure S12), and also by integrating the hydroxyl signal at 4.35–4.92 ppm and at 4.86–5.20 ppm (i.e., $R_{I/II}$ for PHU-2 obtained 0.41/1.06 = 28/72, Figure S12). The determined values of ratios from both signals are included in Table 1. The results indicate that PHUs are equipped with more secondary hydroxyl groups than primary ones. This can be attributed to the presence of electron-withdrawing groups such as $PhOCH_2$, which favors the better transition and stabilization of the secondary hydroxyl group during the polymerization hence favoring the formation of a higher number of secondary hydroxyl groups.[32]

10974628, 2023, 45, Downloaded from https://onlinelibrary.wiley.com/doi/10.1002/app.54647 by Csir-National Chemical, Wiley Online Library on [22/12/2024]. See the Terms and Conditions (https://onlinelibrary.wiley.com/terms-and-conditions) on Wiley Online Library for rules of use; OA articles are governed by the applicable Creative Commons License

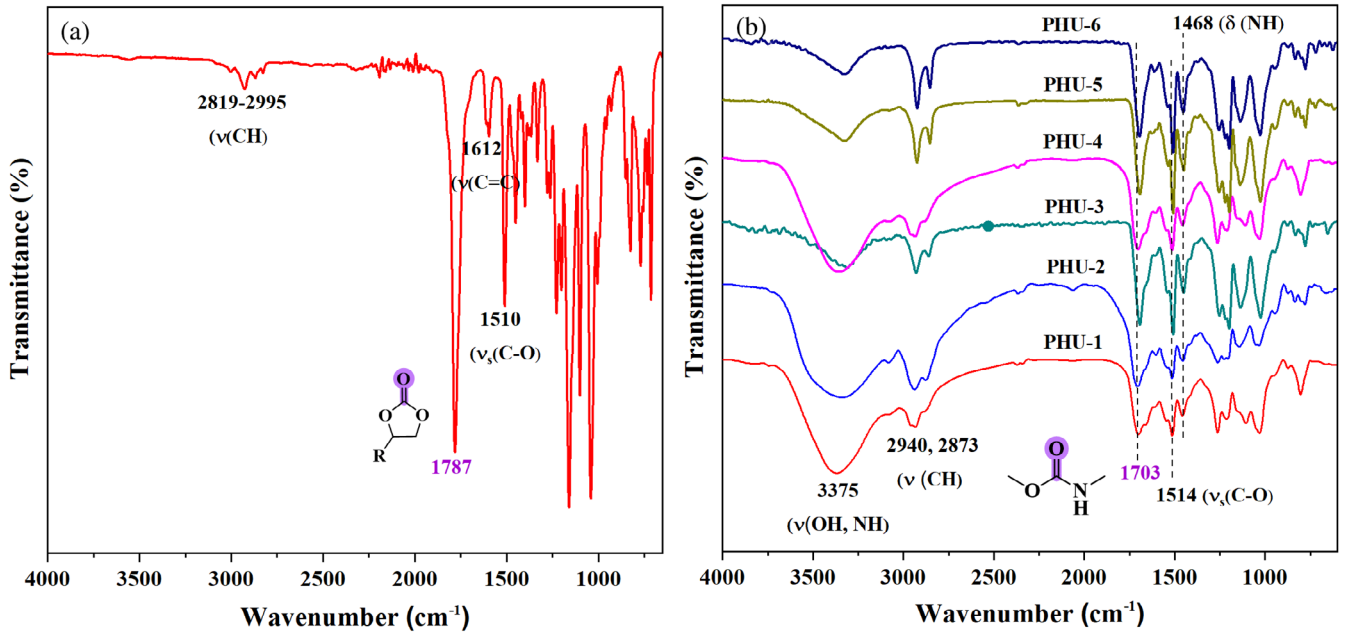

FIGURE 4 FTIR spectrum of (a) DC (b) poly(hydroxy urethanes) (PHUs). [Color figure can be viewed at wileyonlinelibrary.com]

Furthermore, the aliphatic hydrocarbons (diamine precursors) in PHUs (except for PHU-1) displayed the two types of protons in the ^{1}H NMR spectra, where the alpha protons to the urethane —NH were observed at 2.95 ppm while the remaining protons of the aliphatic hydrocarbons appeared in the area of 1.22–1.38 ppm.[29,37] However, in the case of PHU-1, only one signal appeared around 2.95 ppm from the alpha protons adjacent to the urethane —NH.[29,37] Moreover, the NMR signals for the protons related to the opening of the five-membered cyclic carbonate were observed at 3.57–4.87 ppm.[29] The ^{13}C NMR spectra are presented in Figure S17–S22. It revealed the existence of urethane functionality in all PHUs by showing the signal of carbonyl carbon at 156.6 ppm.[37] Both ^{1}H NMR and ^{13}C NMR results confirm the formation of PHU of the desired structure.

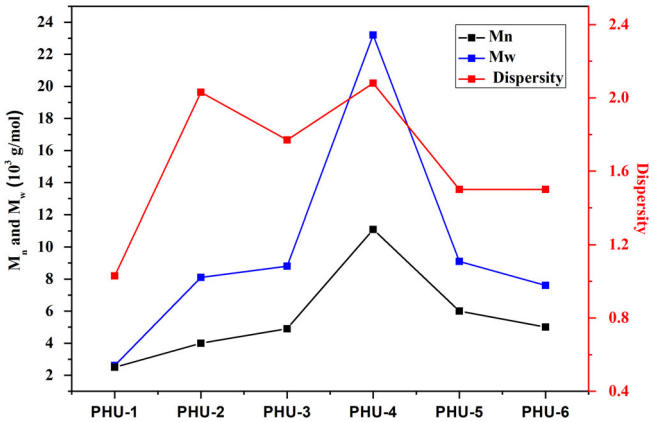

FIGURE 5 Molecular weight distribution of poly(hydroxy urethanes) (PHUs). [Color figure can be viewed at wileyonlinelibrary.com]

3.3.2 | Molecular weight analysis of PHUs

The molecular weight of PHUs was determined by GPC and calibrated with polymethyl methacrylate (PMMA) standards, where DMF containing LiBr (0.1%) was used as the mobile phase. Molecular weights (M_n) of resultant PHUs were observed to vary from 2500 to 11,100 g/mol, and their polydispersity was between 1.03 and 2.08 (Table 1, Figure 5, and Figure S23). However, it has been observed that the synthesized PHUs have a lower molecular weight and polydispersity. The inability of PHUs to achieve higher molecular weights has mainly been attributed to the formation of several oligomers[31] and side reactions during the reaction[11,38] and, secondly, due to the lower reactivity of cyclic carbonate leading to incomplete conversions.[34] Further GPC traces of PHUs further validate the formation of the oligomers, other than a monomodal curve, a multimodel curve was observed for all PHUs (Figure S23).

3.3.3 | Thermal properties of PHUs

The thermal properties of PHUs were determined by DSC and TGA analysis and the results are summarized in Table 2, and corresponding thermographs can be seen in Figure 6a. DSC measurements indicated the

10974628, 2023, 45, Downloaded from https://onlinelibrary.wiley.com/doi/10.1002/app.54647 by Csir-National Chemical, Wiley Online Library on [22/12/2024]. See the Terms and Conditions (https://onlinelibrary.wiley.com/terms-and-conditions) on Wiley Online Library for rules of use; OA articles are governed by the applicable Creative Commons License

amorphous nature of the resulting PHUs. The glass transition temperature (T_g) values of the developed PHUs were found to vary in the range of 28 to 42°C and were found to depend on the chemical structure of diamines. As the length of incorporated diamine in PHU increased, the flexibility of the polymer chain improved, leading to decreased T_g values.[39,40] Moreover, PHUs synthesized from shorter chain diamines can lead to the formation of higher density of hydrogen bonds, which in turn can increase the rigidity of chains.[41] So, the T_g of PHUs with shorter chain diamines was found to be higher than those of PHUs with longer chain diamines.

Thermogravimetric analyses have been performed to examine the thermal stability of the produced PHU systems. The decomposition temperature after 10% weight loss ($T_{d,10\%}$), and the weight % of char content (wt% $_{char}$) at 800°C are listed in Table 2 and the corresponding thermograms of all PHUs are depicted in Figure 6b.

TABLE 2 Thermal properties of PHUs

	DSC	TGA	
Code	**T_g (°C)**	**$T_{d,10\%}$ (°C)**	**Char content[a]**
PHU-1	42	180	0.02
PHU-2	31	214	6.92
PHU-3	38	265	4.53
PHU-4	30	234	9.03
PHU-5	30	247	3.17
PHU-6	28	273	4.48

[a]Char content (wt%) was measured at 800°C.

The results demonstrated that the developed PHUs remained stable up to 180°C and primarily exhibited two-step degradation, and the results were similar to those of the previously reported study.[42] However, the curves of first-step degradation were corresponding to the decomposition of urethane linkages (hard segments), whereas the curves of second degradation were related to soft segments of the PHU backbones (aliphatic and aromatic moieties).[43,44] Moreover, it was observed that the chemical nature of diamines influenced the thermal stability of PHUs, and the thermal stability of PHUs was found to increase as the diamine chain length increased.[42,45] Additionally, the char content of all PHUs has also been estimated, and that was found to be very low (below 10 wt%), the lower char content could be related to the aliphatic nature of diamines since it possesses a very low charring propensity.[31]

3.3.4 | Adhesive properties of PHUs

The application potential of the above synthesized PHU was further explored by evaluating the adhesion performance. It will always be advantageous if the above synthesized bio-based PHU from vanillin can exhibit adhesive properties alternative to traditional petroleum-based products because of its inherent bioactivity, and it represents an inexhaustible resource of monomers.[20,21] Hence, to determine the adhesive performance of synthesized materials, we have performed the lap shear measurements on the aluminum (Al) and stainless steel

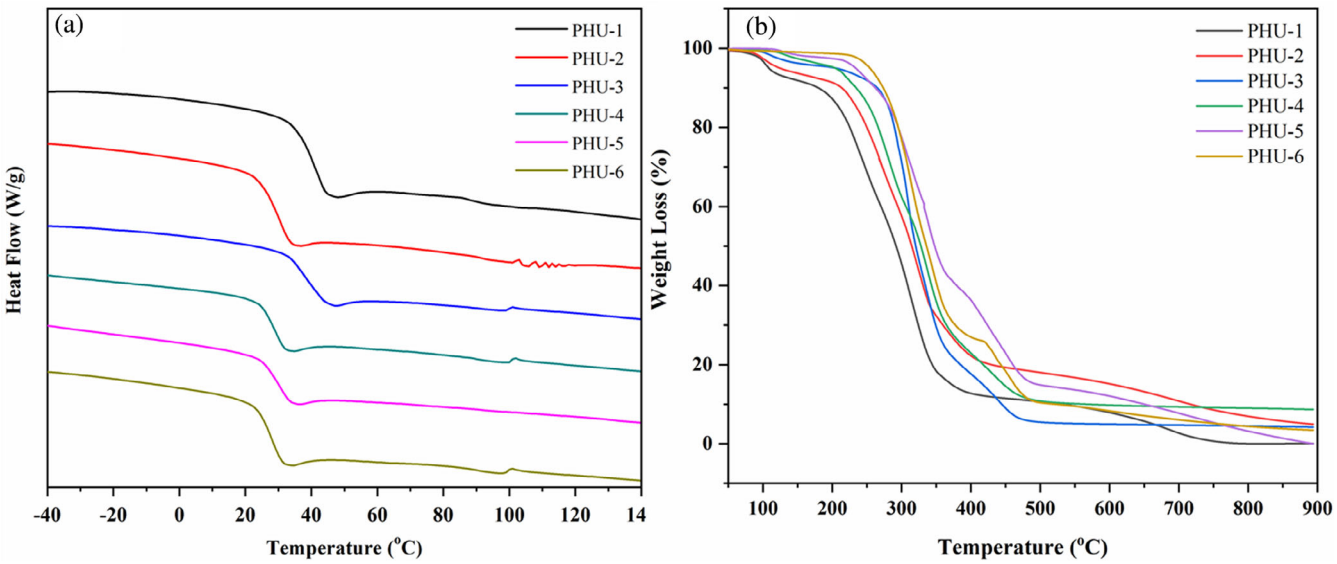

FIGURE 6 (a) DSC curves of poly(hydroxy urethanes) (PHUs) (from second heating curves) (b) Thermograms of the PHUs. [Color figure can be viewed at wileyonlinelibrary.com]

10974628, 2023, 45, Downloaded from https://onlinelibrary.wiley.com/doi/10.1002/app.54647 by Csir-National Chemical, Wiley Online Library on [22/12/2024]. See the Terms and Conditions (https://onlinelibrary.wiley.com/terms-and-conditions) on Wiley Online Library for rules of use; OA articles are governed by the applicable Creative Commons License

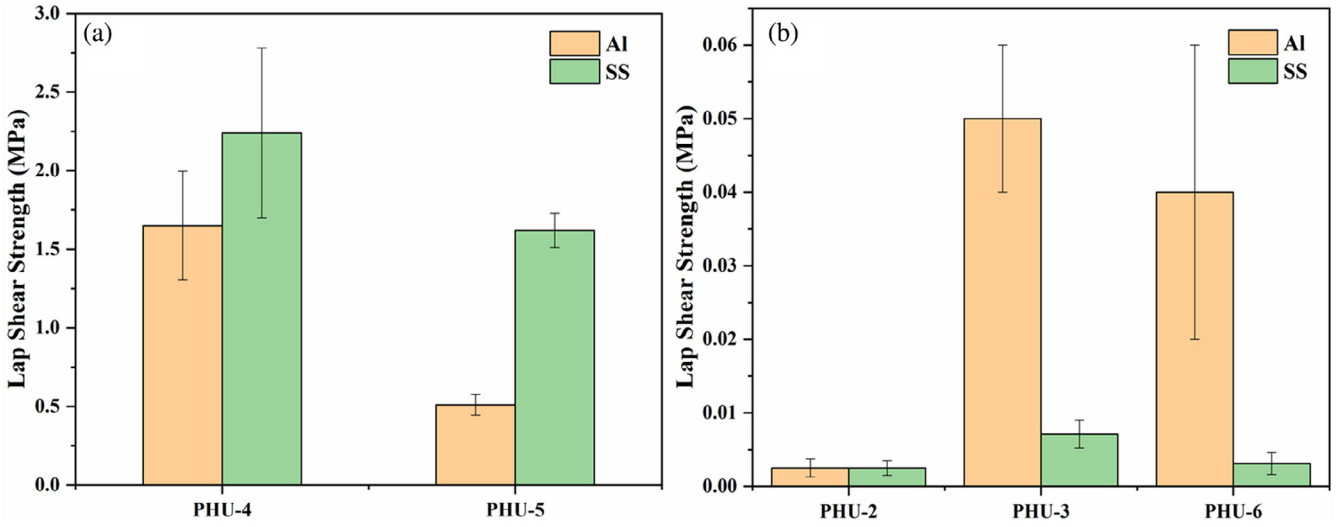

FIGURE 7 Lap shear strength of poly(hydroxy urethanes) (PHUs) evaluated on different sustrates (a) PHU-4 and PHU-5 (b) PHU-2, PHU-3, and PHU-6. The error bars show the representative standard deviation of each sample set of five samples. [Color figure can be viewed at wileyonlinelibrary.com]

(SS) substrate by employing single lap joints (standard: ASTM D1002). The examined PHUs revealed adhesive strength in the range of 0.0025 to 1.65 MPa for aluminum substrate (Table S2, Figure 7, Figure S26–S28) whereas it was in the range of 0.0025 to 2.24 MPa for SS substrates (Table S2, Figure 7, Figure S29). Interestingly, PHU-4 demonstrated better shear strength on both substrate. This enhanced performance of PHU4 can be attributed to their high molecular weight, which resulted in a higher number of primary and secondary hydroxyl groups (hydrogen bonding) and more units of aromatic moieties (π–π interactions), leading to enhanced adhesion properties.[14,46] However, the shear test was not performed in the case of PHU-1 since the flowable nature of the material prevented it from adhering to the substrate. Further, to explore the adhesives repeated applicability, the lap shear-tested substrates were rejoined under similar conditions as of the first application, and measurements were made (Table S2). The rebonded PHUs exhibited comparable or better adhesive strength to their original adhesives.[47] In addition to the adhesive strength, the nature of the adhesive failure was also examined by visual inspection of samples. In all PHUs, cohesive failure was noted (Figure S25).[14] The cohesive force in the PHUs was found to be dominant over the adhesive strength between the PHU and aluminum layer. Even though a few articles explored the applicability of PHUs as adhesives, the dicarbonates utilized for synthesizing these PHUs mainly depend on non-renewable material and often involve further modifications or crosslinking to achieve better adhesive strength.[46–51]

4 | CONCLUSION

In this work, renewable cyclic dicarbonates of vanillin derived by the chemical fixation of greenhouse gas carbon dioxide was reacted with diamines of different chain length, yielding a wide range of PHUs. Further, the chemical structure of the diamine strongly influenced the thermal properties, where PHUs with longer chain diamines exhibited lower T_g values than with shorter chain diamines, leading to flexible and rigid materials. Structural evaluation of PHUs revealed the ring opening of cyclic dicarbonates led to the formation of both primary and secondary hydroxyl groups, which was profoundly found to affect the adhesive properties of polymer. Indeed, the material exhibited an impressive repeatable adhesion strength after several bonding and rebonding studies. Overall, this study highlights the potential of utilizing renewable biobased monomers derived from vanillin for developing PHUs suitable as adhesives.

AUTHOR CONTRIBUTIONS

Gorakh Hiraman Ghuge: Conceptualization (lead); data curation (lead); formal analysis (lead); methodology (lead); writing – original draft (lead). **Karthika Vayalachery Kambikanam:** Formal analysis (supporting); investigation (supporting); project administration (supporting). **Kiran Sukumaran Nair:** Conceptualization (lead); formal analysis (lead); funding acquisition (lead); resources (lead); supervision (lead); writing – review and editing (lead).

10974628, 2023, 45, Downloaded from https://onlinelibrary.wiley.com/doi/10.1002/app.54647 by Csir-National Chemical, Wiley Online Library on [22/12/2024]. See the Terms and Conditions (https://onlinelibrary.wiley.com/terms-and-conditions) on Wiley Online Library for rules of use; OA articles are governed by the applicable Creative Commons License

ACKNOWLEDGMENT

Gorakh Hiraman Ghuge acknowledges the Council of Scientific & Industrial Research (CSIR), New Delhi for the senior research fellowship (SRF) (31/011[1116]/2019-EMR-1), AcSIR registration number: 10CC19J26028. Kiran Sukumaran Nair acknowledges CSIR-NCL for providing the start-up fund (MLP036426) & all the facilities. Kiran Sukumaran Nair acknowledges SERB for the research grant under SRG Scheme (SRG/2020/000954).

CONFLICT OF INTEREST STATEMENT

The authors declare that they have no known competing financial interests or personal relationships that could have appeared to influence the work reported in this article.

DATA AVAILABILITY STATEMENT

The all of analysis results are available in this manuscript and in the supplementary document.

ORCID

Kiran Sukumaran Nair https://orcid.org/0000-0001-6117-2840

REFERENCES

[1] Ellen MacArthur Foundation and World Economic Forum. The New Plastics Economy: Rethinking the future of plastics Ellen MacArthur Found. p 120. **2016**.
[2] A. Das, P. Mahanwar, *Adv. Ind. Eng. Polym. Res.* **2020**, *3*, 93.
[3] W. Wang, C. Wang. Polyurethane for biomedical applications: A review of recent developments, University of Minnesota, USA. **2012**.
[4] J. O. Akindoyo, M. D. H. Beg, S. Ghazali, M. R. Islam, N. Jeyaratnam, A. R. Yuvaraj, *RSC Adv.* **2016**, *6*, 114453.
[5] J. Joseph, R. M. Patel, A. Wenham, J. R. Smith, *Trans. Inst. Met. Finish.* **2018**, *96*, 121.
[6] https://www.precedenceresearch.com/polyurethane-market (**2023**).
[7] D. Bello, C. A. Herrick, T. J. Smith, S. R. Woskie, R. P. Streicher, M. R. Cullen, Y. Liu, C. A. Redlich, *Environ. Health Perspect.* **2007**, *115*, 328.
[8] L. Maisonneuve, O. Lamarzelle, E. Rix, E. Grau, H. Cramail, *Chem. Rev.* **2015**, *115*, 12407.
[9] D. Wołosz, P. G. Parzuchowski, A. Świderska, *Eur. Polym. J.* **2021**, *155*, 110574.
[10] W. Dong, Y. Yoshida, T. Endo, *J. Polym. Sci.* **2021**, *59*, 502.
[11] V. Besse, F. Camara, F. Méchin, E. Fleury, S. Caillol, J. P. Pascault, B. Boutevin, *Eur. Polym. J.* **2015**, *71*, 1.
[12] C. Pronoitis, M. Hakkarainen, K. Odelius, *Polym. Chem.* **2021**, *12*, 196.
[13] M. Blain, A. Cornille, B. Boutevin, R. Auvergne, D. Benazet, B. Andrioletti, S. Caillol, *J. Appl. Polym. Sci.* **2017**, *134*, 1.
[14] S. Panchireddy, B. Grignard, J. M. Thomassin, C. Jerome, C. Detrembleur, *ACS Sustain. Chem. Eng.* **2018**, *6*, 14936.
[15] G. R. Younes, M. Marić, *Macromolecules* **2021**, *54*, 10189.
[16] R. H. Aguirresarobe, S. Nevejans, B. Reck, L. Irusta, H. Sardon, J. M. Asua, N. Ballard, *Prog. Polym. Sci.* **2021**, *114*, 101362.
[17] E. K. Leitsch, G. Beniah, K. Liu, T. Lan, W. H. Heath, K. A. Scheidt, J. M. Torkelson, *ACS Macro Lett.* **2016**, *5*, 424.
[18] F. D. Bobbink, A. P. Van Muyden, P. J. Dyson, *J. Chem. Commun.* **2019**, *55*, 1360.
[19] A. Saravanan, P. Senthil kumar, S. Jeevanantham, V. Bhuvaneswari, V. Anantha Narayanan, P. R. Yaashikaa, S. Swetha, B. Reshma, *Chem. Eng. Sci.* **2021**, *236*, 116515.
[20] M. Fache, B. Boutevin, S. Caillol, *ACS Sustain. Chem. Eng.* **2016**, *4*, 35.
[21] M. Fache, E. Darroman, V. Besse, R. Auvergne, S. Caillol, B. Boutevin, *Green Chem.* **2014**, *16*, 1987.
[22] N. Fanjul-Mosteirín, L. P. Fonseca, A. P. Dove, H. Sardon, *Mater. Adv.* **2023**, *4*, 2437.
[23] C. Zhang, S. A. Madbouly, M. R. Kessler, *Macromol. Chem. Phys.* **2015**, *216*, 1816.
[24] S. Engelen, A. A. Wróblewska, K. De Bruycker, R. Aksakal, V. Ladmiral, S. Caillol, F. E. Du Prez, *Polym. Chem.* **2022**, *13*, 2665.
[25] Y. Ecochard, J. Leroux, B. Boutevin, R. Auvergne, S. Caillol, *Eur. Polym. J.* **2019**, *120*, 109280.
[26] A. Kayan, *J. Appl. Polym. Sci.* **2019**, *136*, 47074.
[27] D. Duraibabu, M. Alagar, S. A. Kumar, *RSC Adv.* **2014**, *4*, 40132.
[28] M. G. González, J. C. Cabanelas, J. Baselga, *Infrared Spectroscopy - Materials Science, Engineering and Technology*, InTech, London, UK **2012**, pp. 261.
[29] Z. Ma, C. Li, H. Fan, J. Wan, Y. Luo, B. G. Li, *Ind. Eng. Chem. Res.* **2017**, *56*, 14089.
[30] C. Mokhtari, F. Malek, A. Manseri, S. Caillol, C. Negrell, *Eur. Polym. J.* **2019**, *113*, 18.
[31] R. Ménard, S. Caillol, F. Allais, *ACS Sustain. Chem. Eng.* **2017**, *5*, 1446.
[32] H. Tomita, F. Sanda, T. Endo, *J. Polym. Sci. Part A Polym. Chem.* **2001**, *39*, 3678.
[33] A. Yuen, A. Bossion, E. Gómez-Bengoa, F. Ruipérez, M. Isik, J. L. Hedrick, D. Mecerreyes, Y. Y. Yang, H. Sardon, *Polym. Chem.* **2016**, *7*, 2105.
[34] Y. Ecochard, S. Caillol, *Eur. Polym. J.* **2020**, *137*, 109915.
[35] A. Steblyanko, W. Choi, F. Sanda, T. Endo, *J. Polym. Sci. Part A Polym. Chem.* **2000**, *38*, 2375.
[36] H. Tomita, F. Sanda, T. Endo, *J. Polym. Sci. Part A Polym. Chem.* **2001**, *39*, 851.
[37] T. Anders, H. Keul, M. Möller, *Des. Monomers Polym.* **2011**, *14*, 593.
[38] A. Bossion, R. H. Aguirresarobe, L. Irusta, D. Taton, H. Cramail, E. Grau, D. Mecerreyes, C. Su, G. Liu, A. J. Müller, H. Sardon, *Macromolecules* **2018**, *51*, 5556.
[39] L. Ubaghs, N. Fricke, H. Keul, H. Höcker, *Macromol. Rapid Commun.* **2004**, *25*, 517.
[40] S. Benyahya, J. P. Habas, R. Auvergne, V. Lapinte, S. Caillol, *Polym. Int.* **2012**, *61*, 1666.
[41] G. Beniah, D. J. Fortman, W. H. Heath, W. R. Dichtel, J. M. Torkelson, *Macromolecules* **2017**, *50*, 4425.
[42] C. Duval, N. Kébir, R. Jauseau, F. Burel, *J. Polym. Sci. Part A Polym. Chem.* **2016**, *54*, 758.
[43] R. Behnam, H. Roghani-Mamaqani, M. Salami-Kalajahi, H. Mardani, *ChemistrySelect* **2020**, *5*, 962.
[44] C. Wang, M. L. Auad, N. E. Marcovich, S. Nutt, A. Si, *J. Appl. Polym. Sci.* **2008**, *109*, 2562.
[45] J. L. J. Van Velthoven, L. Gootjes, D. S. Van Es, B. A. J. Noordover, J. Meuldijk, *Eur. Polym. J.* **2015**, *70*, 125.

10974628, 2023, 45, Downloaded from https://onlinelibrary.wiley.com/doi/10.1002/app.54647 by Csir-National Chemical, Wiley Online Library on [22/12/2024]. See the Terms and Conditions (https://onlinelibrary.wiley.com/terms-and-conditions) on Wiley Online Library for rules of use; OA articles are governed by the applicable Creative Commons License

[46] A. S. Nair, S. Cherian, N. Balachandran, U. G. Panicker, S. K. K. Sankaranarayanan, *ACS Omega* **2019**, *4*, 13042.
[47] A. Gomez-Lopez, N. Ayensa, B. Grignard, L. Irusta, I. Calvo, A. Müller, C. Detrembleur, H. Sardon, *ACS Polym.* **2022**, *2*, 194.
[48] A. Cornille, G. Michaud, F. Simon, S. Fouquay, R. Auvergne, B. Boutevin, S. Caillol, *Eur. Polym. J.* **2016**, *84*, 404.
[49] A. Gomez-lopez, B. Grignard, I. Calvo, C. Detrembleur, H. Sardon, *ACS Appl. Polym. Mater.* **2020**, *2*, 1839.
[50] A. Gomez-Lopez, B. Grignard, I. Calvo, C. Detrembleur, H. Sardon, *Macromol. Rapid Commun.* **2021**, *42*, 1.
[51] A. Gomez-Lopez, B. Grignard, I. Calvo, C. Detrembleur, H. Sardon, *ACS Appl. Polym. Mater.* **2022**, *4*, 8786.

SUPPORTING INFORMATION

Additional supporting information can be found online in the Supporting Information section at the end of this article.

How to cite this article: G. H. Ghuge, K. V. Kambikanam, K. S. Nair, *J. Appl. Polym. Sci.* **2023**, *140*(45), e54647. https://doi.org/10.1002/app.54647

10974628, 2023, 45, Downloaded from https://onlinelibrary.wiley.com/doi/10.1002/app.54647 by Csir-National Chemical, Wiley Online Library on [22/12/2024]. See the Terms and Conditions (https://onlinelibrary.wiley.com/terms-and-conditions) on Wiley Online Library for rules of use; OA articles are governed by the applicable Creative Commons License

ACS APPLIED POLYMER MATERIALS

pubs.acs.org/acsapm

Article

Biobased Reusable Nonisocyanate Polyurethane Hot-Melt Adhesives with Potential Chemical Degradability

Gorakh Hiraman Ghuge, Arun Torris, and Kiran Sukumaran Nair*

Cite This: *ACS Appl. Polym. Mater.* 2024, 6, 11180−11192

Read Online

ACCESS | Metrics & More | Article Recommendations | Supporting Information

ABSTRACT: Hot-melt adhesives (HMAs) derived from renewable resources are always attractive, as they promote less dependence on fossil resources and aid in developing environmentally friendly materials. However, developing sustainable HMAs exhibiting good adhesive performance and biodegradability remains challenging. Herein, reusable biobased HMAs with a high bio content of 88−90%, biodegradability, and tunable adhesive nature were developed as a possible alternative to conventional petroleum-based hot-melt adhesives. Moreover, the structure−property relationship of the product was investigated in detail. By tailoring the monomer composition, NIPU-40 HMA exhibited a good bonding ability with a superior adhesion strength of 6.39 MPa. To the best of our knowledge, this is the highest adhesion strength observed when bonding with an Al substrate among the biobased thermoplastic NIPU-HMAs. Impressively, NIPU-HMAs could display excellent reusability even after three bonding and debonding cycles without a significant drop in the adhesive strength and were found to exhibit good adhesion performance under wet conditions. More importantly, the NIPU-HMAs are prone to degradation under acid-catalyzed conditions. Considering their features, these biobased NIPU thermoplastic hot-melt adhesives offer an opportunity to create environmentally friendly, degradable adhesives that possess excellent adhesive strength and can be reused multiple times.

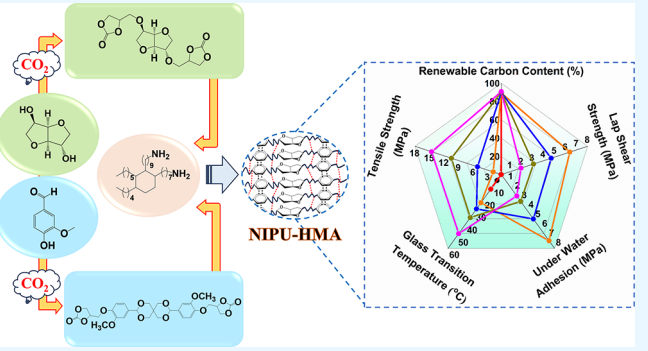

KEYWORDS: *biobased NIPUs, hot melt adhesives, lap shear strength, spiro-aromatic, cyclic carbonates, acid degradability*

Downloaded via NATL CHEMICAL LABORATORY on October 4, 2024 at 02:42:09 (UTC).
See https://pubs.acs.org/sharingguidelines for options on how to legitimately share published articles.

1. INTRODUCTION

Adhesives play a significant role in numerous fields of human endeavor, ranging from basic repairs to advanced engineering.[1] Based on practical implementations, adhesives mainly include water based, solvent-based, two-component, and hot-melt adhesives.[2] Even though widely employed from a sustainable and environmental point of view, solvent-based adhesives and two-component adhesives are not very feasible due to pollution arising from solvent vapors and residual quantities of curing agents and monomers. Hot-melt adhesives (HMAs) are a promising green alternative to other adhesives due to their solvent-free nature, ease of use, and cost-effectiveness. These characteristics make them a popular adhesive choice in various industries, including aerospace, automotive, textile, electronics, and packaging.[3] In fact, the growing demand for HMAs is driving the global market to expand, and it is projected to achieve USD 11.4 billion by 2027.[4] Among the polymers used for hot melt-adhesives, polyurethanes (PUs) are the preferred choice when it comes to formulating high-quality adhesives due to their diverse formulation options, better low-temperature properties, greater flexibility, and excellent adhesion on low-surface roughness materials.[3] The global polyurethane hot-melt adhesive market is valued at 1311 million in 2021 and is projected to reach 2537 million USD by 2030.[5] However, the synthesis of these PUs entirely depends on fossil fuels and involves using hazardous chemicals such as isocyanates, as well as the precursors used for their production such as phosgene, which is a major drawback of the system.[6] Furthermore, the current forms of PU-HMAs are not environmentally friendly, as they are nonbiodegradable and most of the material ends up in landfills, resulting in economic and energy losses.

Scientific efforts to produce sustainable PU-HMAs have led to the development of nonisocyanate polyurethanes (NIPUs), a promising substitute for conventional PUs, as they restrict the usage of allergenic and carcinogenic isocyanates.[7] Additionally, the monomers used in poly(hydroxyurethane)s (PHUs) can be created from precursors utilizing CO_2, an abundant and inexhaustible resource, making the method more sustainable and safer to handle than conventional PU-based

Received: May 17, 2024
Revised: August 29, 2024
Accepted: August 31, 2024
Published: September 10, 2024

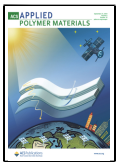

ACS Publications

© 2024 American Chemical Society

HMAs.[8] Despite the recent advancements in the field of NIPU-based adhesives, most studies rely on nonrenewable fossil fuels to synthesize cyclic carbonate and diamine.[9−13] Moreover, most of these studies concentrate on developing thermoset adhesives that are not reworkable, recyclable, or biodegradable, making the disposal/recycling of discarded adhesive products difficult.[14−18] Although limited studies have explored the development of sustainable NIPU-HMAs by utilizing bioderived monomers, they have not yet received much attention as they exhibit inferior adhesion properties and limited recyclable and biodegradable properties.[19−21] Obviously, there is a need for NIPU-HMA systems based on biorenewable monomers, which are reprocessable and could achieve good adhesion and biodegradation properties.

Efforts to develop sustainable NIPUs have led to the utilization of vanillin and isosorbide molecules, which are environmentally friendly, economically viable, sustainable and are produced on an industrial scale. A series of NIPU-HMAs were synthesized by reacting different compositions of vanillin and isosorbide carbonates with Priamine 1074. This study further explored the effect of structure on the thermal properties, mechanical properties, and adhesive behaviors of the NIPUs. In addition to their improved sustainability, the unique molecular architecture of acetal-coupled divanillin utilized in the current study aided in the exploration of convenient degradation of NIPU-HMAs, which can facilitate biodegradation or chemical recycling. Furthermore, the adhesion strength, thermo-reversible adhesion properties, temperature tolerance, and adhesion under wet conditions of the developed NIPUs have been investigated in detail to validate their potential as environmentally friendly and sustainable HMAs.

2. EXPERIMENTAL SECTION

2.1. Materials. Vanillin (>98%), isosorbide (>98%), pentaerythritol (>98%), allyl bromide (>98%), tetrabutylammonium bromide (TBAB, >98%), potassium peroxymonosulfate (oxone), and 1,5,7-triazabicyclo-[4.4.0]dec-5-ene (TBD, >98%) were purchased from TCI Chemicals, India. Priamine 1074 was provided by Croda, Netherlands. Epichlorohydrin (>99%) and para-toluene sulfonic acid monohydrate (pTSA·H_2O) were procured from Sigma-Aldrich. Sodium hydroxide pellets (NaOH, 98%), hydrochloric acid (HCl, 35−38%), and petroleum ether were supplied by the S D Fine Chemical. Sodium sulfate (anhydrous, >99.5%, AR), ethyl acetate, and dichloromethane (DCM) were delivered by Leonid Chemicals. Dimethyl sulfoxide (DMSO-d_6, 99.80% D), acetone-d_6, and chloroform (99.80% D) were purchased from Eurisotop. A CO_2 gas cylinder (99.5%) was obtained from Vadilal Chemical. Sodium bicarbonate ($NaHCO_3$) was procured from SRL Chemicals. *N*-methylpyrrolidinone (NMP) and dimethylformamide (DMF) were distilled over CaH_2 under a nitrogen atmosphere and stored over molecular sieves (4 Å). All chemicals were used as received, unless specified.

2.2. Characterization. The chemical structure of the molecules was determined by ^1H and ^{13}C NMR spectroscopy using a Bruker Advance 500 MHz spectrometer equipped with a QNP z-gradient probe at room temperature. The infrared spectra (IR) were recorded on a Bruker Alpha Fourier transform infrared (FTIR) spectrometer, where 48 scans were recorded in a frequency range of 4000−500 cm^{-1} at a resolution of 4 cm^{-1}. The high-resolution mass spectrometer (ThermoFisher Scientific) was used to detect the molecular weight of compounds. The data were acquired from a hybrid Quadrupole Q-Exactive Orbitrap fitted with an ACCELA PDA detector. Size exclusion chromatography was employed to analyze the molecular weight of NIPUs using a Viscotek SEC Max (VE 2001) with a refractive index as a detector. The measurements were done in DMF (DMF plus lithium bromide 1 g L^{-1}) as an eluent at 1 mL/min using the DT6000 M column at 50 °C. Molecular weights were estimated relative to poly(methyl methacrylate) standards. The X-ray diffraction (XRD) measurement was performed at room temperature using a Rigaku SmartLab X-ray Diffractometer equipped with a Cu, Kα radiation source (operating at 40 kV and 30 mA, λ = 1.5406 nm). The data were recorded in the 2θ range from 5 to 50°.

The glass transition temperature was analyzed on a DSC-Q10 system from TA Instruments. For each sample, two cycles were performed between −40 and 180 °C at 10 °C min^{-1} under a nitrogen atmosphere. The glass transition temperature (T_g) was determined from the second heating cycle. Thermogravimetric studies were performed using a TGA-STA 6000 (PerkinElmer) at a heating rate of 10 °C/min from 50 to 650 °C under a nitrogen atmosphere. The water contact angle (WCA) was determined by using a KRUSS instrument with droplets of Milli-Q water (2 μL). The homogeneous film was prepared prior to analysis by casting polymeric solutions (50 mg in 1 mL of chloroform) on the glass surface (75 × 25 mm). The slides were then kept at room temperature overnight to evaporate the chloroform slowly without leaving any air bubbles on the film. The measurements were taken on a dried homogeneous polymer film after drying at room temperature for 48 h in a desiccator equipped with a high vacuum. To calculate the mean contact angle values, a minimum of five repeated measurements were taken at various locations on each NIPU surface.

The adhesive properties of synthesized NIPUs were investigated at room temperature using an Instron 33R4204 (load cell: 10 KN) with a displacement rate of 1 mm·min^{-1}. The lap shear test was performed on aluminum substrates having dimensions of 54 × 20 × 1.55 mm (L*W*T). 135 mg of polymer materials were applied on the substrate surface, maintaining the adhesive contact area of 200 mm^2 (18 mm × 11.15 mm). Furthermore, the adhesive specimen was prepared by melting at 130 °C while applying gentle pressure. After 20 min, they were left to cool at room temperature overnight before the test. The measurements of each sample were repeated at least six times. The type of failure was further reported after the test based on visual inspection. The following equation determined the lap shear strength,

$$\tau = F/A \quad (1)$$

where:
τ = lap-shear strength (N·mm^{-2} or MPa),
F = maximum shear force (N), and
A = contact area of the adhesive joints (mm^2)

Oscillatory rheological measurements were performed on a stress-controlled rheometer (Physica MCR 301, Anton Paar, Austria) to study the viscoelastic behavior of NIPUs. NIPUs were subjected to sinusoidal oscillatory shear stress to study their viscoelastic response using parallel plate geometry (plate diameter, 25 mm). Strain sweep measurements were performed in the 1% to 10% strain range at a constant temperature (135 °C) and frequency (1 rad/s). Frequency sweep measurements were performed in the frequency range of

https://doi.org/10.1021/acsapm.4c01526
ACS Appl. Polym. Mater. 2024, 6, 11180−11192

Scheme 1. Synthesis Route of ISO−DC from Isosorbide

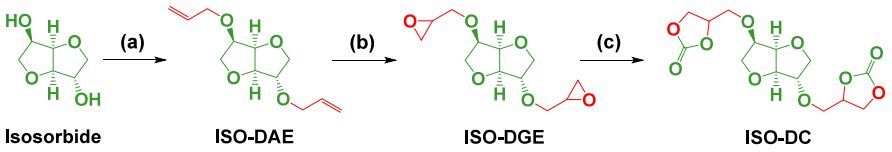

(a) Allyl bromide, aq. NaOH, 65°C, 5h; (b) Oxone, $NaHCO_3$, 0°C, 7h; (c) CO_2, 30 bar, TBAB, 100°C, 24h.

0.5 to 500 rad/s at a constant temperature (135 °C) and strain (2.5%). Temperature ramp measurements were performed in the 5 to 160 °C temperature range, at a constant frequency (10 Hz) and strain (2.5%). The resulting storage modulus, loss modulus, tan delta, and complex viscosity values were recorded and plotted.

Tensile testing was performed at room temperature on an Instron 5944 (load cell: 1 KN) at a speed of 20 $mm.min^{-1}$. The dog-bone-shaped samples were used for analysis; they had the dimensions of length = 2.8 cm and width = 1.2 cm (length and width of narrow fraction = 1.5 and 0.6 cm, respectively). The Young's modulus, tensile strength, and elongation at the break of each polymer were calculated using the average values of at least five specimens. Error represents one standard deviation.

2.3. Preparation of Isosorbide-Derived Cyclic Carbonate. The synthesis of isosorbide dicarbonate has been carried out in three steps using methods described elsewhere in the literature,[22,23] and the synthetic pathways are illustrated in Scheme 1.

2.3.1. Synthesis of Isosorbide Diallyl Ether (ISO−DAE). In a 250 mL round-bottom flask, 30 g of isosorbide (0.205 mol) and 62.06 g of allyl bromide (0.513 mol) were added. Next, an aqueous solution of NaOH (20.52 g, 0.513 mol) was added dropwise, followed by the addition of 1.983 g of tetrabutylammonium bromide (TBAB, 6.155 mmol) as a phase transfer catalyst. The reaction was performed at 65 °C for 6 h. The obtained crude product was extracted with dichloromethane, dried with anhydrous sodium sulfate, and purified by column chromatography (26 g, yield: 76 %).

^1H NMR (500 MHz, $CDCl_3$) δ (ppm): 3.57 (t, 1H, isosorbide ring −C<u>H</u>), 3.89−4.05 (m, 5H, isosorbide ring −C<u>H</u>, and C<u>H_2</u>), 3.89−4.05 (m, 3H, C<u>H_2</u>—CH═CH_2), 4.16−4.20 (dd, 1H, C<u>H_2</u>—CH═CH_2), 4.48 (d, 1H, bridgehead −C<u>H</u>), 4.61 (t, 1H, bridgehead −C<u>H</u>), 5.15−5.30 (m, 4H, —C<u>H_2</u>═CH), 5.82−5.96 (m, 2H, —C<u>H</u>═CH_2) (Figure S2).

^{13}C NMR (500 MHz, $CDCl_3$) δ (ppm): 69.79−70.47 (−C<u>H_2</u>−O, isosorbide ring), 71.59−73.41 (—C═C—C<u>H_2</u>—O), 79.43−80.19 (−C<u>H</u>−O, isosorbide ring), 83.75−86.28 (−C<u>H</u>−O, bridgehead), 117.39−117.72 (—CH═C<u>H_2</u>-), 134.16−134.49 (—C<u>H</u>═CH_2−) (Figure S5).

FTIR (cm^{-1}): 2866−2981 (aliphatic −CH stretch), 1647 (C═C stretch), 1260 (isosorbide C−O stretch), 1023−1137 (isosorbide C−O−C stretch) (Figure S1).

HRMS (ESI) m/z: $[M + H]^+$ calculated for $C_{12}H_{18}O_4$: 227.1283; found: 227.1278.

2.3.2. Synthesis of Isosorbide Diglycidyl Ether (ISO−DGE). The ISO−DAE compound (20 g, 0.088 mol) was dissolved in acetone (161 mL) and DI water (380 mL), and the solution was agitated at 0 °C for 30 min (temperature was maintained using an ice bath). Afterward, oxone (155 g, 0.251 mol) and sodium bicarbonate (63.08 g, 0.750 mol) were added in three to four parts over the course of 1 h. After the addition, the reaction was allowed to run for 7 h while maintaining the temperature at 5 °C. The obtained reaction mixture was filtered, extracted with dichloromethane, and purified by column chromatography to obtain the final product (19.71 g, yield: 86.33 %).

^1H NMR (500 MHz, $CDCl_3$) δ (ppm): 2.54−2.61 (m, 2H, epoxy −C<u>H_2</u>), 2.75−2.78 (m, 2H, epoxy −C<u>H_2</u>), 3.08−3.18 (m, 2H, epoxy −C<u>H</u>), 3.32−3.44 (m, 2H, −O−C<u>H_2</u>), 3.75−3.83 (m, 2H, −O−C<u>H_2</u>), 3.75−3.80 (t, 1H, isosorbide ring −C<u>H</u>), 3.87−4.01 (m, 5H, isosorbide ring −C<u>H</u>, and CH_2), 4.47−4.50 (dd, 1H, bridgehead −C<u>H</u>), 4.60−4.66 (m, 1H, bridgehead −C<u>H</u>) (Figure S3).

^{13}C NMR (500 MHz, $CDCl_3$) δ (ppm): 44.02−44.19 (−C<u>H</u>−O, epoxy), 50.53−50.78 (−C<u>H_2</u>−O, epoxy), 69.79−70.35 (−C<u>H_2</u>−O), 71.07−73.36 (−C<u>H_2</u>−O, isosorbide ring), 80.16−80.63 (−C<u>H</u>−O, isosorbide ring), 84.81−86.16 (−C<u>H</u>−O, bridgehead) (Figure S6).

FTIR (cm^{-1}): 2866−2981 (aliphatic −CH/CH_2 stretch), 1260 (isosorbide C−O stretch), 1023−1137 (isosorbide C−O−C stretch), 905 (asymmetric C−O stretch, epoxy), and 832−847 (symmetric C−O stretch, epoxy) (Figure S1).

HRMS (ESI) *m/z*: $[M + H]^+$ calculated for $C_{12}H_{18}O_6$: 259.1181; found: 259.1176.

2.3.3. Synthesis of Isosorbide Dicarbonate (ISO−DC). ISO−DGE (11 g, 0.0318 mol) and TBAB catalyst (5 mol %) were dissolved in acetone and added to the 50 mL autoclave reactor. The reactor was pressurized with 20 bar of CO_2, and the mixture was heated at 100 °C for 2 h. Upon completion, the reactor was degassed and allowed to cool to room temperature. The crude product was concentrated, extracted with ethyl acetate, and purified by column chromatography using ethyl acetate and petroleum ether as eluents (12.24 g, yield: 83 %).

^1H NMR (500 MHz, $DMSOd_6$) δ (ppm): 3.44−3.52 (m, 1H, isosorbide ring −C<u>H</u>), 3.62−3.81 (m, 5H, isosorbide ring −C<u>H</u>, and C<u>H_2</u>), 3.86−4.09 (dd, 4H, carbonate −C<u>H_2</u>), 4.23−4.26 (dd, 1H, bridgehead −C<u>H</u>), 4.32−4.35 (m, 1H, bridgehead −C<u>H</u>), 4.41−4.62 (dd, 4H, carbonate −C<u>H_2</u>), 4.92 (m, 2H, carbonate −C<u>H</u>) (Figure S4).

^{13}C NMR (500 MHz, $DMSOd_6$) δ (ppm): 66.46 (−C<u>H_2</u>−O, carbonate), 68.69−70.32 (−C<u>H_2</u>−O, isosorbide ring), 72.83−72.94 (−C<u>H</u>−O, carbonate), 75.74−75.94 (−C<u>H_2</u>−O), 80.24−80.59 (−C<u>H</u>−O, isosorbide ring), 84.52−85.87 (−C<u>H</u>−O, bridgehead), 155.36−155.43 (C═O, carbonate) (Figure S7).

FTIR (cm^{-1}): 2866−2981 (aliphatic −CH stretches), 1778 (carbonate C═O stretch), 1175 (isosorbide C−O stretches), 1044 (isosorbide C−O−C stretches) (Figure 1a).

HRMS (ESI) m/z: $[M + H]^+$ calculated for $C_{14}H_{18}O_{10}$: 347.0978; found:347.0973 (Figure S8).

https://doi.org/10.1021/acsapm.4c01526
ACS Appl. Polym. Mater. 2024, 6, 11180−11192

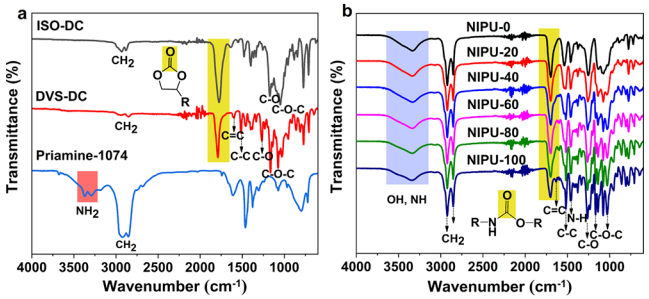

Figure 1. Fourier transform infrared spectroscopy (FTIR) of (a) ISO−DC, DVS-DC, and Priamine-1074 precursors and (b) NIPU polymers.

2.4. Preparation of Vanillin and Pentaerythritol-Derived Cyclic Carbonate. The synthesis of vanillin and pentaerythritol-derived dicarbonate was carried out in three steps,[24] and their synthetic route is presented in Scheme 2.

2.4.1. Synthesis of Divanillin Spiro Diol (DVS-DL). Vanillin (10 g, 0.025 mol) and pentaerythritol (8.95 g, 0.066 mol) were dissolved in a mixture of DMF (22 mL) and petroleum ether (24 mL) in an RB flask equipped with a reflux condenser and Dean−Stark trap. Then, *p*-toluenesulfonic acid monohydrate (pTSA·H_2O, 0.38 g, 2 wt % of the total weight of vanillin and pentaerythritol) was added, and the reaction was carried out at 105 °C for 15 h. The L-shaped tube of the Dean−Stark trap was charged periodically throughout the reaction using a hot gun to increase the vapor speed toward the condenser. The white solid was precipitated with a 3 wt % aqueous solution of $NaHCO_3$, washed multiple times with water, and purified by precipitation in petroleum ether.

^1H NMR (500 MHz, $CDCl_3$) δ (ppm): 3.59 (d, 2H, spirocyclic −CH_2), 3.76 (t, 4H, spirocyclic −CH_2), 3.85 (s, 6H, OCH_3), 4.81 (d, 2H, spirocyclic −CH_2), 5.33 (s, 2H, spirocyclic −CH), 5.59 (s, 2H, aromatic −OH), 6.85 (d, 2H, aromatic −CH), 6.90 (d, 2H, aromatic −CH), 6.96 (s, 2H, aromatic −CH) (Figure S10).

^{13}C NMR (500 MHz, $CDCl_3$) δ (ppm): 32.46 (−C-$(CH_2)_4$-, spirocyclic), 55.94 (OCH_3), 70.59−71.08 (−$CH_2)_4$−O, spirocyclic), 102.29 (O−CH−O, spirocyclic), 108.26−119.51 (C−H, aromatic), 130.15 (C−CH, aromatic), 146.31−146.45 (C−O, aromatic) (Figure S13).

FTIR (cm^{-1}): 3488 (−OH stretch), 2872−2969 (aliphatic −CH/CH_2 stretch), 1613 (aromatic C=C stretch), 1519 (aromatic C−C stretch), 1467 (C−H bend), 1263 (spiroacetal C−O stretch), 1167 (spiroacetal C−O−C stretch) (Figure S9).

HRMS (ESI) m/z: $[M + H]^+$ calculated for $C_{21}H_{24}O_8$: 405.1549; found: 405.1544.

2.4.2. Synthesis of Divanillin Spiro Diglycidyl Ether (DVS-DGE). DVS-DL (8.70 g, 0.022 mol) was added to an RB flask equipped with a reflux condenser and magnetic stirrer, followed by the addition of epichlorohydrin (79.64 g, 0.861 mol) and tetrabutylammonium bromide (TBAB, 10 wt %). The reaction was conducted at a temperature of 75 °C for a duration of 3 h. After completion, the reaction mixture was cooled to room temperature, following which a 50% aqueous solution of NaOH weighing 5.16 g (0.129 mol) was added dropwise. The reaction was then allowed to continue for another 3 h while maintaining a temperature of around 16 °C to promote the ring-closing process. The resulting mixture was filtered, washed with DI water, and dried with anhydrous sodium sulfate. After that, it was precipitated with petroleum ether to obtain a white powder (8.11 g, yield: 72.86 %).

^1H NMR (500 MHz, $CDCl_3$) δ (ppm): 2.73 (m, 2H, epoxy −CH_2), 2.88 (m, 2H, epoxy −CH_2), 3.37 (m, 2H, epoxy −CH), 3.66 (m, 2H, CH_2−OAr), 3.85 (m, 2H, CH_2−OAr), 3.85 (m, 2H, spirocyclic −CH_2), 3.89 (s, 6H, OCH_3), 4.04 (m, 2H, spirocyclic −CH_2), 4.22 (dd, 2H, spirocyclic −CH_2), 4.84 (d, 2H, spirocyclic −CH_{2}), 5.40 (s, 2H, spirocyclic −CH), 6.92 (d, 2H, aromatic −CH), 6.99 (d, 2H, aromatic −CH), 7.04 (s, 2H, aromatic −CH) (Figure S11).

^{13}C NMR (500 MHz, $CDCl_3$) δ (ppm): 32.49 (−C−$(CH_2)_4$-, spirocyclic), 45.00 (CH_2−O, epoxy), 50.14 (CH−O, epoxy), 55.94 (OCH_3), 70.26 (CH_2−OAr), 70.58−71.07 (−$CH_2)_4$−O, spirocyclic), 102.09 (O−CH−O, spirocyclic), 109.51−118.70 (C−H, aromatic), 131.76 (C−CH, aromatic), 148.53−149.56 (C−O, aromatic) (Figure S14).

FTIR (cm^{-1}): 2872−2969 (aliphatic −CH/CH_2 stretch), 1613 (aromatic C=C stretch), 1519 (aromatic C−C stretch), 1467 (C−H bend), 1263 (spiroacetal C−O stretch), 1167 (spiroacetal C−O−C stretch), 908−918 (asymmetric C−O stretch, epoxy), 809 (symmetric C−O stretch, epoxy) (Figure S9).

HRMS (ESI)m/z: $[M + H]^+$ calculated for $C_{27}H_{32}O_{10}$: 517.2073; found: 517.2068.

2.4.3. Synthesis of Divanillin Spiro Dicarbonate (DVS-DC). The DVS-DGE compound (10 g, 0.017 mol) and TBAB catalyst (5 mol %) were dissolved in acetone and poured into the 100 mL autoclave reactor, which was equipped with a mechanical stirrer and temperature controller. Next, 30 bar of

Scheme 2. Synthesis Route of DVS-DC from Vanillin and Pentaerythritol

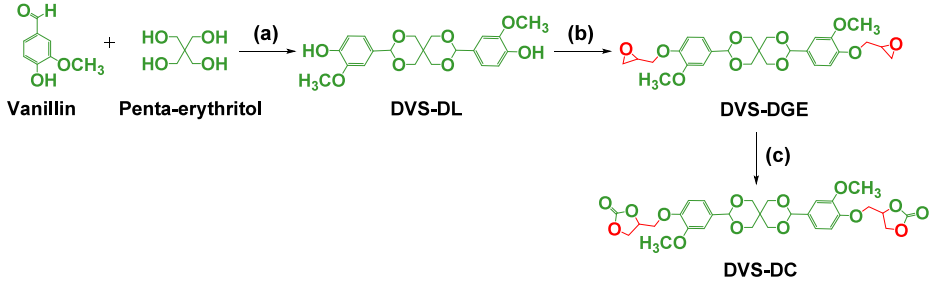

(a) P-TSA, DMF-Pet Ether, Refluxed, 12h; (b) Epichlorohydrin, TBAB, 70°C, 3h, aq. NaOH; (c) CO_2, 30 bars, Acetone, 100°C, 24h.

https://doi.org/10.1021/acsapm.4c01526
ACS Appl. Polym. Mater. 2024, 6, 11180−11192

CO_2 were introduced into the reactor, and the reaction was performed at 100 °C for 24 h. After completion of the reaction, the reactor was degassed and cooled to room temperature. Then, the white solid was precipitated out by adding the reaction mixture to cold water. The crude product was purified by recrystallization in isopropanol. (10.30 g, yield: 88 %).

^1H NMR (500 MHz, $CDCl_3$) δ (ppm): 3.64 (d, 2H, spirocyclic −C$\underline{H}_2$), 3.81 (dd, 4H, spirocyclic −C$\underline{H}_2$), 3.86 (s, 6H, OC$\underline{H}_3$), 4.20 (dd, 4H, carbonate −C$\underline{H}_2$), 4.60 (dd, 4H, carbonate −C$\underline{H}_2$), 4.80 (d, 2H, spirocyclic −C$\underline{H}_2$), 4.99 (m, 2H, carbonate −C$\underline{H}$), 5.41 (s, 2H, spirocyclic −C$\underline{H}$), 6.92 (d, 2H, aromatic −C$\underline{H}$), 7.01 (d, 2H, aromatic −C$\underline{H}$), 7.06 (s, 2H, aromatic −C$\underline{H}$) (Figure S12).

^{13}C NMR (500 MHz, $CDCl_3$) δ (ppm): 32.49 (−$\underline{C}$-$(CH_2)_4$-, spirocyclic), 55.93 (O$\underline{C}H_3$), 66.37 (CH_2−O, carbonate), 69.34 (CH−O, carbonate), 70.54−71.03 (−$\underline{C}H_2)_4$−O, spirocyclic), 74.34 ($\underline{C}H_2$−OAr), 101.83 (O−$\underline{C}$H−O, spirocyclic), 110.09−118.82 ($\underline{C}$-H, aromatic), 133.28 ($\underline{C}$−CH, aromatic), 147.92−150.26 ($\underline{C}$−O, aromatic), 154.71 (C═O, carbonate) (Figure S15).

FTIR (cm^{-1}): 2878−2941 (aliphatic −CH/CH_2 stretch), 1789 (carbonate C═O stretch), 1601 (aromatic C═C stretch), 1518 (aromatic C−C stretch), 1465 (C−H bend), 1269 (spiroacetal C−O stretch), 1167 (spiroacetal C−O−C stretch) (Figure 1a)

HRMS (ESI) m/z: $[M + H]^+$ calculated for $C_{29}H_{32}O_{14}$: 605.1870; found: 605.1865 (Figure S16).

2.5. General Procedure for the Synthesis of NIPUs. The NIPU polymers were prepared according to the compositions summarized in Table 1. The ratio between the cyclic carbonate(s) and Priamine 1074 was maintained at 1:1. In a 50 mL RB flask, the cyclic carbonates, Priamine 1074, and 1,5,7-triazabicyclo-[4.4.0]-dec-5-ene (10 mol %) were added and mixed under an inert atmosphere. Next, the freshly distilled *N*-methyl-2-pyrrolidinone (2 mL per g) was added.[25] The resulting solution was polymerized under continuous stirring at 80 °C for 24 h (Scheme 3). The polymers were precipitated in cold water and further purified by using dichloromethane and petroleum ether. The obtained material was named NIPU-*x*, where "*x*" represents the mole percentages of the aromatic DVS-DC, with respect to ISO−DC in the polymers.

Table 1. Molar Compositions of the Precursors Utilized in NIPU Preparation

Polymers	ISO−DC (mole ratio)	DVS-DC (mole ratio)	Priamine 1074 (mole ratio)
NIPU-0	1.0	0.0	1
NIPU-20	0.8	0.2	1
NIPU-40	0.6	0.4	1
NIPU-60	0.4	0.6	1
NIPU-80	0.2	0.8	1
NIPU-100	0.0	1.0	1

2.6. Acid Degradability of NIPUs. The acid-induced degradation of the DVS-DC monomer and NIPU polymers was examined in HCl/H_2O solution at room temperature. To carry out the experiment, 10 mg of DVS-DC was dissolved in an acetone-d_6/H_2O mixture (9:1, v/v) in NMR tubes. Subsequently, different concentrations of HCl (0.1, 1.0, and 2.0 mol/L) were added, and ^1H NMR was recorded, while samples treated with acetone-d_6/H_2O (9:1, v/v) alone served as the control. Furthermore, the degradation of NIPUs was analyzed by subjecting them (200 mg) to acid degradation in a 1 mol/L HCl solution. The degradation was monitored for 1, 7, and 14 days by measuring the percentage mass loss and by using ^1H NMR and FTIR spectroscopy.

3. RESULT AND DISCUSSION

3.1. Synthesis and Characterization of Cyclic Carbonates. In the past few years, there has been a growing demand for sustainable processes and biobased materials in developing adhesives. The quest for a more sustainable system prompted us to redesign and synthesize monomers suitable for developing NIPU adhesives that are safer to handle and degradable and have less dependency on fossil fuels. Renewable cyclic carbonate monomers derived from bioresources such as isosorbide (57.15% renewable carbon) and vanillin (79.31% renewable carbon) were synthesized and utilized for the development of sustainable NIPUs (Tables S3 and S4). Schemes 1 and 2 illustrate the synthetic pathways for vanillin and isosorbide dicarbonate monomers, respectively. The chemical structure of the prepared monomers (ISO−DC and DVS-DC) was confirmed by using ^1H, ^{13}C, and FTIR spectroscopy. FTIR analysis (Figure 1a) revealed absorption bands around 1786 cm^{-1} (ISO−DC) and 1794 cm^{-1} (DVS-DC), indicating carbonyl groups of carbonate rings,[19,26] whereas the conversion of the oxirane ring to cyclic carbonate was confirmed by the appearance of peaks associated with cyclic carbonates at 3.86−4.09, 4.31−4.52, and 4.92 ppm (Figure S4)[10] for ISO−DC and at 4.20, 4.60, and 5.01 ppm for DVS-DC (Figure S12).[27] Additionally, in the case of ISO−DC, the skeletal protons of the bicyclic ring were observed at 3.44−3.81, 4.24, and 4.66 ppm,[26] whereas in the case of DVS-DC, peaks for the acetal −CH_2 and −CH groups of the spirocyclic backbone were observed at 3.64, 3.84, 4.86, and 5.42 ppm,[28] while the methoxy and aromatic protons were identified at 3.87 and 6.92−7.06 ppm, respectively.[29] Along with ^1H NMR and FTIR, the ^{13}C NMR spectroscopy of the ISO−DC (Figure S7) and the DVS-DC (Figure S15), displayed signals at 155.36, and 154.71 ppm respectively, corresponding to the carbonyl carbon of dicarbonate compounds further supports the successful synthesis of monomers.[30,31]

3.2. Synthesis and Characterization of NIPUs. To prepare NIPUs with balanced adhesion and tunable degradation, we synthesized polymers by reacting different compositions of dicarbonate monomers with Priamine in the presence of TBD catalysts (Scheme 3). Solution polymerization was employed to ensure sufficient mixing of the components, where a minimum of about 2 mL of NMP was used as the solvent. The resulting solution was polymerized under continuous stirring at 80 °C for 24 h to prepare analogous NIPU chains. The chemical structure and composition of the polymers were confirmed by FTIR, ^1H NMR, and ^{13}C NMR spectroscopy, respectively. As shown in Figure 1b, the cyclic carbonate carbonyl band for DVS-DC and ISO−DC around 1786−1794 cm^{-1} disappeared in the formation of NIPU indicating the successful reaction of cyclic carbonate groups with diamine, leading to urethane linkages. Furthermore, NIPUs exhibited two characteristic stretching vibrations, one at 1706 cm^{-1} (strong and sharp), which is ascribed to the —C═O stretch[10,32] and the other at 3150−3600 cm^{-1} (broad), for the hydroxyl as well as the −NH stretch, which verify the formation of hydroxyurethane groups.[16,32] Additionally, new peaks were observed at 1466 cm^{-1} (N−H bending), 2856−

https://doi.org/10.1021/acsapm.4c01526
ACS Appl. Polym. Mater. 2024, 6, 11180−11192

Scheme 3. Preparation of the NIPU-Based Hot-Melt Adhesives from Isosorbide and Vanillin-Derived Cyclic Carbonates: (a) Structure of the Copolymers When two Cyclic Carbonates Were Used and (b,c) Structure of Homopolymers When Individual Monomers Were Used[a]

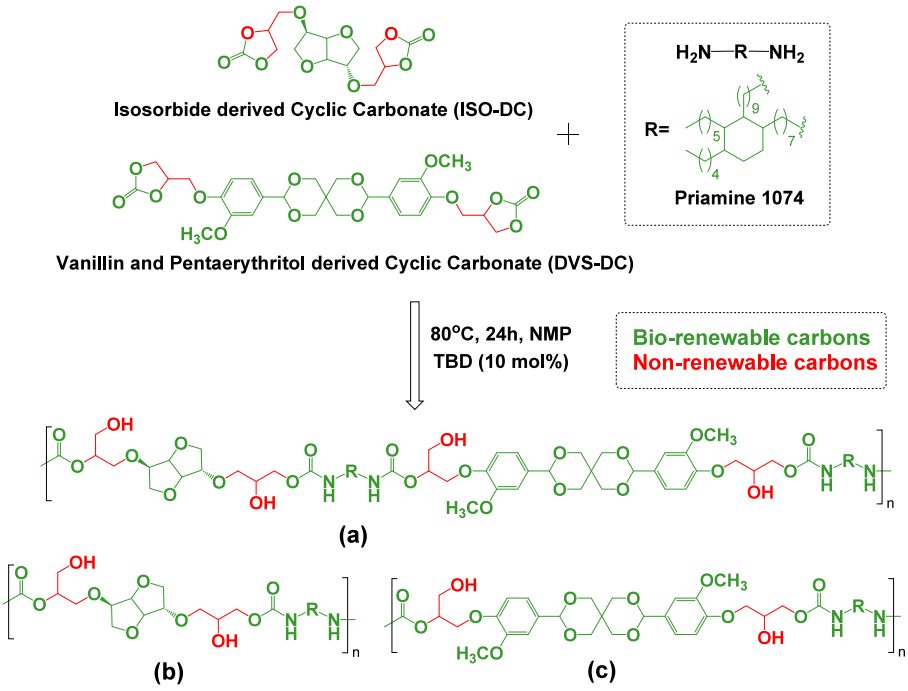

[a]The polymers were named NIPU-*x*, where "*x*" stands for the mole percentages of the aromatic DVS-DC.

2934 cm^{-1} (C−H stretches), and 1592−1638 cm^{-1} (C═C stretching of the aromatic rings), except in the case of NIPU-0.[33] Moreover, the appearance of characteristic bands at 1036, 1080, 1142 cm^{-1}, and 1210−1260 cm^{-1} can be assigned to the C−O−C and C−O stretching, respectively.[33,34]

The polymer structure was further evaluated by ^{1}H NMR analysis (Figures S17−S22), which indicated the emergence of N−H signals at 7.05−7.02 ppm[26,27] and also showed a chemical shift of the α-methylene group of primary amines from 2.61 ppm (Priamine 1074) to 3.13−3.15 ppm due to the formation of new C−N bonds, validating the formation of urethane moieties in the polymer structures.[10] Moreover, the pendant primary and secondary hydroxyl groups generated during the ring-opening reaction were detected at 3.66 and 4.90 ppm, respectively.[27] However, no significant difference in chemical shift for the backbone protons of DVS-DC and ISO−DC was observed upon polymerization, indicating that the basic chemical structure of the backbones is intact. ^{13}C NMR analysis of the polymer (Figures S23−S28) displayed new signals at 156.7 ppm for the carbonyl group of carbamate functionality,[35] and the disappearance of the carbonyl peak of the carbonate precursors at 155.4 ppm (ISO−DC) and 154.71 ppm (DVS-DC), which further supported the successful formation of NIPU thermoplastics.[30,31] Furthermore, based on the monomer composition, the signal intensity corresponding to DVS-DC and ISO−DC showed a consistent variation in the case of copolymers (Table S2). Moreover, the integral of aromatic protons of DVS-DC (signal c, c'), acetal protons of DVS-DC (signals b, b'), and bridge-head protons of ISO−DC (signal a, a') confirmed the incorporated content of DVS-DC in the polymer varied from 19 to 72 mol % (Figure S38).[36] These values were consistent with the initial monomer compositions, indicating good reactivity and stability of the monomers under the optimized polymerization conditions. Moreover, the biorenewable carbon content of these NIPUs was calculated as mentioned in Table S4 and was found to be as high as 88−90%.

3.3. Analysis of the ^{1}H NMR Recorded at Various Temperatures. It is a well-established NIPU that can engage in more hydrogen bonds than regular PUs due to the presence of pendant hydroxyl groups.[37] Studies have shown that these interactions are responsible for segmental stability in NIPUs, which positively impacts the material properties.[38,39] The presence of hydrogen bonds in the synthesized NIPU-40 was investigated using temperature-dependent ^{1}H NMR analysis at four different temperatures (30, 50, 70, and 90 °C) (Figure S29). At room temperature, the signal of the urethane −NH was not visible, as it overlaps with the signals of aromatic protons in the area 7.02−7.05 ppm. However, as the temperature increased, the signal became completely visible and moved upfield, and on cooling to 30 °C, it eventually returned to its original position. Similar shifting was observed with hydroxyl groups where the signals are observed at 3.66 ppm (primary −OH) and 4.90 ppm (secondary −OH) at 30 °C. As the temperature increased, both signals migrated to a lower chemical shift as hydrogen bonds became labile and then immediately returned to their original positions as the temperature dropped to 30 °C. These shifts of the labile protons as a function of temperature indicate that the urethane −NH and both hydroxyl groups (primary and secondary) of NIPUs were involved in the hydrogen bonding.[12]

3.4. Size Exclusion Chromatography. The molecular weight of the synthesized NIPUs was determined by employing SEC and is tabulated in Table 2. All NIPUs exhibited a monomodal distribution (Figure S30), and the molecular weight (M_n) of NIPUs varied between 4400 and

https://doi.org/10.1021/acsapm.4c01526
ACS Appl. Polym. Mater. 2024, 6, 11180−11192

Table 2. Molecular Weight Distribution and Thermal Properties of the NIPUs

	SEC			DSC	TGA	
Polymers	M_n (g/mol)	M_w (g/mol)	$Đ$	T_g (°C)	$T_{d,\ 10\%}$ (°C)[a]	Char yield (%)[b]
NIPU-0	6000	10 400	1.73	4	293	0.58
NIPU-20	4400	7800	1.77	10	305	1.96
NIPU-40	6400	10 500	1.64	17	303	3.35
NIPU-60	5100	9600	1.90	30	315	4.40
NIPU-80	6500	11 800	1.80	36	328	5.28
NIPU-100	6100	10 200	1.58	43	335	5.86

[a]$T_{d,\ 10\%}$ values denote the temperatures at which polymeric materials have lost, respectively, 10% weights of their initial mass. [b]Char yield determined at 600 °C.

6500 g·mol^{-1} with dispersity ranging from 1.58 to 1.90, which is usual for the step-growth polyaddition reaction.[8]

3.5. Thermal Properties. The thermal transitions of the NIPUs were analyzed by differential scanning calorimetry (DSC) and thermogravimetric analysis (TGA). As can be seen from Figure 2a, the second heating curves of all NIPUs lack a

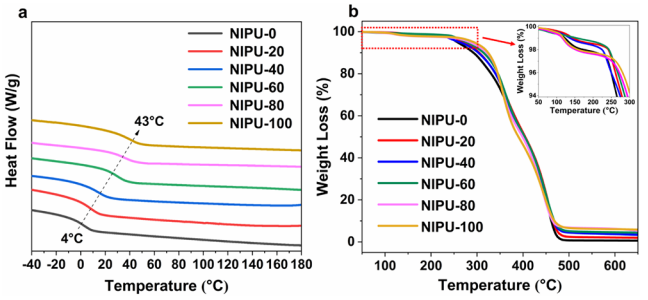

Figure 2. (a) Overlay of the DSC cycles (second heating) and (b) TGA thermograms of the NIPU series.

distinctive melting peak, indicating the amorphous nature. Moreover, only a T_g was observed in DSC for all NIPU copolymers, despite their polymeric backbone being composed of two structurally different dicarbonates (DVS-DC and ISO–DC), indicating good uniformity and better phase mixing behavior in all polymers.[12] As expected, NIPU-0 exhibited a lower T_g of 4 °C, whereas T_g values increased linearly with spiro-aromatic addition, revealing a maximum value of 43 °C for NIPU-100 (Table 2). The improvement in T_g with the addition of DVS-DC can be attributed to the fact that their polymeric matrix comprises less free space due to their backbone's high stiffness, accounting for the restricted mobility of polymer chains.[40,41]

The thermal stability of the prepared NIPUs was examined by TGA under a nitrogen atmosphere, and their corresponding thermograms and decomposition temperature ($T_{d,\ 10\%}$) of the polymers are shown in Figure 2b and Table 2, respectively. The NIPUs developed from isosorbide- and vanillin-derived building blocks showed excellent thermal stability. The $T_{d,\ 10\%}$ values were in the range of 293–335 °C. These $T_{d,\ 10\%}$ values were comparable to or even higher than those of similar NIPU systems.[10,31,42] Furthermore, the thermal stability of NIPUs was found to increase as the DVS-DC content in the polymer chain increased, which in turn can be attributed to the incorporation of the high molar proportion of the rigid aromatic content in the backbone. In DTG curves of NIPUs (Figure S31) indicated two distinct stages of degradation. The first stage degradation between 295 and 400 °C can be attributed to the breakdown of urethane linkages,[43,44] while the decomposition of the other hydrocarbon framework.[44,45] where observed in the second stage between the 400–500 °C range. Moreover, the char yield of the NIPUs was determined at 600 °C and found to be in the range of 0.58 to 5.86% (Table 2). The char yield was also found to enhance with increased incorporation of the spiro-aromatic content in NIPUs, which is indicative of the improved thermal stability upon the incorporation of a rigid aromatic skeleton.[46]

3.6. Water Contact Angle Measurements. The surface wettability of the NIPU films was analyzed by the water contact angle (WCA), and the values obtained are summarized in Table S1 (Figure S32a). The WCA of the NIPU polymers varied in the range of 93.9° ± 1.5° to 105.9° ± 0.9° exhibiting a hydrophobic nature. The hydrophobic nature of these films can be attributed to the strong water-repellent properties of the Priamine architecture due to the long aliphatic backbone and two-pendant alkyl chains.[47,48] However, the WCA changed from 105.9° ± 0.9° to 93.9° ± 1.5° after increasing the molar composition of DVS-DC in NIPUs. The enhanced wettability of films arises from the increase in the concentration of the polar methoxy groups in the polymer architecture, which raises the surface free energy.[49]

3.7. X-Ray Diffraction Spectroscopy. To address the molecular structure and chain arrangement of a polymer, powder X-ray diffraction (XRD) was performed. The XRD results demonstrate that all samples show a broad diffraction peak located within a 2θ range of 12.5° to 27.5° (Figure S32b), indicating the formation of an amorphous phase.[12,50] The amorphous nature of NIPUs can be attributed to the presence of pendant primary and secondary hydroxyl groups, which disrupts the regular packing of polymer chains due to the formation of hydrogen bonds with urethane groups.[39] These results are consistent with DSC findings, as they do not exhibit a melting transition due to the absence of long-range order (Figure 2a).

3.8. Rheological Measurements. To elucidate the effect of molecular composition on the viscoelastic behavior of NIPUs, rheological experiments were performed. Strain (2.5%) within the LVR region was further applied for the frequency sweep and temperature ramp measurements (Figure S33a). Figure 3a exhibits the plot of storage (G') and loss modulus (G'') as a function of frequency for all NIPUs. The NIPU-40 had the highest G' value, indicating higher viscosity compared to other compositions, which is in agreement with the plot of complex viscosity (mean of five values as shown in Figure

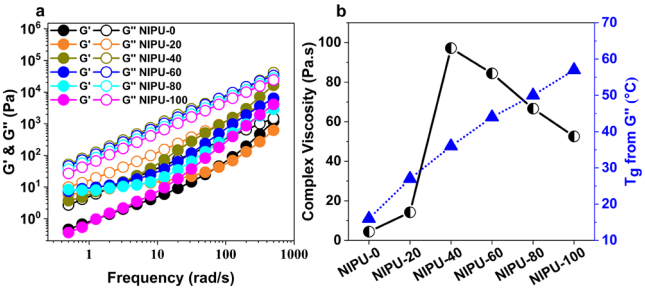

Figure 3. (a) Plot of storage and loss modulus vs angular frequency. (b) Complex viscosity and T_g values obtained from the frequency and temperature sweep measurements, respectively.

https://doi.org/10.1021/acsapm.4c01526
ACS Appl. Polym. Mater. 2024, 6, 11180–11192

S34a) presented in Figure 3b. This enhanced viscosity could be attributed to the synergetic effect of the high density of noncovalent interactions (hydrogen bonds and $\pi-\pi$ interactions), as well as the ordered arrangement of the cycloaliphatic and spiro-aromatic segments present in NIPU-40 (Figure 6).[12,13] As expected, the lowest G'' and complex viscosity were noted for NIPU-0, revealing the absence of $\pi-\pi$ interactions due to the lack of aromatic segments. Moreover, the loss modulus of the synthesized samples follows the trend of NIPU-40 > NIPU-60 > NIPU-80 > NIPU-100 > NIPU-20 > NIPU-0. This may be attributed to the higher segmental stability, supported locally by inter and/or intra-molecular hydrogen bonds formed between primary and secondary hydroxyl groups and urethane linkages of NIPUs.[12] It is interesting to note that except in the case of NIPU-0, the crossover ($G' \approx G''$) points of all other compositions are higher than the measured frequency range. As relaxation time (ω_c) is the reciprocal of the crossover frequency, NIPU-0 possessing negligible noncovalent interaction exhibited the highest relaxation time as compared with other compositions, which is indicative of the lower cohesive force within the polymer chains.[51]

Temperature sweep experiments were conducted to gather more information about the thermal transition of thermoplastic polymers. Figure S33b–d shows the temperature dependence of storage modulus (G'), loss modulus (G''), and tan δ of the NIPUs. The T_g is determined from G'' curves (range of 16 to 57 °C) and is plotted in Figure 3b. These values are in agreement with DSC results, which increased with increasing spiro-aromatic contents. The NIPU-0 exhibited the lowest T_g value (16 °C), while NIPU-100 displayed the highest T_g value (57 °C).

3.9. Adhesive Properties. The application potential of the developed NIPUs as sustainable adhesives was studied by a lap shear test according to the ASTM D1002 standard by directly sandwiching NIPU films between two aluminum joints by thermal treatment (Figure 4a). As displayed in Figures 4b and S35 (Table S1), the shear strength of NIPUs varied between 0.09 and 6.39 MPa based on the monomer composition. A gradual increment in adhesive properties was observed up to 40 mol % of the DVS-DC monomer incorporation in NIPU polymers, above which the adhesion performances declined with the increment in the DVS-DC content. Interestingly, NIPU-40 (40 mol % of the DVS-DC monomer) exhibited higher adhesion strength, up to 6.39 ± 0.39 MPa, representing a 71% increment in strength compared to NIPU-0. Moreover, the adhesive strength expressed by NIPU-40 was much higher than the previously reported results of biobased NIPU hot-melt adhesives.[19−21]

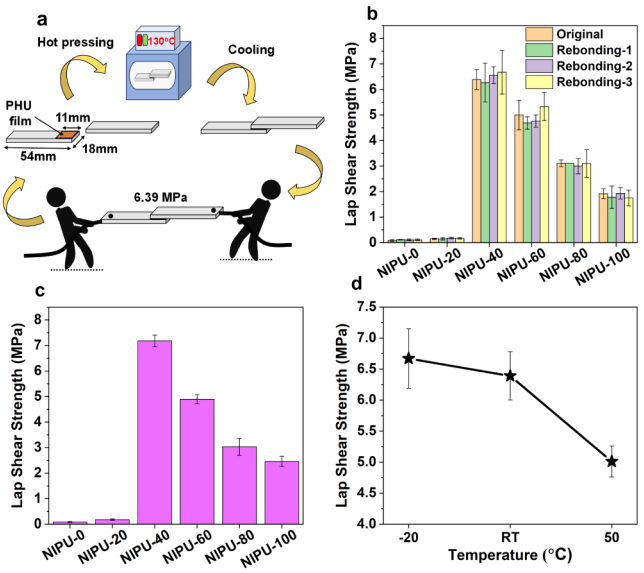

Figure 4. (a) Schematic diagram of the bonding of NIPU adhesives to the aluminum substrate. (b) Original and recycled lap shear strength of NIPU hot melt adhesives assessed on aluminum. (c) Adhesive strength after water soaking for 12 h and (d) Lap shear strength of NIPU-40 at different temperatures.

The improved adhesion property exhibited by NIPU-40 can be concluded to be a synergetic effect arising from noncovalent interactions (hydrogen bonds and $\pi-\pi$ interactions) and can also be attributed to the balanced behavior of the cycloaliphatic and spiro-aromatic segments present in NIPU-40 (Figure 6).[12,13] Further results analyzed by rheological measurements support the improved adhesion exhibited, as high viscosity was observed in the case of NIPU-40, which supports better noncovalent interactions within the network (Figure S34). However, the NIPU-0 and NIPU-20 without or with lower aromatic content exhibited low adhesive strength, indicating the absence of or negligible $\pi-\pi$ interactions, respectively (leading to cohesive failure). However, it was observed that an increment in the incorporation of spiro-aromatic dicarbonate in NIPU-60, NIPU-80, and NIPU-100 leads to decreased adhesive strength. The reduction in adhesive strength can be attributed to the increased steric hindrance caused by aromatic rings, which leads to the disruption of the ordered packing of chain segments and the pattern of noncovalent interactions. Finally, the failure nature of the specimens was examined. It was identified that the mixture of cohesive and adhesive failure occurred in all polymer films except in the case of NIPU-0 and NIPU-20 (Figure S36). Particularly, NIPU-0 and NIPU-20 exhibited cohesive failure (Figure S36a,b).[10]

To explore the robustness of the developed NIPU adhesives thermo-reversible adhesion properties, the temperature tolerance of adhesives and their adhesion performance under wet conditions were explored. The thermoreversible adhesion nature of NIPUs was investigated by repeatedly bonding and debonding of adhesive joints three times. The results showed that almost identical adhesive strengths were observed during the consecutive reuses, which indicates the excellent thermoreversibility of the synthesized adhesives. Upon temperature tolerance adhesion studies, the NIPU adhesive exhibited excellent adherence at low temperatures (−20 °C) and only a slight drop in shear strength (%) at high temperatures (50 °C), indicative of the adhesive applicability for a broad range of temperatures (Figure 4d). The NIPUs also exhibited good adhesion properties even after immersing in deionized water for 12 h (Figure S37). As shown in Figure 4c (Table S1), all NIPU samples retained their original strength after soaking in water, showing the superior adhesion stability and applicability of the material under different conditions. Moreover, the visualization of the remarkable adhesion strength of NIPU-40 can be observed in Figure 5a, where the bonded aluminum slides held over 100 kg of weight. Furthermore, upon a detailed comparison of reported NIPU hot-melt adhesives, it was found that the synthesized NIPU-40 showcased notable adhesion properties and had a high biocontent (Figure 5b). This suggests that it could be a

https://doi.org/10.1021/acsapm.4c01526
ACS Appl. Polym. Mater. 2024, 6, 11180−11192

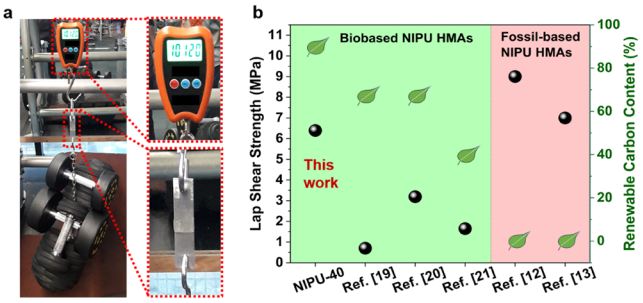

Figure 5. (a) Two aluminum joints bonded by NIPU-40 held 100 kg of weight. (b) Lap shear strength of NIPU-40 compared against thermoplastic NIPU-based hot-melt adhesives reported in the literature.

promising candidate for use in various applications that demand robust and environmentally friendly adhesives.

3.10. Mechanical Properties. The stress−strain curves of NIPUs synthesized by varying the molar composition of dicarbonate/priamine monomers are displayed in Figure 7, and the data are summarized in Table 3. These developed NIPUs were found to have extremely adaptable mechanical properties. NIPU-0 showed considerably inferior modulus, and tensile properties due to the absence of a rigid spiro-aromatic moiety. However, the introduction of DVS-DC in the polymer chain improved the mechanical properties of NIPUs. The observed change in the mechanical properties can be attributed to the incorporation of rigid segments (DVS-DC) leading to restricted mobility of the chains, resulting in a positive impact on the modulus as well as tensile strength values whereas a reduction in elongation.[52,53] These values are considerably higher than those of previously reported thermoplastic NIPUs.[38,39,54,55]

3.11. Acid Degradability of NIPUs. Degradation profiles of the DVS-DC and NIPUs were analyzed as they contained a susceptible acetal group, which is well-known to undergo hydrolysis under acidic conditions.[36,57] The study initially focused on examining the breakdown of the DVS-DC monomer in the presence of acid at room temperature by using ^{1}H NMR. Three different concentrations of HCl (0.1, 1.0, and 2.0 mol/L) were utilized, and the degradation was observed at different time intervals (Figure S40). ^{1}H NMR analysis revealed that the DVS-DC monomer exhibited faster

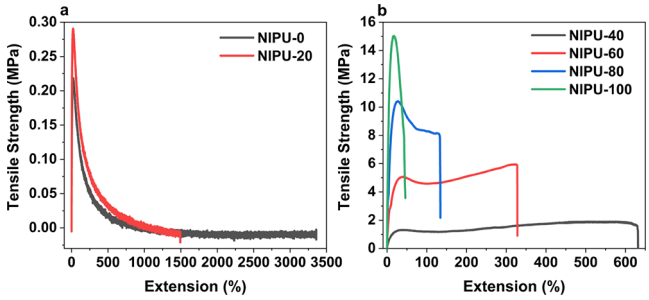

Figure 7. Tensile test curves (stress−strain) of (a) NIPU-0 and NIPU-20, and (b) NIPU-40, NIPU-60, NIPU-80, and NIPU-100.

Table 3. Mechanical Properties and Renewable Carbon Contents of the NIPU Samples

	Tensile Properties			
Polymers	Young's modulus (MPa)	Tensile strength (MPa)	Elongation at break (%)	RCC (%)[a]
NIPU-0	1.22 ± 0.17	0.21 ± 0.01	>2000	88.00
NIPU-20	4.76 ± 0.42	0.27 ± 0.02	1493 ± 395	88.67
NIPU-40	13.54 ± 1.1	1.87 ± 0.30	686 ± 42	89.28
NIPU-60	51.10 ± 2.4	5.11 ± 0.30	312 ± 37	89.83
NIPU-80	151.38 ± 8.0	10.48 ± 0.38	148 ± 10	90.32
NIPU-100	254.07 ± 25	14.56 ± 1.9	59 ± 20	90.76

[a]Renewable carbon content (Tables S3 and S4).[56]

degradation as the HCl concentration increased and afforded a darker solution on degradation (Figures S40 and S41a,b). Compared to the control, samples treated with HCl expressed a reduction in the integration values of the acetal peak at 5.81 ppm (peak 'a') and new intense signals were observed at 9.88 ppm (peak 'b')[58,59] and 3.53−3.72 ppm (peak 'c') . These observations indicate the decomposition of the characteristic acetal bond into aldehyde and pentaerythritol compounds , respectively (Figure S41d). It took 120 h for the complete hydrolysis of the acetal linkage in DVS-DC when treated with 0.1 mol/L HCl, whereas treatment with 1 and 2 mol/L HCl resulted in the complete hydrolysis of the acetal group within 5 h. Furthermore, the potential breakdown products are vanillin

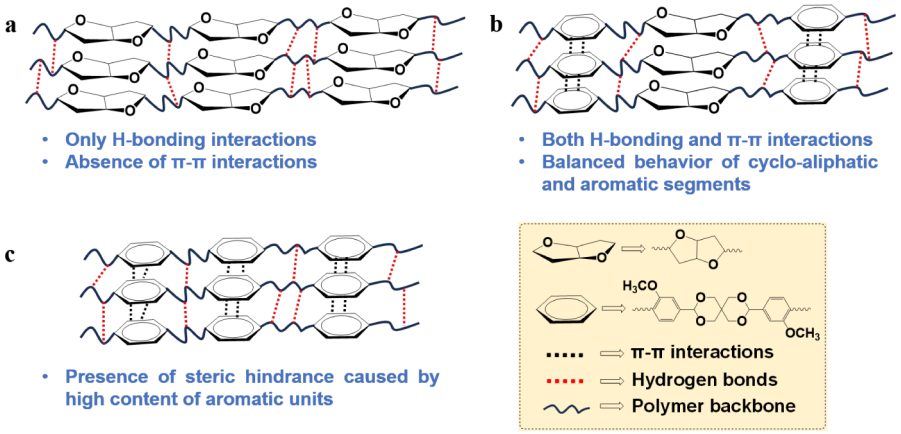

Figure 6. Schematic representation of the possible noncovalent interactions and structural arrangement of cycloaliphatic and aromatic segments in (a) NIPU-0, (b) NIPU-40, and (c) NIPU-100.

https://doi.org/10.1021/acsapm.4c01526
ACS Appl. Polym. Mater. 2024, 6, 11180−11192

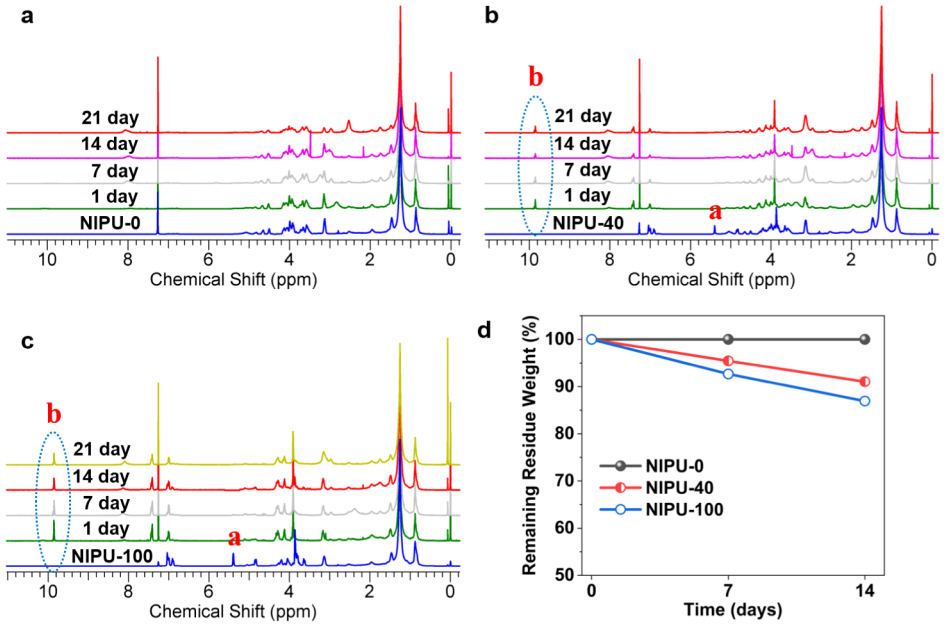

Figure 8. ^{1}H NMR spectra of (a) NIPU-0, (b) NIPU-40, and (c) NIPU-100, before and after degradation (1 mol/L HCl). (d) Weight loss of the NIPUs over different times (under 1 mol/L HCl).

monocarbonate and pentaerythritol, which was confirmed through ^{1}H NMR of the fully decomposed monomer in HCl (1.0 mol/L samples for 5 h) (Figure S39).

Furthermore, the degradation assessment of NIPU-0, NIPU-40, and NIPU-100 samples was analyzed by immersing them in acid solutions (1 mol/L HCl; Figure S42), and their decomposition process was monitored over different periods (1, 7, 14, and 21 days) using ^{1}H NMR and FTIR techniques. NIPU-40 and NIPU-100 samples, which have a significant content of spiro-aromatic monomer, showed complete disappearance of the acetal peak at 5.40 ppm (peak 'a') and the emergence of a new −CHO peak at 9.86 ppm (peak 'b') within 24 h (Figure 8b,c). This indicates the formation of aldehyde functional oligomers and pentaerythritol as a possible degradation product, which clearly demonstrates that NIPUs containing acetal linkages are susceptible to degradation in acidic environments. However, NIPU-0 devoid of acetal linkage did not exhibit any signs of degradation, even after 21 days of treatment with HCl (Figure 8a). Further FTIR analysis of samples showed that NIPU-100 had visible absorbance of −CHO groups at 1680 cm^{-1}, but not in the case of NIPU-0 and NIPU-40 due to their lack or lower of spiro-aromatic content, respectively (Figure S43).

To assess the degradation effect in NIPU samples, the change in mass was measured under 1 mol/L HCl after 7 and 14 days (Figure 8d). NIPU-100 with higher acetal linkages was more prone to weight loss with a percent mass loss of 13.07%, while NIPU-40 with fewer acetal linkages showed a mass loss of 8.96%. In contrast, NIPU-0, which lacks an acetal linkage, did not exhibit any change in mass loss after 14 days of degradation studies. The results indicated that the percentage of mass loss in the NIPU samples corresponded directly to the number of acetal linkages present in them.

4. CONCLUSION

In summary, as a possible alternative to conventional petroleum-based hot-melt adhesives, we successfully constructed a reusable biobased HMA with a biorenewable carbon content of >88%, biodegradability, excellent reusability, and superior adhesive nature. Two biobased cyclic carbonates with high renewable carbon content were synthesized from vanillin and isosorbide, and these monomers were used to prepare NIPU-HMAs with finely tailored physicomechanical properties by step-growth polyaddition. In addition, the structure−property relationship and influence of the monomer composition on the mechanical and thermal properties of the obtained NIPUs were studied in detail. NIPU-HMAs presented excellent mechanical performance including a high adhesion strength, thermo-reversible adhesion properties, good temperature tolerance, and adhesion under wet conditions. The enhanced properties of HMAs were attributed to the synergetic effect of the high density of noncovalent interactions (hydrogen bonds and $\pi-\pi$ interactions), as well as the arrangement of the cycloaliphatic and spiro-aromatic segments. Furthermore, the unique rigid spirocyclic acetal molecular architecture of DVS-DC makes them ideal for enabling facile selective acidic hydrolysis and aiding chemical degradability. Our diligent efforts have paved a pathway in the development of sustainable and environmentally friendly NIPUs with good adhesive and potential degradation properties.

■ ASSOCIATED CONTENT

Data Availability Statement

All of the analysis results are available in this manuscript and in the supplementary document. This work is protected under the Indian patent application number 202311042903.

Supporting Information

The Supporting Information is available free of charge at https://pubs.acs.org/doi/10.1021/acsapm.4c01526.

FTIR, ^{1}H/^{13}C NMR, HRMS data of ISO−DC and DVS-DC compounds; ^{1}H and ^{13}C NMR data of all NIPUs; ^{1}H NMR of NIPU-40 taken at different temperatures; SEC traces, DTG curves, contact angle, XRD profiles, and rheological measurements of NIPU polymers; failure images, and force vs displacement

https://doi.org/10.1021/acsapm.4c01526
ACS Appl. Polym. Mater. 2024, 6, 11180−11192

curves of adhesive joints; calculations for the incorporated mole percentage of dicarbonates in the final NIPUs; calculations for determining the renewable carbon content of dicarbonates and NIPUs; experimental photographs as well as ^{1}H NMR and FTIR data of degradation studies (PDF)

AUTHOR INFORMATION

Corresponding Author

Kiran Sukumaran Nair − *Polymer Science and Engineering Division, CSIR-National Chemical Laboratory, Pune MH-411008, India; Academy of Scientific and Innovative Research (AcSIR), Ghaziabad 201002, India;* orcid.org/0000-0001-6117-2840; Email: s.kiran@ncl.res.in

Authors

Gorakh Hiraman Ghuge − *Polymer Science and Engineering Division, CSIR-National Chemical Laboratory, Pune MH-411008, India; Academy of Scientific and Innovative Research (AcSIR), Ghaziabad 201002, India*

Arun Torris − *Polymer Science and Engineering Division, CSIR-National Chemical Laboratory, Pune MH- 411008, India;* orcid.org/0000-0003-4487-2604

Complete contact information is available at: https://pubs.acs.org/10.1021/acsapm.4c01526

Author Contributions

G.H.G. contributed to: conceptualization, methodology, project administration, data curation, formal analysis, and writing—original draft. A.T. contributed to the rheological studies K.S.N. contributed to conceptualization, resources, formal analysis, supervision, writing—review and editing, and funding acquisition.

Notes

The authors declare no competing financial interest.

ACKNOWLEDGMENTS

Mr. Gorakh H. Ghuge acknowledges the Council of Scientific & Industrial Research (CSIR), New Delhi for the Senior Research Fellowship [31/011(1116)/2019-EMR-1]. Dr. Kiran S. acknowledges the SERB for the research grant under the SRG Scheme (SRG/2020/000954). The authors would like to thank the Director of CSIR-NCL, Pune, for providing the infrastructure, and facilities to conduct this research. We express our immense gratitude to Croda, Netherlands for providing us with Priamine 1074 chemical. We are grateful to Dr. Dinesh Sawant, Dr. Aniket Talanikar, and Ms. V. K. Karthika for contributing to the adhesive studies. We are also thankful to Ms. Nita Patil for her help in conducting the high-temperature ^{1}H NMR study.

REFERENCES

(1) Dinte, E.; Sylvester, B. Adhesives: Applications and Recent Advances. *Applied Adhesive Bonding in Science and Technology*; IntechOpen, 2017, 142156. .

(2) Da Silva, L. F. M.; Ochsner, A.; Adams, R. D. *Handbook of adhesion technology*; Springer Oxford: UK.; 2018.

(3) Vineeth, S. K.; Gadhave, R. V. Sustainable Raw Materials in Hot Melt Adhesives: A Review. *Open J. Polym. Chem.* **2020**, *10*, 49−65.

(4) *Hot Melt Adhesives Market Global Forecast (2022−2027) by Type, Application, and Region*. https://www.marketsandmarkets.com/Market-Reports/hot-melt-adhesives-market-1088.html. (accessed 13 January 2024).

(5) *Polyurethane Hot Melt Adhesive Market Size, Share, and Trend Analysis Report By Type, Application, and Region- Forecast 2020−2030*https://www.straitsresearch.com/report/polyurethane-hot-melt-adhesive-market. (accessed 13 January 2024).

(6) Sardon, H.; Pascual, A.; Mecerreyes, D.; Taton, D.; Cramail, H.; Hedrick, J. L. Synthesis of Polyurethanes Using Organocatalysis: A Perspective. *Macromolecules* **2015**, *48* (10), 3153−3165.

(7) Lockey, J. E.; Redlich, C. A.; Streicher, R.; Pfahles-Hutchens, A.; Hakkinen, P. J.; Ellison, G. L.; Harber, P.; Utell, M.; Holland, J.; Comai, A.; White, M. Isocyanates and Human Health: Multi-stakeholder Information Needs and Research Priorities. *J. Occup. Environ. Med.* **2015**, *57* (1), 44−51.

(8) Maisonneuve, L.; Lamarzelle, O.; Rix, E.; Grau, E.; Cramail, H. Isocyanate-Free Routes to Polyurethanes and Poly(Hydroxy Urethane)S. *Chem. Rev.* **2015**, *115* (22), 12407−12439.

(9) Gomez-Lopez, A.; Grignard, B.; Calvo, I.; Detrembleur, C.; Sardon, H. Accelerating the Curing of Hybrid Poly(Hydroxy Urethane)-Epoxy Adhesives by the Thiol-Epoxy Chemistry. *ACS Appl. Polym. Mater.* **2022**, *4* (12), 8786−8794.

(10) Gomez-Lopez, A.; Grignard, B.; Calvo, I.; Detrembleur, C.; Sardon, H. Monocomponent Non-Isocyanate Polyurethane Adhesives Based on a Sol−Gel Process. *ACS Appl. Polym. Mater.* **2020**, *2* (5), 1839−1847.

(11) Gomez-Lopez, A.; Grignard, B.; Calvo, I.; Detrembleur, C.; Sardon, H. Synergetic Effect of Dopamine and Alkoxysilanes in Sustainable Non-Isocyanate Polyurethane Adhesives. *Macromol. Rapid Commun.* **2021**, *42* (3), 2000538.

(12) Sukumaran Nair, A.; Cherian, S.; Balachandran, N.; Panicker, U. G.; Kalamblayil Sankaranarayanan, S. K. Hybrid Poly(Hydroxy Urethane)s: Folded-Sheet Morphology and Thermoreversible Adhesion. *ACS Omega* **2019**, *4* (8), 13042−13051.

(13) Gomez-Lopez, A.; Ayensa, N.; Grignard, B.; Irusta, L.; Calvo, I.; Müller, A. J.; Detrembleur, C.; Sardon, H. Enhanced and Reusable Poly(Hydroxy Urethane)-Based Low Temperature Hot-Melt Adhesives. *ACS Polym. Au.* **2022**, *2* (3), 194−207.

(14) Panchireddy, S.; Grignard, B.; Thomassin, J. M.; Jerome, C.; Detrembleur, C. Bio-Based Poly(Hydroxyurethane) Glues for Metal Substrates. *Polym. Chem.* **2018**, *9* (19), 2650−2659.

(15) Cornille, A.; Michaud, G.; Simon, F.; Fouquay, S.; Auvergne, R.; Boutevin, B.; Caillol, S. Promising Mechanical and Adhesive Properties of Isocyanate-Free Poly(Hydroxyurethane). *Eur. Polym. J.* **2016**, *84*, 404−420.

(16) Panchireddy, S.; Grignard, B.; Thomassin, J.-M.; Jerome, C.; Detrembleur, C. Catechol Containing Polyhydroxyurethanes as High-Performance Coatings and Adhesives. *ACS Sustainable Chem. Eng.* **2018**, *6* (11), 14936−14944.

(17) Panchireddy, S.; Thomassin, J. M.; Grignard, B.; Damblon, C.; Tatton, A.; Jerome, C.; Detrembleur, C. Reinforced Poly-(Hydroxyurethane) Thermosets as High Performance Adhesives for Aluminum Substrates. *Polym. Chem.* **2017**, *8* (38), 5897−5909.

(18) Anitha, S.; Vijayalakshmi, K. P.; Unnikrishnan, G.; Kumar, K. S. S. CO2 Derived Hydrogen Bonding Spacer: Enhanced Toughness, Transparency, Elongation and Non-Covalent Interactions in Epoxy-Hydroxyurethane Networks. *J. Mater. Chem. A* **2017**, *5* (46), 24299−24313.

(19) Tryznowski, M.;´widerska, A.; Gołofit, T.; Zołek-Tryznowska, Z. Wood Adhesive Application of Poly(Hydroxyurethane)s Synthesized with a Dimethyl Succinate-Based Amide Backbone. *RSC Adv.* **2017**, *7* (48), 30385−30391.

(20) Tryznowski, M.; Gołofit, T.; Swiderska, A. Poly (Hydroxyurethane)s with Diethyl Tartrate-Based Amide Backbone by an Isocyanate-Free Route: Use As Adhesives. *Polymer* **2018**, *144*, 1−6.

(21) Ghuge, G. H.; Kambikanam, K. V.; Nair, K. S. Evaluation of the Adhesive Properties of Vanillin-Derived Polyhydroxy Urethanes. *J. Appl. Polym. Sci.* **2023**, *140*, 1−11.

(22) Lkaszczyk, J.; Janicki, B.; López, A.; Skołucka, K.; Wojdyła, H.; Persson, C.; Piaskowski, S.;´miga-Matuszowicz, M. Novel Injectable

Biomaterials for Bone Augmentation Based on Isosorbide Dimethacrylic Monomers. *Mater. Sci. Eng.: C* **2014**, *40*, 76−84.
(23) Lorenzini, C.; Versace, D. L.; Gaillet, C.; Lorthioir, C.; Boileau, S.; Renard, E.; Langlois, V. Hybrid Networks Derived from Isosorbide by Means of Thiol-Ene Photoaddition and Sol-Gel Chemistry. *Polymer* **2014**, *55* (17), 4432−4440.
(24) Ma, S.; Wei, J.; Jia, Z.; Yu, T.; Yuan, W.; Li, Q.; Wang, S.; You, S.; Liu, R.; Zhu, J. Readily Recyclable, High-Performance Thermosetting Materials Based on a Lignin-Derived Spiro Diacetal Trigger. *J. Mater. Chem. A* **2019**, *7* (3), 1233−1243.
(25) Dong, W.; Yoshida, Y.; Endo, T. Synthesis of Poly(Hydroxyurethane) from 5-Membered Cyclic Carbonate under Mild Conditions in the Presence of Bicyclic Guanidine and Their Reaction Process. *J. Polym. Sci.* **2021**, *59* (6), 502−509.
(26) Besse, V.; Auvergne, R.; Carlotti, S.; Boutevin, G.; Otazaghine, B.; Caillol, S.; Pascault, J. P.; Boutevin, B. Synthesis of Isosorbide Based Polyurethanes: An Isocyanate Free Method. *React. Funct. Polym.* **2013**, *73* (3), 588−594.
(27) Ménard, R.; Caillol, S.; Allais, F. Chemo-Enzymatic Synthesis and Characterization of Renewable Thermoplastic and Thermoset Isocyanate-Free Poly(Hydroxy)Urethanes from Ferulic Acid Derivatives. *ACS Sustainable Chem. Eng.* **2017**, *5* (2), 1446−1456.
(28) Warlin, N.; Garcia Gonzalez, M. N.; Mankar, S.; Valsange, N. G.; Sayed, M.; Pyo, S. H.; Rehnberg, N.; Lundmark, S.; Hatti-Kaul, R.; Jannasch, P.; Zhang, B. A Rigid Spirocyclic Diol from Fructose-Based 5-Hydroxymethylfurfural: Synthesis, Life-Cycle Assessment, and Polymerization for Renewable Polyesters and Poly(Urethane-Urea)S. *Green Chem.* **2019**, *21* (24), 6667−6684.
(29) Zhao, D.; Liang, X.; Wang, J.; Du, J.; Zhu, Y. Vanillin-Based Degradable Polyurethane Thermosets Demonstrating High Bio-Content and Mechanical Properties. *ACS Appl. Polym. Mater.* **2023**, *5* (6), 4536−4545.
(30) Mokhtari, C.; Malek, F.; Manseri, A.; Caillol, S.; Negrell, C. Reactive Jojoba and Castor Oils-Based Cyclic Carbonates for Biobased Polyhydroxyurethanes. *Eur. Polym. J.* **2019**, *113*, 18−28.
(31) Kathalewar, M.; Sabnis, A.; D'Mello, D. Isocyanate Free Polyurethanes from New CNSL Based Bis-Cyclic Carbonate and Its Application in Coatings. *Eur. Polym. J.* **2014**, *57*, 99−108.
(32) Hu, S.; Chen, X.; Torkelson, J. M. Biobased Reprocessable Polyhydroxyurethane Networks: Full Recovery of Crosslink Density with Three Concurrent Dynamic Chemistries. *ACS Sustainable Chem. Eng.* **2019**, *7* (11), 10025−10034.
(33) Ummadisetti, C.; Rachapudi, B. N. P.; Bethala, L. A. P. D. Glycerol-Based SO3H-Carbon Catalyst: A Green Recyclable Catalyst for the Chemoselective Synthesis of Pentaerythritol Diacetals. *Eur. J. Chem.* **2014**, *5* (3), 536−540.
(34) Mankar, S. V.; Gonzalez, M. N. G.; Warlin, N.; Valsange, N. G.; Rehnberg, N.; Lundmark, S.; Jannasch, P.; Zhang, B. Synthesis, Life Cycle Assessment, and Polymerization of a Vanillin-Based Spirocyclic Diol toward Polyesters with Increased Glass-Transition Temperature. *ACS Sustainable Chem. Eng.* **2019**, *7* (23), 19090−19103.
(35) Tryznowski, M.; ˙ołek-Tryznowska, Z. Surface Properties of Poly(Hydroxyurethane)s Based on Five-Membered BIS-Cyclic Carbonate of Diglycidyl Ether of Bisphenol A. *Materials* **2020**, *13* (22), 5184.
(36) Mankar, S. V.; Wahlberg, J.; Warlin, N.; Valsange, N. G.; Rehnberg, N.; Lundmark, S.; Jannasch, P.; Zhang, B. Short-Loop Chemical Recycling via Telechelic Polymers for Biobased Polyesters with Spiroacetal Units. *ACS Sustainable Chem. Eng.* **2023**, *11* (13), 5135−5146.
(37) Blain, M.; Cornille, A.; Boutevin, B.; Auvergne, R.; Benazet, D.; Andrioletti, B.; Caillol, S. Hydrogen Bonds Prevent Obtaining High Molar Mass PHUs. *J. Appl. Polym. Sci.* **2017**, *134* (45), 44958.
(38) Hu, S.; Chen, X.; Torkelson, J. M. Isocyanate-Free, Thermoplastic Polyhydroxyurethane Elastomers Designed for Cold Temperatures: Influence of PDMS Soft-Segment Chain Length and Hard-Segment Content. *Polymer* **2022**, *256*, 125251.
(39) Leitsch, E. K.; Beniah, G.; Liu, K.; Lan, T.; Heath, W. H.; Scheidt, K. A.; Torkelson, J. M. Nonisocyanate Thermoplastic Polyhydroxyurethane Elastomers via Cyclic Carbonate Aminolysis: Critical Role of Hydroxyl Groups in Controlling Nanophase Separation. *ACS Macro Lett.* **2016**, *5* (4), 424−429.
(40) Chantawansri, T. L.; Yeh, I. C.; Hsieh, A. J. Investigating the Glass Transition Temperature at the Atom-Level in Select Model Polyamides: A Molecular Dynamics Study. *Polymer* **2015**, *81*, 50−61.
(41) Aharoni, S. M. Molecular Stiffness and Thermal Properties of Polymers. *J. Appl. Polym. Sci.* **1976**, *20* (10), 2863−2869.
(42) Sheng, X.; Ren, G.; Qin, Y.; Chen, X.; Wang, X.; Wang, F. Quantitative Synthesis of Bis(Cyclic Carbonate)s by Iron Catalyst for Non-Isocyanate Polyurethane Synthesis. *Green Chem.* **2015**, *17* (1), 373−379.
(43) Farhadian, A.; Ahmadi, A.; Omrani, I.; Miyardan, A. B.; Varfolomeev, M. A.; Nabid, M. R. Synthesis of Fully Bio-Based and Solvent Free Non-Isocyanate Poly (Ester Amide/Urethane) Networks with Improved Thermal Stability on the Basis of Vegetable Oils. *Polym. Degrad. Stab.* **2018**, *155*, 111−121.
(44) Ling, Z.; Zhang, C.; Zhou, Q. Synthesis and Characterization of 1 K Waterborne Non-Isocyanate Polyurethane Epoxy Hybrid Coating. *Prog. Org. Coat.* **2022**, *169*, 106915.
(45) Duval, C.; Kébir, N.; Jauseau, R.; Burel, F. Organocatalytic Synthesis of Novel Renewable Non-Isocyanate Polyhydroxyurethanes. *J. Polym. Sci., Part A: polym. Chem.* **2016**, *54* (6), 758−764.
(46) Ecochard, Y.; Leroux, J.; Boutevin, B.; Auvergne, R.; Caillol, S. From Multi-Functional Siloxane-Based Cyclic Carbonates to Hybrid Polyhydroxyurethane Thermosets. *Eur. Polym. J.* **2019**, *120*, 109280.
(47) Wołosz, D.; Fage, A. M.; Parzuchowski, P. G.; ´widerska, A.; Brüll, R. Reactive Extrusion Synthesis of Biobased Isocyanate-Free Hydrophobically Modified Ethoxylated Urethanes with Pendant Hydrophobic Groups. *ACS Sustainable Chem. Eng.* **2022**, *10* (35), 11627−11640.
(48) Younes, G. R.; Maric, M. Increasing the Hydrophobicity of Hybrid Poly(Propylene Glycol)-Based Polyhydroxyurethanes by Capping with Hydrophobic Diamine. *Ind. Eng. Chem. Res.* **2021**, *60* (22), 8159−8171.
(49) Wenzl, I.; Yam, C. M.; Barriet, D.; Lee, T. R. Structure and Wettability of Methoxy-Terminated Self-Assembled Monolayers on Gold. *Langmuir* **2003**, *19* (24), 10217−10224.
(50) Ke, J.; Li, X.; Wang, F.; Jiang, S.; Kang, M.; Wang, J.; Li, Q.; Wang, Z. Non-Isocyanate Polyurethane/Epoxy Hybrid Materials with Different and Controlled Architectures Prepared from a CO2-Sourced Monomer and Epoxy via an Environmentally-Friendly Route. *RSC Adv.* **2017**, *7* (46), 28841−28852.
(51) Novikov, M. B.; Gdalin, B. E.; Anosova, J. V.; Feldstein, M. M. Stress Relaxation during Bond Formation and Adhesion of Pressure-Sensitive Adhesives. *J. Adhes.* **2008**, *84* (2), 164−190.
(52) Xu, X.; Ma, S.; Wu, J.; Yang, J.; Wang, B.; Wang, S.; Li, Q.; Feng, J.; You, S.; Zhu, J. High-Performance, Command-Degradable, Antibacterial Schiff Base Epoxy Thermosets: Synthesis and Properties. *J. Mater. Chem. A* **2019**, *7* (25), 15420−15431.
(53) Türel, T.; Tomović, Ž. Chemically Recyclable and Upcyclable Epoxy Resins Derived from Vanillin. *ACS Sustainable Chem. Eng.* **2023**, *11* (22), 8308−8316.
(54) Beniah, G.; Chen, X.; Uno, B. E.; Liu, K.; Leitsch, E. K.; Jeon, J.; Heath, W. H.; Scheidt, K. A.; Torkelson, J. M. Combined Effects of Carbonate and Soft-Segment Molecular Structures on the Nanophase Separation and Properties of Segmented Polyhydroxyurethane. *Macromolecules* **2017**, *50* (8), 3193−3203.
(55) Beniah, G.; Fortman, D. J.; Heath, W. H.; Dichtel, W. R.; Torkelson, J. M. Non-Isocyanate Polyurethane Thermoplastic Elastomer: Amide-Based Chain Extender Yields Enhanced Nanophase Separation and Properties in Polyhydroxyurethane. *Macromolecules* **2017**, *50* (11), 4425−4434.
(56) Miao, J. T.; Yuan, L.; Guan, Q.; Liang, G.; Gu, A. Biobased Epoxy Resin Derived from Eugenol with Excellent Integrated Performance and High Renewable Carbon Content. *Polym. Int.* **2018**, *67* (9), 1194−1202.
(57) Zhang, W.; Gao, F.; Chen, X.; Shen, L.; Chen, Y.; Lin, Y. Recyclable, Degradable, and Fully Bio-Based Covalent Adaptable

Polymer Networks Enabled by a Dynamic Diacetal Motif. *ACS Sustainable Chem. Eng.* **2023**, *11* (7), 3065−3073.
(58) Hu, H.; Tian, Y.; Kong, Z.; Ying, W. B.; Chen, C.; Li, F.; Zhang, R.; Zhu, J. A High Performance Copolyester with "Locked" Biodegradability: Solid Stability and Controlled Degradation Enabled by Acid-Labile Acetal. *ACS Sustainable Chem. Eng.* **2021**, *9* (5), 2280−2290.
(59) Miao, P.; Liu, J.; He, M.; Leng, X.; Li, Y. Bio-Based Non-Isocyanate Polyurethane with Closed-Loop Recyclability and Its Potential Application. *Chem. Eng. J.* **2023**, *475*, 146398.

https://doi.org/10.1021/acsapm.4c01526
ACS Appl. Polym. Mater. 2024, 6, 11180−11192